TESIS DE LA UNIVERSIDAD DE ZARAGOZA
2021
9

Laura Ceballos Laita

Estudio de la homeostasis de Fe y Mn en plantas mediante aproximaciones proteómicas

Departamento
Bioquímica y Biología Molecular y Celular

Director/es
López Millán, Ana Flor
Abadía Bayona, María Anunciación
Abadía Bayona, Javier

ISSN 2254-7606

Prensas de la Universidad
Universidad Zaragoza

ISSN 2254-7606

Universidad Zaragoza
1542

Tesis Doctoral

ESTUDIO DE LA HOMEOSTASIS DE FE Y MN EN PLANTAS MEDIANTE APROXIMACIONES PROTEÓMICAS

Autor

Laura Ceballos Laita

Director/es

López Millán, Ana Flor
Abadía Bayona, María Anunciación
Abadía Bayona, Javier

UNIVERSIDAD DE ZARAGOZA

Bioquímica y Biología Molecular y Celular

2018

Universidad Zaragoza
1542

TESIS DOCTORAL

Estudio de la homeostasis de Fe y Mn en plantas mediante aproximaciones proteómicas

Laura Ceballos Laita

Memoria presentada para optar al grado de Doctor en Ciencias

Programa de Doctorado en Bioquímica y Biología Molecular

Directores

Dr. Javier Abadía Bayona

Dra. Anunciación Abadía Bayona

Dra. Ana Flor López Millán

Tutor

María Luisa Peleato Sánchez

2018

CONSEJO SUPERIOR DE INVESTIGACIONES CIENTÍFICAS (CSIC)

ESTACIÓN EXPERIMENTAL DE AULA DEI

Departamento de Nutrición Vegetal

Grupo de Fisiología de Estrés Abiótico en Plantas

TESIS DOCTORAL:

Estudio de la homeostasis de Fe y Mn en plantas mediante aproximaciones proteómicas

Memoria presentada por Laura Ceballos Laita, Licenciada en Bioquímica, para optar al grado de Doctor en Ciencias

Dña. Laura Ceballos Laita

Zaragoza, 28 de junio de 2018

AUTORIZACIÓN DE LOS DIRECTORES

El Dr. JAVIER ABADÍA BAYONA, Profesor de Investigación del CSIC, la Dra. ANUNCIACIÓN ABADÍA BAYONA, Profesora de Investigación del CSIC y la Dra. ANA FLOR LÓPEZ MILLÁN, Doctora en Ciencias.

AUTORIZAN

La presentación de la Tesis Doctoral titulada "**ESTUDIO DE LA HOMEOSTASIS DE FE Y MN EN PLANTAS MEDIANTE APROXIMACIONES PROTEÓMICAS**", realizada por la Licenciada en Bioquímica LAURA CEBALLOS LAITA, para optar al Grado de Doctor por la Universidad de Zaragoza, y certifican que ha sido realizada bajo su dirección en la Estación Experimental de Aula Dei del Consejo Superior de Investigaciones Científicas (CSIC).

Y para que conste a los efectos oportunos expiden la presente autorización

En Zaragoza, 28 de junio de 2018

Fdo. Javier Abadía Bayona

Fdo. Anunciación Abadía Bayona

Fdo. Ana Flor López Millán

AUTORIZACIÓN DEL TUTOR ACADÉMICO PARA LA PRESENTACIÓN DE TESIS DOCTORAL

La Dra. MARÍA LUISA PELEATO SÁNCHEZ, Catedrática de la Universidad de Zaragoza

AUTORIZA

La presentación de la siguiente memoria de Tesis Doctoral, titulada "**ESTUDIO DE LA HOMEOSTASIS DE FE Y MN EN PLANTAS MEDIANTE APROXIMACIONES PROTEÓMICAS**" presentada por la Licenciada en Bioquímica LAURA CEBALLOS LAITA, para optar al grado de Doctor por la Universidad de Zaragoza.

Y para que conste a los efectos oportunos expide la presente autorización

En Zaragoza, 28 de junio de 2018

Fdo. María Luisa Peleato Sánchez

Financiación

Los trabajos incluidos en esta Tesis Doctoral han sido financiados por los proyectos de investigación AGL2012-31988, AGL2013-42175-R y AGL2016-75226-R del Ministerio de Economía y Competitividad (MINECO), co-financiados con FEDER, y el Grupo Consolidado A03 de la DGA. La Tesis de Laura Ceballos Laita ha sido financiada por una beca-contrato FPI del MINECO.

Abreviaturas

A	Antheraxanthin
ABC	ATP-binding cassette transporters
ACN	Acetonitrile
ATP	Adenosine triphosphate
AAS	Atomic absortion spectrometry
BPDS	Bathophenantrolinedisulphonic acid
BSA	Bovine serum albumin
CA	Carbonic anhydrase
CAX	Cation exchanger
CCC	Ca^{2+}-sensitive Cross-Complementer
CCX	Calcium cation exchanger
CDF	Cation diffusion facilitator
CDTA	Trans-1,2-Cyclohexylenediaminetetra acetic acid
CHAPS	3-[(3-Cholamidopropyl)dimethylammonio]-1-propanesulfonate
Chl	Chlorophyll
c-mdh	Cytosolic malate dehydrogenase
CPN	Chaperonin
CS	Classical secretory
DE	Dimensional electrophoresis
DIGE	Difference in-gel electrophoresis
DMA	2'-deoxymugineic acid
DNA	Deoxyribonucleic acid
DTT	Dithiothreitol
ECA	Endomembrane-type CA-ATPase
EDTA	Ethylenediamine tetraacetic acid
ER	Endoplasmatic reticulum
ESI	Electrospray ionization
EST	Expressed sequence tag
FAD	Flavin adenine dinucleotide
FCR	Ferric chelate reductase
FLA	Fasciclin-like arabinogalactan protein
FMN	Flavin mononucleotide
FPN	Ferroportin
FRD	Ferric reductase deficient
FRO	Ferric reductase oxidase
FS	Fitosideróforo
G3BP	GTPase-activating protein-binding protein
GFP	Green fluorescent protein
GH	Glycoside hydrolase
GO	Gene onthology
HABP	Hyaluronic acid binding protein
HEPES	4-(2-hydroxyethyl)-1-piperazineethanesulfonic acid
HPLC	High performance liquid chromatography
HSP	Heat shock protein
ICAT	Isotope-coded affinity tag
ICP	Inductively coupled plasma

IEF	Isoelectric focusing
IPG	Immobilized pH gradient
IREG	Iron-regulated
IRT	Iron regulated transporter
ITP	Iron transport protein
iTRAQ	Isotope tagged relative and absolute quantification
KH	K Homology
LEA	Late embryogenesis abundant
LRR	Leucine-rich repeats
MA	Mugineic acid
MALDI	Matrix-assisted laser desorption-ionization
MAR	Multiple antibiotic resistance
MATE	Multidrug and toxic compound extrusion
MFL	Mitoferrin-like
MIT	Mitochondrial iron transporter
MTP	Metal tolerance proteins
MS	Mass spectrometry
MudPIT	Multi-dimensional protein identification technology
MW	Molecular weight
NA	Nicotianamine
NAD(H)	Nicotinamide adenine dinucleotide (reduced)
NAP	Non-intrinsic ABC proteins
NCS	Non-classical secretory
NRAMP	Natural resistance associated-macrophage
NS	No secretory
OEC	Oxygen evolving complex
PAGE	Polyacrylamide gel electrophoresis
PAM	Photosynthesis affected mutant
PAP	Purple acid phosphatases
PCA	Principal component analysis
PEPC	Phosphoenolpyruvate carboxylase
PIC	Permease in chloroplast
PI-PLC	Phosphoinositide phospholipase C
PDR	Pleiotropic drug resistance
PM	Plasma membrane
PMF	Peptide mass fingerprint
PMSF	Phenylmethylsulfonyl fluoride
PPFD	Photosynthetic photon flux density
PR	Pathogenesis related
PSII	Photosystem II
PVDF	Polyvinylidene fluoride
RNA	Ribonucleic acid
ROS	Reactive oxigen species
RP	Reverse phase
RRM	RNA recognition motif
RT-PCR	Real time-polymerase chain reaction
SAM	S-adenosyl-methionine
SCX	Strong cation exchange

SD	Standard deviation
SDS	Sodium dodecyl sulfate
SILAC	Stable isotope labeling by amino acids in cell
SOD	Superoxide dismutase
SPAD	Soil-plant analysis development
TCA	Tricarboxylic acid
TOF	Time of flight
TOM	Transporter of Mugineic Acid
V	Violaxanthin
VIC	Vacuum-infiltration-centrifugation
VIT	Vacuolar iron transporter
YSL	Yellow Stripe Like
Z	Zeaxanthin
ZIP	Zn-regulated transporter/Fe-regulated transpoter-like protein

ÍNDICE

Capítulo 1: Introducción

1.1. La homeostasis en plantas 5
1.2. El Fe en las plantas 6
1.2.1. Adquisición de Fe por la raíz 7
1.2.2 Transporte intracelular e intercelular de Fe 8
Transporte vía xilema 8
Localización, almacenamiento y transporte intracelular 10
Vacuola 10
Mitocondria 12
Cloroplasto 12
Transporte en el floema 14
1.2.3. Estrés por Fe 15
Deficiencia de Fe 16
Respuestas de la planta ante la deficiencia de Fe 17
Medidas correctoras de la deficiencia de Fe 18
1.3. El Mn en las plantas 19
1.3.1. Adquisición de Mn por la raíz 19
1.3.2. Transporte intracelular e intercelular de Mn 21
Translocación del metal a xilema y floema 21
Localización, almacenamiento y transporte intracelular 22
Vacuola 22
Otros compartimentos intracelulares 25
1.3.3. Estrés por Mn 26
Deficiencia de Mn 27
Respuesta de la planta ante la deficiencia de Mn 27
Medidas correctoras de la deficiencia de Mn 28
Toxicidad de Mn 29
Respuesta de la planta ante la toxicidad de Mn 30
Medidas correctoras de la toxicidad de Mn 31
1.4. La proteómica como herramienta de estudio 31
1.4.1. Técnicas clásicas 33
1.4.2. Técnicas de proteómica avanzada 35
Cuantificación mediante marcaje de proteínas o péptidos 36
Cuantificación mediante “Label-free shotgun proteomics” 38

1.4.3. Método de identificación de proteínas 40
1.4.4. Aplicación a los sistemas vegetales 41
Capítulo 2: Objetivos 47
Capítulo 3: Resultados
3.1. Plant fluid proteomics: delving into the xylem sap, phloem sap and apoplastic fluid proteomes 51
3.2. Protein profile of *Beta vulgaris* leaf apoplastic fluid and changes induced by Fe deficiency and Fe resupply 75
3.3. Effects of Fe and Mn deficiencies on the protein profiles of tomato (*Solanum lycopersicum*) xylem sap as revealed by shotgun analyses 99
3.4. Data on xylem sap proteins from Mn- and Fe-deficient tomato plants obtained using shotgun proteomics 123
3.5. Effects of manganese toxicity on the protein profile of tomato (*Solanum lycopersicum*) roots as revealed by two complementary proteomic approaches, two-dimensional electrophoresis and shotgun analysis 129
3.6. Effects of manganese toxicity on the protein profile of tomato (*Solanum lycopersicum*) xylem sap as revealed by shotgun analysis…….. 153
Capítulo 4: Discusión general 179
Capítulo 5: Conclusiones 199
Bibliografía 203

Anexos
I- Effects of Fe deficiency on the protein profiles and lignin composition of stem tissues from *Medicago truncatula* in absence or presence of calcium carbonate 241
II- Curriculum vitae 269

Capítulo 1

INTRODUCCIÓN

1.1. La homeostasis en plantas

El término "homeostasis" fue usado por primera vez en 1926 por Walter Cannon (Cannon, 1926) para referirse al concepto de medio interno descrito por Claude Bernard en 1865 (Bernard, 1865). Dicho término describe el conjunto de mecanismos fisiológicos que se coordinan para mantener en un estado de equilibrio las propiedades físico-químicas del medio interno del organismo. Las plantas necesitan, además de oxígeno, dióxido de carbono y agua, ciertos elementos considerados esenciales para su correcto desarrollo y crecimiento. El sistema de homeostasis de nutrientes se encuentra altamente regulado en las plantas, permitiéndoles mantenerlos en niveles óptimos de concentración. Estos nutrientes esenciales, entre los que podemos distinguir al menos 14 elementos, se obtienen generalmente del suelo y pueden clasificarse, en función de la concentración requerida, como macronutrientes o micronutrientes (Marschner, 1995; Mengel et al., 2001). Entre los macroelementos encontramos N, K, P, Ca, Mg y S, mientras que el grupo de microelementos, denominados así por ser necesarios en cantidades inferiores, está compuesto principalmente por metales de transición como Fe, Mn, Cu, Zn, Ni y Mo y otros no metales como Cl o B. Estos microelementos resultan potencialmente tóxicos si los niveles de exposición son demasiado elevados, y, sin embargo, el organismo no puede crecer ni completar su ciclo biológico sin un suministro adecuado de los mismos, ya que participan en funciones esenciales para la vida. El rango de concentraciones considerado fisiológico para los metales esenciales, comprendido entre los valores que se definen como deficiencia y toxicidad, es muy estrecho y varía en función de la especie, el tejido o las condiciones de crecimiento, y por ello la homeostasis de estos elementos está finamente regulada para ajustarse a las fluctuaciones en su disponibilidad (Marschner, 1995).

Tanto la deficiencia como la toxicidad de micronutrientes en las zonas agrícolas pueden reducir el crecimiento y la producción de los cultivos (MacNicol y Beckett, 1985; Marschner, 1995; Mengel et al., 2001; Álvarez-Fernández et al., 2003). Se considera "deficiente" aquella concentración que impide que el crecimiento del cultivo alcance el 90 % del rendimiento máximo. Ante una deficiencia de micronutrientes la planta activa mecanismos involucrados en su obtención con la finalidad de aumentar su capacidad de adquisición. Por otro lado, se utiliza el término "toxicidad" cuando la concentración del micronutriente en el cultivo es excesiva y provoca una disminución en el crecimiento de la planta de más de un 10 % (White y Brown, 2010). Los daños ocasionados en el crecimiento de la planta se deben con frecuencia a la actividad redox de muchos de estos micronutrientes. Altas concentraciones de estos metales generan especies reactivas de oxígeno que son potencialmente tóxicas debido a oxidaciones inespecíficas ocasionadas en proteínas, lípidos de membrana y ácidos nucleicos (Schützendübel y Polle, 2002). Asimismo, semejanzas en el tamaño y las características de estos metales pueden llevar a procesos de competición, reemplazándose unos a otros cuando actúan como cofactores

de proteínas. Del mismo modo que en las situaciones de escasez, cuando estos elementos se encuentran en exceso la planta desarrolla mecanismos orientados hacia su almacenaje y desintoxicación.

Para una correcta nutrición de la planta el suministro de nutrientes debe estar equilibrado. Las plantas poseen mecanismos específicos para la absorción, translocación y almacenamiento de estos nutrientes, que varían en función de la movilidad del elemento en el suelo, la entrada al interior de las células de la raíz, su transporte a la parte aérea y su posible movilización a compartimentos de almacenamiento. La red de sistemas vasculares de la planta, constituida por los vasos de xilema y el floema, transporta y distribuye los nutrientes, así como los productos de la fotosíntesis y otras moléculas señalizadoras como las hormonas, a sus lugares de utilización. Metales esenciales para la planta, como Fe y Mn, han sido localizados en la vacuola, el cloroplasto o la mitocondria. Tanto el cloroplasto como la mitocondria necesitan de la presencia de estos metales para llevar a cabo sus funciones biológicas, debido a su importante papel en las cadenas de transporte electrónico y a su función como cofactores de numerosas enzimas (Vigani et al., 2009) y, al mismo tiempo, estos compartimentos sub-celulares actúan como reservorios de metales (Pilon et al., 2009; Puig y Peñarrubia, 2009).

En las últimas décadas, muchos estudios en el área de la nutrición vegetal se han centrado en ampliar el conocimiento existente tanto sobre los mecanismos involucrados en la asimilación y distribución de los nutrientes como sobre los procesos que conducen a su homeostasis, necesaria para el correcto crecimiento y desarrollo de la planta (Marschner et al., 1995; Mengel et al., 2001; Karley y White, 2009; Miller et al., 2009; Miwa et al., 2009; Puig y Peñarrubia, 2009; White y Broadley, 2009). En esta Tesis Doctoral se presentan los resultados obtenidos mediante la aplicación de aproximaciones proteómicas en el estudio de la homeostasis de dos microelementos, Fe y Mn, imprescindibles para llevar a cabo las funciones vitales de la planta por estar implicados en importantes procesos del metabolismo vegetal.

1.2. El Fe en las plantas

El Fe presenta una gran versatilidad en sus funciones biológicas debido principalmente al potencial del par redox Fe^{3+}/Fe^{2+}, que varía dependiendo del ligando al que se encuentre unido, permitiendo así su uso en forma de grupos hemo (citocromos, nitrato reductasas, catalasas o peroxidasas), grupos sirohemo y cluster Fe-S (nitrito reductasas o sulfito reductasas y ferredoxinas) u otros grupos conteniendo Fe (lipooxigenasas). Así, este metal es un constituyente indispensable de un gran número de enzimas y proteínas con funciones redox que intervienen en algunas de las principales funciones del metabolismo vegetal, como son la respiración (Clark, 1983), la fotosíntesis, la fijación de nitrógeno, la síntesis de clorofila, el

mantenimiento de la estructura del cloroplasto (Abadía y Abadía, 1993) y la síntesis de DNA y hormonas (Marschner, 2012).

Aproximadamente el 80 % del Fe total de la planta se encuentra localizado en el cloroplasto, y más del 50 % del Fe presente en las hojas se encuentra formando parte de proteínas (Young y Terry, 1982). La concentración de Fe que la planta necesita para mantener un crecimiento y desarrollo normal varía entre 10^{-9} a 10^{-4} M. Concentraciones superiores de Fe en estado libre pueden generar especies reactivas de oxigeno (ROS) (Marschner, 1995), y por ello, la absorción, transporte, utilización y compartimentación de este elemento en la planta requiere una estrecha regulación tanto a nivel celular como molecular.

1.2.1. Adquisición de Fe por la raíz

El Fe es el cuarto elemento más abundante en la corteza terrestre, estimándose que representa en torno al 3,8 % de la misma. Este elemento puede encontrarse en el suelo formando especies ferrosas (Fe^{2+}) o férricas (Fe^{3+}) dependiendo del potencial redox y del pH del mismo. En suelos con buena aireación, la concentración de oxígeno está próxima a la atmosférica y predominan las especies férricas. El pH de algunos suelos es ácido, lo que favorece la disolución de óxidos de Fe e incrementa los niveles de especies de Fe^{3+} en disolución. Sin embargo, en otros suelos que tienen un pH neutro o alcalino, como es el caso de los suelos calizos presentes en un 30 % de los suelos cultivables en el mundo, el Fe se encuentra en forma de óxidos que presentan niveles de solubilidad mínimos y son difícilmente asimilables para las plantas (Colombo et al., 2014).

Atendiendo a los mecanismos de adquisición de Fe por las células radiculares, las plantas se dividen en dos grupos: las pertenecientes a la Estrategia I (dicotiledóneas y monocotiledóneas no gramíneas) y las que pertenecen a la Estrategia II (gramíneas). Las plantas que utilizan la Estrategia I incorporan Fe en forma de ión divalente, previa reducción mediante una reductasa férrica situada en la membrana plasmática de las células de la raíz y perteneciente a la familia FRO (Ferric Reductase Oxidase) (Robinson et al., 1999). Este Fe se transporta al citoplasma celular en su forma divalente (Fe^{2+}) a través del transportador IRT1 (Iron Regulated Transporter) (Eide et al., 1996; Vert et al., 2002) con la ayuda de una enzima ATPasa que disminuye el pH de la rizosfera mediante la secreción de H^+, aumentando así la solubilidad del metal (Santi y Schmidt, 2009). Además, las plantas de Estrategia I liberan compuestos de bajo peso molecular como carboxilatos, compuestos fenólicos, flavinas y flavonoides, que favorecen la captación de Fe de la rizosfera (Abadía et al., 2011). Las plantas que utilizan la Estrategia II adquieren Fe en forma de quelato de Fe^{3+} mediante la secreción de fitosideróforos (Fe^{3+}-FS) (Abadía et al., 2011). Los fitosideróforos (FSs) pertenecen a una clase de compuestos denominados ácidos mugineicos (MAs; Ma y Nomoto, 1996) cuya biosíntesis comienza con la

condensación de tres moléculas de S-adenosil-metionina que forman el precursor nicotianamina (NA; Shojima et al., 1990; Ma et al., 1995). Este mecanismo de adquisición exuda los FSs mediante un transportador TOM (Nozoye et al., 2011) e introduce el quelato Fe^{3+}-FS al interior celular a través de un transportador específico de la familia "Yellow Stripe-Like" (YSL) localizado en las zonas apicales de la raíz (Curie et al., 2001; Murata et al., 2006). Una vez en el citoplasma, el quelato Fe^{3+}-FS se disocia en una reacción mediada por ascorbato que tiene como resultado la formación de un complejo terciario (Weber et al., 2008). A pesar de haberse definido dos estrategias de adquisición tan claramente diferenciadas, se han descrito especies que poseen elementos propios de ambas estrategias en función de las condiciones de cultivo, como p. ej. arroz o cacahuete (Ishimaru et al., 2006; Xiong et al., 2013). Los esquemas de ambas Estrategias se muestran en la Figura 1.1.

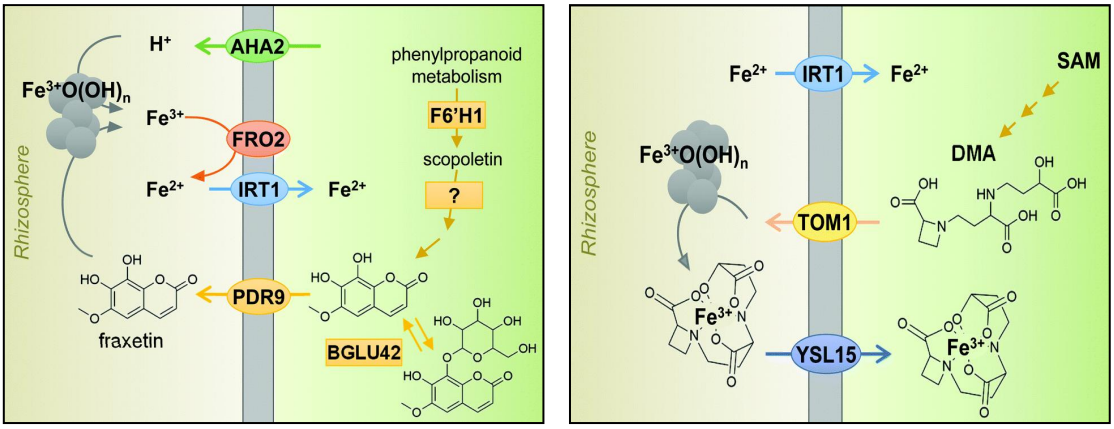

Figura 1.1. *Esquema de la adquisición de Fe por la raíz en plantas pertenecientes a la Estrategia I (Arabidopsis; A) y en plantas que utilizan la Estrategia II (arroz; B). Imagen adaptada de Connorton et al., 2017.*

Además de las estrategias mencionadas anteriormente, el Fe puede ser introducido en las células radiculares a través de transportadores de otros metales, que a veces poseen cierta inespecificidad. Dicha inespecificidad es debida a que los metales presentan características químicas similares, y refleja así la complejidad de los mecanismos de adquisición de micronutrientes en la planta.

1.2.2. Transporte intracelular e intercelular de Fe

Transporte vía xilema

Una vez adquirido por las células de la epidermis de la raíz, el Fe es dirigido al sistema vascular para su translocación a la parte aérea. En esta translocación, puede ser adsorbido por la pared celular, transportado *via* simplasto y/o apoplasto, y/o almacenado en orgánulos celulares en la raíz. El apoplasto es el espacio extracelular que constituye la interfase acuosa entre la membrana plasmática de células adyacentes donde el Fe puede difundir libremente. Sin

embargo, el transporte a través de la *via* apoplástica en raíz se encuentra limitado por las bandas de Caspary (Enstone et al., 2002), lo que implica que la ruta simplástica sea la mayoritaria para el transporte del metal (Stephan et al., 1996). Durante este proceso de transporte radial, la alta reactividad del Fe hace que la quelación resulte imprescindible, para evitar el estrés oxidativo y facilitar la translocación del metal a través de la vasculatura (Pich, 2001). Se ha propuesto que tanto la NA como el citrato sean los quelantes dominantes durante este transporte hacia el sistema vascular, aunque los transportadores involucrados aún no han sido descritos. Estudios previos han demostrado que la NA, que está presente tanto en plantas de Estrategia I como de Estrategia II, forma complejos con Fe, Mn, Co, Zn, Ni y Cu, y junto con los FSs facilita el transporte del metal a larga distancia (Von Wirén et al., 1999). Por otro lado, el destino del Fe^{3+} introducido mediante el complejo Fe^{3+}-FS en las gramíneas no está claro, aunque la presencia de complejos de Fe^{3+}-NA puede sugerir igualmente una quelación del metal hasta su canalización a otros sitios de transporte o almacenamiento (Hell y Stephan, 2003). Finalmente, el Fe libre que no haya sido quelado puede oxidarse y precipitar como hidróxido o sales de fosfato, formando depósitos de Fe apoplástico, y se ha propuesto que estos reservorios podrían ser utilizados en condiciones de escasez del metal (Bienfait et al., 1985).

Para su transporte a larga distancia, el Fe debe ser cargado al xilema. El xilema es un espacio apoplástico, por lo que, tras pasar la banda de Caspary, el Fe debe ser transportado fuera de la célula radicular. Aunque el transportador responsable de este proceso no ha sido descrito, se ha sugerido que la proteína ferroportin 1/iron-regulated 1 (AtFPN1/ AtIREG1) identificada en *Arabidopsis thaliana* sea un posible candidato (Morrisey et al., 2009). El Fe se oxidaría química o enzimáticamente al ser liberado a los vasos del xilema y una vez en el fluido se transportaría en forma de Fe^{3+}, acomplejado con citrato u otros carboxilatos que forman complejos estables al pH ligeramente ácido del xilema (5,5-6,0; López-Millán et al., 2000a; Rellán et al., 2010; Flis et al., 2016). Aunque el conocimiento de este proceso es aún limitado, miembros de la familia de transportadores MATE (Multidrug And Toxic compound Extrusion) parecen estar involucrados en el transporte del citrato a los vasos del xilema. Así, la proteína FRD3 presenta grandes similitudes con transportadores de la familia MATE que confieren tolerancia al Al en cebada a través del eflujo de citrato de la raíz al suelo (Furukawa et al., 2007; Magalhaes et al., 2007). Se ha descrito que los mutantes del gen *frd3* en *Arabidopsis* contienen un 40 % menos de citrato y un 49 % menos de Fe en hojas que las plantas silvestres (Green y Rogers, 2004). Por otro lado, una proteína ortóloga a FRD3, OsFRDL1, ha sido descrita en arroz y sus mutantes de deleción presentan fenotipos similares a los del mutante *atfrd3* de *Arabidopsis* (Inoue et al., 2004; Yokosho et al., 2009). De esta forma, a pesar de tener mecanismos distintos en la adquisición del metal, parece que plantas de Estrategia I y II

comparten procesos comunes de translocación de Fe de la raíz a la parte aérea (Conte y Walker, 2011).

El transporte de agua y solutos desde la raíz hasta las hojas *vía* xilema se lleva a cabo mediante la presión hidrostática creada por la transpiración del agua en las hojas. Aproximadamente el 80 % del Fe adquirido por la raíz se transporta a la parte aérea de la planta. En *Arabidopsis* miembros de la familia YSL han sido propuestos como mediadores en la descarga del Fe transportado por el xilema. Los genes YSL han sido descritos en varias especies y sus sustratos incluyen a los complejos metal-NA (DiDonato et al., 2004; Kioke et al., 2004; Roberts et al., 2004; Gendre et al., 2007; Harada et al., 2007). Tal y como se ha mencionado anteriormente, el Fe se transporta en xilema acomplejado con carboxilatos, por lo que el intercambio del ligando a NA debe suceder antes de que el complejo llegue a estos transportadores (Curie et al., 2009). La expresión de los transportadores AtYSL1, AtYSL2 y AtYSL3 de *Arabidopsis* disminuye en condiciones de deficiencia de Fe, sugiriendo que estos transportadores no están involucrados en la adquisición de Fe aunque sí juegan un papel importante en la homeostasis del metal. En hoja, estas tres proteínas se localizan en las células vasculares próximas al xilema y se les asigna un papel esencial en el movimiento del Fe transportado por el xilema a través del apoplasto y/o simplasto hasta su compartimento de destino (DiDonato et al., 2004; Waters et al., 2006). Por tanto, las concentraciones de metales y otros solutos en el fluido apoplástico vienen determinadas por un equilibrio de importación/exportación a través de la red de fluidos del xilema y el floema que, junto con el apoplasto, conforman el sistema vascular de transporte en las plantas superiores, permitiendo así la distribución de nutrientes.

Localización, almacenamiento y transporte intracelular

El Fe en la célula se acumula principalmente en la vacuola, la mitocondria y el cloroplasto. Además, en el caso del cloroplasto y la mitocondria, su disponibilidad en estos compartimentos resulta imprescindible para llevar a cabo un correcto desarrollo de sus funciones (Bashir et al., 2011; Vigani et al., 2013). En el transporte intracelular de Fe se encuentran implicados varios transportadores de membrana.

Vacuola

Los primeros transportadores de Fe asociados a la vacuola que fueron descritos pertenecen a la familia NRAMP (Natural Resistance Associated-Macrophage) (Curie et al., 2000; Thomine et al., 2000). En *Arabidopsis*, NRAMP3 y NRAMP4 median el eflujo de Fe desde la vacuola al citosol y juegan un papel determinante en su removilización desde este compartimento tanto en las etapas de germinación como en la vida adulta de la planta,

especialmente en tejidos senescentes (Thomine et al., 2003; Lanquar et al., 2005). Estudios en *Arabidopsis* han demostrado que su sobreexpresión permite aumentar los niveles de Fe en el citosol y reduce la expresión de *IRT1* y *FRO2* en condiciones de deficiencia de Fe (Thomine et al., 2003). El papel de estos transportadores no ha sido definido únicamente para Fe, sino que median también el transporte de otros metales divalentes como Mn o Cd (Thomine et al., 2000). El responsable del proceso inverso en *Arabidopsis*, el transportador involucrado en la movilización del Fe al interior de la vacuola (VIT1), fue descubierto con posterioridad (Kim et al., 2006). Para el estudio de este proceso se utilizó como base la proteína CCC1 (Ca^{2+}-sensitive Cross-Complementer) descrita en levadura, que media el transporte de Fe y Mn al interior de la vacuola en este organismo. Estudios de sobreexpresión de CCC1 en levadura mostraron un aumento en la concentración de Fe vacuolar, mientras que el mutante de deleción del transportador presentaba bajos niveles de Fe vacuolar y mayor sensibilidad a la toxicidad por Fe (Li et al., 2001). La tolerancia a la toxicidad por Fe se restauró al expresar en el mutante de deleción la proteína de *Arabidopsis* VIT1 (Vacuolar Iron Transporter), que presenta una similitud del 58 % con la correspondiente en levadura (Kim et al., 2006). En planta, VIT1 se expresa tanto en la raíz como en la parte aérea y su papel se presupone opuesto a NRAMP3 y NRAMP4, introduciendo el Fe en la vacuola donde es almacenado (Grotz y Guerinot, 2006). Otras proteínas similares a VIT han sido descritas en *Arabidopsis* (VTL-VIT1 Like proteins) con un papel activo en la transferencia de Fe del citoplasma al interior vacuolar (Gollhofer et al., 2014). No está clara la necesidad de tantos transportadores de Fe en *Arabidopsis*, y podría suceder que se encontrasen también implicados en el transporte de otros metales, como ocurre en el caso de VIT1 y VIT2 en arroz que, además de transportar Fe, facilitan el transporte de Mn y Zn (Zhang et al., 2012). Una vez en el interior de la vacuola, el Fe se encontraría en forma de complejos con fitato de forma globoide que resultan altamente insolubles (Clemens, 2014). La Figura 1.2. muestra el esquema de proteínas involucradas en el transporte de Fe a la vacuola.

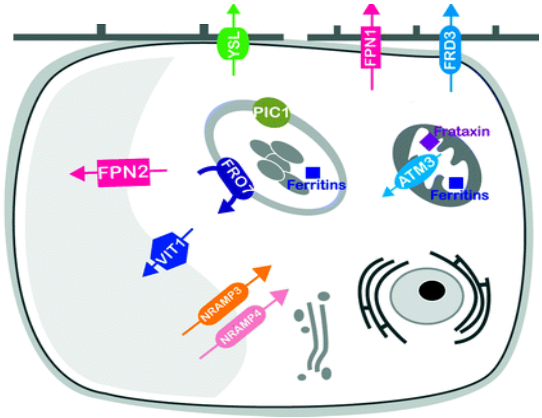

Figura 1.2. *Localización subcelular de los transportadores implicados en el transporte de Fe a la vacuola y en su exportación al citosol. (Imagen adaptada de Thomine y Lanquar, 2011).*

Mitocondria

La mitocondria en la planta actúa como el centro de regulación de las reacciones redox y de conversión de energía, uniendo las rutas metabólicas provenientes de diversos compartimentos subcelulares en las que el Fe juega un papel esencial. Estas propiedades hacen de la mitocondria un buen sensor que refleja el estado metabólico y energético de la célula, así como el estado nutricional con respecto al Fe (Schwarzländer et al., 2012; Vigani et al., 2013). En arroz, el transporte de Fe desde el citoplasma al interior de la mitocondria está mediado por el transportador MIT (Mitochondrial Iron Transporter). El mutante de deleción de MIT en esta especie presenta un fenotipo letal (Bashir et al., 2011), mostrando el papel fundamental que juega esta proteína. Estudios en *Arabidopsis* han permitido la identificación de varios miembros de la familia ABC (ATP-binding cassette transporters), AtATM3 y AtATM1, como responsables del transporte de complejos de Fe-S o de sus precursores desde la mitocondria al citoplasma, donde participarían en el ensamblaje de proteínas citosólicas con centros Fe-S (Kushnir et al., 2001; Chen et al., 2007). Por otro lado, dos miembros de la familia de reductasas férricas (FRO) en *Arabidopsis*, FRO3 y FRO8, localizados en el sistema vascular, contienen péptidos diana mitocondriales (Wu et al., 2005; Mukherjee et al., 2006; Tarantino et al., 2010) y además estudios proteómicos han localizado a uno de ellos, FRO8, en la membrana mitocondrial (Heazlewood et al., 2004). Aunque estas proteínas no han sido caracterizadas funcionalmente, por similitud con la función de la reductasa férrica de raíz se ha sugerido que podrían jugar algún papel en la adquisición de Fe en la mitocondria (Jain et al., 2014). Finalmente, se ha propuesto que la frataxina puede actuar como una proteína chaperona de Fe actuando en el transporte de este metal en el interior de la mitocondria, en una situación similar a la descrita en la homeostasis de Cu, en la que chaperonas como la CCH juegan un papel esencial en su homeostasis (Busi et al., 2006; Vazzola et al., 2007).

Cloroplasto

Los mecanismos que rigen el transporte de Fe al interior del cloroplasto todavía no se conocen con detalle, aunque está generalmente aceptado que pueda suceder tanto en forma de catión divalente como trivalente, utilizando transportadores de Fe^{2+} o una reductasa de Fe^{3+} como ocurre en cianobacterias (Katoh et al., 2001; Kranzler et al., 2014). Estudios basados en la proteína FRO7 de *Arabidopsis* han demostrado que el cloroplasto emplea un mecanismo basado en la reducción para la adquisición de Fe. La proteína FRO7 está localizada en la envoltura interna del cloroplasto (Solti et al., 2014) y la pérdida de su función produce una reducción significativa de la actividad reductasa férrica en la superficie de este orgánulo, lo que lleva a una disminución del contenido de Fe cloroplástico de aproximadamente un 30 % (Jain et al., 2014). Además, el fenotipo del mutante de deleción muestra un descenso en la eficiencia fotosintética,

reforzando la hipótesis que sitúa el papel de FRO7 como fundamental a la hora de proporcionar el Fe necesario para el correcto ensamblaje de los complejos fotosintéticos (Jain et al., 2014). Trabajos recientes en remolacha han reafirmado la existencia de un mecanismo de adquisición de Fe en el cloroplasto basado en estrategias de reducción (Solti et al., 2012, 2014). Por otro lado, también se ha identificado un posible transportador de Fe al interior del cloroplasto en la envoltura interna, PIC1 (Duy et al., 2007) aunque no está claro si transporta Fe^{2+} o Fe^{3+}. Otras proteínas posiblemente involucradas en la homeostasis de Fe en el cloroplasto incluyen MAR1 (un homólogo de la ferroportina 1 y 2) que puede actuar como quelante de Fe (Conte et al., 2009), MFL1/2 (que pertenece a la familia de mitoferrinas pero actúa en el cloroplasto) (Tarantino et al., 2011) y NAP14 (una proteína ABC localizada en plástidos de *A. thaliana* que participa activamente en la homeostasis del Fe) (Shimoni-Shor et al., 2010). Finalmente, igual que en la mitocondria, se ha descubierto una proteína de tipo NEET localizada en el cloroplasto que podría participar en el transporte de centros Fe-S hacia sus apoproteínas (Nechushtai et al., 2012).

En los cloroplastos y plástidos, el exceso de Fe libre se almacena en proteínas denominadas fitoferritinas. Estos complejos multiméricos se localizan en los plástidos de brotes y raíces y son capaces de almacenar hasta 4.000 átomos de Fe, evitando así daños por estrés oxidativo en la planta (Savino et al., 1997; Briat et al., 1999). En condiciones normales, la presencia de ferritina se limita al estroma del cloroplasto, por lo que el 90 % del Fe en las células de las hojas se encuentra en los cloroplastos. Estudios previos sugieren un papel importante de la NA en la mediación entre las distintas formas de almacenamiento de Fe y su homeostasis (Stephan y Scholz 1993, Stephan et al., 1996, Pich et al., 2001). De acuerdo con esta hipótesis, miembros de la familia YSL en *Arabidopsis* (YSL4 y YSL6) localizados en el cloroplasto parecen participar activamente en el eflujo del complejo Fe-NA desde el cloroplasto, principalmente en etapas de embriogénesis y senescencia (Divol et al., 2013). El esquema del transporte del Fe en el cloroplasto se muestra en la Figura 1.3.

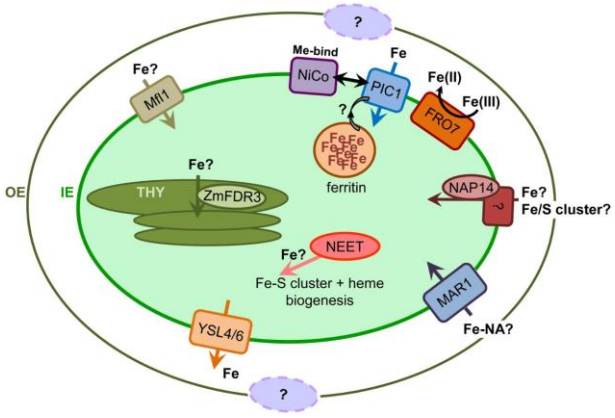

Figura 1.3. *Transportadores involucrados en el transporte de Fe en el cloroplasto. Imagen tomada de López-Millán et al., 2016. IE: envoltura interna; OE: envoltura externa; THY: membrana tilacoidal.*

Transporte en el floema

El sistema de transporte vascular actúa como un canal de comunicación entre la raíz y la parte aérea de la planta, en un proceso en el que participan múltiples transportadores y agentes quelantes de Fe. Así, el Fe almacenado en los distintos compartimentos puede ser translocado a los tejidos en crecimiento que precisen del metal, posiblemente a través de la ruta simplástica. El floema está implicado en el transporte a larga distancia en ambas direcciones, siendo el responsable tanto de la removilización desde los tejidos sumidero a las distintas partes de la planta (Van Bel, 2003), como del transporte del metal a órganos en desarrollo como ápice o semillas, donde el flujo de xilema generado por los procesos de transpiración resulta ineficiente (Kim y Guerinot, 2007). El Fe se transporta en floema acomplejado con agentes quelantes, evitando su posible precipitación debida al pH de este fluido, que es más elevado que el pH del xilema. El 77 % del Fe presente en el floema se encuentra formando complejos de elevado peso molecular. Hasta el momento se han descrito complejos con la molécula DMA (ácido deoximugineico, un derivado de la NA; Nishiyama et al., 2012) o la proteína ITP (Iron Transport Protein; Krüger et al., 2002). Aunque dos proteínas de bajo peso molecular presentes en el floema también han sido identificadas como ligandos de Fe mediante técnicas basadas en cromatografía de afinidad, no es probable que presenten ninguna función en su transporte (Lattanzio et al., 2013).

En el mutante de tomate "chloronerva", que se caracteriza por una NA sintetasa disfuncional que produce la pérdida de la síntesis de NA (Herbik et al., 1999; Higuchi et al., 1999; Ling et al., 1999), se han encontrado niveles de Fe muy elevados en las hojas maduras. Este exceso del metal no es transportado a las hojas más jóvenes, que siguen presentando deficiencia de Fe (Scholz et al., 1985; Becker et al., 1992), sugiriéndose así un papel de la NA en la removilización del Fe a través del fluido floemático, lo que además se ve reforzado por estudios que indican que el complejo Fe-NA puede existir al pH básico de este compartimento (von Wirén et al., 1999; Rellán-Álvarez et al., 2008; Conte y Walker, 2011). Por tanto, los graves defectos reproductivos que presentan las plantas deficientes en NA pueden estar relacionados con un transporte comprometido del Fe a través del floema. Además, el grado de removilización del metal a través de esta vía parece depender de la especie vegetal. Tan sólo un pequeño porcentaje del Fe presente en el floema se encuentra como Fe^{2+}, indicando que la NA podría tener un papel activo en la carga y descarga al fluido (Curie y Briat, 2003; Schuler et al., 2012).

En arroz se ha visto que OsYSL2 es un transportador involucrado en el transporte de metales en floema como complejos metal-NA (Fe^{2+}-NA y Mn^{2+}-NA), y que su expresión aumenta drásticamente en las células del floema de los haces vasculares de las hojas en condiciones de deficiencia de Fe, si bien no presenta variaciones en las células radiculares. Esta

localización en las células del cilindro vascular permite formular la hipótesis de que OsYSL2 está implicado en el transporte de Fe a larga distancia a través del floema, pero no en su captación del suelo (Koike et al., 2004). Una vez el complejo Fe^{2+}-NA se encuentra en el floema, el Fe se podría oxidar y transportar como Fe^{3+}. Algunos estudios recientes han demostrado la existencia de otras especies, posiblemente de carácter peptídico, implicadas en el transporte del metal una vez ha sido cargado al floema como complejo Fe-NA (Schmidke et al., 1999; Álvarez-Fernández et al., 2014). Un candidato para soportar esta suposición es la proteína de transporte de Fe (ITP), miembro de la familia de proteínas LEA (Late Embryogenesis Abundant) que se propuso que transportara Fe en forma férrica (Krueger et al., 2002). Este hecho implicaría la existencia de un sistema de oxidación-reducción que debe operar dentro del fluido floemático. Aunque se ha hipotetizado sobre la posible implicación de una citocromo b5 reductasa (Curie y Briat, 2003), hasta el momento se desconocen los posibles responsables de este proceso.

1.2.3. Estrés por Fe

El efecto del estrés por Fe en el fenotipo de la planta depende del grado de deficiencia o toxicidad del metal. En ambos casos la planta ve comprometidos su crecimiento y floración, presentando un menor número de frutos y de menor tamaño. No es habitual encontrar concentraciones de Fe asimilable lo suficientemente elevadas como para provocar toxicidad en los cultivos. En condiciones normales, aun cuando exista mucho Fe^{2+} en la rizosfera, el oxígeno liberado por la superficie de la raíz permite su oxidación a formas no inmediatamente disponibles para la planta, controlando así su adquisición en exceso. Por tanto, la toxicidad por Fe sólo se produce en suelos ácidos o, como en el caso de los cultivos de arroz, en suelos que presentan una inundación constante que hace que la planta sufra una reducción en la capacidad de oxidación radicular por inhibición de los procesos de respiración, con lo que el Fe en la solución del suelo no se puede oxidar fácilmente a formas no disponibles.

Mientras que la toxicidad por Fe no resulta un estrés nutricional generalizado importante desde un punto de vista agronómico, la deficiencia de dicho metal sí que supone un problema cada vez más común en los suelos cultivables. Este estrés nutricional resulta uno de los factores limitantes más importantes en la producción agrícola y afecta a un porcentaje elevado de plantaciones frutales del área mediterránea (Sanz et al., 1992; Tagliavini et al., 2000) y de cultivos de soja en el medio oeste de Estados Unidos (Froelich et al., 1981; Coloumbe et al., 1984; Lin et al., 1997). La deficiencia de Fe es un problema complejo en el que influyen diversos factores, incluyendo la escasa solubilidad y movilidad del metal en determinados suelos, la predisposición genética de la planta, dificultades en la adquisición de Fe y otros muchos factores relacionados con el metabolismo de la planta. Sin embargo, la presencia de un

pH elevado resulta determinante a la hora de limitar su disponibilidad. Algunos suelos presentan altos niveles de humedad y elevadas cantidades de arcillas, fosfatos e iones bicarbonato (HCO_3^-) capaces de tamponar el pH entre valores de 7,5-8,5 que reducen considerablemente la solubilidad de los óxidos de Fe (Lindsay y Schwab, 1982; Lucena, 2000). La distribución del pH del suelo a nivel global se muestra en la Figura 1.4. Una estimación de la concentración de Fe disponible en este tipo de suelo da niveles dos órdenes de magnitud más bajos que los óptimos necesarios para una nutrición adecuada de las plantas (Lindsay y Schwab, 1982; Guerinot y Yi, 1994; Guerinot, 2001).

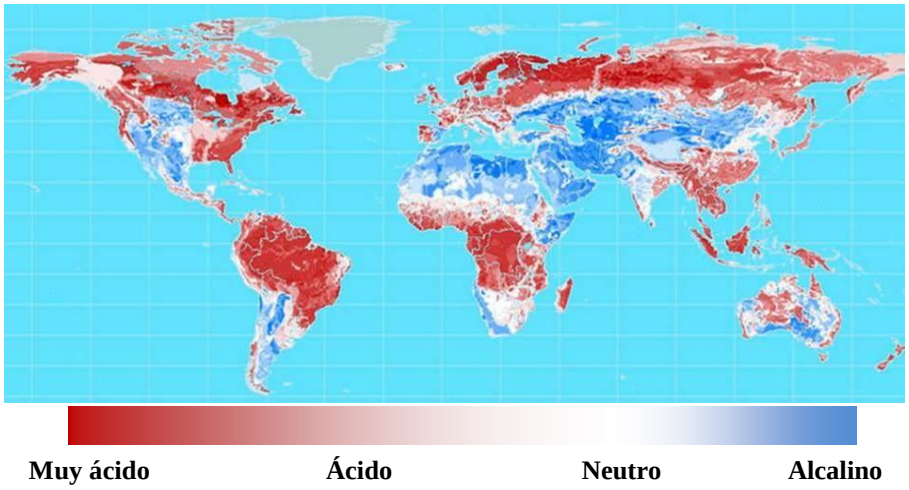

Figura 1.4. *Distribución global del pH del suelo. Figura adaptada del mapa incluido en el Atlas de la Biosfera (Center for Sustainability and the Global Environment, University of Wisconsin, Madison 1998).*

Como ya se ha dicho, aproximadamente el 30 % de la superficie cultivable presenta suelos calizos, en los que la deficiencia de Fe reduce la calidad y el rendimiento de los cultivos (Korcak, 1987; Hansen et al., 2006). Los suelos de toda la Cuenca Mediterránea, incluido el Valle Medio del Ebro, presentan este problema. Entre las plantaciones más afectadas por esta deficiencia se encuentran manzano (*Malus domestica*), peral (*Pyrus communis*), melocotonero (*Prunus persica*), ciruelo (*Prunus domestica*), cerezo (*Prunus avium*) o cítricos (*Citrus spp.*) (Sanz et al., 1992).

Deficiencia de Fe

La deficiencia de Fe se caracteriza por el amarilleamiento de la zona internerval de las hojas jóvenes (clorosis férrica), causada por disminuciones en la síntesis de clorofila y el desarrollo del cloroplasto que afectan tanto al crecimiento y desarrollo de la planta como a la calidad del fruto (Álvarez-Fernández et al., 2003). Si la situación de deficiencia se prolonga pueden presentarse lesiones necróticas y llegar a la muerte prematura de la planta (Sanz et al., 1992). En la Figura 1.5. se muestran los síntomas de la deficiencia de hierro en plantas de cultivo.

Junto con las características del suelo, la baja removilización del metal en los distintos tejidos es otra de las causas más frecuentes de deficiencia de Fe. Como se ha mencionado anteriormente, el 80 % del Fe adquirido por la raíz se transporta a las hojas. Estudios previos exponen que la concentración de Fe en las hojas cloróticas en árboles frutales puede ser elevada, en lo que se conoce como "paradoja de la clorosis férrica" (Morales et al., 1998; Römheld, 2000), lo que demuestra la importancia de un correcto almacenaje que haga posible posteriormente su disponibilidad (Mengel y Geurtzen, 1986). Estos datos reflejan la necesidad de una regulación fina no sólo de la adquisición del metal, sino también de su transporte y distribución entre los diferentes órganos y compartimentos celulares, a fin de evitar su acumulación, manteniendo al mismo tiempo un suministro adecuado.

Figura 1.5. *Cultivo de soja crecido en condiciones de suficiencia de Fe y afectado por la deficiencia de Fe; imagen tomada de "Agriculture Trends", 2017 (https://www.ag.ndsu.edu).*

Respuestas de la planta ante la deficiencia de Fe

Ante una escasez de Fe la planta desarrolla cambios morfológicos encaminados a aumentar la superficie de contacto entre la raíz y el suelo. La raíz primaria disminuye y aumenta el número de raíces laterales que presentan un engrosamiento de las puntas apicales y, en algunas especies, un amarilleamiento de las mismas (Römheld y Marschner, 1981; Moog et al., 1995; López-Millán et al., 2000b).

Junto con los cambios morfológicos se desarrollan cambios fisiológicos encaminados a mejorar la adquisición del metal por la raíz. Las plantas de Estrategia I aumentan la actividad de la reductasa férrica y la ATPasa, así como la expresión del transportador IRT y la exudación de compuestos de bajo peso molecular, como carboxilatos, fenoles y flavinas, a la rizosfera, mientras que las plantas de Estrategia II incrementan los mecanismos de síntesis y exudación de sideróforos así como la expresión del transportador Fe^{3+}-FS (Murata et al., 2006). Además, la planta sufre una reorganización de su metabolismo con el fin de mantener las necesidades energéticas y de poder reductor demandadas por el incremento en los mecanismos de adquisición del metal. La baja especificidad de ciertos transportadores involucrados en la adquisición de Fe, como los pertenecientes a la familia IRT o NRAMP, hace que la deficiencia

de este metal también afecte a la homeostasis de otros cationes divalentes, como el caso de Mn que se comentará posteriormente.

Los cambios a nivel bioquímico más consistentes entre especies se producen en el metabolismo del carbono (López-Millán et al., 2013). La deficiencia de Fe provoca un aumento en la fijación anaplerótica de carbono a nivel radicular por medio de la actuación combinada de la enzima fosfoenolpiruvato carboxilasa (PEPC) y determinadas enzimas del ciclo de los ácidos tricarboxílicos, como malato deshidrogenasa y citrato sintasa (López-Millán et al., 2000b). Parte de este carbono fijado en la raíz es capaz de actuar como sustrato para la obtención de poder reductor y ATP a fin de sostener la demanda producida por la inducción de las enzimas reductasa férrica y ATPasa, y otra parte se transporta a la parte aérea para suplir la disminución de fijación fotosintética de C (López-Millán et al., 2000b; Zochi, 2006).

La deficiencia de Fe también altera el metabolismo del nitrógeno (N), ya que causa una recirculación del N proteico cuyo fin es paliar el descenso en la asimilación de N provocado por la inactivación de la nitrito reductasa, que requiere Fe para su correcto funcionamiento (Borlotti et al., 2012). Estos cambios en los metabolismos de C y N, así como en proteínas involucradas en el estrés oxidativo, han sido descritos de forma generalizada en varios sistemas vegetales y se presuponen independientes de la especie vegetal (López-Millán et al., 2013). Sin embargo, otras rutas metabólicas presentan cambios cuando la planta se encuentra ante una deficiencia del metal, siendo muchas de estas respuestas específicas para cada especie, dependiendo también de las condiciones de cultivo y el grado de deficiencia. Un ejemplo claro de esta diversidad de respuestas es el incremento en la exudación de carboxilatos, flavinas y compuestos fenólicos (Cesco et al., 2010; Mimmo et al., 2014). Compuestos fenólicos de tipo cumarina han sido descritos en *A. thaliana* como componentes esenciales en la adquisición de Fe cuando la planta crece en condiciones de escasez del metal (Rodríguez-Celma et al., 2013a; Fourcroy et al., 2014; Schmid et al., 2014; Sisó-Terraza et al., 2016a). Del mismo modo, *Medicago truncatula* o *Beta vulgaris* secretan derivados de riboflavina que actúan de forma similar ante situaciones de escasez de Fe (Rodríguez-Celma et al., 2011; Sisó-Terraza et al., 2016b).

Medidas correctoras de la deficiencia de Fe

Las medidas correctoras de esta deficiencia en cultivos suponen un gasto de millones de euros al año (Sanz et al., 1992; El Jendoubi et al., 2011). Entre los mecanismos de corrección de la clorosis férrica, una de las técnicas más utilizadas es la aplicación de Fe al suelo en forma de quelatos sintéticos. Este tratamiento conlleva un gasto económico importante, que se estima entre 200-400 € por hectárea en el caso de árboles frutales (Rombolà y Tagliavini, 2006). Además, la alta solubilidad de estos quelatos sintéticos de Fe facilita su lixiviación, lo que puede llegar a causar problemas medioambientales. Una alternativa a este tipo de técnicas es el

uso de la fertilización foliar (Fernández et al., 2009; Abadía et al., 2011; Rios et al., 2016). Sin embargo, la escasa reproducibilidad en los estudios de este tipo de aplicaciones, causada por factores ambientales, fisicoquímicos y relacionados con la planta, normalmente lleva a un uso limitado de esta técnica. La falta de conocimiento acerca del rendimiento de estas pulverizaciones restringe su uso, que a menudo se limita a una utilización como complemento de la aplicación de Fe al suelo.

Las prácticas agrícolas extensivas (uso de variedades de alto rendimiento, sistemas intensivos de riego y aumento en la fertilización) están causando una fuerte disminución de nutrientes en el suelo y acrecentando los problemas de deficiencia, que son cada vez más frecuentes, afectando actualmente a cultivos que antes no sufrían estas limitaciones como en el caso del olivo (Sánchez-Rodríguez et al., 2013). Un mayor conocimiento sobre los mecanismos de adquisición, transporte, acumulación y removilización del metal por parte de la planta cada vez resulta más importante, ya que el desarrollo de técnicas más respetuosas con el medio ambiente que corrijan esta deficiencia comienza con la comprensión de estos procesos en la planta.

1.3. El Mn en las plantas

La importancia del Mn como micronutriente esencial para las plantas fue demostrada a principios del siglo XX (McHargue, 1922). El Mn desempeña funciones esenciales en la fotosíntesis al formar parte del complejo oxigénico del fotosistema II, en la síntesis de proteínas, lípidos, ligninas o carbohidratos, así como en la activación de hormonas (Burnell et al., 1988; Schmidt et al., 2016). Además, el Mn tiene un papel crítico en los procesos de división celular y elongación de las puntas de la raíz. Este microelemento presenta un papel tanto estructural, p. ej. en el caso de la concavalina A, como enzimático, formando parte de enzimas tan importantes como superóxido dismutasa (Mn-SOD), catalasa, oxalato oxidasa, RNA polimerasa, enzima málico, isocitrato deshidrogenasa o PEPC, entre otras (Broadley et al., 2012; Socha y Guerinot, 2014). La planta necesita cantidades relativamente pequeñas de Mn (20-40 mg Mn kg^{-1} de peso seco; Marschner et al., 2012) y su homeostasis es de vital importancia, ya que tiene la capacidad de reemplazar al Mg^{2+} en muchas reacciones químicas. El Mn adquirido por la raíz es transportado por el sistema vascular de la planta y se acumula principalmente en los tejidos de almacenamiento de las hojas más viejas, así como en los tejidos del peciolo (Gilbert, 1957; Masui et al., 1980).

1.3.1. Adquisición de Mn por la raíz

El Mn es el duodécimo elemento más abundante en la corteza terrestre, el segundo metal de transición más frecuente en la misma después del Fe, y se encuentra distribuido en una gran

variedad de especies químicas, en las que presenta estados de oxidación de 1^+ a 7^+, siendo la forma 2^+ la más frecuente en la naturaleza. Su solubilidad, al igual que en el caso del Fe, depende del pH y de las condiciones redox del suelo (Hernández-Soriano et al., 2012; Marschner, 2012), de forma que el Mn disponible en el suelo presenta un amplio rango de concentración que se sitúa entre 20 y 3.000 mg kg^{-1} (Rengel, 2015). Además de la cantidad asociada a la composición mineral del propio suelo, el Mn, igual que el resto de los metales pesados, puede llegar al suelo tanto por vía aérea (aerosoles, partículas minerales, polvos suspendidos y transportados por el aire...) como terrestre (fertilizantes, plaguicidas, residuos sólidos…), y se pierde por la absorción por las plantas o por fenómenos de lixiviación o erosión. Los numerosos factores que influyen en las características del suelo y por tanto en la disponibilidad de Mn, así como la gran variabilidad entre los valores de deficiencia y toxicidad en función de la especie vegetal, implican la necesidad de estrategias de regulación fina que permitan la homeostasis de Mn en la planta. En suelos ricos en Mn se ha encontrado que las plantas pueden contener cantidades del metal entre 30-500 mg Mn kg^{-1} de peso seco, una cantidad a menudo superior a la que en realidad requieren para su correcto metabolismo (20-40 mg Mn kg^{-1} de peso seco), lo que muestra la variabilidad de concentración del metal en función del suelo y la existencia de una escasa regulación en cuanto al proceso de absorción (Millaleo et al., 2010; Shao et al., 2017).

El Mn se toma por la planta en forma de Mn^{2+} (Marschner, 2012) y su adquisición se lleva a cabo a través de transportadores de la familia NRAMP localizados en la membrana plasmática de las células de la raíz. En *Arabidopsis* el responsable es AtNRAMP1, capaz de mediar también el transporte de Fe y Co (Caillatte et al., 2010). Se han descrito homólogos de este transportador tanto en arroz (OsNRAMP5) como en cebada (HvNRAMP5) (Sasaki et al., 2012; Wu et al., 2016). Los transportadores de las células radiculares encargados de la adquisición de micronutrientes con frecuencia no son específicos para un único elemento, por lo que es habitual que el Mn también se incorpore utilizando las rutas de asimilación de otros metales de características similares, teniendo lugar este proceso con mayor relevancia en situaciones fisiológicas concretas en las que estos transportadores se encuentran inducidos o cuando la concentración de Mn en el suelo es elevada (Grotz y Guerinot, 2006; Broadley et al., 2007). Por ejemplo, se ha descrito que el transportador de Fe de la membrana plasmática de raíz AtIRT1 también es capaz de transportar Mn (Connolly et al., 2002; Curie et al., 2000). De un modo similar, los canales permeables a Ca que se encuentran localizados en la membrana plasmática de las células radiculares pueden, aunque en menor medida, transportar también Mn^{2+} (White et al., 2002; Socha y Guerinot, 2014). Esta falta de especificidad, ya mencionada en el caso de Fe, lleva a que la alteración en uno de estos micronutrientes se traduzca en variaciones en las cantidades de otros elementos.

Por otro lado, al igual que en el caso de Fe, se han descrito mecanismos de exudación a la rizosfera de H^+, de compuestos reductores o de ligandos de unión a Mn que facilitan la posterior adquisición del metal por la raíz (Rengel, 2015). Estos compuestos reductores y quelantes son sustancias de bajo peso molecular exudadas por la raíz o por la microflora del suelo cuya naturaleza no está clara. En *Medicago sativa* se ha demostrado que la exudación de carboxilatos distintos a malonato y maleato se incrementa ante condiciones de deficiencia de Mn (Gherardi y Rengel, 2004), si bien a valores de pH elevados, donde es más factible la deficiencia de Mn, la quelación de Mn por estos ácidos no parece ser importante (Rengel, 2000). Además, el Mn en su forma divalente es capaz de unirse a las matrices homopoligalacturonadas de la planta (Irwin et al., 1988), lo que aumenta su concentración en el apoplasto de la raíz, y por lo tanto, en las inmediaciones de los sitios de captación de la membrana plasmática. Finalmente, la oxidación de la forma divalente del metal da lugar a MnO_2 que es capaz de permanecer en la superficie de la raíz. Se ha observado que los sitios de máxima oxidación del metal se encuentran a unos 5 mm del vértice de la raíz, en la epidermis, la endodermis y el xilema (Aoba et al., 1977).

1.3.2. Transporte intracelular e intercelular de Mn

La mayor parte del Mn absorbido por las células radiculares es translocado a la parte aérea de la planta donde es utilizado y almacenado (Gilbert, 1958). Sin embargo, una fracción del mismo puede almacenarse en la vacuola de las células de la raíz. Aunque se desconoce el transportador encargado de introducir Mn a la vacuola en las raíces, se ha descrito que AtZIP1, miembro de la familia ZIP (Zn-regulated transporter/Fe-regulated transporter-like Protein) y localizado en el tonoplasto, removiliza Mn de las vacuolas al citoplasma (Milner et al., 2013). Un segundo miembro de esta familia, AtZIP2, localizado en la membrana plasmática, media la absorción de Mn por las células del cilindro vascular (Milner et al., 2013).

Translocación del metal a xilema y floema

El Mn se transporta hacia las partes aéreas *via* xilema, aunque los mecanismos de carga y descarga en este fluido no se conocen con exactitud. Además de la participación de AtZIP2 en la descarga de Mn al parénquima xilemático desde la estela de la raíz (Milner et al., 2013), comentada anteriormente, tan sólo se han descrito dos transportadores más de Mn en arroz, OsYSL2 (Koike et al., 2004) y OsNRAMP3 (Yamaji et al., 2013), que participan en la descarga al xilema y floema, respectivamente.

En plantas gramináceas como arroz o cebada, los nodos juegan un papel importante en la distribución de los elementos minerales (Yamaji et al., 2013, 2014; Shao et al., 2017). El transportador OsNRAMP3, localizado en la membrana plasmática, se encuentra altamente expresado en los nodos y está presente, entre otras células, en las células de transferencia del

xilema y en los haces vasculares difusos del floema (DVBs). Aunque sus niveles de expresión no se ven afectados por la concentración externa de Mn, la proteína se degrada con rapidez ante niveles elevados de Mn en el interior celular, actuando como un interruptor en la distribución de Mn, que se activa o desactiva en respuesta a las fluctuaciones de las concentraciones de este elemento (Shao et al., 2017). Este hecho indica una regulación post-traduccional del transporte de Mn una vez ha sido tomado por la raíz.

Por otro lado, aunque las proteínas YSL caracterizadas hasta el momento transportan principalmente complejos Fe^{2+}-NA, estudios en oocitos de *Xenopus laevis* muestran que la proteína OsYSL2 de arroz también es capaz de transportar complejos Mn^{2+}-NA (Koike et al., 2004). OsYSL2 se encuentra involucrado en el movimiento lateral de los complejos de Mn^{2+}-NA a través del floema y su carga a las semillas en desarrollo (Koike et al., 2004). Como se ha comentado anteriormente, la inducción de la expresión de OsYSL2 en las células del cilindro vascular en condiciones de deficiencia de Fe ha permitido establecer su papel en el transporte del Fe *via* floema, aunque no se observa un aumento en su expresión ante una escasez de Mn (Koike et al., 2004). Estudios fisiológicos llevados a cabo en plantas dicotiledóneas sugieren que la NA es necesaria en la redistribución de Fe, Zn, y Mn a través del fluido floemático (Stephan et al., 1994), y este hecho, junto con la presencia de transportadores del complejo metal-NA en arroz y su expresión en las células del floema, refuerza la hipótesis de una participación de dicho compuesto en la descarga a floema de Fe y Mn.

A pesar de que no hay evidencias hasta el momento en el reino vegetal, ciertas especies de carácter peptídico podrían encontrarse involucradas en el transporte de Mn *vía* xilema. Esta hipótesis está basada en la existencia de metalo-chaperonas en otros organismos que intervienen en el movimiento intercelular de metales esenciales a los compartimentos correspondientes, procurando una correcta localización y evitando la acumulación de los mismos (Mira et al., 2001). Así, el Mn se ha encontrado asociado a péptidos de bajo peso molecular en el floema de *Ricinus communis*, sugiriendo una posible función de estos péptidos en el transporte de Mn en fluidos vegetales (van Goor y Wiersma, 1976). La redistribución del Mn en el floema parece depender de la especie y del estado de desarrollo de la misma (Herren y Feller, 1994) presentando una movilidad más elevada en su transporte a las semillas que en su translocación hacia la raíz (Nable y Loneragan, 1984; Loneragan, 1988).

Localización, almacenamiento y transporte intracelular

Vacuola

A nivel celular, el Mn se almacena principalmente en la vacuola, aunque también puede encontrarse en cloroplasto, mitocondria y aparato de Golgi (Pittman, 2005). Los responsables del secuestro del Mn en el interior de la vacuola son miembros de varias familias de

transportadores entre las que se encuentran CAX (CAtion eXchanger), CCX (Calcium Cation eXchanger), CDF (Cation Diffusion Facilitator) y VIT.

Los miembros de la familia CAX fueron descritos originalmente como transportadores de Ca^{2+}, aunque posteriormente se ha demostrado la capacidad de algunos de sus miembros para transportar Mn. Sin embargo, muestran una baja afinidad por este metal y, en general, parece que presentan un papel activo sólo cuando las concentraciones de Mn son elevadas, interviniendo de este modo en los mecanismos de detoxificación del metal (Shigaki et al., 2003; Pittman, 2005; Socha y Guerinot, 2014). En *Arabidopsis*, AtCAX2 se encuentra expresado en todos los tejidos, aunque con niveles de expresión bajos y que no responden a los cambios en la disponibilidad de Mn (Hirschi et al., 2000). A pesar de que los mutantes *Atcax2* acumulan niveles de Mn en vacuola inferiores al genotipo silvestre (Pittman et al., 2004), los mutantes de deleción de este transportador no se encuentran altamente afectados, sugiriendo la presencia de otros transportadores vacuolares que compensarían la ausencia de AtCAX2. Entre los candidatos se encuentran AtCAX4 y AtCAX5, que del mismo modo que AtCAX2, se localizan en la membrana vacuolar de todos los tejidos con una baja expresión constitutiva (Cheng et al., 2002; Edmond et al., 2009). La expresión de AtCAX5 es predominante en tallo y raíz, mientras que AtCAX4 se encuentra principalmente en las células radiculares, presentando un papel crucial en el crecimiento de la raíz bajo condiciones de estrés de metales pesados como la toxicidad de Mn^{2+} (Edmond et al., 2009; Mei et al., 2009). En el caso de estos dos transportadores, los niveles de RNA sí que se ven incrementados ante un exceso de Mn^{2+} (Cheng et al., 2002; Edmond et al., 2009; Mei et al., 2009), aumentando así la tolerancia de la planta al metal. Otros miembros de la familia de proteínas CAX también han sido descritos como transportadores de Mn en especies como arroz (OsCAX1a y OsCAX3) (Kamiya y Maeshima, 2004; Kamiya et al., 2005), cebada (HvCAX2) o tomate (LeCAX2) (Edmond et al., 2009).

Junto con las proteínas CAX, los transportadores CCX, que forman parte de la superfamilia de transportadores CaCA (Ca^{2+}/catión antiporters), han sido descritos como transportadores de Mn a la vacuola. Concentraciones elevadas de Mn inducen la expresión de AtCCX3 en raíces y flores de *Arabidopsis* (Morris et al., 2008), aunque, del mismo modo que ocurre con los transportadores CAX, los mutantes de este transportador no presentan grandes alteraciones fenotípicas debido a la diversidad de transportadores del metal en la membrana vacuolar.

Además de las proteínas CAX y CCX, miembros de la familia CDF presentan una expresión dependiente de la concentración de Mn y la especie. En *Arabidopsis*, un transportador perteneciente a esta familia, AtMTP8, secuestra el exceso de Mn en compartimentos prevacuolares o de tipo Golgi (Delhaize et al., 2007; Peiter et al., 2007). Por otro lado, su homólogo en arroz se encuentra expresado en el tonoplasto de células de tejidos en desarrollo (OsMTP8.1) y su homólogo en pepino (CsMTP8) ha sido localizado en el tonoplasto de células radiculares, mostrando funciones

similares pero con variaciones a nivel de expresión en función de la especie. Se ha descrito que su expresión aumenta tanto en condiciones de exceso de Mn como de deficiencia de Fe (Chen et al., 2013; Migocka et al., 2014; Eroglu et al., 2016; Shao et al., 2017).

Finalmente, algunos transportadores de Mn en plantas han sido descritos por homología con otros transportadores caracterizados en sistemas heterólogos como la levadura. Este es el caso de AtVIT1 de *Arabidopsis*, ortólogo de CCC1 (Ca^{2+}-sensitive Cross Complementer 1) que transporta Fe y Mn al interior de la vacuola en levadura (Li et al., 2001). Estudios de expresión de AtVIT1 en el mutante *ccc1* mostraron evidencias de acumulación de Mn en la vacuola en este organismo (Kim et al., 2006). Sus ortólogos funcionales en arroz (OsVIT1 y OsVIT2) están localizados en la vacuola y transportan Mn, Fe y Zn en levadura, aunque estudios fisiológicos en planta sugieren un papel activo tan sólo en el transporte de Fe y Zn (Zhang et al., 2012), por lo que el transporte de Mn mediado por AtVIT1 en *Arabidopsis* requiere estudios adicionales. El esquema del transporte de Mn en la célula se muestra en la Figura 1.6.

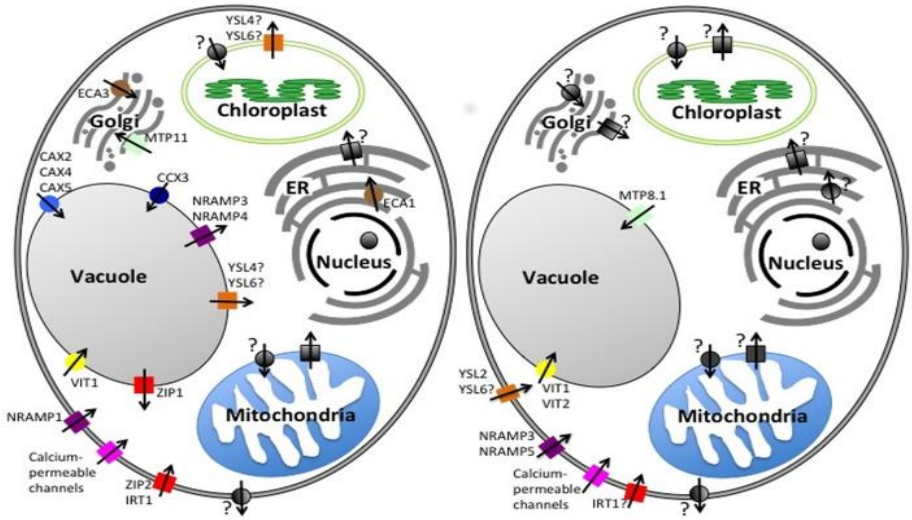

Figura 1.6. *Localización subcelular de los transportadores de Mn en plantas de Estrategia I (Arabidopsis thaliana; A) y Estrategia II (Oryza sativa; B). Los transportadores representados mediante un rectángulo corresponden a la importación desde el citosol, mientras que los transportadores representados mediante círculos describen vías de exportación al citosol. (Imagen tomada de Socha y Guerinot, 2014).*

Por otro lado, los transportadores que median la exportación de Mn desde el interior de la vacuola para ser redistribuido en función de las necesidades de la planta son menos conocidos. Hasta el momento se han descrito tres proteínas implicadas en este transporte, AtNRAMP3, AtNRAMP 4 y AtZIP1 (Fetch-Christoffers et al., 2003; Milner et al., 2013; Thomine et al., 2003). AtNRAMP3 y AtNRAMP4, situados en el tonoplasto en *Arabidopsis*, son los responsables del transporte de Fe y Mn desde el interior vacuolar a las células del mesófilo en las hojas de las plantas adultas (Lanquar et al., 2010). Estudios utilizando el doble mutante *nramp3nramp4* mostraron un fuerte efecto de la mutación en el PSII en condiciones de deficiencia de Mn; sin embargo, la actividad de la MnSOD mitocondrial no se vio afectada en

estas condiciones. Estos resultados sugieren un importante papel de los reservorios de Mn en vacuola en el suministro de este metal al cloroplasto en condiciones de deficiencia de Mn y que este suministro estaría mediado por los transportadores AtNRAMP3 y 4 (Lanquar et al., 2010). Del mismo modo, AtZIP1, localizado en el tonoplasto de las células radiculares incrementa sus niveles de expresión en situaciones de deficiencia de Mn y se ha sugerido que pueda desempeñar un papel importante en la reubicación del Mn de la vacuola al citoplasma en raíces, pudiendo contribuir al movimiento radial de este elemento en el parénquima xilemático (Milner et al., 2013).

Otros compartimentos intracelulares

Al contrario que para el Fe, la información disponible sobre las proteínas implicadas en el transporte de Mn a las diferentes localizaciones subcelulares es limitada y transportadores involucrados en el transporte de este metal a compartimentos tan importantes como el cloroplasto o la mitocondria todavía no se conocen. Se ha sugerido que dos de los 18 genes putativos de YSL descritos en arroz pudieran estar implicados en la homeostasis de Mn (OsYSL2 y OsYSL6). Mientras que OsYSL2, como se ha comentado anteriormente, participaría en la descarga de Mn al floema, OsYSL6 sería necesario para la desintoxicación de este metal cuando se encuentra en exceso (Sasaki et al., 2011). Estudios de localización intracelular de OsYSL6 usando la proteína de fusión con GFP (Green Fluorescent Protein) no han tenido resultados concluyentes; sin embargo el éxito obtenido en estudios de complementación realizados en el mutante de levadura *smf1* (que carece del transportador de Mn) sugieren que OsYSL6 se encontraría localizado en la membrana plasmática y presentaría la capacidad de transportar el complejo Mn^{2+}-NA. Si bien cuando se utilizan sistemas heterólogos para estudios de transporte debe tenerse siempre presente que el hecho de que una proteína muestre capacidad de transportar un metal no implica que esta actividad tenga relevancia fisiológica en la planta (Pittman, 2005), el hecho de que las plantas que carecen de este transportador presenten síntomas de toxicidad, acumulándose el exceso de Mn en el apoplasto de dichos tejidos, parece reforzar la hipótesis de su localización en la membrana plasmática (Socha y Guerinot, 2014). Puesto que cuando el Mn^{2+} se acumula en el apoplasto se oxida rápidamente a Mn^{3+}, capaz de oxidar proteínas y lípidos (Fecht-Christoffers et al., 2003), se ha sugerido que cuando las plantas estén expuestas a niveles altos de Mn, OsYSL6 sería capaz de transportar el Mn desde el apoplasto al simplasto, donde se almacenaría de forma adecuada evitando estos efectos adversos (Socha y Gueinot, 2014).

Hasta el momento, además de los transportadores descritos en la membrana vacuolar, dos miembros de la familia de ATPasas tipo P, AtECA1 y AtECA3, se han descrito como transportadores implicados en el secuestro de Mn en el retículo endoplasmático y en el aparato de Golgi, respectivamente, mientras que AtMTP11, también localizado en el aparato de Golgi,

se encontraría involucrado en la exocitosis de Mn (Peiter et al., 2007). AtECA1 se considera que tiene un papel importante en el control de la toxicidad por Mn en la célula (Wu et al., 2002), mientras que AtECA3 y AtMTP11 participan en la detoxificación del Mn (Peiter et al., 2007; Li et al., 2008). Los homólogos en cebada (HvMTP8.1 y HvMTP8.2), también localizados en el aparato de Golgi, parecen presentar el mismo papel esencial en la carga del metal al orgánulo y su liberación mediante vesículas de secreción (Pedas et al., 2014). Por otro lado, ensayos de complementación en mutantes de levadura deficientes en los transportadores de Fe y Mn han destacado el importante papel de NRAMP2 en el transporte intracelular de Mn, aunque no de Fe (Curie et al., 2000; Alejandro et al., 2017). La pérdida parcial de este transportador se traduciría en una mayor sensibilidad a la deficiencia de Mn debida a una distribución defectuosa del metal. Se ha hipotetizado que NRAMP2 participa activamente en la descarga de Mn desde el aparato de Golgi a la vacuola a través del citosol (Salomé, 2017).

Finalmente, en el cloroplasto de *Arabidopsis* se ha descrito AtPAM71, que se presupone como necesaria para la incorporación del metal a los tilacoides, permitiendo asegurar de este modo el rendimiento óptimo del PSII. Estas suposiciones están basadas en estudios realizados en el mutante de deleción *pam71* de *Arabidopsis*, el cual mostró menos Mn unido al PSII causando una disminución de la actividad fotosintética. Esta actividad se restauraba al suplementar el mutante con Mn^{2+}, indicando que PAM71 participa en la absorción de Mn^{2+} en los tilacoides y garantiza el correcto funcionamiento del PSII (Schneider et al., 2016).

1.3.3. Estrés por Mn

La presencia de formas de Mn asimilables para las plantas depende de las características del suelo. Al contrario que en el caso del Fe, el Mn disponible para las plantas varía entre concentraciones que resultan deficientes y concentraciones lo suficientemente elevadas como para provocar su toxicidad. Los síntomas causados por la deficiencia y la toxicidad de Mn se muestran en la Figura 1.7.

Figura 1.7. *Síntomas de la deficiencia de Mn en hoja de vid (izquierda) y de la toxicidad de Mn en hoja de batata (derecha) (Imágenes tomadas de http://www.omafra.gov.on.ca y https://keys.lucidcentral.org, respectivamente).*

Deficiencia de Mn:

Como se ha comentado anteriormente, la disponibilidad de Mn para la planta depende de su estado de oxidación, siendo Mn^{2+} la forma en la que la planta es capaz de adquirirlo. La disponibilidad de Mn en la rizosfera está controlada por el efecto combinado de las propiedades del suelo, las características de la planta y la interacción de la raíz de la planta con los microorganismos y el entorno (Bowen y Rovira, 1992). La acidificación de la rizosfera juega un papel importante en la movilización del Mn, de forma que la deficiencia de Mn se presenta principalmente en suelos alcalinos, situación que afecta al 30 % de los suelos cultivables. Ambas alteraciones nutricionales (Fe y Mn) suponen un problema agronómico de gran importancia en toda el área mediterránea. Asimismo, la deficiencia de Mn es prevalente en suelos arenosos en el norte de Europa y Reino Unido (Hebbern et al., 2005; Husted et al., 2009; George et al., 2014), y en los últimos años se ha extendido al norte de USA y Canadá, y al sur de Australia (Pallotta et al., 2000).

Las plantas presentan síntomas de deficiencia de Mn cuando la concentración del metal en las hojas jóvenes es inferior a los 10-20 mg Mn kg^{-1} peso seco (Reuter et al., 1997). El fenotipo deficiente muestra una inhibición del crecimiento y un descenso de la biomasa de la planta, junto con una clorosis intervenal de las hojas (más acusada en las hojas más jóvenes) en las que las nervaduras permanecen de coloración verde, alcanzando la necrosis foliar, si la deficiencia es prolongada, debida a la acumulación de especies reactivas de oxígeno dentro de los cloroplastos (Hannam y Ohki, 1988). Además, la deficiencia de Mn provoca deformación de las semillas (Walton, 1978), reducción de la fertilidad del polen y del rendimiento del grano (Sharma et al., 1991). La acumulación de Mn en las plantas sigue normalmente un gradiente que presenta los valores más elevados en la raíz y disminuye conforme se avanza en tallo, hoja y por último semilla (Rogers et al., 2008). La estratificación de los síntomas se debe a la escasa movilidad del Mn en el floema que impide la removilización del metal desde los tejidos de almacenamiento a las hojas más jóvenes.

Respuesta de la planta ante la deficiencia de Mn

Los mecanismos de respuesta a nivel radicular presentan diferencias en función de la especie. El transportador involucrado en la absorción de Mn en *Arabidopsis*, AtNRAMP1, sigue la misma tendencia de expresión que en condiciones de deficiencia de otros nutrientes y se encuentra moderadamente inducido ante una deficiencia de Mn, lo que no sucede con sus homólogos en arroz (OsNRAMP5) o cebada (HvNRAMP5) (Curie et al., 2000; Cailliate et al., 2010; Vatansever et al., 2016; Wu et al., 2016; Shao et al., 2017). Las diferencias probablemente se relacionen con una adaptación debida al crecimiento en condiciones de

inundación en las que se cultiva el arroz. Tendencias de expresión opuestas se han encontrado también en los miembros de la familia ZIP (Zn-regulated transporter/Fe-regulated transporter-like Protein). Si bien estos transportadores no ven afectada su expresión ante la deficiencia de Mn en *Arabidopsis* (Milner et al., 2013), su homólogo en cebada (HvIRT1) sí que presenta inducción en estas condiciones (Pedas et al., 2008). Las diferencias entre especies pueden ser atribuidas a cambios en la estructura de la raíz, capacidad de absorción del metal o condiciones de crecimiento de la especie.

A nivel metabólico, unas 35 enzimas diferentes necesitan Mn para llevar a cabo correctamente su función. Entre ellas, la fenilalanina amonio-liasa es clave en el metabolismo de fenólicos, y cataliza la desaminación de la fenilalanina a ácido cinámico. En consecuencia, la deficiencia de Mn se traduce en una disminución de la producción de lignina y compuestos fenólicos (Brown et al., 1984; Marschner, 2012; Salvador et al., 2013; Barros et al., 2015), lo que podría conllevar un aumento de la susceptibilidad de las raíces a la infección por patógenos (Rengel et al., 1993). Si la deficiencia es prolongada estos cambios metabólicos llevan a una reducción de la longitud de las raíces (Neumann y Steward, 1968), seguida de la reducción del crecimiento y desarrollo de la planta (Kriedemann et al., 1985; Gong et al., 2010). Estos síntomas pueden llevar a un uso excesivo, y en ocasiones innecesario, de pesticidas. En algunas especies como la cebada, la degradación de la capa cérea cuticular provoca una mayor transpiración de la planta, haciendo que sea menos tolerante a la sequía y a las fluctuaciones en la disponibilidad de agua en el suelo (Morales y Warren, 2012). La deficiencia de Mn también causa alteraciones en enzimas del ciclo de Krebs (Morgan et al., 2008), disminuye la concentración de los glicolípidos de los tilacoides y los ácidos grasos poliinsaturados (Constantopoulos, 1970) e inhibe la fotosíntesis, resultando en clorosis foliar. En la mayoría de estas enzimas la función del Mn puede ser reemplazada por otro metal divalente como por ejemplo el Mg, cuya concentración en las células es entre 50-100 veces mayor. Sin embargo, algunas enzimas involucradas en procesos redox como la SOD requieren específicamente de Mn como cofactor (Allen et al., 2007).

Medidas correctoras de la deficiencia de Mn

Para paliar la deficiencia de Mn pueden añadirse al suelo o vía foliar fertilizantes que contienen sulfato de Mn (Carrasco-Gil et al., 2016). Además de resultar una práctica costosa, el Mn añadido puede ser fijado en el suelo, lo que impide que esté disponible para la planta. Estudios combinando la aplicación del fertilizante a suelo y foliar han mostrado mayores rendimientos en el grano y una disminución de los síntomas ocasionados por la deficiencia del metal (Reuter et al., 1973; Heckman et al., 2008). Sin embargo, una alternativa más rentable y respetuosa con el medio ambiente es el uso de plantas capaces de crecer en suelos con bajas

concentraciones del metal. En los últimos años, se ha dedicado un gran esfuerzo a identificar las especies de cultivo que se consideran eficientes y pueden tolerar el crecimiento a bajos niveles de Mn, ya sea almacenándolo en mayor cantidad o presentando una mayor capacidad para su absorción (Pedas et al., 2008). Los mecanismos que hacen a una planta más eficiente no están bien definidos, por lo que, al igual que en el caso del Fe, el entendimiento de los mecanismos de absorción, transporte y acumulación del metal se hace indispensable.

Toxicidad de Mn

La cantidad de Mn presente en el suelo en formas libres divalentes es muy variable (entre 0,1 y 800 μM) y aumenta considerablemente conforme el pH disminuye (5,0) (Barber, 1995; Lynch y St. Clair, 2004; Watmough et al., 2007), de forma que en suelos con pH ácido puede incluso resultar tóxico para las plantas (Mukhopadhyay y Sharma, 1991). La exudación de H^+ y ácidos orgánicos al suelo puede disminuir el pH de los suelos alcalinos y así incrementar la disponibilidad de este micronutriente (Marschner, 1987). El contenido de metales en el suelo varía en función de la composición del material original y de los procesos edafogenéticos, pero la actividad humana ha incrementado el contenido de estos metales en cantidades considerables, y la entrada de metales en el suelo ha aumentado mucho desde que comenzó la industrialización. Las actividades antropogénicas, como las actividades mineras y los residuos de incineración o de procesos industriales, han provocado el enriquecimiento en metales del medio ambiente, originándose una acumulación de 100 a 1.000 veces más alta en relación con su proporción natural en la corteza terrestre, con la excepción del Fe y el Hg (Wedepohl, 1991). Además de la industrialización, las prácticas agrícolas constituyen una importantísima fuente de metales en el suelo en muchas partes del mundo, especialmente en zonas de actividad intensa (Alloway, 1995).

A grandes rasgos, los síntomas físicos de la toxicidad de los metales en las plantas son a menudo similares a los generados por sus deficiencias (Di Toopi y Gabrielli, 1999; Socha y Guerinot, 2014), e incluyen disminuciones en la biomasa y crecimiento de la planta, manchas necróticas en las hojas y daños a nivel de raíz (Bona et al., 2007; Kieffer et al., 2008; 2009). Además, las plantas con niveles tóxicos de Mn presentan clorosis intervenal, deformación de las hojas jóvenes (Ducic y Polle, 2005), pérdida de la dominancia apical y formación de brotes auxiliares (Gangwar et al., 2011). Al contrario de lo que ocurre en la deficiencia de Mn, los valores considerados como tóxicos no están establecidos y varían en función de la especie, existiendo especies denominadas hiperacumuladoras que almacenan niveles muy elevados de Mn muy superiores a sus requerimientos fisiológicos (Shao et al., 2017). En general, las plantas son más resistentes a los incrementos en la concentración de micronutrientes que a las deficiencias. La sensibilidad de los cultivos ante un exceso de metales es muy variable, así

como la tendencia a acumularlos en partes que luego pasen al consumo animal o humano. Uno de los principales problemas de la acumulación de este tipo de metales en plantas es que pueden resultar una amenaza para la salud humana si pasan a formar parte de la cadena alimentaria (Islam et al., 2007; Fu et al., 2008). Las plantas constituyen una parte muy importante de la dieta humana, por lo que la posible contaminación de verduras, cereales o frutas con metales supone un alto riesgo para la calidad y seguridad de la alimentación (Muchuweti et al., 2006).

Respuesta de la planta ante la toxicidad de Mn

Ante la presencia de altas concentraciones de Fe y Mn en el suelo, las plantas generalmente acumulan niveles superiores de Mn que de Fe, de ahí que la toxicidad por Fe sea menos frecuente. Esto sucede porque el oxígeno liberado de la superficie de la raíz es suficiente para oxidar Fe^{2+} pero no Mn^{2+}, ya que la oxidación de Mn^{2+} requiere un potencial redox superior (Kirk, 2003; Mansfeldt, 2004). A pesar de los avances realizados durante las últimas décadas, la mayor parte de la información disponible acerca de la toxicidad de Mn proviene de estudios realizados en plantas hiperacumuladoras, como son *Phytolacca americana* o *Gossia bidwillii*, siendo limitado el conocimiento de la fisiología de especies de interés agronómico sometidas a este estrés.

Los síntomas de toxicidad de Mn conllevan depósitos de coloración marrón en las hojas maduras (Ducic y Polle, 2005), resultado de la activación de peroxidasas que llevan a la acumulación de compuestos fenólicos oxidados y óxidos de Mn en el fluido apoplástico (Wissemeier y Horst, 1987; Fecht-Christoffers et al., 2003; Führs et al., 2009). Se reducen los niveles de carotenoides y clorofila (Gangwar et al., 2011), se produce una inhibición de la fotosíntesis (Sinha et al., 2002) y aumenta la producción de ROS (Millaleo et al., 2010). Además, el exceso de Mn puede generar deficiencias en otros metales como Ca, Mg, Fe y Zn debido a la inespecificidad de los transportadores de metales (Horst, 1988; De Varennes et al., 2001), así como causar la inactivación de enzimas debido a la unión de Mn a determinados grupos funcionales, al desplazamiento de otros cationes que actúan como cofactores del centro activo y/o a cambios estructurales provocados por el metal que interrumpen el funcionamiento normal de las mismas (Haydon y Cobbett, 2007).

Las plantas crecidas en condiciones de toxicidad de Mn aumentan la expresión de transportadores implicados en el secuestro de Mn en la vacuola o el apoplasto y activan los mecanismos de movilización del metal al interior del retículo endoplasmático y el aparato de Golgi (Wu et al., 2002; Delhaize et al., 2003; Socha y Guerinot, 2014). Como se ha descrito anteriormente, AtECA1 parece tener un papel importante en situaciones de toxicidad de Mn (Wu et al., 2002) y AtECA3 y AtMTP11 participan en los procesos de detoxificación mediante exocitosis *via* aparato de Golgi (Peiter et al., 2007; Li et al., 2008). Por otro lado,

transportadores localizados en la membrana plasmática como OsNRAMP3, reducen rápidamente sus niveles para evitar la absorción en exceso del metal en plantas de arroz (Shao et al., 2017). Sin embargo, como se ha comentado previamente, el incremento o descenso de los niveles de los transportadores de Mn varía significativamente en función de la especie, lo que confiere a las plantas diferentes mecanismos de respuesta ante estas condiciones de estrés. Finalmente, la quelación de los iones de Mn^{2+} libre con ácidos orgánicos los convierte en formas inactivas, aumentando la tolerancia de la planta al metal (Pittman, 2005; Fernando et al., 2010). La tendencia a la quelación y compartimentación del Mn, así como la reducción de la cantidad de Mn translocado desde la raíz a las partes aéreas (Zhou et al., 2013; You et al., 2014; Chen et al., 2016), resultan mecanismos indispensables de protección que reducen el exceso del metal en las áreas metabólicamente activas de la planta, incrementando su tolerancia ante situaciones de estrés (Memon et al., 1981; Williams y Pittman, 2010; Xu et al., 2015).

Medidas correctoras de la toxicidad de Mn

En respuesta a este problema, las investigaciones en esta área han centrado sus esfuerzos en entender la naturaleza de los mecanismos de adquisición, tolerancia y toxicidad de Mn en las plantas. Algunos de los avances más importantes alcanzados han sido el desarrollo de variedades tolerantes capaces de crecer en suelos contaminados y el descubrimiento de nuevas variedades que pueden extraer los metales del suelo, con el objetivo de que este vuelva a ser útil para la agricultura, una práctica que se conoce como fitorremediación (Salt et al., 1995; Pulford y Watson, 2003; Xue et al., 2004; Min et al., 2007).

1.4. La proteómica como herramienta de estudio

El desarrollo de las técnicas denominadas "-ómicas" ha permitido aumentar el conocimiento acerca del efecto que ocasionan determinados estreses bióticos y abióticos sobre los sistemas vegetales, llevando a cabo el análisis de un gran volumen de datos en un tiempo reducido. El término "-ómicas" hace referencia a disciplinas como la genómica, la proteómica, la transcriptómica y la metabolómica. A su vez, estas tres últimas pueden encontrarse agrupadas bajo la denominación de "genómica funcional" y surgen a raíz de la publicación de la secuencia completa del Proyecto Genoma Humano en 2004. El entendimiento de cómo las variantes genéticas regulan el fenotipo celular se conoce como "Post-Genómica" y plantea una visión global de los procesos biológicos, ya que estudia los productos de la expresión de los genes. El sufijo "-oma" tiene origen latino y significa "conjunto de". Es por tanto que la adición de este sufijo a diferentes estudios en biología cubre las nuevas aproximaciones masivas en las que se está enfocando la biología en la actualidad. La cantidad de información obtenida con estas técnicas requiere el uso de potentes técnicas estadísticas e informáticas que ayuden a interpretar

los datos obtenidos. Tanto la bioinformática como el uso de técnicas de análisis rápidas y automatizadas de alto rendimiento (high-throughput techniques) son imprescindibles en el desarrollo de cualquier ciencia "-ómica".

Inicialmente, los estudios "-ómicos" sobre nutrición vegetal se centraron en el uso de la transcriptómica para el estudio de los genes que se expresan en un momento dado. Tanto los proteomas como los transcriptomas son sistemas con mucha variabilidad, y los cambios a nivel transcripcional no necesitan estar correlacionados con cambios a nivel traduccional. El ratio mRNA/proteína puede variar considerablemente en función del nivel de transcripción, la estabilidad de la proteína, procesos post-transcripcionales (5'-capping, poli-adenilación, "splicing", transporte nuclear) y procesos post-traduccionales (ubiquitinaciones, glicosilaciones, fosforilaciones), entre otros. La proteómica es una disciplina relativamente reciente, ideada inicialmente como técnica complementaria a la genómica. De hecho, el término "proteómica" fue acuñado en 1997 por analogía con genómica; la palabra "proteoma" fue empleada por Wilkins en 1994 como abreviatura de "el complemento proteico del genoma (the PROTEin complement of the genOME)" (Wilkins, 1994). La consolidación definitiva de la espectrometría de masas (MS) como técnica aplicada al análisis de moléculas biológicas y el crecimiento exponencial en el número de entradas correspondientes a genes y/o proteínas en las bases de datos, combinados con el empleo de potentes métodos de fraccionamiento y separación de péptidos y proteínas como la electroforesis de poliacrilamida de dos dimensiones (2-DE PAGE) y la cromatografía líquida de alta resolución (High Performance Liquid Cromatography, HPLC), han permitido consolidar la proteómica, desde mediados de los años 90, como disciplina científica para el análisis y estudio masivo de proteínas. Las técnicas proteómicas descritas a lo largo de este apartado se resumen en la Tabla 1.1.

Tabla 1.1. *Tabla resumen de las técnicas, métodos de detección y software de análisis descritos en el apartado 1.4 de esta Tesis Doctoral.*

	Tipos	Método de cuantificación	Software de análisis
Técnicas clásicas	IEF-SDS-PAGE	Coomassie Tinción con plata Fluorocromos (DIGE)	PDQuest BioImage
Técinas avanzadas	ICAT SILAC	Marcadores isotópicos	MaxQuant, msInspect/AMT, SuperHirn, Census, OpenMS/TOPP, Progenesis LC-MS, SIEVE, Scaffold o Mascot Distiller
	iTRAQ	Marcadores isobáricos	
	Label-free shotgun proteomics	Correlación de areas/ conteo espectral	

1.4.1. Técnicas clásicas

Un estudio proteómico requiere una extracción y purificación del proteoma, incluyendo una etapa de fraccionamiento subcelular, en función del objeto de estudio, que disminuya la complejidad de la muestra (Cordwell et al., 2000). Las aproximaciones proteómicas clásicas llevan a cabo la separación de las proteínas presentes en la muestra mediante técnicas electroforéticas o de cromatografía líquida de intercambio iónico, exclusión por tamaño o afinidad y fase reversa. En esta Tesis Doctoral se ha elegido la electroforesis en dos dimensiones mediante el uso de geles de poliacrilamida como método clásico para la separación de proteínas en el estudio de los proteomas apoplasto de remolacha y de raíz de tomate (ver Capítulos 3.2 y 3.5).

La electroforesis bidimensional (2-DE) fue descrita por O`Farrell y Klose en 1975 y está basada en el uso de características físicas como la carga y la masa molecular (Klose, 1975). La combinación del isoelectroenfoque y la electroforesis en gel con dodecil sulfato de sodio (IEF-SDS-PAGE) permite que se separen muestras de proteínas complejas con una alta resolución. La focalización isoeléctrica (IEF) separa las proteínas según su punto isoeléctrico (pI) en una primera dimensión, mientras que la electroforesis en gel de poliacrilamida, en presencia de SDS como detergente aniónico (SDS-PAGE), separa las proteínas en función de su masa molecular en una segunda dimensión, dando lugar a proteínas aisladas en lo que se denominan "spots". Esta técnica permite llevar a cabo análisis tanto cuantitativos, basados en la intensidad de señal del "spot", como cualitativos, como son la identificación de isoformas proteicas o modificaciones post-traduccionales, ya que proporciona información del pI y la masa molecular de la proteína. El uso de geles de poliacrilamida para la separación de proteínas requiere de métodos de tinción para llevar a cabo su visualización, siendo los más rutinarios la tinción por Coomassie (Fakezas et al., 1963) y por plata (Switzer et al., 1979). Paquetes de software como PDQUEST de BioRad o BioImage están especializados en la detección de "spots", realización de análisis cuantitativos, comparación de geles y generación de imágenes virtuales que engloban la información recogida en varios geles individuales. Estos programas de análisis llevan a cabo el alineamiento de imágenes, la normalización, la eliminación del ruido y la cuantificación de los "spots" basándose en el volumen de los mismos, es decir, en la intensidad de señal de cada uno de los píxeles que componen la imagen. La intensidad de señal se expresa en unidades de densidad óptica, y mediante un modelado Gaussiano los "spots" se transforman en una representación tridimensional que permite su cuantificación relativa. Además, estos programas utilizan paquetes estadísticos multivariables, como el análisis de varianza, usando el tamaño e intensidad de los "spots" (Abdallah et al., 2012). El mayor inconveniente de la electroforesis bidimensional radica en la dificultad a la hora de visualizar proteínas minoritarias. Estudios previos demuestran que la resolución de esta técnica disminuye al aumentar la cantidad de

proteína aplicada (Fey y Larsen, 2001), lo que puede llevar a un enmascaramiento de las proteínas menos abundantes por aquellas que se encuentran en cantidades mayores.

El desarrollo de marcadores fluorescentes ha permitido aumentar el rango dinámico de la cuantificación y la reproducibilidad de las tinciones. Un ejemplo del uso de fluorocromos es la electroforesis diferencial DIGE ("Difference In-Gel Electrophoresis") que utiliza derivados de la cianina CyDye, similares a los utilizados para análisis de microarrays de cDNA diferencial, pero optimizados para 2-DE (Tonge et al., 2001). En esta técnica se marcan, mediante uniones covalentes, dos extractos proteicos diferentes con dos fluorocromos que tienen espectros de excitación y emisión distintos. Las muestras se mezclan y las proteínas de ambas se separan en un mismo gel 2-D. La diferencia en los espectros permite tanto una rápida cuantificación como la distinción entre proteínas presentes en cada uno de los extractos originales. Generalmente, se utiliza un tercer extracto marcado que sirve como estándar interno y permite la normalización. Esta técnica DIGE reduce el número de réplicas necesarias y mejora la reproducibilidad de resultados. La tinción DIGE ha sido utilizada en el estudio de estreses abióticos como la sequía en el roble o las bajas temperaturas en *Arabidopsis* (Li et al., 2011; Sergeant et al., 2011) y más recientemente, en el estudio del floema de plantas de melón en respuesta a la infección por virus (Serra-Soriano et al., 2015). Sin embargo, esta técnica ha sido menos aplicada a estudios con plantas debido al alto coste de los marcadores y del equipo necesario, así como a la limitación del análisis a dos o tres condiciones diferentes en el proteoma estudiado (Miller et al., 2006). En la Figura 1.8. se compara el esquema de flujo de trabajo utilizado en las técnicas de electroforesis bidimensional y DIGE.

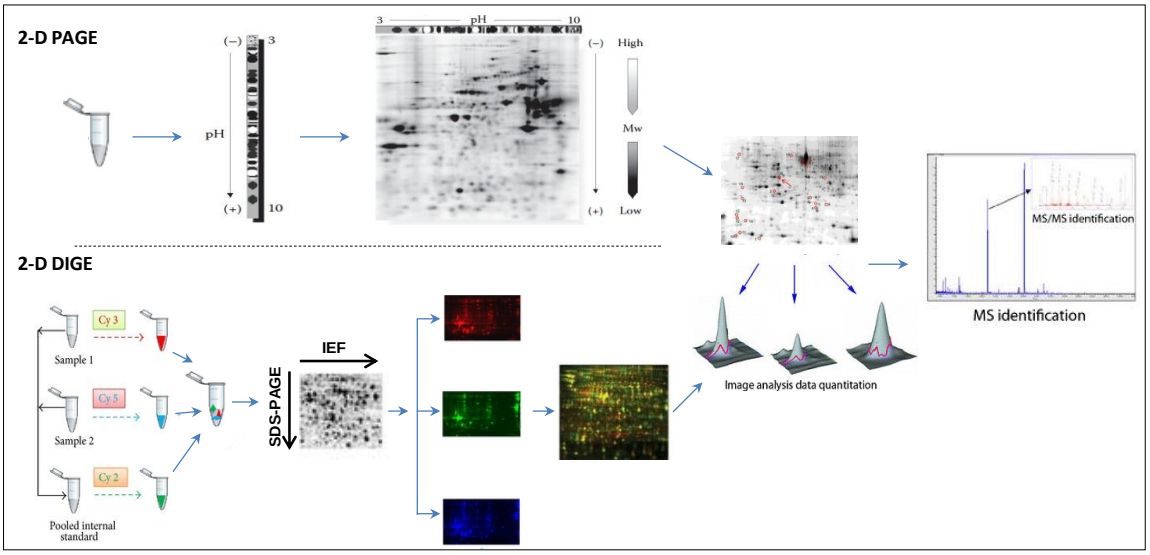

***Figura 1.8**. Flujo de trabajo en las técnicas de electroforesis bidimensional y DIGE.*

A pesar de los avances conseguidos en los últimos años, la separación de proteínas mediante el uso de geles de poliacrilamida presenta ciertas limitaciones. Por un lado, la

solubilización en la primera dimensión de la electroforesis bidimensional resulta un factor limitante a la hora de identificar proteínas hidrofóbicas, como es el caso de las proteínas de membrana. Este tipo de proteínas con carácter hidrofóbico resultan difíciles de solubilizar y por tanto, no es infrecuente que no sean detectadas mediante 2-DE. Por otro lado, proteínas con puntos isoeléctricos muy ácidos o básicos pueden ser difíciles de focalizar en esta primera dimensión, ya que su carga las desplaza a las zonas más externas del gel. Estas dificultades técnicas implican que las poblaciones proteicas caracterizadas por 2-DE estén generalmente sesgadas hacia moléculas más hidrofílicas, que son fácilmente solubilizables. Durante años, la electroforesis en dos dimensiones ha sido la metodología con mayor poder resolutivo utilizada para la identificación de proteínas en mezclas complejas. Actualmente, a pesar de las limitaciones comentadas anteriormente y del desarrollo tecnológico de las denominadas técnicas de proteómica avanzada, la electroforesis bidimensional sigue siendo una de las técnicas más utilizadas, ya que permite la detección de isoformas y modificaciones post-traduccionales con relativa facilidad.

1.4.2. Técnicas de proteómica avanzada

En las últimas décadas, el uso de instrumentos de HPLC conectados en línea con equipos de espectrometría de masas en tándem (MS/MS) se ha generalizado y se dispone de muchas combinaciones para la etapa de separación cromatográfica, encaminadas a enriquecer la muestra con aquellas proteínas menos abundantes o a obtener subproteomas más simples y fáciles de analizar. Además, el desarrollo de métodos de alta resolución también ha permitido el análisis de mezclas complejas de proteínas sin necesidad de una separación previa. En este caso, el conjunto de proteínas se digiere simultáneamente y la mezcla de péptidos obtenida se separa mediante métodos cromatográficos, siendo posible la combinación de dos o más tipos de cromatografía en casos de elevada complejidad o si el objeto de estudio lo requiere (separación multidimensional). Por tanto, las técnicas cromatográficas pueden aplicarse en el fraccionamiento tanto de mezclas de proteínas como de péptidos y generalmente incluyen columnas de cromatografía de fase reversa, exclusión molecular, intercambio iónico o afinidad (Righetti et al., 2005). Pese a la complejidad de la muestra, este nuevo procedimiento supone un avance en la identificación de muchas proteínas que no podían ser visualizadas en gel, como las proteínas poco abundantes en la muestra, debido a la utilización de equipos cada vez más sensibles, o aquellas de carácter hidrofóbico o de membrana, ya que los digeridos sí que resultan solubles (Washburn et al., 2001). Finalmente, este tipo de técnicas avanzadas conlleva una mayor automatización de los análisis que permite aumentar el número de muestras en comparación con las técnicas clásicas. Esta diversidad de combinaciones a la hora de simplificar la muestra ha llevado a que los espectrómetros de masas se hayan convertido en instrumentos

analíticos cada vez más atractivos para este tipo de estudios, debido en parte a los nuevos métodos de ionización más suaves, que permiten el análisis tanto de proteínas como de péptidos, y a las mejoras en precisión, resolución, sensibilidad y facilidad de uso. Estas nuevas tecnologías han extendido el uso de la espectrometría de masas a la caracterización de grandes macromoléculas intactas tales como proteínas, y en consecuencia han permitido el desarrollo de la proteómica como herramienta de uso habitual.

Una de las primeras combinaciones utilizadas de manera efectiva para catalogar péptidos en mezclas de proteínas totales ha sido el Mud-PIT (Multi-Dimensional Protein Identification Technology), usada en el estudio de proteomas de varios organismos como levadura o arroz (Washburn et al., 2001; Koller et al., 2002; Whitelegge, 2002). El Mud-PIT combina un microcapilar empaquetado con fase reversa (RP) y una cromatografía de intercambio catiónico (SCX) en línea con un espectrómetro de masas en tándem (Fournier et al., 2007), con lo que se pueden analizar mezclas complejas de péptidos, aunque su reproducibilidad no es suficiente para obtener información cuantitativa. Otra de las combinaciones más utilizadas es GeLC-RP-MS/MS, en la que las proteínas se separan en función de su tamaño en un gel monodimensional SDS-PAGE, el carril se corta en bandas que son digeridas y analizadas por RP-MS/MS (Schirle et al., 2003; Taylor et al., 2003; Rezaul et al., 2005).

La proteómica comparativa es una de las aplicaciones que más interés suscita, y para llevar a cabo análisis diferenciales con este tipo de técnicas se necesita obtener una cuantificación de las proteínas, ya sea de forma absoluta o relativa. El salto de la proteómica cualitativa (o descriptiva) a la proteómica cuantitativa ha venido determinada por una serie de desarrollos en los procesos de cuantificación, basados ya sea en el marcaje de proteínas o bien en la correlación de péptidos presentes en las distintas muestras.

Cuantificación mediante marcaje de proteínas o péptidos

En un primer momento, las técnicas de cuantificación se basaron en el marcaje (isotópico o isobárico) de las proteínas o péptidos. Entre las metodologías que utilizan un marcaje isotópico se encuentran las técnicas ICAT ("Isotope-Coded Affinity Tag"), desarrollada en las últimas década para mejorar las comparaciones cuantitativas en ausencia de 2-DE (Gygi et al., 1999) y SILAC ("Stable Isotope Labeling by Amino acids in Cell") que incorpora al medio de crecimiento celular aminoácidos marcados con isótopos pesados estables no radiactivos (Ong et al., 2002). Los isótopos estables más utilizados son los de hidrógeno -deuterio- (H^1/H^2), carbono (C^{12}/C^{13}) y nitrógeno (N^{14}/N^{15}). La técnica ICAT se basa en la separación de los péptidos marcados mediante el uso de cromatografía de afinidad por avidina. Los reactivos ICAT están constituidos por tres partes funcionales: un grupo de unión, un grupo reactivo (iodoacetamida) capaz de unirse de manera covalente a los grupos sulfhidrilos de las cisteínas del grupo de unión

y un marcador de biotina. El grupo de unión contiene, generalmente, ocho átomos de H^1 (isótopo ligero) o H^2 (isótopo pesado), aunque también existe una variante que usa isótopos de carbono (Yi et al., 2005). El esquema de flujo de trabajo de las técnicas ICAT y SILAC se describe en la Figura 1.9.

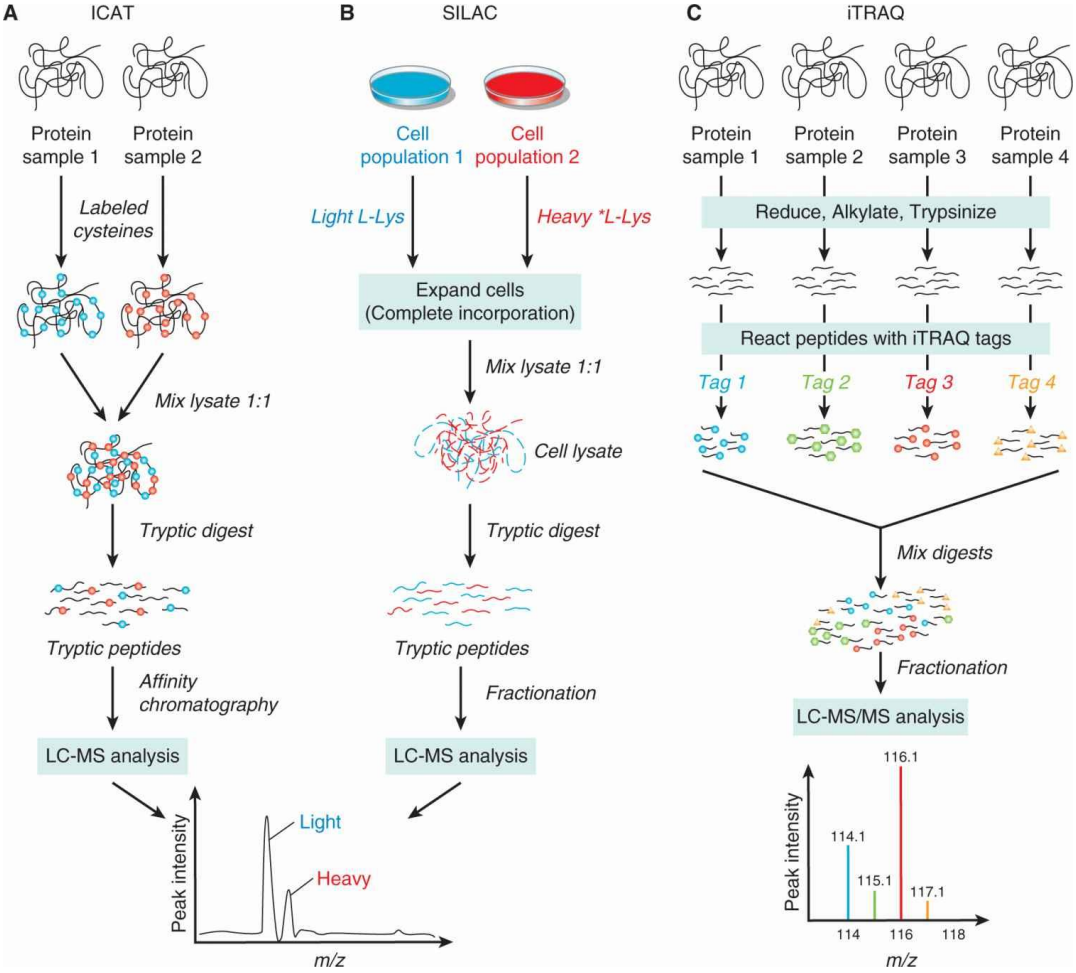

Figura 1.9. *Flujo de trabajo en las técnicas ICAT (A), SILAC (B) e iTRAQ (C). Imagen tomada de (https://oncohemakey.com/methods-of-molecular-analysis).*

Por otro lado, en la técnica SILAC tanto los aminoácidos no marcados como los que presentan marcaje son incorporados a las proteínas celulares durante la síntesis proteica. Los aminoácidos más utilizados son la H^2-leucina, C^{13}-lisina y C^{13}/N^{15}-arginina (Ong et al., 2002). El marcaje de las proteínas mediante isótopos estables (ligero y pesado), incorporados metabólicamente, de forma química o enzimática, permite que los péptidos marcados generen en el análisis por espectrometría de masas parejas de picos con una diferencia de m/z característica dependiendo de los isótopos usados (Goshe y Smith, 2003; Ong y Mann, 2005; Corthals y Rose, 2007). La abundancia relativa de los péptidos se obtiene por comparación de las áreas de los picos. Como ocurría en la técnica DIGE, el número de muestras analizadas simultáneamente es limitado, debido al precio de los materiales necesarios para el marcaje y al número de isótopos estables disponibles. La reproducibilidad y el número de réplicas requeridas

que determinan la significancia estadística en la técnica ICAT no están completamente optimizadas (Rabilloud, 2002). Esta técnica ha sido utilizada en el estudio de endomembranas de *Arabidopsis* o cloroplastos de maíz (Dunkley et al., 2004; Majeran et al., 2005). Sin embargo, la metodología SILAC permite la cuantificación relativa sin ninguna derivatización química o manipulación en un procedimiento simple, barato y preciso, que se puede utilizar como herramienta para estudios de proteómica cuantitativa en cualquier sistema de cultivo celular, aunque no resulta posible el análisis de proteínas procedentes de fluidos o tejidos celulares. La incorporación de los aminoácidos con esta metodología ha limitado su uso en plantas debido a su ineficiencia, aunque un estudio reciente en *Arabidopsis* ha propuesto un procedimiento más eficaz que incluye marcaje de argininas y lisinas (Lewandowska et al., 2013).

Al contrario que en el marcaje isotópico, los péptidos marcados isobáricamente presentan la misma masa tras su marcaje, si bien en el análisis de MS/MS los marcadores producen distintos fragmentos iónicos que pueden ser utilizados para la cuantificación. Este es el caso de la metodología iTRAQ ("Isotope Tagged Relative and Absolute Quantification"), que se basa en la aplicación de tres partes funcionales. Un grupo reactivo derivado de la N-hidroxisuccimida reacciona con los residuos de lisina y el extremo N-terminal, por lo que se incorpora a todos los péptidos presentes en la muestra, un segundo grupo compensador y un tercer grupo reportero derivado de la N-metilpiperacina, siendo constante la suma de masa de las tres partes. Durante la fragmentación en MS/MS los grupos reporteros se liberan y son detectados en el espectro como picos con una relación de m/z determinada (Ross et al., 2004; Pierce et al., 2008). Esta técnica permite la comparación de más de 4 muestras en el mismo experimento y además ha sido usada como metodología complementaria a la electroforesis bidimensional en aquellas regiones del gel donde los spots no estaban resueltos suficientemente (Rudella et al., 2006). Recientemente, ha sido utilizada en el estudio de la respuesta del alga *Pyropia haitanensis* al estrés por temperatura (Shi et al., 2017) o en plantas de *Arabidopsis* cultivadas con exceso de Zn (Fukao et al., 2011). El flujo de trabajo que utiliza la técnica iTRAQ se detalla en el esquema de la Figura 1.9.

Cuantificación mediante "Label-free shotgun proteomics"

Posteriormente, en el campo de la espectrometría de masas aplicada a la proteómica se ha desarrollado una nueva metodología basada en la digestión proteolítica de un proteoma dado, la separación cromatográfica de los péptidos obtenidos y su análisis por espectrometría de masas en tándem. Esta metodología recibió en 2001 el nombre de "Label-free shotgun proteomics" (Wolters et al., 2001). Este desarrollo se debe en gran medida al avance tecnológico de los espectrómetros de masas. La rápida aparición de la genómica y la proteómica como disciplinas

altamente financiadas y potencialmente rentables en las ciencias de la vida ha proporcionado un impulso adicional al desarrollo de espectrómetros de masas muy automatizados y relativamente fáciles de usar. Actualmente se dispone de una amplia gama de instrumentos específicamente diseñados para satisfacer las necesidades de los investigadores en proteómica, puesto que se hace hincapié no sólo en el rendimiento técnico, lo que incluye la precisión y la sensibilidad de la determinación de masas, sino también en la automatización. Los espectrómetros más nuevos incluyen software que facilita la identificación de proteínas, proporcionando puentes entre los espectros de masas y las bases de datos de secuencias públicas. A esto hay que añadir el desarrollo de herramientas bioinformáticas con gran capacidad para recolectar, almacenar, procesar y visualizar la enorme cantidad de datos que se generan en un análisis proteómico.

Se han desarrollado programas que usan la combinación de los tiempos de retención y masas de ion precursor para correlacionar péptidos de diversos archivos de datos brutos procedentes de LC–MS/MS. Las áreas de los picos correspondientes a los péptidos correlacionados se comparan para dar lugar a una relación de abundancia (Chelius y Bondarenko, 2002; Wang et al., 2003), por lo que esta cuantificación puede aplicarse a cualquier tipo de muestra y no requiere de preparaciones previas como en las cuantificaciones por marcaje. Este método es sencillo y presenta una buena reproducibilidad y linealidad en las comparaciones.

Una alternativa a este método es el conteo espectral, que contabiliza el número de espectros MS/MS atribuidos a un mismo ión precursor (Liu et al., 2004). La frecuencia de estos espectros refleja la abundancia del péptido en la muestra, facilitando una rápida adquisición de los datos. Este tipo de cuantificación requiere de un funcionamiento estable del instrumento, y, en ocasiones, la relación entre el número de espectros y la abundancia no es lineal, como ocurre en el caso de proteínas de gran tamaño o con pocos sitios de corte.

Estudios recientes han comparado los dos métodos de cuantificación, encontrando concordancia entre ambos. El conteo espectral mostró una mayor sensibilidad, mientras que la comparación de áreas de los picos mostró una mayor precisión (Old et al., 2005). Como se ha comentado anteriormente, en ambos casos es necesario asumir que ya sea la intensidad de señal de cada péptido en el espectro de masas o bien el número de espectros MS/MS y la concentración de dicho péptido sigue una tendencia lineal. Estos análisis requieren de un potente poder computacional, un funcionamiento estable del instrumento y un algoritmo que relacione las intensidades medidas y lleve a cabo la alineación de los picos obtenidos, asegurando la obtención de los parámetros necesarios para poder llevar a cabo la cuantificación, utilizando el tiempo de retención y la masa/carga de los precursores como señales. El desarrollo de equipos como Orbitrap o Q-TOF permite obtener una relación masa/carga de los precursores con alta resolución (100.000 FWHM) y exactitud (< 1 ppm) (Norbeck et al., 2005). La

reproducibilidad en los tiempos de retención cromatográficos se consigue con tecnologías de última generación como Agilent HPLC-Chip (Vollmer y Van de Goor, 2009). El potente desarrollo instrumental ha ido acompañado de la aparición de programas informáticos que permiten el procesado del complejo conjunto de datos obtenidos, ya sea mediante plataformas académicas como MaxQuant (Cox et al., 2007), msInspect/AMT (May et al., 2007), SuperHirn (Mueller et al., 2007), Census (Park et al., 2008) u OpenMS/TOPP (Sturm et al., 2008), o bien plataformas comerciales como Progenesis LC-MS (Nonlinear Dynamics; Waters), SIEVE (Thermo Scientific), Scaffold (Via ScaffoldBatch) o Mascot Distiller (MatrixScience), entre muchos otros. En general, estas plataformas funcionan con archivos nativos ("raw") que provienen de los análisis de MS/MS y presentan diferentes formatos de entrada y salida de datos que, en ocasiones, requieren de inter-conversiones. Mascot Distiller, Progenesis LC-MS y Scaffold son capaces de soportar una amplia variedad de formatos y, aunque todas las plataformas que existen en el mercado pueden procesar datos de alta resolución, solo algunos paquetes, como OpenMS/TOPP y Census (Park et al., 2008), son capaces de trabajar con datos de baja resolución (Nahnsen et al., 2013).

1.4.3. Método de identificación de proteínas

Actualmente, la identificación de proteínas a partir de los datos obtenidos de la espectrometría de masas en tándem (MS/MS) resulta el procedimiento más habitual cuando hablamos de proteómica. Inicialmente, la identificación se obtenía mediante la denominada huella peptídica ("Peptide Mass Fingerprint"; PMF) generada por las masas de los péptidos de un "spot" digerido con tripsina, utilizando instrumentos como MALDI/TOF (Matrix-Assisted Laser Desorption/Ionization Time-Of-Flight). Esta huella se comparaba con la información disponible en las bases de datos y la proteína se identificaba en base al emparejamiento *in silico* de las masas peptídicas determinadas experimentalmente frente a predicciones, en algunos casos, incluyendo la información del pI aparente y predicho y la masa molecular obtenida mediante los geles 2-D. Este enfoque es rápido pero los resultados son algo ambiguos y dependen de la disponibilidad de una secuencia genómica, o al menos de una colección EST (Expressed Sequence Tag) suficiente para la especie bajo estudio.

La gran variabilidad en las secuencias de aminoácidos, la distribución relativa de los sitios de acción de las proteasas en función de la proteína y el hecho de que sea inusual que el conjunto completo de péptidos para una proteína dada sea ionizado y detectado experimentalmente por determinados instrumentos llevó al desarrollo de una alternativa en la cuantificación de proteínas, la secuenciación *de novo* utilizando los espectros de MS/MS. Este tipo de metodología la utilizan instrumentos como los espectrómetros de masas en tándem con ionización por electrospray (ESI) MS/MS. La muestra, una vez ionizada, se separa en función

de la relación masa/carga de los iones primarios. Los picos seleccionados del primer espectro MS obtenido son fragmentados y se detectan los correspondientes iones (espectros MS/MS). Este proceso permite determinar una fracción de la secuencia peptídica que se compara con el patrón teórico de fragmentación disponible en las bases de datos, validando así la identificación. Este tipo de identificación tiene un rendimiento más lento pero, generalmente, proporciona un resultado más concluyente en cuanto a la identificación definitiva de una proteína, así como el valor añadido de permitir el estudio de las modificaciones post-traduccionales y otras características estructurales.

1.4.4. Aplicación a los sistemas vegetales

La proteómica se ha utilizado como una herramienta potente para el estudio de la homeostasis de metales en plantas y, como se ha comentado anteriormente, su aplicación a sistemas vegetales se debe al desarrollo de nuevas metodologías que han ido ganando en complejidad y precisión (Jorrín-Novo et al., 2009). Las aproximaciones proteómicas permiten aumentar el conocimiento de las rutas metabólicas compartidas en los procesos de deficiencia y desintoxicación y arrojar luz sobre los complejos mecanismos utilizados para mantener la homeostasis de nutrientes en las plantas. El conocimiento de los procesos derivados del estrés por metales pesados y deficiencia de micronutrientes en la planta es el primer paso para desarrollar aplicaciones que puedan evitar problemas agrícolas como la deficiencia y toxicidad de metales en cultivos, así como mejorar el contenido en nutrientes de los alimentos vegetales y a facilitar la fitorremediación de suelos contaminados por metales pesados. A pesar de los grandes avances realizados, la aplicación de las aproximaciones proteómicas a sistemas vegetales sigue un paso por detrás del desarrollado en cultivos celulares, y se encuentra muy lejos de las aplicaciones en estudios humanos.

Una de las limitaciones iniciales en los estudios vegetales fue la dificultad en la identificación de proteínas vegetales debido a la escasez de genomas vegetales secuenciados (van Wijk, 2001) que llevó a que plantas modelo como *A. thaliana* y arroz fueran las especies predominantes. Sin embargo, en los últimos años el número de especies vegetales de las que se ha secuenciado su genoma ha aumentado, incluyendo especies de interés agronómico como tomate, trigo, maíz y patata entre otros. En esta línea, el reciente desarrollo de bases de datos como la PPDB ("Plant Proteome DataBase"; Sun et al., 2009), la PODB ("The Plant Organelles Database"; Mano et al., 2008¨), la AtCHLORO (Ferro et al., 2010) y la P3DB ("Plant Protein Phosphorylation Database"; Yao et al., 2014) han permitido aumentar la fiabilidad de las identificaciones. Además, uno de los mayores logros ha sido el establecimiento de una base de datos de MS/MS con entradas de *Arabidopsis*, *Chlamydomonas reinhardtii*, *M. truncatula*, *Solanum tuberosum* (patata), *Solanum lycopersicum* (tomate) y otras especies vegetales

(ProMEX; http://promex.mpimp-golm.mpg.de/home.shtml; Hummel et al., 2007). Como resultado de estos avances, el número de estudios de proteómica vegetal también ha aumentado considerablemente y está ganando en importancia en los últimos años. Los trabajos en proteómica aplicados a sistemas vegetales se basan en estudios de proteómica diferencial o en la caracterización de proteomas de alta complejidad, en los que los mayores avances corresponden a la caracterización del proteoma de diferentes compartimentos subcelulares, como el cloroplasto, la envoltura cloroplástica, la mitocondria, la membrana plasmática, el fluido apoplástico o las savias de xilema y floema (Jorrín-Novo et al., 2007; Meisinger et al., 2008; Joyard et al., 2010; Schmidt et al., 2010; Lattanzio et al., 2013; Gutierrez-Carbonell et al., 2014, 2015, 2016; Ceballos-Laita et al., 2015, 2018; Rodríguez-Celma et al., 2016a).

En el ámbito de la nutrición vegetal, la proteómica se convierte en una potente herramienta para el conocimiento de los mecanismos moleculares responsables de la adaptación de la planta ante alteraciones nutricionales de macronutrientes, como P o N, o micronutrientes, como Fe o Mn (Hossain et al., 2013; Liang et al., 2013; Cvjetko et al., 2014). Esta Tesis Doctoral se ha centrado en el estudio de la homeostasis de dos micronutrientes que están suponiendo importantes problemas en áreas agrícolas de todo el mundo: Fe y Mn. El estrés por Fe ha sido más estudiado desde un punto de vista proteómico que el estrés por Mn. Los primeros estudios sobre Fe fueron en tejidos vegetales completos como la raíz y las hojas, y aún hoy en día los trabajos en estos tejidos son mayoritarios (López-Millán et al., 2013; Mai et al., 2016). Se ha utilizado la electroforesis bidimensional en el estudio del efecto de la deficiencia de Fe en raíz de *Beta vulgaris* (Rellán-Álvarez et al., 2010), *M. truncatula* (Rodríguez-Celma et al., 2011) *Prunus dulcis* × *Prunus persica* (Rodríguez-Celma et al., 2013b), *Cucumis sativus* (Donnini et al., 2010), *Hyoscyamus albus* (Khandakar et al., 2013) o *S. lycopersicum* (Brumbarova et al., 2008; Li et al., 2008). Sin embargo, el análisis de sub-proteomas resulta crucial para el entendimiento de la homeostasis de estos metales e incluye el estudio tanto de los orgánulos aislados como de los fluidos de la planta y las preparaciones de membrana purificada, puesto que estos últimos forman parte fundamental en el transporte y translocación de estos nutrientes en planta. En esta dirección, se han publicado estudios para el entendimiento del efecto de la deficiencia de Fe en la membrana plasmática de raíz mediante DIGE y "shotgun proteomics" (Meisrimler et al., 2011; Hopff et al., 2013) y en el floema mediante 2-DE (Gutierrez-Carbonell et al., 2015), aunque la información disponible es todavía limitada. En esta Tesis Doctoral, se pretende aumentar el conocimiento existente mediante el estudio del efecto de la deficiencia de Fe en el proteoma de raíz, xilema y apoplasto.

El efecto del estrés por Mn en los sistemas vegetales ha sido menos estudiado y, por tanto, la información disponible sobre la respuesta a este estrés nutricional es limitada. Recientemente, se han estudiado los efectos que la deficiencia del metal provocan en la raíz de

Arabidopsis a nivel génico (Rodríguez-Celma et al., 2016b). Sin embargo, los trabajos publicados hasta el momento a nivel de proteoma se han centrado en plantas con características hiperacumuladoras (Führs et al., 2010). Estudios en hoja han revelado que hay un efecto negativo del exceso del metal sobre la fotosíntesis y que lleva a un gran incremento de ROS (Fecht-Christoffers et al., 2003; Führs et al., 2008). Los cambios en el proteoma a nivel radicular, al contrario que ocurre con el Fe, sólo han sido estudiados en dos especies de *Citrus* (*C. sinensis y C. grandis*) (You et al., 2014) y en *Glycine max* (Chen et al., 2016), mostrando alteraciones en la estructura y lignificación de la pared celular. El efecto de esta alteración nutricional en subproteomas de la planta es prácticamente desconocido debido a que los trabajos hasta el momento son limitados (hay una única excepción sobre la respuesta de las peroxidasas presentes en el apoplasto de hoja ante condiciones de toxicidad de Mn; Führs et al., 2009).

En este trabajo de Tesis Doctoral se utiliza la proteómica diferencial como herramienta de estudio de los cambios inducidos por estos dos estreses nutricionales (Fe y Mn), muy frecuentes en zonas agrícolas, en raíz de plantas de tomate y en sub-proteomas tan importantes para el transporte de nutrientes como son la savia de xilema o el fluido apoplástico de hoja, de plantas de tomate y remolacha, respectivamente. El uso de la proteómica diferencial en estos estreses y subproteomas puede proporcionar información sobre los procesos de adaptación de las plantas, así como apuntar hacia posibles estrategias para combatirlos.

Capítulo 2

OBJETIVOS

El objetivo general de esta Tesis Doctoral es incrementar el conocimiento existente acerca de los efectos que causan la deficiencia de Fe y la deficiencia y toxicidad por Mn en los proteomas vegetales implicados en la absorción y el transporte de estos nutrientes. Se pretende dibujar, con un enfoque proteómico, un mapa general de las alteraciones metabólicas producidas por ambos estreses nutricionales en las plantas. El estudio de estos procesos permitirá incrementar el conocimiento existente sobre la homeostasis de estos metales y así asentar las bases para mejorar la calidad y productividad de los cultivos, elaborar posibles estrategias de fitoremediación y desarrollar fertilizantes eficientes y respetuosos con el medio ambiente.

Se plantean los siguientes objetivos específicos:

1. Describir la categorización funcional de los perfiles proteicos de los tres fluidos principales en plantas, fluido apoplástico y savia de xilema y floema, considerando los estudios proteómicos recientemente publicados.

2. Caracterizar, usando técnicas de 2-DE, los perfiles proteicos del fluido apoplástico de remolacha (*Beta vulgaris*), tanto en plantas control como afectadas por deficiencia de Fe y en las mismas plantas tras el suministro de Fe a las raíces.

3. Caracterizar, mediante técnicas de "shotgun proteomics", los cambios inducidos por las deficiencias de Fe y Mn en el perfil proteico de la savia de xilema de plantas de tomate (*Solanum lycopersicum*).

4. Caracterizar, mediante técnicas de 2-DE y "shotgun proteomics", los efectos de la toxicidad de Mn sobre los perfiles proteicos de la raíz y de la savia de xilema de plantas de tomate (*Solanum lycopersicum*).

Capítulo 3

RESULTADOS

3.1. Plant fluid proteomics: Delving into the xylem sap, phloem sap and apoplastic fluid proteomes

Jorge Rodríguez-Celma [a], Laura Ceballos-Laita [b], Michael A. Grusak [c], Javier Abadía [b], Ana-Flor López-Millán [b,c]

[a]*University of East Anglia/John Innes Centre, Norwich Research Park, Norwich, United Kingdom*
[b]*Department of Plant Nutrition, Aula Dei Experimental Station, Consejo Superior de Investigaciones Científicas (CSIC), Zaragoza, Spain*
[c]*USDA-ARS Children's Nutrition Research Center, Department of Pediatrics, Baylor College of Medicine, Houston, TX, USA*

Published in Biochimica et Biophysica Acta (2016) 1864, 991-1002 (*doi: 10.1016/j.bbapap.2016.03.014*)

ABSTRACT

The phloem sap, xylem sap and apoplastic fluid play key roles in long and short distance transport of signals and nutrients, and act as a barrier against local and systemic pathogen infection. Among other components, these plant fluids contain proteins which are likely to be important players in their functionalities. However, detailed information about their proteomes is only starting to arise due to the difficulties inherent to the collection methods. This review compiles the proteomic information available to date in these three plant fluids, and compares the proteomes obtained in different plant species in order to shed light into conserved functions in each plant fluid. Inter-species comparisons indicate that all these fluids contain the protein machinery for self-maintenance and defense, including proteins related to cell wall metabolism, pathogen defense, proteolysis, and redox response. These analyses also revealed that proteins may play more relevant roles in signaling in the phloem sap and apoplastic fluid than in the xylem sap. A comparison of the proteomes of the three fluids indicates that although functional categories are somewhat similar, proteins involved are likely to be fluid-specific, except for a small group of proteins present in the three fluids, which may have a universal role, especially in cell wall maintenance and defense. This article is part of a Special Issue entitled: Plant Proteomics - a bridge between fundamental processes and crop production, edited by Dr. Hans-Peter Mock.

3.1.1. Introduction

The vascular system of land plants is essential for long- and short-distance transport and distribution of nutrients and signals. The vascular transport system consists of the xylem and

phloem conduits, with the apoplast compartment acting as an interface between them and cells and also between cells. The xylem is composed of long treachery elements and shorter cells that are dead at maturity and have primary and secondary cell walls; these elements are connected together forming long tubes known as xylem vessels. The xylem mainly transports water and mineral nutrients taken up by the roots from the soil to the aerial part of the plant, although it also contains a number of other organic compounds, including carboxylates, hormones, amino acids, peptides and proteins (Lucas et al., 2013). Transport in the xylem is passive and driven by shoot transpiration, which causes a negative pressure that pulls the xylem fluid from the roots, and/or by root pressure, which can occur after soil solution enters the root by osmosis, and causes the sap to move towards the shoot (Fisher, 2000). A major role of the xylem is to provide water and nutrients to the shoots, but it also plays an important role in the root to shoot signaling system.

In contrast, the phloem conduit is a living tissue, whose major role is to transport the photosynthates from a photosynthetically active source to sink tissues. The conducting portion of the phloem is composed of two cell types, the sieve elements and the companion cells. At maturity, sieve elements are arranged to form the sieve tube; sieve elements lack a nucleus and contain pores at their ends, forming sieve plates that allow sap flow. The companion cells are metabolically active and usually contain a large number of ribosomes and mitochondria (Lucas et al., 2013). These cells are in close association with the sieve elements and support their function (Oparka and Cruz, 2000; Van Bel, 2003). The exchange of molecules between these two cells occurs *via* plasmodesmata (Oparka and Cruz, 2000). While transport in xylem sap is unidirectional (upwards), transport of the phloem sap is multidirectional and driven by positive hydrostatic pressures created by the gradients in sugar concentration between source and sink tissues. The phloem sap is rich in sugars, but also contains inorganic ions, other organic compounds including proteins and small signaling molecules such as hormones, systemic wound signals and mRNAs (Oparka and Cruz, 2000; Van Bel, 2003; Thompson and Schulz, 1999). Furthermore, the phloem sap is also a conduit for the trafficking of pathogens and foreign compounds such as herbicides and other xenobiotics (Van Bel, 2003; Fiehn, 2003).

The apoplast is the free diffusional space outside the plasma membrane and comprises the cell wall matrix and the fluid in the intercellular spaces. The apoplast occupies less than 5 % of the plant tissue volume in aerial organs (Parkhurst, 1982; Steudle and Lüttge, 1980) and the root cortex (Vakhmistrov, 1967) and its composition reflects the exchange between xylem and phloem compartments and the export and import of molecules by individual cells (Parkhurst, 1982). Therefore, small changes in these fluxes could produce large differences in the solute composition of the apoplast. The apoplast plays important roles in a wide array of physiological processes, including water and nutrient trafficking (Sattelmacher et al., 1998), plant defense,

cell interactions, cell wall maintenance, and in the transduction of environmental and developmental signals (Dietz et al., 2000; Geilfus et al., 2015; Hoson, 1998; Sakurai, 1998; Ohyama et al., 2009).

The study of plant fluid dynamics can be approached by means of non-destructive methodologies such as those used to measure sap flow velocity and pressure or to visualize vessel structures (reviewed and discussed in Kim et al., 2014). Other approaches include the use of isotope labeling to study fluxes of specific compounds (Orera et al., 2010). However, studies of the chemical composition, including their proteomes, often require the use of harsh techniques to collect these plant fluids. While information about the chemical composition of these plant fluids is ample with regard to minerals, sugars and small organic compounds such as carboxylates and amino acids (Álvarez-Fernández et al., 2014), information about their proteomes has arisen more recently. Proteomic studies can provide useful information about processes occurring in plant fluids and also to target proteins putatively involved in them for future studies. Most of the proteomic studies in plants were initially carried out with whole tissue samples (Jorrín-Novo et al., 2015; López-Millán et al., 2103), and later on with subcellular organelles such as the mitochondria (Huang et al., 2014), chloroplast (Ferro et al., 2010), and different membrane systems (Ephritikhine et al., 2004; Gutierrez-Carbonell et al., 2015; Marmagne et al., 2004), as well as with cell walls (Albenne et al., 2013; Rose and Lee, 2010) and plant fluids (see references in Table 3.1.1).

A major constraint for the proteomic analysis of plant fluids is the limited amount of sample that can be obtained. In the case of the xylem sap, another constraint is the low protein concentration, which is only in the ng μl^{-1} range. An additional constraint is an inherent consequence of the sampling methodologies: the presence of proteins not intrinsic to these fluids, which can be considered either as contaminants or as the result of protein-protein interactions occurring in vivo or during isolation (see below). Methodological progress in the proteomic field has shed light not only into the protein composition of these plant fluids, but also into their functionality. This includes the development of high-throughput technologies such as shotgun proteomics and LC–MS/MS that allow for the analysis of small sample volumes and for the detection of low abundance proteins, as well as the constant improvement in plant proteome databases, which have led to the construction of several mapping datasets (see Table 3.1.1 for references).

The aim of this review is to provide a general overview of the proteomic studies carried out in the three plant fluids mentioned. We have considered as outside the scope of this review, which is mainly focused into describing these plant fluid proteomes in healthy plants, a number of differential proteomic studies focused on the specific effects of biotic stresses, including pathogen systemic dissemination and plant defense mechanisms.

3.1.2. Plant fluid collection

The main limitations for obtaining reliable plant fluid proteomes have been the technical difficulties in the collection of plant fluids, which usually imply a disruption of the vascular tissues, and the small volumes and sometimes dubious purity of the samples obtained.

Table 3.1.1. *Summary of proteomic bibliography reviewed. Functional classification and number of identified proteins are depicted as reported in the original publications.*

Ref.	Species	Technique	Material	Separation	Identified	Functional Classification
Buhtz et al., 2004	*B. napus* *B. oleracea* *C. máxima* *C. sativus*	Stem de-top	Xylem	1-DE	14	Redox response, plant defense, proteolysis
Kehr et al., 2005	*B. napus*	Stem de-top	Xylem	2-DE	69	Plant defense, cell wall
Álvarez et al., 2006	*Z. mays*	Stem de-top	Xylem	2-DE	154	Cell wall, plant defense, proteolysis
Djordjevic et al., 2007	*G. max*	Stem de-top	Xylem	1&2DE, 2D-LC	24	Proteolysis, cell wall, redox stress, metabolism
Aki et al., 2011	*O. sativa*	Stem de-top	Xylem	2D-LC	118	Metabolism, cell wall, pathogenesis related, redox stress
		Stylectomy	Phloem	1DE followed by 2D-LC	107	Metabolism, pathogenesis related, redox stress, signal transduction
Ligat et al., 2011	*B. oleracea*	Stem de-top	Xylem	1DE followed by 2D-LC	189	Carbohydrate metabolism, proteolysis, cell wall, oxido-reductases
Krishnan et al., 2011	*G. max*	Stem de-top	Xylem	2-DE	38	
Zhang et al., 2011	*G. hirsutum*	Stem de-top	Xylem	LC	455	Carbohydrate metabolism, cell wall, stress response, signal transduction
Boudart et al., 2005	*A. thaliana*	VIC	Leaf apoplast	2-DE, 1-DE	93	Cell wall, defense related, protein interaction, proteinases
Soares et al., 2007	*M. truncatula*	VIC and IB	Leaf apoplast	2-DE	81	Defense, redox, transport, cell wall, pathogenesis related
Pechanova et al., 2010	*P. deltoides*	Pressure chamber	Leaf apoplast	2-DE, 2D-LC	144	Cell wall, stress defense, proteolysis
Witzel et al., 2011	*Z. mays*	VIC	Leaf apoplast	2-DE	67	Cell wall, defense, transport
Delaunois et al., 2013	*V. vinifera*	VIC	Leaf apoplast	2-DE	89	Defense, cell wall, proteolysis
Ceballos-Laita et al., 2015	*B. vulgaris*	Leaf centrifugation	Leaf apoplast	2-DE	164	Stress and defense, cell wall, metabolism

(Continued)

Table 3.1.1: continued

Ref.	Species	Technique	Material	Separation	Identified	Functional Classification
Barnes et al., 2004	*R.communis*	Stem puncture	Phloem	2-DE	18	Sugar metabolism, redox regulation, chaperones
Walz et al., 2004	*C. sativus, C. maxima*	Stem puncture	Phloem	1-DE, 2-DE	45	Redox response, proteinase inhibitors, signaling, defense proteins
Giavalisco et al., 2006	*B. napus*	Stem puncture	Phloem	2-DE and 1-DE	140	Redox stress, signaling, structural, RNA binding, metabolism
Dafoe et al., 2009	*P. trichocarpa x P. deltoides*	Phloem flow from a cut stem into solution	Phloem	2-DE	48	Metabolism, signaling, stress, structural
Lin et al., 2009	*C. maxima*	Stem puncture	Phloem	2D-LC	1121	Embryo development, ubiquitination, proteolysis, RNA binding, metabolism
Rodríguez-Medina et al., 2011	*L.albus*	Stem puncture	Phloem	2-DE	86	Metabolism, protein modification, redox regulation, stress/defense, structural components
Lattanzio et al., 2013	*L. texensis*	Stem puncture	Phloem	2-DE and 1-DE	54	Protein modification, metabolism, redox stress, cell wall

Xylem sap is frequently obtained by de-topping plant shoots, cleaning the cut area, and subsequently collecting the fluid that bleeds out, but this requires plant species with sufficient root pressure and turgid stems. This can be done with some dicots, including *Solanum lycopersicum*, *Brassica napus* and *Brassica oleracea*, and with most of the monocots (*Oryza sativa*, *Zea mays*, etc.) (Schurr, 1998). The collection of phloem sap is commonly achieved by bleeding after performing small incisions in the peduncles of plant species with slow sieve element wound closure. However, there are only a limited number of "phloem bleeder" species, mostly including members of the *Curcubitaceae*, *Brassicaceae* and the genus *Lupinus* (Atkins et al., 2011). Therefore, usual collection techniques limit the use of model plants such as *Arabidopsis thaliana* for the study of plant fluids, and force the use of non-canonical model plant species, thus delaying progress in the knowledge of these proteomes. The limited number of plant species that can be studied may be not relevant for mineral or metabolomic studies, but it is crucial for proteomic techniques, where the use of non-sequenced species decreases the number of confidently identified proteins.

Among the three plant fluids, xylem sap can usually be obtained in sufficient quantities; however, the protein concentration in the xylem sap is generally low, thus limiting the proteomic approaches to be used (Aki et al., 2008). Volume yields collected by de-topping shoots of hydroponically grown healthy plants can reach several ml h^{-1} of acceptably pure

xylem sap (Goodger et al., 2005). The mapping studies of the xylem sap proteome published to date have used root pressure as a means to obtain xylem sap; and protein yields ranged from 5 to 12 ng μl^{-1} (Table 3.1.1). Although none of these studies assessed the possible sap contamination by cytoplasmic proteins by experimental work, *in silico* prediction of localization as secreted or intracellular proteins was used in *B. oleracea* to assess the quality of the xylem sap proteome (Ligat et al., 2011). Several other methods to obtain xylem sap have been published, and their advantages and disadvantages have been reviewed recently (Álvarez-Fernández et al., 2014; Kehr and Rep, 2007).

As commented above, the collection of phloem sap is carried out using "phloem bleeder" species, making direct incisions in the phloem vessels located in peduncles, or alternatively by stylectomy using aphids or other sucking insects (Kehr and Rep, 2007). The latter technique requires very specialized expertise, provides low volumes of sample (in the nl range), is time-consuming and is only achievable with some plant-insect combinations (Atkins et al., 2011). Advantages and disadvantages of sampling methods for phloem sap and for purity assessment have been critically reviewed (Atkins et al., 2011; Kehr and Rep, 2007). The phloem sap proteomes published so far have been obtained by collecting exuded sap from direct incisions in *B. napus* (Gutierrez-Carbonell et al., 2015; Giavalisco et al., 2006; Zhang et al., 2012), *Cucurbita maxima* and in two *Lupinus species* (36-38), and by aphid stylectomy in *O. sativa* (Aki et al., 2008). With the direct incision method volumes collected were in the several hundred µl range (Gutierrez-Carbonell et al., 2015; Zhang et al., 2012; Lattanzio et al., 2013), whereas protein yields ranged from 0.2 $\mu g\ \mu l^{-1}$ found in rice and *Lupinus* species (Aki et al., 2008; Lattanzio et al., 2013; Rodríguez-Medina et al., 2011) to 35-60 $\mu g\ \mu l^{-1}$ in Curcubitaceae (Atkins et al., 2011; Walz et al., 2004).

The most common methodology used to collect apoplastic fluid is vacuum infiltration-centrifugation (VIC), which can be used with roots, leaves and stems (Boudart et al., 2005; Dani et al., 2005; Husted and Schjoerring, 1995; Lohaus et al., 2001). Briefly, the tissue is infiltrated with a buffer while applying vacuum and the infiltrated intercellular fluid (considered as a diluted apoplastic fluid) is thereafter collected by centrifugation. A study of the variables in this method, including the pH and composition of the buffer, as well as applied centrifugal force and time, indicated that centrifugal forces below 1000 × *g* do not lead to significant contamination, whereas the composition and pH of the solution affect the metabolite composition of the fluid collected (Lohaus et al., 2001). From a proteomic point of view, a detailed study of the influence of the composition of the infiltration solution on the number and nature of proteins collected indicated that the lowest number of intracellular protein contaminants and the largest number of extracellular proteins was obtained in *Z. mays* using 100 mM Na phosphate buffer, whereas water alone led to the highest contamination (Witzel et al., 2011). In *Arabidopsis*

rosette leaves, the efficiency of several VIC solutions for the collection of apoplastic proteins was also assessed, with 0.2 M $CaCl_2$ yielding the largest number of solubilized proteins among the salts studied (Boudart et al., 2005). Buffers with different ionic strengths have been applied in order to extract proteins more tightly or loosely bound to the cell wall (Soares et al., 2007). Following VIC, approximately 100 μL of apoplastic fluid per g of tissue can be obtained without significant cytosolic contamination (references in Table 3.1.1). Direct centrifugation without infiltration can also be applied to obtain apoplastic fluid, leading to similar yields but in general implying a slightly higher contamination (Ceballos-Laita et al., 2015, Chapter 3.2).

Another major limitation for the study of plant fluid proteomes is their purity. The collection methods, although optimized, cannot completely avoid intracellular fluid leakage. The major source of contamination for these three fluids consists of soluble cytosolic proteins; since the concentration of proteins in the cytosol is usually much higher than in the intercellular space, a relatively small cytosolic leakage (e.g., the rupture of a few cells) could lead to markedly altered protein profiles. Several methods have been used to assess the purity of the plant fluids. Among the xylem mapping studies reviewed (Table 3.1.1), purity was assessed only in one study by means of *in silico* prediction of secreted proteins (Ligat et al., 2011). However, the low protein yields obtained and the fact that only a small amount of cytosolic proteins were identified may suggest an acceptable level of purity. Common phloem sap purity assessment tests are based in the measurement of sugar concentrations as well as the reducing to non-reducing sugar ratio, the presence of Rubisco, and the measurement of certain enzymatic activities as cytosolic contaminant markers (Gutierrez-Carbonell et al., 2015; Giavalisco et al., 2006; Lattanzio et al., 2013; Rodríguez-Medina et al., 2011; Mendoza-Cozatl et al., 2008). A thorough assessment of purity was performed in the study of the *B. napus* proteome (Giavalisco et al., 2006), where the purity of the phloem was studied using four independent techniques: sugar composition, western blot and RT-PCR of Rubisco, as well as the comparison of the 2-DE protein maps of the phloem sap with those from full leaf extracts. Given the harsher techniques used for the collection of apoplastic fluid, this plant fluid is more prone to contain products of cytosolic leakage. Apoplastic fluid contamination is usually assessed by measuring the activity of cytosolic enzymes, such as malate dehydrogenase or hexose-phosphate isomerase, as markers (Soares et al., 2007; Ceballos-Laita et al., 2015, Chapter 3.2). When the extraction buffer used in VIC is not compatible with the enzymatic activity assays, antibody detection of cytosolic contamination has also been used as an alternative (Delaunois et al., 2013). The contamination level measured by these techniques was below 5 % in all the studies reviewed. However, the meta-analysis of all the proteins identified in these apoplastic fluid proteomes indicates that approximately 10 % of the proteins identified are known to be cytosolic, suggesting that these purity control methods may underestimate the presence of cytoplasmic components.

3.1.3. Approach for plant fluid proteome comparisons

Given the difficulties to compare proteomes from different plant species and also the fact that some of the published proteomes have a certain degree of duplicity (e.g., containing the same protein identified in different databases, plant species, or in different gel spots), we have produced a "non-redundant proteome" for the three plant fluids reviewed (included in Supplementary Tables S1-3). BLAST searches of each dataset were performed against the TAIR10 database, the closest *Arabidopsis* orthologue (E-values lower than 10-30) was selected and duplicates deleted, thus obtaining a unique AGI number per protein.

Functional classification of these three non-redundant proteomes was then carried out using the Gene Ontology (GO) annotation included for these proteins in the TAIR database, and the GO categories were manually checked and grouped. The classification includes categories as follows: polysaccharide metabolism, proteolysis, oxido-reductases, general metabolism (including lipid, amino acid, nucleotide and miscellaneous metabolism), regulation, plant defense, unknown, and miscellaneous (including cytoskeleton related, nutrient reservoir, cell division, protein synthesis, photosynthesis, and transport). When the GO annotation was too general, references or functional domains included in the TAIR entry were used as additional criteria. These non-redundant proteomes of xylem sap, phloem sap and leaf apoplastic fluid are presented in Tables S1, S2 and S3, respectively.

The subcellular localization database for *Arabidopsis* proteins (SUBA3, http://suba3.plantenergy.uwa.edu.au) was used to predict protein subcellular localization in the proteome sets. SUBA3 combines manual literature curation of large scale subcellular proteomics, fluorescent protein visualization and protein-protein interaction (PPI) datasets with subcellular targeting output results from 22 prediction software packages (Tanz et al., 2012). The SUBA3 output includes a consensus location (SUBAcon, Table S4), based on Bayesian probabilities, which allows for an automated evaluation of large datasets. In this study, a protein was considered as extracellular when SUBAcon indicated extracellular location. A summary of these results is shown in Table S4. Although *in silico* prediction is a powerful tool to analyze large datasets, the existence of non-canonical secretory proteins and the limitations of the prediction algorithms make recommendable using alternative experimental methods to verify the true extracellular nature of proteins classified as such. It should be noted that all three non-redundant proteomes contain a significant amount of intracellular proteins (43, 99 and 57 % in the xylem sap, phloem sap and leaf apoplastic fluid, respectively), which likely reflect some degree of cytoplasmic contamination. Their unequivocal assignment to the respective proteomes deserves further studies.

3.1.4. The xylem sap proteome

The xylem sap proteome has been studied in eight plant species, including two monocots, *Z. mays* (Alvarez et al., 2006) and *O. sativa* (Aki et al., 2008), two Brassicaceae species, *B. oleracea* (Ligat et al., 2011) and *B. napus* (Buhtz et al., 2004; Kehr et al., 2005), two Curcubitaceae, *C. maxima* and *Cucumis sativus* (Buhtz et al., 2004), the legume *Glycine max* (Djordjevic et al., 2007; Krishnan et al., 2011) and the Malvaceae *Gossypium hirsutum* (Zhang et al., 2015). These mapping studies used the 'root pressure' method (Goodger et al., 2005) for xylem sap collection in most species, and 'root pressure' applying vacuum in *G. max* (Djordjevic et al, 2007). Different proteomic techniques (1-DE (Buhtz et al., 2004; Djordjevic et al, 2007; Krishnan et al., 2011), 2-DE (Ligat et al., 2011; Alvarez et al., 2006; Kehr et al., 2005; Krishnan et al., 2011) and 2D-LC (Aki et al., 2008; Ligat et al., 2011; Zhang et al., 2015)) were used to obtain the xylem sap proteome. The number of xylem sap proteins identified by 1-DE was low and ranged from 14 to 24, whereas the number of proteins identified by 2-DE and 2D-LC ranged from 69 to 154 and from 118 and 455, respectively. In *B. oleracea*, both the xylem sap proteome and N-glycoproteome were studied, the latter one using Concanavalin A affinity chromatography followed by LC–MS/MS (Ligat et al., 2011). This study reported 81 glycoproteins in the xylem sap, from which 25 were probably low abundance ones, since they were not detected in the direct xylem sap proteome analysis (Ligat et al., 2011).

The comparison of the reviewed xylem sap proteomes led to the assignment of 354 unique AGI proteins (Table S1), with 57 % of them predicted as extracellular (Table S4). Given that the number of proteins obtained in the 1-DE studies was low, only the non-redundant proteomes obtained by 2D techniques in *O. sativa*, *Z. mays*, *B. oleracea*, *B. napus* and *G. hirsutum* were compared in order to identify putative proteins conserved between species. The overlap between them was limited, with no common proteins found in the five species compared and only ten proteins identified in at least four of them (Table 3.1.2). Interestingly, this small subset contains only proteins related to the polysaccharide metabolism (5), oxido-reductases (3), plant defense (1) and proteolysis (1) categories (Table 3.1.2), suggesting that these are conserved functional categories of the xylem sap proteome and that these specific proteins may have a species-independent role in the xylem sap. However, it should be noted that given the differences in resolution of the proteomes studied and the low coverage in some of the plant species this hypothesis needs further support. Among these ten proteins, nine were predicted by SUBA3con to be extracellular (Table 3.1.2).

The functional classification of the 354 non-redundant proteins of the xylem sap proteome is presented in Figure 3.1.1. The major functional categories found were polysaccharide metabolism (28 %), general metabolism (22 %), oxido-reductases (14 %) and proteolysis (12 %).

Table 3.1.2. *The consistent xylem sap proteome. The list contains ten non-redundant Arabidopsis-referenced proteins present in at least four of the following xylem sap proteomes: maize (Z. mays), rice (O. sativa), cabbage (B. oleracea), rapeseed (B. napus) and cotton (G. hirsutum). Accession identifiers are those reported for Z. mays (Alvarez et al., 2005), O. sativa (Aki et al., 2008), B. oleracea (Ligat et al., 2011), B. napus (Buhtz et al., 2004; Kehr et al., 2005) and G. hirsutum (Zhang et al., 2015). Annotation corresponds to the TAIR10 description from the BLAST-matched Arabidopsis proteins. Exracellular localization (Y) or non-extracellular localization (N) was described according to the SUBA3 consensus prediction.*

Z. mays	*O. sativa*	*B. oleracea*	*B. napus*	*G. hirsutum*	AGI	Annotation
gi|13398412	Os12g0128700	TC43276		Q76LU3	AT3G10740	Arabinoxylan arabinofurano-hydrolase isoenzyme (Y)
gi|2109457	Os03g0418000	TC15913		A7LAB9	AT3G12500	Chitinase (Y)
gi|30692538	P0644B06.40	TC25741/ TC461514	AT3G61490		AT3G61490	Polygalacturonase-like protein (Y)
gi|50931079	Os05g0104200		AAM94869	Q2HYU7	AT5G06860	Putative polygalacturonase inhibitor (Y)
gi|7451375	Os01g0860500	TC17043		A9XTK9	AT5G24090	Acidic endochitinase (Y)
gi|7442163	Os12g0629700	TC540954	AAN23104		AT4G11650	Thaumatin-like pathogenesis-related protein (Y)
gi|28400794	Os04g0651000	TC352237	gi|15239075	Q7XYR7	AT5G05340	Peroxidase (Y)
gi|7433034	Os03g0235000	TC558054	AT5G19890	B9T8I2	AT5G19890	Peroxidase (EC 1.11.1.7) (Y)
gi|50940455		TC589344	AT4G33420	F4YAW4	AT4G33420	Putative peroxidase 47 precursor (N)
gi|21593457	OsI_030760	ES901600/ TC56831/ TC462494	AT1G20160		AT1G20160	Subtilisin-like serine protease (Y)

Many (approximately 65 %) of the enzymes identified in the polysaccharide metabolism category are cell wall hydrolases (glucanases, galactosidases and xylosidases) involved in primary cell wall degradation and cell wall remodeling (Ross et al., 1995; Van der Ende et al., 2004). This degradation is needed for the formation of secondary cell walls (Demura et al., 2002). This group of enzymes can also play a role in modifying the cell wall surface in conjunction with pectic enzymes and hemicellulases (Minic, 2008; Numan and Bhosle, 2006). Lignin and secondary cell wall provide structural support for xylem vessels, being essential for its function (Boyce et al., 2004). Lignin deposition requires polymerization and de-polymerization of monolignols from the phenylpropanoid metabolism, and these reactions involve hydrogen peroxide (Boerjan et al., 2003).

The second most important functional group found is general metabolism, including proteins related to carbohydrate (22), lipid (20), nucleotide (seven) and amino acid metabolisms (ten) (Table S1). There are several possible explanations for the presence of such a large number of metabolic enzymes in xylem sap. The first plausible explanation would be that they are cytosolic contaminants due to the sampling process. The fact that most of them are not present

in the overlaps (Table 3.1.2) and that only 47 % of them are predicted to be extracellular (Tables S1 and S4) would argue in favor of this explanation. Another possibility would be that at least some of these enzymes are needed for the production of cellulose and lignin; these include the carbohydrate metabolism enzymes, phenylalanine ammonialyase and 4-coumarate-CoA ligase (Van den Ende, et al., 2004). Further studies are needed to clarify the presence and functions of these proteins in the xylem sap.

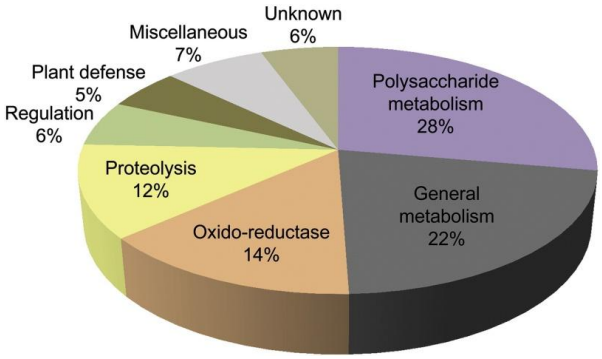

Figure 3.1.1. *Functional classification of the non-redundant xylem sap proteome. The 354 Arabidopsis non-redundant proteins obtained from the BLAST of species-specific protein sets against that of A. thaliana were classified based on their gene ontology (GO) biological process and TAIR annotations.*

Proteins classified as oxido-reductases include several enzymes of the ascorbate–glutathione cycle, Cu, Zn-SOD and several redox enzymes such as thioredoxin H and glutaredoxin (Table S1). A large number of peroxidases (26 of the 50 identified proteins that belong to the oxido-reductase category) were also found in the studies reviewed (Table S1), and although most authors in the studies assigned them to redox response, they could also well be associated with cell wall processes and lignification. Approximately 90 % of these peroxidases were predicted to be extracellular (Tables S1 and S4). The presence of proteins involved in the response to redox homeostasis in the xylem sap proteome of non-stressed plants supports the existence of a constitutive basal defense mechanism, which may be especially useful given that xylem cells do not have the protein machinery to synthesize proteins when submitted to a stress situation.

Proteolysis related proteins accounted for 12 % of the non-redundant xylem proteome. Most of the proteases, including pepsins, subtilisins, and serine and cysteine peptidases are known to have an extracellular localization, and accordingly 63 % of them were classified as extracellular. In addition to a role in the degradation of damaged proteins for the maintenance of xylem sap, extracellular proteases may also constitute a basal defense strategy against pathogen infection (Shabab et al., 2008; Xia et al., 2004). Plant defense related proteins accounted for 5 % of the non-redundant xylem proteome. Many plant defense proteins, such as thaumatins and chitinases, have been found in the xylem sap of different plant species (Buhtz et al., 2004; Rep

et al., 2003), and they are consistently found in the proteomic studies reviewed. This already established defense system found in plant fluids is thought to create a hostile environment to prevent pathogen infection (Delaunois et al., 2013; Pechanova et al., 2010).

In summary, from a proteomic point of view the bulk xylem sap composition is relatively simple. It contains proteins involved in maintaining the xylem conduit architecture, as well as a battery of proteins; including redox and plant defense ones in addition to proteases, which constitutes a basic defense barrier that provides a rapid and local first response against possible stress situations and pathogen infection.

3.1.5. The phloem sap proteome

A large number of proteomic studies have focused on deciphering the phloem sap proteome. Initial studies used 1-DE approaches and yielded a limited number of proteins (Dani et al., 2005; Schobert et al., 2000). More recently, the development of high throughput proteomic methods, such as two dimensional electrophoresis (2-DE) and especially LC–MS/MS, have allowed a more thorough characterization of the phloem sap proteome. Phloem sap in these studies was obtained either by using stylectomy in *O. sativa* (Aki et al., 2008) or by sap exudation after incision in *Ricinus communis* (Barnes et al., 2004), *B. napus* (Gutierrez-Carbonell et al., 2015; Giavalisco et al., 2006), *C. maxima* (Lin et al., 2009; Walz et al., 2004), *C. sativus* (Walz et al., 2004), *Populus trichocarpa* × *Populus deltoides* (Dafoe et al., 2009), *Lupinus albus* (Rodríguez-Medina et al., 2011) and *Lupinus texensis* (Lattanzio et al., 2013). The number of phloem sap proteins identified by 2-DE was similar, irrespective of the gel size, and ranged from 45 in *C. maxima* to 140 in *B. napus*, with 86 and 54 identified in *L. albus* and *L. texensis*, respectively. The number of phloem proteins identified by LC–MS/MS was larger, and included 1121 proteins in *C. maxima* and 107 in *O. sativa*.

Comprehensive comparisons of the phloem sap proteomes of these different plant species have already been performed (Lattanzio et al., 2013; Lin et al., 2009). These inter-species comparisons were approached by using the phloem protein data sets from *C. maxima*, *O. sativa*, *B. napus* and *R. communis* to perform BLAST searches against *A. thaliana* and by creating a "total non-redundant phloem proteome" containing 688 proteins (Figure 2A in Lin et al., 2009). A similar approach was used to compare the phloem proteome of *L. texensis* to the previously reported non-redundant proteome and found only 12 new protein species (Lattanzio et al., 2013). From these, two proteins were previously described in *L. albus* (Rodríguez-Medina et al., 2011) and the remaining ten novel protein species had non-redundant identifiers, but had functions similar to other protein species already described in the phloem of other plant species (Figure 2C in Lattanzio et al., 2013). The comparison of the reviewed phloem sap proteomes led

to the assignment of 720 unique AGI proteins (Figure 3.1.2; Tables S2 and S4). Comparisons of the non-redundant phloem proteomes previously described (Lattanzio et al., 2013; Lin et al., 2009) revealed that approximately 60 proteins were found in the phloem sap of at least two plant species, with 13 of them being consistently detected in at least four of the five plant species considered (Table 3.1.3). Among these 13 proteins, none were predicted to be extracellular (Table 3.1.3). Proteins in this list were representative of the most abundant functional categories found in the phloem sap proteome (see below).

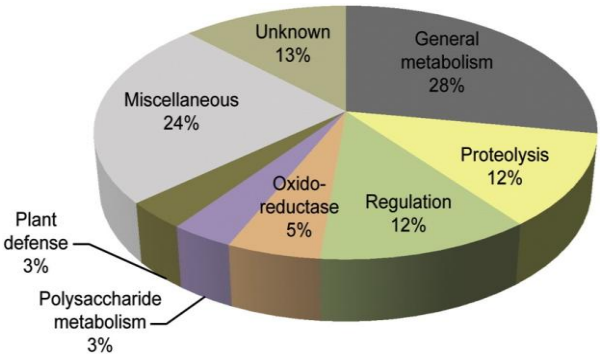

Figure 3.1.2. *Functional classification of the non-redundant phloem sap proteome. The 720 Arabidopsis non-redundant proteins obtained from the BLAST of species-specific protein sets against that of A. thaliana were classified based on their gene ontology (GO) biological process and TAIR annotations.*

The functional classification and cellular localization of the non-redundant phloem sap proteome (Figure 3.1.2; Tables S2 and S4) clearly reflects the complex nature of this fluid, which results from the exchange between companion cells and sieve elements along the translocation pathway. On one hand, categories such as oxido-reductases (5 %), plant defense (3 %), and proteolysis (12 %) are enriched in this fluid, as also seen in the xylem sap and apoplastic fluid (see references in Table 3.1.1). These categories provide a basal defense mechanism against pathogens and stress or are involved in the maintenance and stability of the sieve elements. On the other hand, other enriched categories such as general metabolism (28 %) and miscellaneous (24 %) (the latter including the sub-categories protein synthesis (9 %) and macromolecular trafficking (8 %)) reflect exchange processes occurring between the metabolically active companion cells and the enucleate sieve elements (Figure 3.1.2 and Table S2). The category of regulation, including RNA binding, is also enriched (12 %) in the phloem sap proteome and may represent proteins that are being translocated (references in Table 3.1.1). Furthermore, *in silico* prediction of the localization of the non-redundant phloem proteome indicated that 99 % of them are intracellular (Tables S2 and S4), suggesting that the contribution of companion cells to the phloem sap proteome is very significant, or alternatively that there may be some contamination from other cell types.

Proteins in the oxido-reductase category typically found in phloem sap include enzymes of the ascorbate–glutathione cycle, glutaredoxins and glutathione transferases, with thioredoxin

being one of the most abundant proteins in this group in most plant species (Table S2). Defense related proteins include pathogenesis related proteins, LRR disease resistance proteins and several hormone responsive proteins.

In addition to extracellular proteases such as cysteine or serine proteases (16 of the 26 phloem proteases were predicted to be extracellular), components of the proteasome 26S were also found in the non-redundant proteome, although none of them were predicted as extracellular. Furthermore, the *C. maxima* proteome, the most detailed proteome described so far, contains all the components to form a functional 26S proteasome as well as a large set of proteins related to ubiquitin related processes (Lin et al., 2009), suggesting that the sieve tube system has retained the capacity for proteolysis *via* the ubiquitin-proteasome 26S pathway. The presence of protein degrading enzymes in sieve elements could be related to protein turnover or also constitute a defense mechanism. Cell structural components such as actin and profilin and actin-depolymerizing factors are also common proteins in the non-redundant phloem sap proteome (23 cytoskeleton related proteins) (Table S2 and references in Table 3.1.1). In *R. communis*, these proteins are constantly delivered into the sieve elements and are mobile in the translocation stream (Schobert et al., 2000), but their specific role in sieve elements remains to be determined.

A general overview of the proteins identified in different plant species in the general metabolism category indicates the existence of a wide array of metabolic processes in phloem sap, including carbohydrate metabolism, synthesis and breakdown of organic-, amino- and fatty-acids as well as secondary metabolites and nucleotides (Table S2, references in Table 3.1.1), suggesting that these processes might still be active in sieve elements. However, only 1.5 % (three out of the 200 proteins in this category; Table S2) were classified as extracellular, highlighting the special nature of the phloem sap proteome and raising doubts about their possible origin.

A large array of molecules related to regulation (12 %) has been described in the phloem sap proteome. The regulation category would include those proteins involved in protein modification and folding and those acting as mobile signals for systemic signaling. The first group includes chaperones such as peptidyl-prolyl isomerases, several heat shock proteins and proteins involved in phosphorylation such as protein kinases, and in Ca-dependent signaling such as annexins, calmodulins and C2 domain containing proteins (Table S2, references in Table 3.1.1). Overall, these proteins are involved in signal processing, protein phosphorylation, folding and unfolding of proteins for protein trafficking between companion cells and sieve elements and microRNA regulation of gene expression (Rodríguez-Medina et al., 2011). Among putative mobile signals, the flowering locus FT is ubiquitously found in most plant species (Table 3.1.3) (Aki et al., 2008; Giavalisco et al., 2006). The presence of extracellular

RNA binding proteins such as cyclophilins (one of them, cyclophilin 19, although predicted as intracellular, was found in all species compared here, Table 3.1.3), lectins, and the glycine rich proteins in the phloem sap is consistent with RNA transport in phloem as ribonucleoprotein complexes, which are most likely involved in long distance signaling. Secreted lectins have been shown to translocate RNAs (Gómez and Pallás, 2004). Many of the glycine-rich proteins have been associated with stress and hormone treatments (Nomata et al., 2004), supporting their possible role in RNA homeostasis and signaling (Lucas et al., 2001; Yoo et al., 2004), whereas some of the glycine-rich proteins (such as AT2G21660 and AT3G03773 found in the non-redundant phloem proteome, Table S2) are possibly involved in the formation of secondary walls (Mangeon et al., 2010).

Table 3.1.3. *The consistent phloem sap proteome. The list contains 13 non-redundant Arabidopsis-referenced proteins present in at least four of the following phloem sap proteomes: pumpkin (C. maxima), rice (O. sativa), rapeseed (B. napus), Lupinus texensis and Lupinus albus. Accession identifiers are those reported for C. maxima (Lin et al., 2008), O. sativa (Aki et al., 2008), B. napus (Giavalisco et al., 2006), L. texensis (Lattanzio et al., 2013) and L. albus (Rodríguez-Medina et al., 2011). Annotation correspond to the TAIR10 description from the BLAST-matched Arabidopsis proteins. Extracellular localization (Y) or non-extracellular localization (N) was described according to the SUBA3 consensus prediction.*

C. maxima	*O. sativa*	*B. napus*	*L. texensis*	*L. albus*	**Annotation**
FG226997_3	gi|115458768	AT3G04120		CAI83772	Glyceraldehyde-3-phosphate dehydrogenase subunit 1 (N)
FG227596_2	gi|115481260	AT2G36530		CAB75428	Enolase 2 (N)
FG227348_3	gi|115447399	AT5G03300		XP_002531678	Adenosine kinase 2 (N)
FG227154_3	gi|115461741	AT1G75270		AAL71857	Dehydroascorbate reductase 2 (N)
gil26985219	gi|115456247b	AT5G28540	gil1143427		Heat shock cognate 70-kDa protein 1 (N)
FG227112_2	gi|115443875	AT2G16600	gi|6014890	O49886	Cyclophilin 19 (N)
FG227050_1	gi|115465581	AT5G20020	gil4336905		RAS-related GTP-binding nuclear protein 2 (N)
FG227803_2	gi|115489714	AT2G21660		BAF34340	Cold, circadian rhythm, and RNA binding 2 (N)
gil157346142	gi|115461424	AT3G52560		NP_566968	Ubiquitin E2 variant 1D-4 (N)
FG227133_5	gi|115473151	AT1G69410	gil13094963		Eukaryotic translation initiation factor 5A-1 (N)
gil115343291	gi|115468204	AT1G65480		BAJ33494	Flowering locus T (N)
FG227096_3	gi|115455697	AT3G46000	gil7339501		Actin-depolymerizing factor 2 (N)
gil118481204	gi|115454971	AT5G09810	gil9965319	AAD03741	Actin7 (N)

Finally, the non-redundant phloem proteome contains 67 proteins related to protein synthesis and only eight were structural components of the ribosome (Table S2); in addition,

none of the proteins in this sub-category were predicted as extracellular (Table S2). Most of these proteins come for the high-throughput analysis of the *C. maxima* proteome (Lin et al., 2009), which contains around 100 proteins involved in t-RNA aminoacylation, translation initiation, elongation, and termination, but very few components of the ribosomal complexes, which prompted the authors to suggest the existence of protein synthesis in the sieve element. A limited number of translation initiation factors have been detected in several plant species, with one of them, the intracellular eiF-5A, being found in most species compared (Table 3.1.3). Given that some of them bind RNA, including eiF-5A, a role in RNA transport in phloem has also been suggested for these proteins in phloem sap (Giavalisco et al., 2006). The large number of this set of proteins in *C. maxima* could reflect a larger contribution of companion cells in this proteome, the high sensitivity of the proteomic approach used in this study, or to the specific characteristics of the phloem sap in Curcubitaceae species, which is mostly composed of extra-fascicular phloem sap and may have a peculiar composition (Zhang et al., 2012; Turgeon and Oparka, 2010).

3.1.6. The leaf apoplastic fluid proteome

The proteome of the leaf apoplastic fluid has been described in six plant species so far (Table 3.1.1). This fluid was collected by the VIC technique using buffers of different ionic strengths in four of them: *Z. mays* (Witzel et al., 2011), *Medicago truncatula* (Soares et al., 2007), *Vitis vinifera* (Delaunois et al., 2013) and *A. thaliana* (Boudart et al., 2005). In *Populus deltoides*, the leaf apoplastic fluid was collected using a pressure chamber (Pechanova et al., 2010) and in *Beta vulgaris* it was obtained by direct leaf centrifugation (Ceballos-Laita et al., 2015, Chapter 3.2). Protein yields were only reported in three studies, including sugar beet apoplastic fluid obtained by direct leaf centrifugation (400-800 μg protein mL^{-1}; Ceballos-Laita et al., 2015, Chapter 3.2) and grapevine and *M. truncatula* apoplastic fluids obtained by VIC (6 and 50 μg protein g^{-1} FW, respectively) (Soares et al., 2007; Delaunois et al., 2013). 2-DE analysis detected a similar number of protein spots: 328, 220, 306, and 203 in the apoplastic fluid of *Z. mays*, *M. truncatula*, *V. vinifera* and *B. vulgaris*, respectively (Witzel et al., 2011; Soares et al., 2007; Ceballos-Laita et al., 2015, Chapter 3.2; Delaunois et al., 2013); whereas the combination of 2-DE and 2D-LC in *P. deltoides* (Pechanova et al., 2010) and of 2-DE and sepharose fractioning followed by 1-DE in *A. thaliana* (Boudart et al., 2005) yielded a somewhat lower number of identified apoplastic proteins: 144 and 133, respectively. However, it should be noted that redundancy existed in the 2- DE approaches, and the number of unique proteins identified was in the one hundred range (from 67 in *Z. mays* to 164 in *B. vulgaris*) (Table 3.1.1). In addition to these mapping studies there is a significant number of studies on the effect of biotic stresses in the leaf apoplast proteome, which as stated above are out of the scope of this review

(Floerl et al., 2008, 2012; Goulet et al., 2010; Kim et al., 2013; Petriccione et al., 2014; Shenton et al., 2012).

The comparison of the leaf apoplastic fluid proteomes led to the assignment of 373 unique AGI proteins (Table S3), with 43 % being predicted as extracellular (Table S4). Although no AGIs were found in all plant species reviewed, the overlap between these leaf apoplastic fluid proteomes was significant, with 77 non-redundant AGIs identified in at least two plant species (Table S3) and a total of 25 proteins found in at least three plant species (Table 3.1.4). This small subset contains 22 extracellular proteins related to polysaccharide metabolism (13), oxido-reductases (three), proteolysis (three), plant defense (two), and general metabolism (one) categories, suggesting that these are conserved functionalities of the leaf apoplastic fluid (Table 3.1.4). Two chloroplast proteins were found among the non-redundant proteins present in at least two plant species (Table 3.1.4) and this underlines the difficulty of obtaining pure apoplastic fluid. Within this subset, *Z. mays, P. deltoides* and *V. vinifera* were the plant species containing the most proteins in common (Table 3.1.4).

Functional classification of this non-redundant leaf apoplastic fluid proteome showed that general metabolism was the most abundant category (27 %) followed by polysaccharide metabolism (21 %), proteolysis (12 %), oxido-reductase (11 %), plant defense (7 %), and regulation (7 %) (Figure 3.1.3). Some of the general metabolism proteins (70 %) have an intracellular localization and most likely reflect some degree of cytoplasmic contamination; this is also clear for the 23 photosynthesis related proteins present in this non-redundant proteome (Table S3). These proteins were found in all the studies regardless of their purity assessment, but their percentages were higher when pressure chamber (18 %) or direct leaf centrifugation (25 %) were used, suggesting that leaf VIC may be better at preventing leakage of proteins from the cytoplasm (Lohaus et al., 2001; Witzel et al., 2011). The overlapping degree of these metabolism-related proteins between species was low (Table S3), suggesting that this category might be over-represented in the non-redundant proteome that compiles proteins from all plant species. Some of the proteins in this group, such as the six lipid transfer proteins and eight extracellular lipases, are indeed annotated as secretory proteins and their presence in the apoplastic fluid may suggest an active role of this fluid in the maintenance of the leaf cell plasma membranes and/or in cuticle biogenesis (Girard et al., 2012). The presence of proteins related to this array of metabolic pathways deserves further studies to clarify the intrinsic metabolic processes occurring in the apoplast.

As described for xylem sap, polysaccharide related proteins accounted for a large proportion of the leaf apoplastic fluid proteome (21 %), with glucosidases and galactosidases being the two larger families present (Table S3). Typical cell wall proteins such as α-mannosidase, chitinase, β-1,3-D-glucosidase, xyloglucan, heparanase, endotransglucosylase-

hydrolase and α- and β-galactosidases (Table S3) have been identified as prominent constituents in different studies, playing various roles in cell wall modification during plant development (Witzel et al., 2011; Zhang et al., 2008). The presence of a high number of hydrolases in this non-redundant proteome confirms that the apoplast is a highly glycolytic compartment (Dietz et al., 2000).

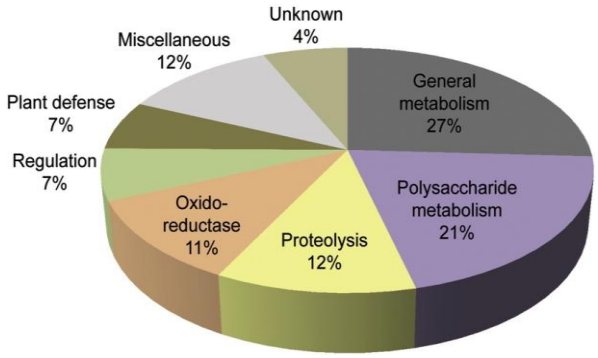

Figure 3.1.3. *Functional classification of the non-redundant leaf apoplast proteome. The 373 Arabidopsis non-redundant proteins obtained from the BLAST of species-specific protein sets against that of A. thaliana were classified based on their gene ontology (GO) biological process and TAIR annotations.*

Plant defense and proteolysis accounted for approximately 19 % of the leaf apoplastic fluid proteome. The plant defense category contains a large number of pathogenesis related proteins (five; four of them extracellular), and disease resistance proteins containing LRR domains (seven; five of them extracellular) (Table S3), which frequently increase in xylem sap and apoplastic fluids when plants experience biotic stresses (Floerl et al., 2008; Islas-Flores et al., 2015; Johansson et al., 2006; Joosten and Wit, 1989; Watson et al., 2004) and, as commented for the xylem sap, constitute a basal plant defense mechanism in non-stressed conditions. The disease resistance proteins with LRR domains may also be involved in signaling (Boudart et al., 2005). Other proteins in this category included extracellular osmotin-like (AT4G11650) and a basic secretory protein (AT2G15130) (Table S3). The proteolysis-related proteins included 24 extracellular peptidases, such as serine-carboxypeptidases, cysteine and aspartic proteases, subtilisin-like serine proteases, and four proteinase inhibitors, most of them similar to cystatin (Table S3). Four proteins related to the proteasome, although not predicted as extracellular, were also found in the non-redundant apoplastic fluid proteome; while it is clear that the apoplastic fluid is enriched in extracellular proteases, the presence of proteasome components was only detected in the sugar beet apoplastic fluid proteome (Ceballos-Laita et al., 2015, Chapter 3.2). It has been hypothesized that the proteolytic composition of the apoplastic fluid is species-dependent (Witzel et al., 2011), and therefore the presence of some components of the proteasome in sugar beet may be species-specific or reflect a possible intracellular contamination.

***Table 3.1.4**. The consistent apoplastic fluid proteome. The list contains 25 non-redundant Arabidopsis-referenced proteins present in at least three of the six plant species for which the leaf apoplast proteome has been described. Accession identifiers are those reported for A. thaliana (Boudart et al., 2005), B. vulgaris (Ceballos-Laita et al., 2015, Chapter 3.2), M. truncatula (Soares et al., 2007), Z. mays (Witzel et al., 2011), V. vinifera (Delaunois et al., 2013) and P. deltoides (Pechanova et al., 2010). Protein identifiers (AGI) and description correspond to the TAIR10 annotation from the BLAST-matched Arabidopsis proteins. Extracellular localization (Y) or non-extracellular localization (N) was described according to the SUBA3 consensus prediction.*

A. thaliana	*B. vulgaris*	*M. truncatula*	*Z. mays*	*V. vinifera*	*P. deltoides*	AGI	Description
AT5G08370			gi|242039251 gi|29468168		Q84VQ7	AT5G08370	α-Galactosidase 2 (Y)
AT3G57240		AF435088		gi|225441379 gi|225441375 gi|163914215 gi|225441373		AT3G57240	β-1,3-Glucanase 3 (Y)
AT2G28470				gi|157337481 gi|157332401 gi|157329180	Q93X57	AT2G28470	β-Galactosidase (Y)
AT5G13980	A9PG55		gi|219887203 gi|241935426 gi|115485699	gi|157343878	Q8LPJ3	AT5G13980	α-Mannosidase (Y)
AT5G64570	V4SY44		gi|146762261 gi|223975771 gi|241939802	gi|157355824 gi|157350003	Q2MCJ5	AT5G64570	β-D-Xylosidase 4 (Y)
AT4G16260	B9GI31	AF239617 O23473 Q6S9W0 Q8GT15 Q9ZP12		gi|170243	Q56AP0	AT4G16260	Putative β-1,3-endoglucanase (Y)
			gi|238908875 gi|195623744 gi|241943398 gi|108707861 gi|77548573	gi|225440254	Q7X9G7	AT3G10740	α-L-Arabino-furanosidase 1 (Y)
			gi|125535042	gi|225426168	Q84LI7	AT3G61490	Polygalacturonase-like (Y)
			gi|255640568 gi|2204224 gi|22240	gi|147810287	Q2MK92	AT5G08380	α-Galactosidase 1 (Y)
			gi|195615700 gi|308081951	gi|157360089	Q9FZP1	AT5G34940	Glucuronidase 3 (Y)
		AAD34596 CAA64868 Q42428 Q7X9F6 Q9SDY6	gi|226507679 gi|241939007 gi|2340043	gi|10880381		AT3G12500	Basic chitinase B (Y)
	Q8LST3	P29024	gi|7687414	gi|225462669	Q09Y38	AT5G24090	Acidic endochitinase (Y)
	P42820 P36910		gi|413937682 gi|116329	gi|15213852 gi|116333 gi|266324 gi|225434076 gi|157353734	Q9M2U5	AT3G54420	Endochitinase EP3 (Y)

(Continued)

Table 3.1.4: continued

A. thaliana	*B. vulgaris*	*M. truncatula*	*Z. mays*	*V. vinifera*	*P. deltoides*	AGI	Description
AT5G20630	I3SGS4	CAC34417	gi|226504688	gi|225444754		AT5G20630	Germin-like protein subfamily 3 member 3 (Y)
	D7SXW6	AY185207		gi|225429295	Q9XIY9	AT2G15220	Basic secretory protein family (Y)
AT5G67360	XP_ 006466502		gi|125544798 gi|226508174 gi|195647626 gi|223947903	gi|1771160 gi|157335622 gi|157345245	Q8RVJ7	AT5G67360	Subtilisin-like protease SBT1.7 (Y)
	E0CQB3		gi|242048242	gi|157335112	Q8LAE1	AT1G20160	Serine-type endopeptidase (Y)
	XP_ 008235895		gi|226533158	gi|157348245	Q8L7B2	AT4G12910	Serine carboxypeptidase-like 20 (Y)
	Q38745	O04364	gi|226505234	gi|225426801 gi|225426793	Q8GUQ2	AT4G11650	Osmotin (Y)
			gi|257644672	gi|223635592	Q9ZNZ5	AT1G05260	Peroxidase (Y)
	H9BQP8	AAC14127		gi|134684	A9PJW9	AT2G28190	Superoxide dismutase [Cu-Zn] 2 (N)
			gi|125597507	gi|157355447 gi|225459180	Q58GF4	AT5G05340	Peroxidase 52 (Y)
	XP_ 007014796		gi|226493671	gi|225435616	Q42517	AT5G19890	Peroxidase 59 (Y)
		CAA26709	gi|130280		P00299	AT1G20340	Plastocyanin major isoform (N)
	B0L802	AW559699	gi|157482855			AT1G06680	Oxygen-evolving enhancer protein 2-1 (N)

Among the proteins classified as oxido-reductases (11 %), 19 were predicted to be extracellular. These included a large number of peroxidases (ten), cupro-redoxins (three), and FAD-binding proteins (three), among others (Table S3). Furthermore, three peroxidases were found in three or more plant species (Table 3.1.4) suggesting that their presence is highly conserved in this fluid. Five thioredoxins were also found in the non-redundant apoplastic fluid proteome, although only one of them was predicted as extracellular. Thioredoxins are also abundant in the phloem sap proteome (Ishiwatari et al, 1995) and, in addition to redox homeostasis, some thioredoxins have been associated with inter-cellular communication and may be required for redox signaling (Meng et al., 2010) (Table S3).

Interestingly, as it occurs in phloem sap, the apoplastic fluid also contains proteins involved in regulation including RNA binding (7 %), although only two proteins were predicted as extracellular. This set of extracellular proteins included an auxin-independent growth promoter-like protein (AT5G63390) and a homolog of CLAVATA 1b (a putative receptor kinase) (Table S3). The latter one was probably identified as a proteolytic fragment belonging to

the extracellular domain (Boudart et al., 2005). The presence of these proteins in the apoplast may suggest a role of this compartment in signaling that deserves further study.

In summary, the functional categorization of the apoplastic fluid proteome indicates that a large part of this proteome is involved in basal defense and in the maintenance of the cell wall and possibly the leaf cell plasma membrane. The functional categorization also reveals a possible role in regulation and points out candidates which deserve further study. However, it should be kept in mind that 57 % of the non-redundant apoplastic fluid proteome is predicted to be intracellular and therefore some of these enriched functional categories may arise from cytoplasmic contamination and deserve additional studies.

3.1.7. The root apoplastic fluid proteome

To the best of our knowledge, a comprehensive description of the root apoplastic fluid proteome has not been published yet. There are two studies in rice describing the effects of H_2O_2 and salt stress on the proteome of the root apoplastic fluid (Zhang et al., 2009; Zhou et al., 2011). Both studies used VIC and 2-DE to obtain 400 and 100 spots using 24 and 13 cm IPG strips, respectively. Although mapping was not performed in these studies, proteins identified as responsive to NaCl and H_2O_2 belong to two of the categories, defense and redox, described in the leaf apoplastic fluid proteome.

3.1.8. Conclusion and outlook

The overlap of the non-redundant plant fluid proteomes (Figure 3.1.4) indicates that xylem and apoplastic fluid share more proteins between them (117) than with the phloem sap (40 and 38 proteins in common in each comparison, respectively), highlighting the peculiar composition of the phloem sap proteome. Although the overlap in unique identifiers is somewhat limited, there are functional categories, including polysaccharide metabolism, defense, proteolysis and oxido-reductases that occur in the three fluids, altogether accounting for large percentages of their proteomes. These categories indicate that plant fluids contain the machinery needed for the maintenance of xylem vessels, phloem sieve elements and cell walls, and for basal defense processes. It is also interesting to note that a significant number of proteins in these categories, such as peroxidases or proteases, have dual roles in both defense and structural maintenance. The relatively low number of common identifiers may indicate that the specific proteins in charge of these functions are fluid-specific. On the other hand, the category regulation is enriched to a higher extent in phloem sap (Figure 3.1.2) than in xylem sap (Figure 3.1.1) and apoplastic fluid (Figure 3.1.3), highlighting the role of phloem sap in long distance signaling and communication. The comparison of the non-redundant proteomes reveals 14 proteins commonly found in the three plant fluids (Table 3.1.5, Figure 3.1.4), among them, four of them

being predicted as extracellular. These included three extracellular glycosidase hydrolases from the families 17, 18 and 38 as well as peroxidase 54, indicating a possible universal role of these proteins in cell wall maintenance and defense. Functional classification of the remaining ten intracellular proteins indicates that plant fluid proteomes share proteins related to general metabolism (three proteins), amino acid metabolism (two), oxido-reductases (two), as well as in nucleotide metabolism (nucleoside diphosphate kinase 1) and photosynthesis (small subunits 3B and 1A of Rubisco). These intracellular proteins may reflect intracellular contamination and their presence in these fluids needs to be further addressed. The pairwise overlaps indicate that xylem and apoplastic fluids share a large number of polysaccharide metabolism related proteins (41 proteins, accounting for 35 % of the shared proteins), whereas phloem and xylem or apoplast share proteins related to general metabolism and oxido-reductase categories, accounting for approximately 50 % of the common proteins (Figure 3.1.4).

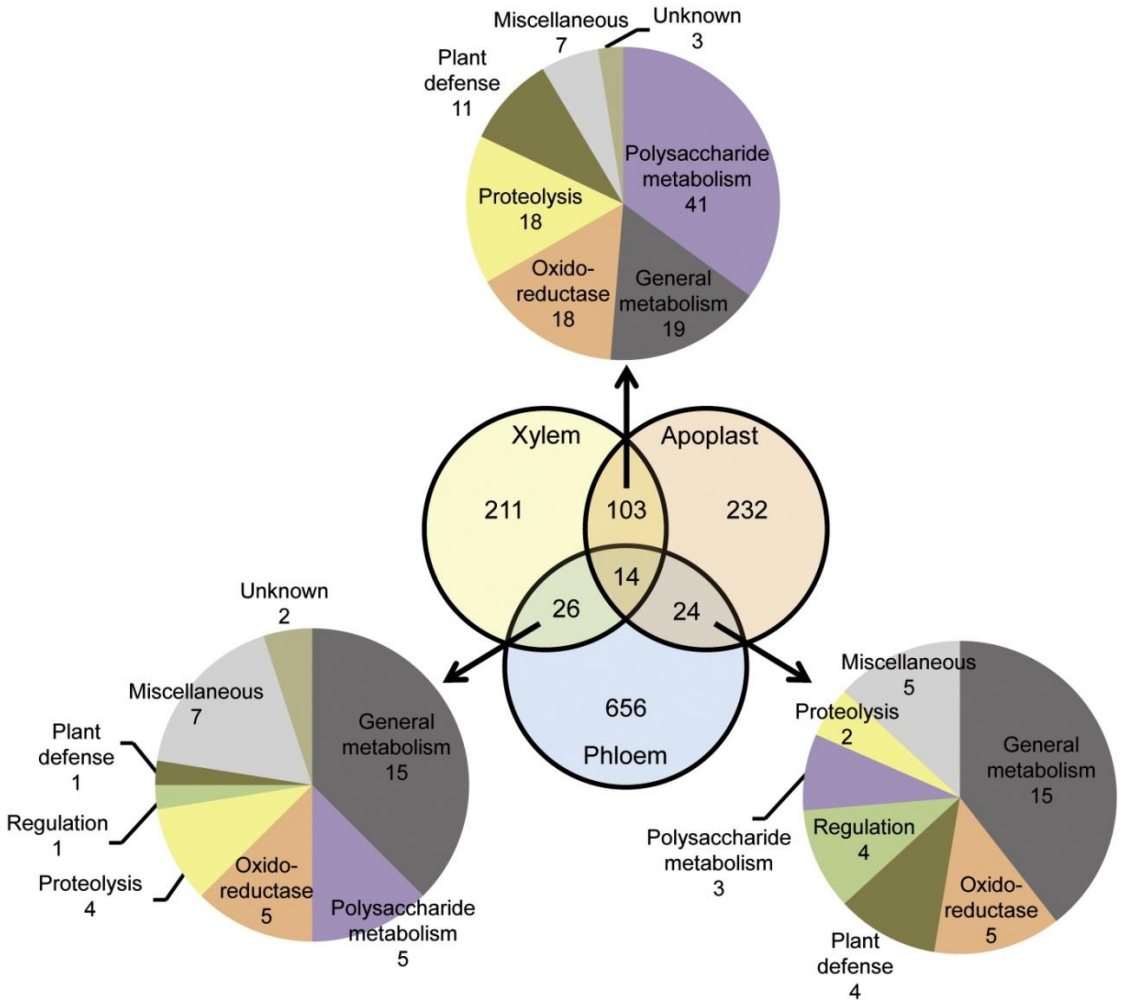

Figure 3.1.4. *Overview of the similarities among xylem sap, phloem sap and leaf apoplastic fluid proteomes. The Venn diagram shows the overlap of the non-redundant plant fluid proteomes provided in Tables S1–3. Functional analysis is presented for each of the pair-wise overlaps. The 14 overlapping proteins among the three fluids are listed in Table 3.1.5.*

Extracellular proteins accounted for 57, 43 and 1 % of the xylem sap, leaf apoplastic fluid and phloem sap proteomes, respectively. These data clearly distinguish the phloem sap proteome from those of the leaf apoplastic fluid and xylem sap. When specifically looking at peroxidases as an example, the phloem sap non-redundant proteome only contained four peroxidases, with one of them being extracellular, whereas xylem sap and apoplastic fluids contained a larger number of peroxidases, most of them being extracellular. These results also point out that significant percentages of these non-redundant proteomes are predicted to be intracellular, and therefore additional experiments are needed to ascertain the presence and possible role of these proteins in plant fluids.

The compilation of the studies reviewed has allowed us to obtain a composite picture of each plant fluid proteome and has clarified major functions occurring in these compartments. The comparison between these three plant fluid proteomes highlights their differences and commonalities, thus providing hints into possible functionalities specific and shared by them and has pointed out several candidates for which their functions in these compartments deserve further studies (i.e., proteins presented in Tables 3.1.2–5, especially the extracellular ones).

Table 3.1.5*. List of the 14 proteins present in the proteomes of xylem sap, phloem sap and apoplastic fluid. Symbols and description correspond to TAIR10 annotation.*

AGI	Symbol	Extracellular*	Annotation
AT2G36530	ENO2	N	Enolase 2
AT3G04120	GAPC1	N	Cytosolic GADPH-1
AT5G43330	MDH2	N	Malate dehydrogenase
AT5G17920	MS1	N	Methionine synthase
AT4G31990	ASP5	N	Aspartate aminotransferase
AT4G09320	NDK1	N	Nucleoside diphosphate kinase 1
AT5G13980		Y	Glycosyl hydrolase family 38 protein
AT4G16260		Y	Putative β-1,3-endoglucanase
AT5G24090	CHIA	Y	Chitinase A (class III)
AT1G07890	APX1	N	L-ascorbate peroxidase 1
AT1G11840	GLX1	N	Lactoylglutathione lyase
AT5G38410	RBCS3B	N	Rubisco small subunit 3B
AT1G67090	RBCS1A	N	Rubisco small chain 1A
AT5G06730	PRX54	Y	Peroxidase 54

* *Localization according to the SUBA3 consensus prediction.*

However, there are still many gaps that need to be addressed to obtain a complete picture. On one hand, the use of the high-throughput and more sensitive LC–MS/MS proteomic approaches can increase the inventory of these proteomes. On the other hand, ProteoMiner protein enrichment technologies (Frohlich et al., 2012; Righetti et al., 2008) may help to reveal low abundance proteins such as those involved in signaling that might be underrepresented in protein extracts, but that still play important roles in the long-distance communication system. Indeed, this technique has been recently used to study root cell wall proteins in *Arabidopsis*

allowing one to identify low abundance proteins never described before in cell walls (Nguyen-Kim et al., 2016). These studies need to be performed in a variety of plant species to reveal fluid specific and species-specific processes occurring in these plant fluids. Furthermore, given the high enrichment of these plant fluids in glycoproteins, specific studies of this subproteome and progress in bioinformatics tools to predict plant-specific glycoproteins will provide further insights into these plant fluids.

Given the invasive nature of the methods used for the collection of these fluids, clear criteria and well-established protocols to assess their purity are needed, including the establishment of thresholds for contamination and the use of data validation *via* complementary techniques such as Western blot, immuno- and GFP-localization techniques. Although the coverage of plant fluid proteomes has improved considerably, its integration with other high-throughput techniques is still lacking. Proteomic data combined with small RNA sequencing and metabolomics using a system biology approach could provide a holistic view of plant fluids and provide new insights into their functions. Finally, while there is no doubt that some proteins found in phloem and xylem sap are being translocated, this information is lacking for other proteins and experiments are needed to clearly demonstrate that these proteins are being unloaded into the target tissues. This is especially relevant for putative signaling proteins for which, in addition to delivery, a function in the sink tissue needs to be proven.

Supplementary material

Supplementary data to this article can be found online at http://dx.doi.org/10.1016/j.bbapap.2016.03.014: **Table S1.** Non-redundant xylem sap proteome. Protein identifiers (AGI), functional categorization and description correspond to the TAIR10 annotation; **Table S2.** Non-redundant phloem sap proteome. Protein identifiers (AGI), functional categorization and description correspond to the TAIR10 annotation; **Table S3.** Non-redundant apoplastic fluid proteome. Protein identifiers (AGI), functional categorization and description correspond to the TAIR10 annotation; **Table S4.** Protein localization by SUBA3.

3.2. Protein profile of *Beta vulgaris* leaf apoplastic fluid and changes induced by Fe deficiency and Fe resupply

Laura Ceballos-Laita [a], Elain Gutierrez-Carbonell [a], Giuseppe Lattanzio [a], Saul Vázquez [a], Bruno Contreras-Moreira [b,c], Anunciación Abadía [a], Javier Abadía [a] and Ana-Flor López-Millán [a]

[a] *Department of Plant Nutrition, Aula Dei Experimental Station, Consejo Superior de Investigaciones Científicas (CSIC), Zaragoza, Spain*

[b] *Laboratory of Computational and Structural Biology, Aula Dei Experimental Station, Consejo Superior de Investigaciones Científicas (CSIC), Zaragoza, Spain*

[c] *Fundación ARAID, Zaragoza, Spain*

Published in Frontiers in Plant Science (2015) 6, 145 (*doi: 10.3389/fpls.2015.00145*)

ABSTRACT

The fluid collected by direct leaf centrifugation has been used to study the proteome of the sugar beet apoplastic fluid as well as the changes induced by Fe deficiency and Fe resupply to Fe-deficient plants in the protein profile. Plants were grown in Fe-sufficient and Fe-deficient conditions, and Fe resupply was carried out with 45μM Fe(III)-EDTA for 24 h. Protein extracts of leaf apoplastic fluid were analyzed by two-dimensional isoelectric focusing-SDS-PAGE electrophoresis. Gel image analysis revealed 203 consistent spots, and proteins in 81 % of them (164) were identified by nLC–MS/MS using a custom made reference repository of beet protein sequences. When redundant UniProt entries were deleted, a non-redundant leaf apoplastic proteome consisting of 109 proteins was obtained. TargetP and SecretomeP algorithms predicted that 63 % of them were secretory proteins. Functional classification of the non-redundant proteins indicated that stress and defense, protein metabolism, cell wall and C metabolism accounted for approximately 75 % of the identified proteome. The effects of Fe deficiency on the leaf apoplast proteome were limited, with only five spots (2.5 %) changing in relative abundance, thus suggesting that protein homeostasis in the leaf apoplast fluid is well-maintained upon Fe shortage. The identification of three chitinase isoforms among proteins increasing in relative abundance with Fe deficiency suggests that one of the few effects of Fe deficiency in the leaf apoplast proteome includes cell wall modifications. Iron resupply to Fe-deficient plants changed the relative abundance of 16 spots when compared to either Fe-sufficient or Fe-deficient samples. Proteins identified in these spots can be broadly classified as those responding to Fe resupply, which included defense and cell wall related proteins, and non-responsive, which are mainly protein metabolism related proteins and whose changes in relative abundance followed the same trend as with Fe deficiency.

3.2.1. Introduction

Iron is the fourth most abundant element in the earth's crust and it is an essential micronutrient for all living organisms including plants. However, its low availability in neutral or alkaline soils, which account for approximately 30 % of the world's arable soils, causes Fe deficiency (Abadía et al., 2004). Iron deficiency is the most common nutritional disorder in many plants and typical symptoms include chlorosis of young leaves (leaf yellowing) and reduced crop yield and quality, which result in increased orchard management costs (Álvarez-Fernández et al., 2006; Rombolà and Tagliavini, 2006; Abadía et al., 2011).

Plants have developed two main mechanisms to allow Fe uptake from the soil: a strategy based on Fe (III) chelation (Strategy II) used by graminaceous plants, and a strategy used by non-graminaceous plants based on Fe(III) reduction (Strategy I) (Römheld and Marschner, 1986; Curie and Briat, 2003; Abadía et al., 2011). When challenged with Fe shortage, Strategy I plants such as *Beta vulgaris* increase the activity of several enzymes at the root plasma membrane level. These changes are aimed at increasing Fe uptake and include increases in a Fe(III) reductase (FRO, Ferric Reductase Oxidase; Robinson et al., 1999), an Fe transporter (IRT1, Iron Regulated Transporter) which introduces Fe(II) into the root cell (Eide et al., 1996; Fox and Guerinot, 1998) and an H^+-ATPase that lowers the pH of the rhizosphere increasing soil Fe solubility (Santi et al., 2005; Santi and Schmidt, 2008, 2009). Also, several changes occur at the metabolic level in order to support the increased demand of energy and reducing power of Fe-deficient Strategy I roots (Zocchi, 2006). These changes include increased activity of the glycolytic pathway and TCA cycle, shifts in the redox state of the cytoplasm and in the mitochondrial electron transport chain (Schmidt, 1999; López-Millán et al., 2000b; Zocchi, 2006; Vigani, 2012).

While it is well-known that Fe is transported to the shoot *via* xylem, complexed by citrate (López-Millán et al., 2000a; Rellán-Álvarez et al., 2010), the mechanisms for Fe loading and unloading from the vasculature system are not yet fully understood. These processes could take place *via* parenchyma cells or by passive diffusion to the apoplastic space driven by transpiration (Abadía et al., 2011). Also, Fe uptake by mesophyll cells is not as well-studied as in roots. An Fe-reductase activity has been detected in leaf cells and protoplasts (Nikolic and Römheld, 1999; González-Vallejo et al., 2000; Jeong and Connolly, 2009) and AtFRO6 has been located in leaf PM-membranes (Mukherjee et al., 2006; Jeong et al., 2008). However, *fro6* mutant plants do not display any Fe deficiency symptoms (Jeong and Connolly, 2009) therefore suggesting the existence of other reducing mechanisms. Factors such as differences in apoplastic pH and carboxylate concentrations as a result of Fe deficiency may also regulate leaf Fe reductase activity. On the other hand, light has also been proposed to directly photoreduce Fe (III)-citrate complexes in the leaf apoplast (Nikolic and Römheld, 2007).

The apoplast is a free diffusional space outside the plasma membrane that occupies less of 5 % of the plant tissue volume in aerial organs (Steudle et al., 1980; Parkhurst, 1982) and the root cortex (Vakhmistrov, 1967). Among other important functions, such as transport and storage of minerals (Starrach and Mayer, 1989; Wolf et al., 1990; Zhang et al., 1991) or signal transmission (Hartung et al., 1992), the apoplast plays a major role in plant defense (Pechanova et al., 2010). Given that the composition of the apoplastic fluid results from the balance between xylem and phloem transport and mesophyll cell uptake processes, small changes in these fluxes could produce large changes in the solute concentrations in the apoplast. Changes in the apoplastic composition have been described in biotic and abiotic stresses such as Fe deficiency, air pollutants, heavy metal toxicity, drought, salinity, and extreme temperature (Griffith et al., 1992; Brune et al., 1994; Covarrubias et al., 1995; Dietz, 1997; López-Millán et al., 2000a; Fecht-Christoffers et al., 2003). For instance, Fe deficiency causes a slight decrease in the pH of the apoplast and has a strong impact on the carboxylate composition, with major increases in the concentrations of citrate and malate (López-Millán et al., 2000a). These Fe deficiency induced changes in the leaf apoplast chemical environment have been suggested to play a role in Fe homeostasis (López-Millán et al., 2000a).

Apoplastic fluid isolation is always carried out using some degree of force (e.g. vacuum perfusion, leaf centrifugation or pressure using a Schölander bomb), therefore leading to the presence of some cytosolic components in the samples (Lohaus et al., 2001). This contamination may be originated by the rupture of a certain fraction of the leaf mesophyll cells, or, alternatively, by the rupture of the plasmodesmata that communicate neighboring cells. The degree of contamination is usually assessed using cellular marker enzymes such as cytosolic malate deshidrogenase (c-mdh) or other cytoplasmic or internal organelle components, with values ≤ 3 % considered acceptable (Dannel et al., 1995; Lohaus et al., 2001).

Proteomic approaches are useful to understand the general effect that a given stress exerts on metabolic processes (Jorrín-Novo et al., 2009). These approaches have been previously used to study the effects of Fe deficiency in several plant tissues, including thylakoids and roots (López-Millán et al., 2013). Most of the leaf apoplastic proteomic studies so far have been devoted to the study of the protein profile or the effect of biotic stresses. However, knowledge about the effects of nutritional stresses such as Fe deficiency in the apoplastic fluid protein profile is still very limited. Therefore, the aim of this study was first to obtain an overview of the leaf apoplast proteome in sugar beet plants and second to characterize the changes induced by Fe deficiency and resupply in the protein profile of this compartment, with the final goal of shedding light into the major processes taking place in the apoplast and the effect of Fe deficiency on them.

3.2.2. Material and methods

Plant material and growth conditions

Sugar beet (*Beta vulgaris* L. cv. Orbis) was grown in a growth chamber with a photosynthetic photon flux density (PPFD) of 350 μmol m^{-2} s^{-1} photosynthetically active radiation, 80 % relative humidity and a photoperiod of 16 h, 23 ºC/8 h, 18 ºC day/night regime. Seeds were germinated and grown in vermiculite for 2 weeks. Seedlings were grown for an additional 2 weeks period in half-strength Hoagland nutrient solution with 45 μM Fe(III)-EDTA, and then transplanted to 20 L plastic buckets (four plants per bucket) containing half-strength Hoagland nutrient solution with either 0 or 45 μM Fe(III)-EDTA. Iron-free nutrient solutions were buffered at pH 7.7 with 1 mM NaOH and 1 g L^{-1} of $CaCO_3$. Young leaves from plants grown for 10 d in the presence and absence of Fe were used to collect the apoplastic fluid in all experiments. In the Fe resupply experiment, 45 μM Fe (III)-EDTA was added to the nutrient solution of plants grown for 10 d in the absence of Fe. The apoplastic fluid of these plants was collected 24 h after Fe addition.

Experimental design

The experiment was repeated four times with independent sets of plants. Each batch of plants consisted of four buckets per treatment with four plants per bucket. Apoplastic fluid was isolated from the four to five youngest leaves of each plant. Cytosolic contamination was assayed in each sample as described below. Samples with less than 3 % of cytosolic contamination from a given treatment per batch were pooled together and considered as a biological replicate (n = 4).

Collection of leaf apoplastic fluid

Leaf apoplastic fluid was obtained from whole sugar beet leaves by direct centrifugation (López-Millán et al., 2000a). Briefly, leaves were excised at the base of the petiole and each leaf was rolled and placed into a plastic syringe barrel. Leaf-filled syringes were first centrifuged at low speed (2500 × *g*, 4 ºC, 15 min) to remove the xylem sap from the main vein and the fluid collected was discarded. A second centrifugation was then carried out at 4 ºC, 4000 × *g* for 15 min and the fluid collected was considered as soluble apoplastic fluid. The activity of cytosolic malate dehydrogenase (c-mdh; EC 1.1.1.37) in the collected fluid was measured immediately and used as a cytosolic contamination marker. The activity of c-mdh was measured spectrophotometrically at 340 nm in a final reaction mixture containing 46.5 mM Tris (pH 9.5), 0.1 mM NADH, 0.4 mM oxaloacetate and 5 μL of apoplastic fluid and referred to activity

measured in a whole leaf extract (López-Millán et al., 2000a). For the activity in whole leaf extracts, approximately 0.1 g of leaf tissue was homogenized with 2 mL of a buffer (pH 8.0) containing 100 mM HEPES, 30 mM sorbitol, 2 mM DTT, 1 mM $CaCl_2$, 1 % (w/v) bovine serum albumin and 1 % (w/v) polyvinylpyrrolidone. The supernatant was collected and analyzed immediately after a 10 min centrifugation at 10,000 × *g*.

Protein extraction

Proteins in approximately 1 mL of apoplastic fluid were precipitated by adding five volumes of cold 10 % trichloroacetic acid. Samples were incubated for at least 14 h at 4 ºC and then centrifuged at 10,000 × *g* for 15 min. The pellet was washed twice with cold methanol, dried with N_2 gas and solubilized in a sample rehydration buffer containing 8 M urea, 2 % (w/v) CHAPS, 50 mM DTT, 2 mM PMSF and 0.2 % (v/v) IPG buffer pH 3-10 (GE Healthcare, Uppsala, Sweden). After rehydration, samples were incubated in a Thermomixer Confort device (Eppendorf AG, Hamburg, Germany) at 42 ºC and 1000 rpm during 3 h, then centrifuged at 10,000 × *g* for 10 min at room temperature and filtered (0.45 μm ultrafree-MC filters, Millipore, Bedford, USA). Protein concentration in the samples was quantified immediately with the Bradford method in microtiter plates using an Asys UVM 340 spectrophotometer (Biochrom Ltd., Cambridge, UK) and BSA as standard.

2-DE

A first dimension IEF separation was carried out on 7 cm ReadyStrip IPG Strips (BioRad, Hercules, CA, USA) with a linear pH gradient 3-10 in a Protean IEF Cell (BioRad). Strips were passively rehydrated for 16 h at 20 ºC in 125 μL of rehydration buffer containing 80 μg of apoplast proteins and a trace of bromophenol blue and then strips were transferred onto a strip electrophoresis tray. IEF was run at 20 ºC, for a total of 14,000 V h (20 min with 0-250 V linear gradient; 2 h with 250-4000 V linear gradient and 4000 V until 10,000 V h). After IEF, strips were equilibrated for 10 min in equilibration solution I [6 M urea, 0.375 M Tris-HCl, pH 8.8, 2% (w/v) SDS, 20 % (v/v) glycerol, 2 % (w/v) DTT] and for another 10 min in equilibration solution II [6 M urea, 0.375 M Tris-HCl pH 8.8, 2 % (w/v) SDS, 20 % (v/v) glycerol, 2.5 % (w/v) iodoacetamide]. For the second dimension, polyacrylamide gel electrophoresis (SDS-PAGE) and equilibrated IPG strips were placed on top of vertical 12 % SDS-polyacrylamide gels (8 × 10 × 0.1 cm) and sealed with melted 0.5 % agarose in 50 mM Tris-HCl (pH 6.8) containing 0.1 % SDS. SDS-PAGE was carried out at 20 mA per gel for approximately 1.5 h at 4 ºC, until the bromophenol blue reached the plate bottom, in a buffer containing 25 mM Tris Base, 192 mM glycine, and 0.1 % SDS. Gels were subsequently stained with Coomassie blue G-250 (Serva, Barcelona, Spain). For each treatment, gels were made from four independent

apoplast protein extracts (n = 4), each of them obtained by pooling the apoplastic fluid collected from 5 to 6 leaves in a given batch.

Gel image and statistical analysis

Stained gels were scanned with an Epson Perfection 4990 Photo Scanner (Epson Ibérica, Barcelona, Spain), previously calibrated using the SilverFast 6 software (LaserSoft Imaging AG, Kiel, Germany) using an IT8 reference card. Experimental Mr values were calculated by mobility comparisons with Precision Plus protein standard markers (BioRad) run in a separate lane on the SDSgel, and pI was determined by using a 3-10 linear scale over the total dimension of the IPG strips. Spot detection, gel matching and interclass analysis were performed with PDQuest 8.0 software (BioRad). Normalized spot volumes based on total intensity of valid spots were calculated for each 2-DE gel and used for statistical calculations of protein abundance; for all spots present in the gels, pI, Mr, and normalized volumes (mean values and SD) were determined. Only spots present in all four replicates from at least one treatment were considered as consistent and used in further analysis. The spots were also manually checked, and a high level of reproducibility between normalized spot volumes was found in all four different replicates.

Univariate and multivariate statistical analyses were carried out. Protein response ratios were defined as the relative abundance in a given treatment divided by the relative abundance in the control; when ratios were lower than one the inverse was taken and the sign changed. Spots changing in relative abundance were defined using a Student *t*-test and a significance level of $p < 0.05$. Among these, only protein species with mean response ratios above 2.0 or below -2.0 were considered relevant and are discussed in this study. Principal component analysis (PCA) analysis was also carried out, using Statistical software (v. 10.0) and including only those spots showing differential accumulation as a result of the Fe deficiency and Fe resupply treatments.

Protein in gel digestion

Consistent spots were excised automatically using a spot cutter EXQuest (BioRad), transferred to 500 μL Protein LoBind Eppendorf tubes, distained in 400 μL of 40 % [v/v] acetonitrile (ACN) and 60 % [v/v] 200 mM NH_4HCO_3 for 30 min and dehydrated in 100 % ACN for 10 min. Gel pieces were dried at room temperature and then in gel digested with 15 μL Trypsin solution (Sequencing Grade Modi- fied Trypsin V511, Promega, Madison, WI, US; 0.1 μg μL^{-1} in 40 mM NH_4HCO_3 / 9 % ACN). After incubation for 5 h at 37 ºC, the reaction was stopped by adding 1 μL of 1 % trifluoroacetic acid. The peptide solution was finally analyzed using mass spectrometry (MS).

Reference repository of beet protein sequences

Proteomes of five sequenced beet accessions (RefBeet, KDHBv, YMoBv, UMSBv and YTiBv) were downloaded from http://bvseq.molgen.mpg.de/Genome/Download, corresponding to gene models annotated as of February 2013. In addition, all *B. vulgaris* protein sequences annotated in Uniprot (www.uniprot.org) were retrieved, and added to the set, which was subsequently filtered to remove redundant sequences with software CD-HIT (http://www.ncbi.nlm.nih.gov/pubmed/ 23060610) with cutoff-c 1.0 and otherwise default parameters. The final non-redundant set contained 82,368 protein sequences.

Protein identification by nano-liquid chromatography-tandem mass spectrometry (nLC-ESI-MS/MS)

Peptides present in 6 μL of sample were pre-concentrated on line onto a 300 μm i.d. × 5 mm, 5 μm particle size ZORBAX 300SB-C18 trap column (Agilent Technologies, Waldbronn, Germany), using a 100 μL min^{-1} flow rate of 3 % ACN, 0.1 % formic acid, in a nano-HPLC system 1200 series (Agilent Technologies). Backflow elution of peptides from the trap column was carried out, and separation was done with a 75 μm i.d. × 150 mm, 3.5 μm particle size ZORBAX 300SB-C18 column (Agilent Technologies), using a 300 nL min^{-1} nano-flow rate and a 55 min linear gradient from solution 97 % A (0.1 % formic acid) to 90 % of solution B (90 % ACN, 0.1 % formic acid). The nano-HPLC was connected to a HCT Ultra high-capacity ion trap (Bruker Daltoniks, Bremen, Germany) using a PicoTip emitter (50 μm i.d., 8 μm tip i.d., New Objective, Woburn, MA, USA) and an on line nano-electrospray source. Capillary voltage was × 1.8 kV in positive mode and a dry gas flow rate of 10 L min^{-1} was used with a temperature of 180 ºC. The scan range used was from 300 to 1500 m/z. The mass window for precursor ion selection was ± 0.2 Da and the rest of parameters were those recommended by the manufacturer for MS/MS proteomics work. Peak detection, deconvolution and processing were performed with Data Analysis 3.4 software (Bruker Daltoniks).

Protein identification was carried out using the Mascot search engine v. 2.5.0 (Matrix Science; London, UK) and the non-redundant *B. vulgaris* 20140811 (82,368 sequences; 28,127,547 residues), NCBI 20130310 (23,641,837 sequences; 8,123,359,852 residues), and Plants_EST EST_114 20140804 (158,278,518 sequences; 27,948,288,346 residues). Search parameters were: monoisotopic mass accuracy, peptide mass tolerance ± 0.2 Da, fragment mass tolerance ± 0.6 Da, one allowed missed cleavage, fixed modification carbamidomethylation (Cys), and variable modification oxidation (Met). Positive identification was assigned with Mascot p-values below the threshold ($p < 0.05$), at least two identified peptides with a score above homology, 10 % sequence coverage and similar experimental and theoretical MW and pI

values. We used the GO biological process annotation (http://www.geneontology.org) for classification of each individual protein identified. The secretion of apoplastic proteins was predicted using TargetP (www.cbs.dtu.dk/services/TargetP) (Emanuelsson et al., 2007), and SecretomeP (www.cbs.dtu.dk/services/SecretomeP) analysis to predict classical and non-classical secreted proteins, respectively (Bendtsen et al., 2004, 2005).

Quantitative RT-PCR

Expression of chitinase and thaumatin genes was analyzed by qRT-PCR in two batches of plants. Total RNA from *B. vulgaris* leaves was isolated using the RNeasy Plant mini kit from QIAGEN (QIAGEN Inc., Valencia, CA, USA) according to the manufacturer's instructions. Samples were treated with DNAsa (recombinant DNase from Macherey-Nagel, Düren, Germany) to remove contaminating genomic DNA. The concentration of RNA and cDNA was determined with a Nanodrop system (Thermo Fisher Scientific, Waltham, MA, USA) and the structural integrity the RNA was checked using non-denaturing agarose gel stained with SybrSafe (Invitrogen, Carlsbad, CA, USA). One μg of total RNA was reverse transcribed to cDNA by using the SuperScript III reverse transcriptase and 2.5μM poly$(dT)_{20}$ primer in a final volume of 20 μl according to the manufacturer's instructions (Invitrogen, Carlsbad, CA, USA). Quantitative real time polymerase chain reactions were performed in a AB7500 Fast Real-Time PCR system (Applied Biosystems by Life Technologies, Grand Island, New York) with equal amount of cDNA for all samples and 10 μl SYBR green master mix (Applied Biosystems, Warrington, UK) using gene specific primers and two different housekeeping genes (actin and tubulin) in a final volume of 20 μl. Primer sequences and fragment sizes are listed in Table S1. The qPCR program was 50 ºC for 2 min, 95 ºC for 10 min, 40 cycles of 95 ºC for 15 s and 60 ºC for 1 min; and a final dissociation stage of 95 ºC for 15 s, 60 ºC for 1 min, and 95 ºC for 30 s. A previous experiment was performed to assess for primer efficiency with different sets of primers for each target gene. Primer efficiencies of the chosen sets are listed in the Table S1.

Low-temperature scanning electron microscopy

Leaf pieces were mounted on aluminum stubs with adhesive (Gurr®, optimum cutting temperature control; BDH, Poole, UK), cryo-fixed in slush nitrogen (-196 ºC), cryo-transferred to a vacuum chamber at -180 ºC, and then fractured using a stainless steel spike. Once inside the microscope, the samples underwent superficial etching under vacuum (-90 ºC, 120 s, 2 kV), and then were overlaid with gold for observation and microanalysis. This freeze-fracture procedure leads to cell rupture only at the fracture plane, whereas the general internal leaf structure is well-preserved. Fractured samples were observed at low temperature with a digital scanning electron microscope (Zeiss DSM 960, Oberkochen, Germany) using secondary and back-scattered

electrons. Secondary electron images (1024 × 960 pixels) were obtained at 133 eV operating at a 35º take-off angle, an accelerating voltage of 15 kV, a working distance of 25 mm and a specimen current of 1-5 nA. Microscopy was run in the Institute of Agricultural Sciences-CSIC (ICA-CSIC), Madrid, Spain.

3.2.3. Results

Sugar beet plants showed Fe deficiency symptoms 5 days after the treatment onset, with a marked yellowing of the younger leaves (Table S2). A freeze-fracture electron microscopy micrograph provided a representative image of a *B. vulgaris* leaf, with the apoplastic space surrounding mesophyll cells, as well as the epidermal cells and the minor vein tissues (Figure 3.2.1). The micrograph also shows the presence of plasmodesmata that communicate neighboring cells.

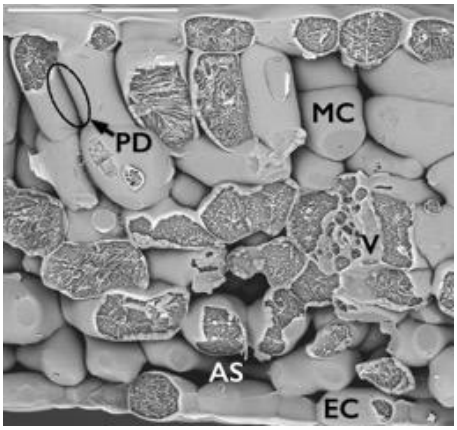

Figure 3.2.1. *Freeze-fracture low-temperature scanning electron micrograph of a transversal section from a Beta vulgaris leaf. This leaf transversal section gives three-dimensional information on the internal structure of the leaf. Apoplastic space (AS in white letters) surrounds mesophyll (MC) and epidermal cells (EC). The image also shows the presence of plasmodesmata (PD) that communicate neighboring mesophyll cells.*

The apoplastic fluid collected from these leaves was assayed for c-mdh activity and only samples with contamination levels < 3 % (mean 1.72 %, expressed on a total leaf activity basis) were used for 2-DE protein profiling (Table S2). Typical protein extraction yields ranged between 0.4 and 0.8 μg protein μL^{-1} of apoplastic fluid (Table S2).

Protein profiles of the apoplastic fluid

The protein profile of apoplast extracts from *B. vulgaris* leaves was studied by 2-DE IEF-SDS-PAGE electrophoresis. Experimental conditions allowed for the separation of proteins within pI and MW ranges from 3.5 to 8 and from 18 to 106 kDa, respectively. Typical real scans of 2-DE gels obtained from apoplastic fluid protein extracts of Fe-sufficient (+Fe), Fe-deficient (-Fe), and Fe-resupplied Fe-deficient plants (-FeR) are shown in Figure 3.2.2A-C, respectively. The

average number of detected spots (mean ± SD) was 210 ± 12, 216 ± 11, and 211 ± 20 in gels from plants grown in +Fe, -Fe, and -FeR conditions, respectively (Table S3 and Figure S1). The total number of spots consistently detected in the whole experiment (present in all four gels of at least one treatment) was 203. A composite averaged virtual map containing all consistent spots is shown in Figure 3.2.2D.

All consistent spots were analyzed by MS, and proteins were unambiguously identified in 78 % of the cases (158 spots) (Table S4 and Figure S1). A large percentage (97 %) of identifications was achieved using the beet custom reference repository. To identify UniProt entries, BLAST searches (E-values < $1e^{-30}$) of the unambiguously identified protein hits were run when needed. This approach revealed a high degree of redundancy in the identified protein species. When duplicates (same UniProt entry) were removed, the 158 identified proteins were reduced to 109 non-redundant proteins and this protein set was considered as the leaf apoplastic protein profile (Table 3.2.1). However, it should be noted that there may be still certain degree of redundancy left, since some hits correspond to the same protein description but from different plant species (Table 3.2.1).

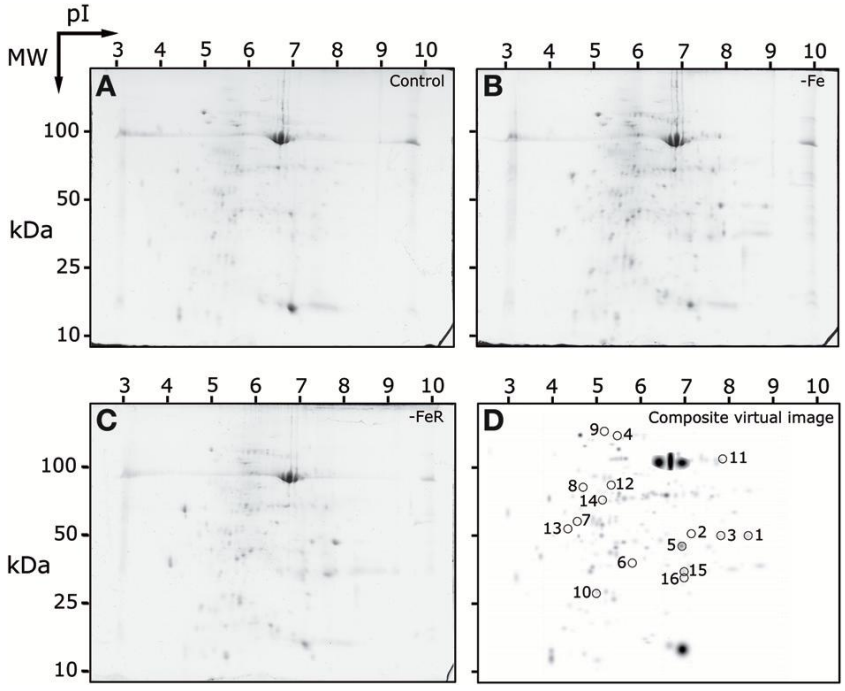

Figure 3.2.2. *2-DE IEF-SDS PAGE protein profile maps of leaf apoplastic fluid extracts from sugar beet plants. Scans of typical gels from Fe-sufficient (+Fe), Fe-deficient (-Fe) and Fe-resupplied Fe-deficient (-FeR) plants are shown in (A-C), respectively. To facilitate visualization of the studied spots, a virtual composite image (D) was created containing all spots present in the real gels (A-C). In (D) spots whose intensities changed in relative abundance as a result of the treatments are circled and numbered as in Table 3.2.2.*

The distribution of non-redundant proteins according to the biological process in the sugar beet leaf apoplast indicated that the major functional categories within the apoplastic proteome

Table 3.2.1. *Non-redundant proteome of the leaf apoplastic fluid of sugar beet plants.*

N. of spots[a]	Protein description[b]	UniProt[c]	TargetP[d]	SecretomeP[e]	Go:P[f]
		Protein metabolism			
2	Proteasome subunit α type	D7T9I6, I6U5E4	-,M	-,nCS	Ubiquitin-dependent proteolysis
1	Proteasome subunit α type-5	Q9M4T8	-	-	Ubiquitin-dependent proteolysis
1	Proteasome subunit α type-6-like isoform X1	XP_004488480	-	-	Ubiquitin-dependent proteolysis
1	Proteasome subunit β type-6	M4D453	-	nCS	Ubiquitin-dependent proteolysis
1	Proteasome subunit α type-7	XP_008393990	-	-	Ubiquitin-dependent proteolysis
1	Cysteine proteinase RD19a/like	I1LJ95	S	CS	Proteolysis
1	Cysteine protease	A5HIJ1	S	CS	Proteolysis
1	Aspartic protease	A0A067FW02	S	CS	Proteolysis
2	Serine carboxypeptidase	W9SXH8, B9SMP4	S,S	CS,CS	Proteolysis
2	Serine carboxypeptidase-like 20-like	XP_008235895	S	CS	Proteolysis
2	Unknown protein with peptidase domain	E0CQB3	-	nCS	Serine-type endopeptidase activity
1	Subtilisin-like protease-like	XP_006466502	S	CS	Serine-type peptidase activity
1	Chaperonin 20	A0A061GL19	C	-	Protein folding
3	Peptidyl-prolyl cis-trans isomerase	B9RN18, O49939	C,C	-,nCS	Protein folding
1	Rubisco subunit binding-protein α subunit	B9MZ75	C	-	Protein folding
1	Heat shock 70 protein	O22664	-	-	Protein folding
1	Predicted heat shock cognate 70 kDa protein 2-like	XP_004505872	-	-	Protein folding
1	Elongation factor Tu	A0A067FTF8	C	nCS	Translation
		Carbon metabolism			
4	Enolase	Q43130	-	nCS	Glycolytic process
4	Triosephosphate isomerase	B0LT90, K4FXE7, P48496	-,-,C	-,nCS, nCS	Glycolytic process
11	Fructose-bisphosphate aldolase	F1AHC9, O04975, Q6RSN7	C,-,-	nCS, nCS,-	Glycolytic process
1	2,3-Bisphosphoglycerate-independent phosphoglycerate mutase	Q42908	-	-	Glycolytic process
1	Phosphoglucomutase	P93262	-	-	Glucose metabolic process
3	Glyceraldehyde-3-phosphate dehydogenase	A3FMH0	-	-	Glucose metabolic process
2	Ribose-5-phosphate isomerase	Q8RU73	C	nCS	PPS, non-oxidative branch
1	Ribulose-phosphate 3-epimerase	Q43157	C	nCS	Calvin cycle; PPS, oxidative branch
3	Transketolase	O20250, Q14K68	C,-	nCS,nCS	Calvin cycle; PPS, oxidative branch

(Continued)

Table 3.2.1: continued

N. of spots[a]	Protein description[b]	UniProt[c]	TargetP[d]	SecretomeP[e]	Go:P[f]
1	Phosphoglycerate kinase	P29409	C	-	Calvin cycle, glycolytic process
1	Sedoheptulose-1,7-bisphosphatase	O20252	C	nCS	Calvin cycle
1	Phosphoribulokinase	P09559	C	-	Calvin cycle
6	Ribulose-1,5-bisphosphate carboxylase/oxygenase	Q08184, Q6JXV6, XP_004144069, P16032, A0A023ZPS4	C,-, C,C,-,	nCS,nCS,-, nCS,nCS,	Carbon fixation
3	23 KDa OEC protein	B0L802	-	-	Photosynthesis
1	Oxaloacetase (*D. caryophyllus*)	Q05957	-	-	Metabolic process
5	Malate dehydrogenase, cytoplasmic	Q9SML8	-	nCS	Cellular carbohydrate metabolic process
5	Carbonic anhydrase	P16016, U5GK55	C,S	nCS,CS	One-carbon metabolic process
	Stress and defense				
3	Osmotin-like protein	Q38745	S	CS	Defense response
4	Thaumatin-like protein	Q6PP01, A9ZMG1, A9ZMG0, XP_004297839	-,S,S,S	nCS,CS, CS,CS	Defense response
1	Abscisic acid stress ripening-related protein	A0A059SPX5	-	-	Response to stress
1	Protein IN2-1 homolog B-like	XP_003632205	C	nCS	Glutathione metabolic process
1	Uncharacterized protein with Bet_v_I_allergen domain	M0ZYA5	-	-	Defense response
1	Ascorbate peroxidase	Q94CF7	-	-	Response to oxidative stress
1	Monodehydroascorbate reductasa	Q93YG1	S	CS	Response to oxidative stress
1	Peroxidase superfamily protein	XP_007014796	S	CS	Response to oxidative stress
1	Peroxidase	P93547	S	CS	Response to oxidative stress
3	Peroxiredoxin	H6VND7	C	nCS	Cell redox homeostasis
1	Type II peroxiredoxin	I0CC96	M	nCS	Cell redox homeostasis
1	Cu/Zn superoxide dismutase	H9BQP8	C	CS	Superoxide metabolic process
6	Lactoylglutathione lyase	M0ZHD0, D2D330, Q8W593, GI:697188226, GI:697141977	C,-,C, -,C	nCS,-, nCS,-,-	Methylglyoxal catabolic process to D-lactate
2	Lactoylglutathione lyase isoform X2	GI:694332574, XP_008385524	-,-	-,-	Methylglyoxal catabolic process to D-lactate
1	Predicted isoflavone reductase homolog	XP_008377292	S	CS	Oxidation-reduction process
	Polysaccharide metabolism				
2	3-Glucanase family protein	B9GI31	S	CS	Carbohydrate metabolic process
2	Acidic endochitinase SP2	P42820	S	CS	Polysaccharide catabolic process

(Continued)

Table 3.2.1: continued

N. of spots[a]	Protein description[b]	UniProt[c]	TargetP[d]	SecretomeP[e]	Go:P[f]
1	Acidic endochitinase SE2	P36910	S	CS	Polysaccharide catabolic process
4	Chitinase	Q8LST3	S	CS	Carbohydrate metabolic process
2	β-Xylosidase/α-L-arabinofuranosidase	XP_008218886	S	CS	Xylan catabolic process
1	UDP-Glucuronic acid decarboxylase 1	W9R277	C	nCS	UDP-D-Xylose biosynthetic process
2	β-Fructofuranosidase	Q8VXS6, S49256	-,-	nCS,nCS	Carbohydrate metabolic process
1	Uncharacterized protein with hydrolase domain	V4SY44	M	CS	Carbohydrate metabolic process
1	Unknown protein with hydrolase domain	A9PG55	-	nCS	Mannose metabolic process
	Amino acid metabolism				
3	Serine hydroxymethyltransferase	XP_007034218, XP_007034219	-,-	-,-	L-Serine metabolism
1	Serine transhydroxymethyltransferase	P50433	M	-	L-Serine metabolism
1	Aminomethyltransferase	P93256	M	nCS	Glycine catabolism
3	Glutamine synthetase	Q9AWA8, Q9AXD1	C,-	-,-	Glutamine biosynthesis
2	Aspartate aminotransferase	B9HAW0	C	nCS	Cellular amino acid metabolic process
	Lipid metabolism				
1	3-Hydroxybutyryl-CoA dehydratase	B9RPB0	M	nCS	Enoyl-coa hydratase activity
1	Uncharacterized protein with lipase domain	U5FE87	S	CS	Lipid metabolic process
1	Uncharacterized protein with lipase domain	D7TJU3	S	CS	Lipid metabolic process
	Other				
1	Ferredoxin--NADP reductasa	B9SB31	C	nCS	Oxidation-reduction process
3	Alcohol dehydrogenase	B9SHB0	C	-	Oxidation-reduction process
1	Flavoprotein wrba-like	XP_004294313	-	-	Oxidation-reduction process
2	Acylpyruvase FAHD1	XP_004508199	-	-	Hydrolase activity
1	Cytosolic ATP sulfurylase	G9B7N0	-	-	Sulfate assimilation
1	Nucleoside diphosphate kinase 2	Q01402	C	nCS	Nucleotide metabolic process
1	Thiamine thiazole synthase	XP_008244366	C	nCS	Thiamine biosynthetic process
1	Uncharacterized germin protein	I3SGS4	S	CS	Nutrient reservoir activity
1	Soluble inorganic pyrophosphatase 1	A0A061E4X1	M	nCS	Pyrophosphatase activity
	Unknown function				
1	Putative protein (*H. vulgare*)	F2EID0	-	-	Nucleotide binding
1	CSP41A protein	E5KGE2	-	-	Cellular metabolic process

(Continued)

Table 3.2.1: continued

N. of spots[a]	Protein description[b]	UniProt[c]	TargetP[d]	SecretomeP[e]	Go:P[f]
4	Uncharacterized protein (*V. Vinifera*)	D7SXW6	S	CS	
1	Uncharacterized protein (*J. Curcas*)	A0A067KSH6	M	nCS	
1	Uncharacterized protein (*J. Curcas*)	A0A067KHD5	-	nCS	
1	Jasmonate-induced protein (*A. Canescens*)	P42764	-	nCS	
2	No blast result				
1	Hypothetical protein CICLE_v10029208mg (*C. Clementina*)	V4SBG5	S	CS	
	No identified				
45					

[a] *Number of spots with the same protein description.*
[b] *Protein description.*
[c] *UniProt entries sharing same protein description.*
[d] *TargetP algorithm predictions: C, M, S, and – indicate chloroplast, mitochondrion, secretory pathway and any other location, respectively.*
[e] *SecretomeP algorithm predictions: CS, nCS and – indicate classical secreted, non-classical secreted, and non-secreted proteins, respectively.*
[f] *Description of the GO: P (biological process) term.*

were C metabolism (25 %; 27 protein species), stress and defense (21 %; 23 proteins), and protein related processes (19 %; 21 proteins), followed by cell wall related processes (9 %, 10 proteins) (Table 3.2.1, Figure 3.2.3A).

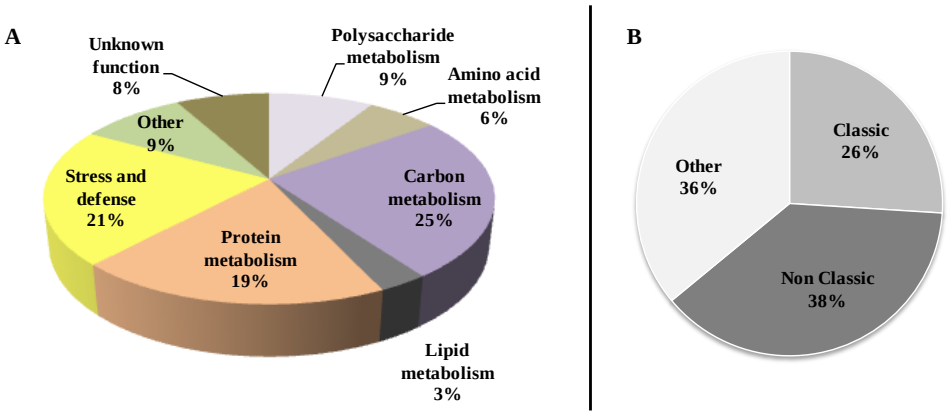

Figure 3.2.3. *(A) Functional classification of the non-redundant leaf apoplastic proteome of sugar beet. Pathways related to the identified proteins were integrated according to the GO annotation. (B) Protein distribution of the non-redundant leaf apoplastic proteome according to TargetP and SecretomeP algorithms; CS and nCS indicate classical and non-classical secretory proteins, respectively, whereas "Other" represents proteins ascribed to other cellular compartments and unclassified.*

From the non-redundant leaf apoplastic proteins, 26 % (28 protein species) were predicted to have a signal peptide sequence using the TargetP or SecretomeP softwares, whereas

SecretomeP revealed that 38 % (41 proteins) were assigned to non-classical secreted proteins lacking a signal peptide (Table 3.2.1, Figure 3.2.3B).

Effect of Fe deficiency and Fe resupply on the leaf apoplastic fluid protein profile

The statistical analysis ($p < 0.05$; *t*-Student) of averaged 2- DE maps indicated that 8 % (16 spots) of the total number of consistent spots changed significantly and > 2-fold in relative abundance in the whole experiment (spots labeled 1-16 in Figure 3.2.2D). Among them, 88 % of the spots (14) matched reliably to known proteins and were identified by database searches (1-14, Figure 3.2.2D). Their metabolic functions were assessed manually by GO annotation and identified proteins were classified into five functional categories: cell wall related processes (4 spots, 2 proteins), protein metabolism (4 proteins), and defense, amino acid and C-related pathways, with two proteins each (Table 3.2.2). The principal component analysis of differentially accumulated spots showed a good separation between treatments, with the first and second components explaining approximately 48 and 38 % of the variation, respectively (Figure 3.2.4).

Table 3.2.2. *Spots showing differences in relative abundance (Student t-test $p < 0.05$) as a result of Fe deficiency and Fe resupply. All proteins were identified in Beta vulgaris specie.*

N. of spot[a]	N. of SSP[b]	-Fe *vs* +Fe[c]	-FeR vs +Fe[d]	-FeR vs -Fe[e]	Protein[f]	Uniprot[g]	GO:P[h]	Secretome P[i]
Polysaccharide catabolism								
1	9403	***new***	*new*	-8.1	Chitinase *(P. americana)*	Q8LST3	Carbohydrate metabolic process	CS
2	7404	**8.7**	**5.3**	-1.6	Chitinase *(P. americana)*	Q8LST3	Carbohydrate metabolic process	CS
3	8401	**4.2**	3.0	-1.4	Chitinase *(P.americana)*	Q8LST3	Carbohydrate metabolic process	CS
4	3805	1.4	-3.6	**-5.0**	β-Xylosidase/α-L-arabinofuranosidase *(P.mume)*	XP_ 008218886*	Xylan catabolic process	CS
Protein related								
5	1402	-1.8	**-6.5**	-3.7	Cysteine proteinase RD19a-like *(G. max)*	I1LJ95	Proteolysis	CS
6	2203	-1.1	**-3.6**	-3.2	Peptidyl-prolyl cis-trans isomerase *(R. communis)*	B9RN18	Protein folding	nCS
7	1602	-3.1	**-7.9**	-2.6	Peptidyl-prolyl cis-trans isomerase *(S. oleracea)*	O49939	Protein folding	nCS
8	2902	1.2	-2.1	**-2.4**	Cytosolic heat shock 70 protein *(S. oleracea)*	O22664	Protein folding	-
Defense								
9	1404	**19.5**	**11.5**	-1.7	Thaumatin-like protein 1 *(F. Vesca)*	XP_ 004297839*	Defense response	CS
10	2503	1.2	-2.0	**-2.3**	Lactoylglutathione lyase *(G. Hirsutum)*	D2D330	Methylglyoxal catabolic process to D-lactate	nCS

(Continued)

Table 3.2.2: continued

N. of spot[a]	N. of SSP[b]	-Fe *vs* +Fe[c]	-FeR vs +Fe[d]	-FeR vs -Fe[e]	Protein[f]	Uniprot[g]	GO:P[h]	Secretome P[i]
Amino acid metabolism								
11	8710	-1.7	**-5.0**	-3.0	Serine hydroxymethyltransferase *(T. cacao)*	XP_ 007034218*	L-Serine metabolic process	-
12	2610	2.3	-6.3	**-14.2**	Glutamine synthetase	Q9AXD1	Glutamine biosynthesis	-
Carbon metabolism								
13	7302	**-2.2**	-1.8	1.2	Carbonic anhydrase *(S. oleracea)*	P16016	One-carbon metabolic process	nCS
14	4307	ND	-12.2	***new***	23 KDa OEC protein *(S. veneta)*	B0L802	Photosynthesis	-
No identified								
15	7202	1.5	**6.1**	**4.1**				
16	7204	4.7	**2.4**	-2.0				

[a] *Spot number as in Figure 3.2.1.*
[b] *Spot number as in Table S3.*
[c-e] *Fold change in the Fe-deficient vs. Fe-sufficient, Fe-resupplied vs. Fe-sufficient and Fe-resupplied vs. Fe-deficient comparisons, respectively, values in bold indicate significant changes and when the ratios were lower than one the inverse was taken and the sign changed.*
[f] *Protein description.*
[g] *Uniprot entry (* denotes protein entry in UniParc).*
[h] *GO:P term description.*
[i] *SecretomeP algorithm predictions: CS, nCS and – indicate classical secreted, non-classical secreted and non-secreted proteins, respectively.*

When the protein profile of -Fe samples was compared to that of the +Fe samples, only five spots changed in relative abundance. Four of them increased, including three spots (spots 1-3) identified as chitinase and one (spot 9) identified as a thaumatin-like protein. Only one spot (spot 13) decreased as a result of Fe deficiency and it was identified as carbonic anhydrase (Figure 3.2.2D, Table 3.2.2).

In the comparison of -FeR *vs.* +Fe, eight spots changed in relative abundance, four of them increased whereas the other four decreased (Figure 3.2.2D, Table 3.2.2). Two of the spots increasing in relative abundance were identified as chitinase and thaumatin (spots 2 and 9, respectively) whereas the other two could not be identified (spots 15 and 16). The spots decreasing in relative abundance were identified as a cysteine proteinase RD19-like protein (spot 5), a peptidyl-prolyl cis-trans isomerase (spots 6, 7) and a serine hydroxymethyltransferase (spot 11) (Table 3.2.2). When the -FeR samples were compared to the -Fe ones, six spots changed in relative abundance (Table 3.2.2). Among them, one spot was detected de novo (spot 14) and identified as the 23 kDa OEC protein and a second one (spot 15) could not be identified. Four spots showed significant decreases in relative abundance (Table 3.2.2, Figure 3.2.2D), and

they were identified as β-xylosidase/α-L-arabinofuranosidase (spot 4), a cytosolic heat shock 70 protein (spot 8), lactoylglutathione lyase (spot 10) and glutamine synthetase (spot 12).

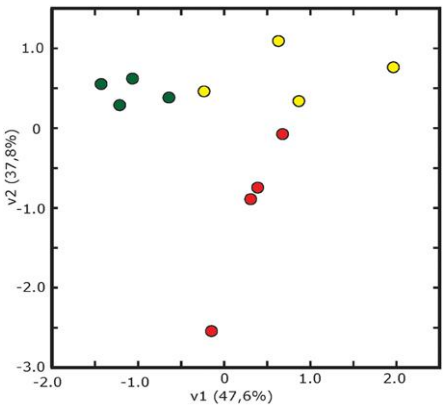

Figure 3.2.4. *Multivariate statistical analysis (Principal Component Analysis, PCA) of 2-DE gels. Score scatter PCA plot of component 1 vs. component 2 after analysis of spots showing differences in relative abundance from leaf apoplastic fluid of sugar beet plants grown in Fe-sufficient (green circles), Fe-deficient (yellow circles) and Fe-resupplied Fe-deficient (red circles) conditions.*

Relative transcript abundance of target genes

The chitinase and thaumatin-like 1 proteins identified in spots 1 and 9 (Table 3.2.2 and Table S4, Figure 3.2.2), respectively, showed the highest increases in relative abundance as a result of Fe deficiency and were selected to study transcript abundances using q-PCR. Sequences containing the peptides matched during protein identification, KDHBv_S14175_58500.t1 for chitinase and BQ584258 for the thaumatin-like 1 protein, were selected to design primers for specific amplification of target genes (Table S1).

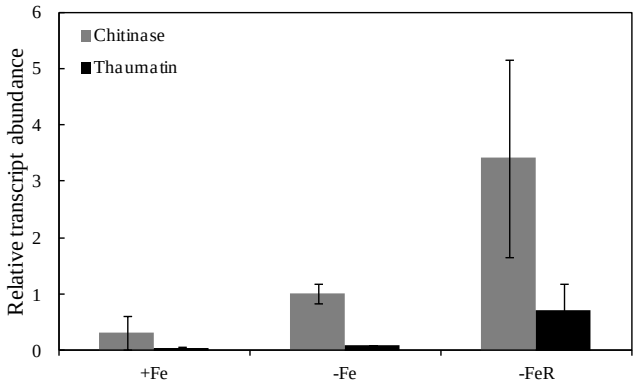

Figure 3.2.5. *Relative abundances of chitinase and thaumatin-like 1 transcripts measured in leaves by qRT-PCR using tubulin as housekeeper gene. Sequences containing the peptides matched during protein identification, KDHBv_S14175_58500.t1 for chitinase and BQ584258 for the thaumatin-like 1, were selected to design primers for specific amplification (Table S1). Data are means ± SD of two experiments with four biological and two technical replicates per treatment in each experiment. Different letters indicate statistically significant differences at $p < 0.05$.*

In Fe-deficient leaves, the relative abundances of chitinase and thaumatin-like 1 protein transcripts increased 3- and 2- fold, respectively, when compared to controls (Figure 3.2.5),

whereas upon Fe resupply the relative abundance of chitinase transcript was higher and that of thaumatin-like 1 protein was not significantly different at $p < 0.05$ (Figure 3.2.5). When compared to the Fe-deficient controls, changes in transcript abundances upon Fe resupply were not statistically significant at $p < 0.05$ (Figure 3.2.5).

3.2.4. Discussion

Leaf apoplastic protein profile

The 2-DE proteomic approach allowed us to resolve 203 spots, with 158 of them (78 %) being identified and 109 accounting for non-redundant proteins. These results are similar to those reported for gel-based leaf apoplastic proteome studies in other plant species, which ranged between 93 and 470 spots, with an average of 200 spots in most of the studies (Table 3.2.3 and references therein). Functional classification of the non-redundant leaf apoplastic proteins of sugar beet indicates that stress and defense, protein metabolism, cell wall and C metabolism account for approximately 75 % of the identified proteome (Figure 3.2.3A).

Stress and defense related proteins accounted for 21 % of the non-redundant sugar beet apoplastic proteome. Similar to what has been reported in other plant species (references in Table 3.2.3), proteins identified were peroxidases, osmotin-like, thaumatinlike, and pathogenesis-related proteins. Our results also indicate the presence in the leaf apoplast of enzymes participating in defense against oxidative stress (two peroxiredoxins, CuZnSOD and two enzymes from the ascorbate-glutathione cycle: ascorbate peroxidase and monodehydroascorbate reductase) and in the detoxification of methylglyoxal (two UniProt entries described as glyoxalase I). These proteins have also been found in the leaf apoplast from poplar (Pechanova et al., 2010) and are also present in fluids from the vascular tissue (Lattanzio et al., 2013; Lucas et al., 2013). The presence of this wide spectrum of defense proteins in non-stressed plants has been attributed to a preformed defense that creates a hostile environment for pathogens (Pechanova et al., 2010; Delaunois et al., 2013).

The contribution of protein metabolism-related proteins to the sugar beet apoplastic proteome (19 %, with 14 of the 21 UniProt entries being proteases) is within the range reported in other studies using grapevine, *Arabidopsis*, and rice (16-20 %; Floerl et al., 2012; Delaunois et al., 2013; Kim et al., 2013), but higher than percentages described for other plant species, which range from 6 to 10 % (Boudart et al., 2005; Goulet et al., 2010; Pechanova et al., 2010). The presence of such a high number of proteolysis-related proteins in the apoplast has been proposed to be species-dependent (Delaunois et al., 2013). Subtilisin-like, serine-carboxypeptidases, and aspartic proteases found in this study have been consistently described in the apoplast of several plant species (Goulet et al., 2010; Floerl et al., 2012; Delaunois et al.,

2013). In addition, our results indicate that sugar beet apoplast also contains several subunits of the proteasome (six UniProt entries), which is involved in the ubiquitin dependent degradation of damaged and miss-folded proteins (Kurepa and Smalle, 2008). These apoplastic proteases may play a role in plant defense against pathogens and also in signaling (Van Der Hoorn and Jones, 2004; Xia et al., 2004; Pearce et al., 2010).

The cell wall related category accounted for 9 % (10 proteins) of the sugar beet leaf proteome and included nine glycoside hydrolases. Glycoside hydrolases modify cell walls by metabolizing carbohydrate compounds from plant cell polysaccharides and by interacting with hemicellulases and pectic enzymes (Numan and Bhosle, 2006; Minic, 2008). The percentage of cell wall related proteins found in sugar beet is similar to those reported in grapevine and tobacco but lower than those found in rice, poplar or maize (Table 3.2.3). On the other hand, the percentage of proteins participating in C-related processes in the leaf apoplast of sugar beet was slightly higher (25 %, 27 proteins) than those reported in other plant species (Table 3.2.3 and references therein). However, these values vary depending on the functional classification of certain proteins, such as peroxidases that are included in defense or cell wall depending on the study, and on the consideration of carbohydrate metabolism and cell wall as one or two functional categories.

The relatively high percentage of C-related proteins found in the sugar beet leaf proteome may have several causes. First, a large number of the spots identified as proteins participating in C metabolism have a low spot intensity and therefore they are over-represented in the functional categorization based on protein number. Second, the sugar beet apoplastic proteome was obtained by direct leaf centrifugation, whereas most of the proteomes from other plant species were obtained using leaf vacuum infiltration followed by centrifugation (Table 3.2.3 and references therein); this later technique may be somewhat better at preventing leakage of proteins from the cytoplasm (Lohaus et al., 2001; Witzel et al., 2011). Interestingly, the percentage of C-related proteins in the stem apoplast of poplar (18 %) as well as the identity (TCA and glycolysis-related) (Pechanova et al., 2010), are similar to those found in sugar beet (25 %). This comparison might suggest that the sugar beet apoplastic fluid obtained by direct centrifugation of the leaves could have a high contribution of the fluid contained in the xylem sap vessels of the main vein of the leaf.

The presence of cytoplasmic contamination in our samples was always lower than 3 %, with an average value of 1.5 %, as assessed by the activity of c-mdh (Table S2). However, *in silico* analysis of the non-redundant proteome using the TargetP and the Secretome P algorithms (for classical and non-classical secretory proteins) predicted 26 % (28 proteins) and 38 % (41 proteins) of the non-redundant proteome as classical and nonclassical secretory proteins, respectively, whereas 36 % of the proteins were predicted to be non-secretory (Table 3.2.1,

Figure 3.2.3B). This percentage (64 %) of secretory proteins is within the range of those reported in the leaf apoplast proteome of other plant species (from 50 % in *Arabidopsis* to 80 % in grapevine and poplar; Casasoli et al., 2008; Pechanova et al., 2010; Delaunois et al., 2013). The fact that our samples contain a relative large number of proteins tagged as non-secretory is not surprising, since the c-mdh assay indicates that up to 3 % of the leaf cells could have delivered cytosolic components into the isolated apoplastic fluid. Furthermore, the release of cytosolic components may be in part associated to the rupture of the pasmodesmata that exist in these leaves (Figure 3.2.1), even if mesophyll cells remain intact. On the other hand, RuBisCO was identified in six spots of the total 203 of the leaf apoplastic proteome map (Table S4). In addition there were 10 more spots whose identification yielded proteins related to the Calvin cycle and are, most likely, plastid located (Table 3.2.1). Therefore, we could assume that at least 16 spots (approximately 8 % of the total) are probably a result of cell leakage. These results may suggest that the real contamination by cell rupture is likely to be higher than that estimated by the use of c-mdh as a contamination marker.

Changes induced by Fe deficiency in the leaf apoplastic proteome

The largest part of the changes caused by Fe deficiency and Fe resupply corresponded to proteins tagged as secretory proteins (10 spots), probably corresponding to true components of the apoplast. Changes also occurred in a relatively small number (four) of the apoplastic fluid proteins tagged as non-secretory ones, and possibly associated to cell or plasmodesmata rupture (these are marked by ∗ in the following paragraphs).

Iron deficiency caused changes in the relative abundance of five spots (2.5 % of the consistent spots of the leaf apoplast proteome), suggesting that protein homeostasis in the leaf apoplast fluid is well-maintained upon Fe shortage. This number of changes is markedly low when compared to those induced by Fe deficiency in other proteomes, including those of roots and thylakoids of sugar beet plants (44 and 53 %, respectively; Andaluz et al., 2006; Rellán-Álvarez et al., 2010) and falls within the lower range of the number of changes caused by other abiotic stresses in the leaf apoplast (Table 3.2.3; Dani et al., 2005; Casasoli et al., 2008).

Three spots identified as chitinase increased in relative abundance as a result of Fe deficiency (spots 1-3; Figure 3.2.2, Table 3.2.2). These three spots had the same molecular weight and different pIs (8.2, 7.1, and 7.6), indicating that Fe deficiency alters the isoform pattern of this enzyme, with one of the isoforms identified de novo in Fe-deficient samples. Chitinases are hydrolytic enzymes that break down glycosidic bonds, removing xylosyl residues of xyloglucan oligosaccharides in the cell wall (Sampedro et al., 2001). Therefore, these increases in chitinase suggest the existence of Fe deficiency-induced cell wall modifications.

Table 3.2.3. *Summary of proteomic studies on leaf apoplast.*

Ref.	Specie	Technique	Leaf material	Study	Separation		N. of spots	Analysis	Changes	Functional classification in control
Fecht-Christoffers et al., 2003	*V. unguiculata*	VIC-(water)	Whole leaf	Mn toxicity	18 cm	3-10 NL	Not reported		10	Not reported
					18 cm	BN-PAGE				
Boudart et al., 2005	*A.thaliana*	VIC-(0.3 M mannitol)	Whole rossete leaves	Mapping	7 cm	4-7	46	93 identified	–	32 % cell wall modifying proteins, 21 % defense-related, 20 % proteins with interacting domains, 11 % proteinases
		VIC-(1 M NaCl, 0.2 M $CaCl_2$, 2 M LiCl or 0.3 M CDTA)	Whole rossete leaves		Sepharose fractioning followed by 1DE		87		-	
Dani et al., 2005	*N. tabacum*	VIC- (50 mM phosphate buffer, 200 mM NaCl, pH 7)	1-2 cm2 leaf strips	Salt stress	7 cm	3-10	150		20	Not reported
Soares et al., 2007	*M. truncatula*	VIC-(15 mM sodium acetate buffer, pH 4.5)	Leaf pices	Mapping	Not specified	3-10 NL	220	45 analyzed and 19 identified	–	38 % defense, 58 % unknown
Casasoli et al., 2008	*A.thaliana*	VIC-(25 mM Tris-HCl pH7.4, 50 mM EDTA, 150 mM $MgCl_2$)	Seedlings	Oligo-galacturonides	DIGE-13 cm	3-10	180-220	62 analyzed and 55 identified	16	30 % secretory pathway, 20 % chloroplast, 14 % cell wall
Floerl et al., 2008	*B.napus*	VIC-(100 mM KCl, 0.01 % Triton)	Leaf without midrib	Fungus infection	18 cm	3-10	170	31 analyzed and 19 identified		Chitinases, proteases, peroxidases, glucanases, germin, cell wall modification
Soares et al., 2009	*M. truncatula*	VIC-(water)	Leaf-halves	Wounding	Not specified	3-10 NL	110	35 analyzed and identified	28	Defense or unknown
Pechanova et al., 2010	*P. deltoides*	pressure chamber	Whole leaf	Mapping	24 cm	3-10 NL	84	144 analyzed and identified	-	25 % cell wall, 24 % stress-defense, 12 % proteolysis, 8 % cell wall, 4 % carbohydrate
					2D-LC		106		-	

(Continued)

Table 3.2.3: continued

Ref.	Specie	Technique	Leaf material	Study	Separation		N. of spots	Analysis	Changes	Functional classification in control
Goulet et al., 2010	*N. benthamiana*	VIC (10 mM MES, pH 5.8)	Whole leaf	Agrobacterium infection	13 cm	3-10 NL	Ca. 200	91 analyzed and 73 identified	44	29 % defense, 15 % cell wall, 6 % proteases
Witzel et al., 2011	*Z. mays*	VIC-(water/ 100 mM sodium phosphate buffer/25 mM Tris-HCl/ 100 mM sorbitol/ 20 mM ascorbic acid and 20 mM $CaCl_2$/ 50 mM NaCl)	5.5 cm leaf segments	Infiltration technique	7 cm	3-10	171/107/ 131/133/ 133/114 328 total	67 identified as apoplastic proteins by in silico (20%)	–	58 % carbohydrate metabolism and cell wall, 22 % defense , 10 % protein transporting function, 27 % cytosol proteins, 13 % chloroplast proteins
Floerl et al., 2012	*A. thaliana*	VIC (100 mM KCl, 0.005% Triton X-100)	Whole leaf	Fungus infection	18 cm	3-10	217	45 analyzed and identified	7	25 % carbohydrate metabolism, 18 % proteases, 21 % oxido-reductases
Shenton et al., 2012	*O sativa*	VIC-(50 mM NaP buffer pH 7.5, 600 mM NaCl, 0.01% Tween-20, 0.1% β-mercapto ethanol)	Whole leaf	Fungus infection	11 cm	3-11 NL	Not reported		-	Not reported
Delaunois et al., 2013	*V. vinifera*	VIC-(150 mM Tris-HCl, pH 8.5, 6 mM CHAPS)	1 cm2 leaf cuts	Mapping	18 cm	3-10 NL	306	177 analyzed and 89 identified	-	On protein number basis: 28 % defense, 18 % cell wall / on spot volume basis: 51 % defense, 16 % proteases, 12 % cell wall
Kim et al., 2013		CA-VIC (200 mM $CaCl_2$, 5 mM Na-acetate, pH 4.3)	5 cm leaf cuts	Fungus infection	18 cm	4-7	27		12	21 % carbohydrate metabolism, 20 % protein metabolism, 30 % defense, 12 % energy pathway
					MudPIT		283		-	
Petriccione et al., 2014		VIC-(100 mM Tris-HCl, pH 7.5, 10 mM KCl, 1mM phenylmethanesulfonyl-fluoride)	Leaf without midrib	Pseudomonas infection	7 cm	3-10	ca. 220		60	Not reported
Kim et al., 2014	*O. sativa*	CA-VIC-(200 mM $CaCl_2$, 5 mM Na-acetate, pH 4.3)	5 cm leaf cuts	Fungus infection	Shotgun		470	174 secreted proteins by in silico analyses	-	Not reported

VIC stands for vacuum infiltration followed by centrifugation.

This is in agreement with the changes elicited by Fe deficiency in leaf morphology, which include reduction of xylem vessel size (Fernández et al., 2008; Eichert et al., 2010). Furthermore, changes in lignification have been reported in roots of Fe-deficient pear and quince cultivars (Donnini et al., 2009) and cell wall related proteins commonly show changes in abundance in proteomic studies of Fe-deficient plants (see López-Millán et al., 2013 for a review).

A spot identified as a thaumatin-like protein 1 (spot 9) also increased in relative abundance as a result of Fe deficiency. Thaumathins are pathogenesis-related (PR) proteins from the PR5 subfamily, which are induced by biotic and abiotic stresses. Some members of PR5 subfamily have been described to play distinctive roles in the defense system that protects against high-salt stress or osmotic imbalance (Tachi et al., 2009), which is likely to occur in the Fe deficiency treatment in the presence of $CaCO_3$. A PR5b protein also showed increases in abundance in roots and stems of Fe-deficient *M. truncatula* plants grown in the presence of $CaCO_3$ (Rodríguez-Celma et al., 2011), suggesting that thaumatins are ubiquitously up-regulated by Fe deficiency. Interestingly, both chitinase and the thaumatin-like 1 protein were also affected in the leaf proteome of cowpea submitted to Mn toxicity (Fecht-Christoffers et al., 2003).

Only one protein, identified as carbonic anhydrase (CA; spot 13), decreased as a result of Fe deficiency. Carbonic anhydrase interconverts CO_2 and bicarbonate to maintain the acid-base balance. A decrease in CA activity could be attributed to the presence of bicarbonate in the nutrient solution that may reach the leaf apoplast *via* xylem (Nikolic and Römheld, 2007). Although some mammalian CA isoforms are extra-cellular and have been described in saliva and milk (Karhumaa et al., 2001; Leinonen et al., 2001), and CA is classified as a non-classical secretory protein by SecretomeP, plant isoforms are distinct from an evolutionary standpoint and have been mainly localized in the chloroplast or the cytosol.

Changes induced by Fe resupply in the leaf apoplastic proteome

Iron resupply to Fe-deficient plants caused significant changes in the relative abundance of 13 spots when compared to either Fe-sufficient or Fe-deficient plants. These spots can be roughly classified into two major groups. The largest group (seven spots) was composed by those spots increasing in relative abundance (significantly or not) with Fe deficiency and decreasing significantly with Fe resupply when compared either with the control or with Fe-deficient samples. This group contained two cell wall related proteins [chitinase (spot 2), and β-xylosidase (spot 4)], three stress-related proteins [a heat shock 70 protein (spot 8*), thaumatin-like 1 protein (spot 9), glyoxalase I (spot 10)], glutamine synthase (spot 12*) and the unidentified spot 16. These results indicate that Fe resupply causes changes in the short-term (within 24 h) in cell wall and stress-related processes of the Fe-resupplied plants toward values found in the Fe-sufficient controls. One more protein (spot 14*, the 23 kDa OEC protein, which

nuclear-encoded and synthesized in the cytosol) was also responsive to short term Fe resupply but followed a different trend, not-detected in Fe-deficient samples but detected upon Fe resupply. This likely reflects transitory increases in the cytosolic levels of this protein upon short term Fe resupply, which are necessary for the slight recovery of the photosynthetic system at this resupply stage (Larbi et al., 2004).

On the other hand, a second group of four spots (spots 5-7 and 11*) decreased in relative abundance with Fe deficiency (although not significantly) and decreased significantly upon Fe resupply when compared either with controls or Fe-deficient samples. This group included two proteins identified as protein-metabolism related [a cysteine protease (spot 5), a peptidyl-prolyl cis-trans isomerase (spots 6, 7)] and a serine hydroxymethyltransferase (spot 11*). One more spot (spot 15, unidentified protein) followed the opposite behavior (increased). This group of proteins can be classified as not responsive to short term Fe resupply, since they may require a time longer than 24 h to reset to control values after resupply.

3.2.5. Concluding remarks

In summary, this study provides information on the composition of the apoplast proteome in *B. vulgaris* leaves, which appears to be quite similar to that of other previously studied plant species. The study shows that Fe deficiency and Fe resupply cause significant changes in a limited number of proteins in the leaf apoplast, and none of them is expected to play a significant role in metal homeostasis. This is in contrast with the intense changes previously found in the concentrations of metabolites (e.g., carboxylates) that could interact with metals in the same compartment. Data found contribute toward the understanding of metal homeostasis, and in particular on the still poorly known mechanisms of Fe acquisition by plant mesophyll cells. Results presented here open an interesting line of work regarding possible modifications of cell wall that ultimately may affect permeability or transport of Fe across the plasma membrane.

Supplementary material

Supplementary data to this article can be found online at: http://www.frontiersin.org/journal/10.3389/fpls.2015.00145/abstract: **Figure S1.** Virtual composite image containing all consistent spots present in the real gels. Numbers are as in Table S4 (SSP); **Table S1.** Forward and reverse primers used for qPCR analyses and primer set efficiencies; **Table S2.** Summary of the 2-DE protein profiling results; **Table S3.** Univariate statistical analysis of 2-DE gels; **Table S4.** Proteins identified in 2-DE IEF-SDS PAGE gels of sugar beet leaf apoplast.

3.3. Effects of Fe and Mn deficiencies on the protein profiles of tomato (*Solanum lycopersicum*) xylem sap as revealed by shotgun analyses

Laura Ceballos-Laita [a], Elain Gutierrez-Carbonell [a], Daisuke Takahashi [b,c], Anunciación Abadía [a], Matsuo Uemura [b,c], Javier Abadía [a], Ana Flor López-Millán [d]

[a] *Department Plant Nutrition, Aula Dei Experimental Station, Consejo Superior de Investigaciones Científicas (CSIC), Zaragoza, Spain*

[b] *United Graduate School of Agricultural Sciences, Iwate University, Morioka, Japan*

[c] *Cryobiofrontier Research Center, Faculty of Agriculture, Iwate University, Morioka, Japan*

[d] *USDA-ARS Children's Nutrition Research Center, Department of Pediatrics, Baylor College of Medicine, Houston, TX, USA*

Published in Journal of Proteomics (2018) 170, 117-129 (*doi.org/10.1016/j.jprot.2017.08.018*)

ABSTRACT

The aim of this work was to study the effects of Fe and Mn deficiencies on the xylem sap proteome of tomato using a shotgun proteomic approach, with the final goal of elucidating plant response mechanisms to these stresses. This approach yielded 643 proteins reliably identified and quantified with 70 % of them predicted as secretory. Iron and Mn deficiencies caused statistically significant and biologically relevant abundance changes in 119 and 118 xylem sap proteins, respectively. In both deficiencies, metabolic pathways most affected were protein metabolism, stress/oxido-reductases and cell wall modifications. First, results suggest that Fe deficiency elicited more stress responses than Mn deficiency, based on the changes in oxidative and proteolytic enzymes. Second, both nutrient deficiencies affect the secondary cell wall metabolism, with changes in Fe deficiency occurring *via* peroxidase activity, and in Mn deficiency involving peroxidase, Cu-oxidase and fasciclin-like arabinogalactan proteins. Third, the primary cell wall metabolism was affected by both nutrient deficiencies, with changes following opposite directions as judged from the abundances of several glycoside-hydrolases with endo-glycolytic activities and pectin esterases. Fourth, signaling pathways *via* xylem involving CLE and/or lipids as well as changes in phosphorylation and N-glycosylation also play a role in the responses to these stresses.

Biological significance

In spite of being essential for the delivery of nutrients to the shoots, our knowledge of xylem responses to nutrient deficiencies is very limited. The present work applies a shotgun proteomic approach to unravel the effects of Fe and Mn deficiencies on the xylem sap proteome. Overall,

Fe deficiency seems to elicit more stress in the xylem sap proteome than Mn deficiency, based on the changes measured in proteolytic and oxido-reductase proteins, whereas both nutrients exert modifications in the composition of the primary and secondary cell wall. Cell wall modifications could affect the mechanical and permeability properties of the xylem sap vessels, and therefore ultimately affect solute transport and distribution to the leaves. Results also suggest that signaling cascades involving lipid and peptides might play a role in nutrient stress signaling and pinpoint interesting candidates for future studies. Finally, both nutrient deficiencies seem to affect phosphorylation and glycosylation processes, again following an opposite pattern.

3.3.1. Introduction

The xylem is a key component of the vascular transport system of land plants, essential for long- and short-distance transport and distribution of nutrients and signals. The major role of the xylem is to transport water and mineral nutrients from roots to shoots. The flow of the fluid through the treachery elements that compose the xylem vessels, known as xylem sap, is mainly driven by the negative pressure created by transpiration, whereas differences in water potential between the soil and the root system can also create a positive root pressure that contributes to the xylem sap flow (Fisher et al., 2000).

The xylem sap is mainly composed by water and mineral nutrients, but also contains a wide array of other minor compounds, including carbohydrates, hormones, secondary metabolites, polyamines, amino acids, peptides and proteins (Carella et al., 2016; Dickson, 1979; Escher et al., 2004; Friedman et al., 1986; López-Millán et al., 2000a; Rodríguez-Celma et al., 2016a; Satoh et al., 1992, 2006). In spite of the fact that the treachery elements that compose the xylem have lost their nuclei and cellular content during differentiation and are therefore unable to synthesize proteins, the xylem sap has been widely reported to have a characteristic protein profile (Rodríguez-Celma et al., 2016a, Álvarez et al., 2006; Fukuda, 1996; Ligat et al., 2011). Many of the xylem sap proteins contain predicted N-terminal signals and are synthetized in the roots and subsequently loaded in the xylem sap *via* the secretory pathway (Satoh et al., 2006; Djordjevic et a., 2007; Masuda et al., 1999; Sakuda and Satoh, 2000), whereas others may arise from cytoplasmic contamination from neighboring tissues (Rodríguez-Celma et al., 2016a).

Proteomic studies have allowed generating a detailed xylem sap protein repertoire. Since one of the major limitations for these studies is the low protein concentration present in xylem sap, which ranges between 10 and 300 μg mL^{-1} (see Rodríguez-Celma et al., 2016a for a review), initial studies performed by means of one dimensional electrophoresis only provided a

limited number of protein species (Álvarez et al., 2006). Later on, the development of more sensitive high-throughput proteomic techniques allowed to decipher in detail the xylem sap proteome of a significant number of plant species, including tomato (see Rodríguez-Celma et al., 2016a for a review). A comprehensive analysis of these proteomes, which included between 100 and 500 proteins, indicated that the major functional category in the xylem is polysaccharide metabolism, including mainly cell wall hydrolases (Carella et al., 2016, Rodríguez-Celma et al., 2016a, Ligat et al., 2011). The xylem proteome, as it also occurs in other plant fluids, contains a battery of proteins related to redox homeostasis, plant defense and proteases, which are thought to constitute a local defense barrier against biotic and abiotic stresses (Rodríguez-Celma et al., 2016a; Buhtz et al., 2004; Pechanova e al., 2010; Rep et al., 2003; Xia et al., 2004).

The xylem sap also participates actively in the root to shoot signaling pathway that helps regulating vegetative growth depending on the root environment conditions (Lucas et al., 2013). In situations such as plant-symbiotic associations or nutrient deficiencies, the xylem serves as a conduit for signaling metabolites (Lucas et al., 2013; Dodd, 2005), with many of them being hormones. For instance, in P- and N-deficient conditions xylem-mobile cytokinins regulate the nutrient starvation response (Ghanem et al., 2011; Hirose et al., 2008; Martin et al., 2000; Rahayu et al., 2005; Rouached et al., 2011; Ruffel et al., 2011; Takei et al., 2002). Interestingly, the xylem sap proteome also contains a small number of proteins involved in regulatory processes that could participate in root to shoot signaling, including transcription factors, fasciclin-like arabinogalactan proteins and kinases (Carella et al., 2016; Rodríguez-Celma et al., 2016a; Aki et al., 2008; Krishnan et al., 2011; Zhang et al., 2015).

Minerals such as Fe and Mn are essential micronutrients for living organisms including plants (Marschner, 1995; Williams and Pittman, 2010). Both metals are cofactors for numerous enzymes and play important roles in photosynthesis, with Mn being required in the catalytic center of the oxygen evolving complex (Williams and Pittman, 2010; Nickelsen et al., 2013; Socha and Guerinot, 2014; Pittman, 2005) and Fe participating in electron transfer reactions of the photosynthetic apparatus as well as in the synthesis of chlorophyll (Msilini et al., 2011; Raven et al., 1999; Tottey et al., 2003). Deficiencies of both nutrients often occur in alkaline soils where there is limited availability of metals, leading to reduced growth and yield and affecting the nutritional quality of plant crops (Marschner, 1995; Williams and Pittman, 2010; Socha and Guerinot, 2014; Abadía et al., 2004, 2011; Briat et al., 2015; Jiang, 2006). In the xylem sap, Fe is found complexed with carboxylates (Flis et al., 2016; Rellán-Álvarez et al., 2010) whereas it has been estimated that 60 % of the xylem Mn is in the form of Mn^{2+} (White et al., 1981). In spite of the fact that proteins are unlikely to play a direct role in the transport of these metals in the xylem, they might play important roles in root to shoot nutrient signaling and

protection against metal-induced ROS, among others. Comparative proteomics can provide useful information not only about processes occurring in xylem sap during the adaptation to nutrient stresses, but also can help to target proteins putatively involved in systemic regulation for future studies (Kosová et al., 2011; Timperio et al., 2008). A significant number of proteomic studies have focused into the effect on different sub-proteomes of nutrient stresses such as Fe (see López-Millán et al., 2013; Mai and Bauer, 2016 for reviews) and Mn (Fecht-Christoffers et al., 2003; Rodríguez-Celma et al., 2016a), but the number of proteomic studies devoted to the effect of nutrient deficiencies and/or toxicities in the xylem sap has been limited, to the best of our knowledge, to studies on the effects of salt stress, K deficiency and N starvation or overload (Fernández-García et al., 2011; Liao et al., 2012; Zhang et al., 2016).

Therefore, the aim of this work was to study the effects of Fe and Mn deficiencies on the protein profile of the xylem sap of tomato (*Solanum lycopersicum*), with the aim of elucidating plant response mechanisms to these nutritional stresses. Tomato was chosen as a model plant because the tomato genome has been published and this plant species has adequate root pressure and turgid stems that permit xylem sap sampling in sufficient amounts by de-topping. The high-throughput shotgun analysis has permitted to identify and quantified a large number of low abundance proteins in the tomato xylem sap.

3.3.2. Materials and methods

Plant material and xylem sap collection

Tomato (*Solanum lycopersicum*, cv. Tres Cantos) plants were grown hydroponically in a controlled environment chamber (Fitoclima 10.000 EHHF, Aralab, Lisbon, Portugal) with a photosynthetic photon flux density (PPFD) of 400 μmol m^{-2} s^{-1} photosynthetically active radiation, 80 % relative humidity and a photoperiod of 16 h, 23 °C/8 h, 18 °C day/night regime. In the Fe deficiency experiment, seeds were germinated in vermiculite for 13 days in half-strength Hoagland nutrient solution containing 45 μM Fe-EDTA and 4.6 μM $MnCl_2$. Seedlings were then transplanted to 10 L plastic buckets (16-18 plants per bucket) containing half-strength Hoagland nutrient solution and grown for an additional 13-day period. After this time, solutions were renewed and control (45 μM Fe(III)-EDTA, 4.6 μM $MnCl_2$) and Fe deficiency treatments (0 μM Fe(III)-EDTA) imposed. In the Mn experiment the time line and experiment design (including control conditions) were the same, but Mn-deficient plants (0 μM $MnCl_2$) were germinated and grown without Mn and with 45 μM Fe(III)-EDTA throughout the experiment. Plants were analyzed and xylem sap collected eight days after treatment onset. At this time, plants were de-topped approximately 5 mm above the mesocotyl using a carbon steel disposable scalpel (Nahita, Beriain, Spain) and the exudate fluid was collected from the cut surface. The

initial sap collected during the first 5 min was discarded to minimize contamination with other plant fluids and broken cells, and then the xylem sap was collected for 30 min using a micropipette tip. Samples were kept on ice during the entire collection period.

Experimental design

The experiment was repeated six times with independent batches of plants. Each batch of plants consisted of one 10-L bucket per treatment with 16-18 plants per bucket. In each batch of plants, the xylem sap fluid from all plants in a given treatment was pooled together and considered as a biological replicate (n = 6).

Mineral analysis and chlorophyll estimation

The concentration of micronutrients (Fe, Mn, Cu and Zn) in the collected fluid was determined by ICP-MS (Inductively Coupled Plasma Mass Spectrometry; model Agilent 7500ce; Agilent Technologies, Tokyo, Japan) after digestion with 1 % HNO_3 (TraceSELECT Ultra, Sigma-Aldrich, Madrid, Spain).

Leaf chlorophyll content was estimated using a SPAD 502 apparatus (Minolta Co., Osaka, Japan). The SPAD values of young and old expanded leaves were recorded at sampling time (8 days after treatment onset) and an average per treatment obtained.

Protein extraction

Proteins in the collected fluid were precipitated immediately by adding five volumes of cold 0.1 M ammonium acetate in methanol, containing 0.07 % β-mercaptoethanol. Samples were kept overnight at -20 °C and then centrifuged at 20,000 × *g* for 20 min. The pellet was washed twice with cold methanol, dried with N_2 gas and solubilized in a sample rehydration buffer containing 8 M urea, 2 % (w/v) CHAPS, 50 mM DTT, 2 mM PMSF and 0.2 % (v/v) IPG buffer pH 3-10 (GE Healthcare, Uppsala, Sweden). After rehydration, samples were incubated in a Thermomixer comfort device (Eppendorf AG, Hamburg, Germany) at 42 °C and 1,000 rpm during 3 h, then centrifuged at 10,000 × *g* for 10 min at room temperature and filtered (0.45 µm ultrafree-MC filters, Millipore, Bedford, USA). Protein concentration in the samples was quantified immediately with the Bradford method using an Asys UVM 340 spectrophotometer with microtiter plates (Biochrom Ltd., Cambridge, UK) and BSA as standard.

Label free liquid chromatography-tandem mass spectrometry (LC-MS/ MS)

Sample preparation for label free LC–MS/MS was carried out according to (Takahashi et al., 2014). Briefly, 5 µg of total proteins were subjected to 1-DE to remove non-protein compounds.

The resulting gel bands were cut into six pieces, proteins were in gel digested with trypsin, and peptides were subsequently extracted.

Peptide solutions were concentrated in a trap column (Lcolumn Micro 0.3 × 5 mm; CERI, Japan) using an ADVANCE UHPLC system (Michrom Bioresources, Auburn, CA, USA). Elution was carried out with 0.1 % (v/v) formic acid in ACN and concentrated peptides were separated in a Magic C18 AQ nano column (0.1 × 150 mm; Michrom Bioresources) using a linear gradient of ACN (from 5 to 45 %) and a flow rate of 500 nL min^{-1}. Peptide ionization was carried out with a spray voltage of 1.8 kV using an ADVANCE spray source (Michrom Bioresources). Mass spectrometry analysis was carried out on an LTQ Orbitrap XL (Thermo Fisher Scientific, Waltham, MA, USA) equipped with Xcalibur software (v. 2.0.7, Thermo Fisher Scientific) and mass data acquisition parameters were set as described elsewhere (Gutierrez-Carbonell et al., 2016).

Mass data analysis was performed according to (Takahashi et al., 2013). Protein identification was carried out using the full peptide list with the Mascot search engine (version 2.4.1, Matrix Science, London, UK) and NCBI 20141009 database (50,750,890 sequences; 18,190,226,827 residues). Search parameters were: peptide mass tolerance ± 5 ppm, MS/MS tolerance ± 0.6 Da, one allowed missed cleavage, allowed fixed modification carbamidomethylation (Cys), and variable modification oxidation (Met) and peptide charges were set to +1, +2 and +3. Positive protein identification was assigned with at least two unique top-ranking peptides with scores above the threshold level ($p < 0.05$). Protein information was exported from Mascot .xml format and imported to Progenesis software (v. 2.0, Nonlinear Dynamics, Newcastle upon Tyne, UK), which then associate peptide and protein information. The MS proteomics data have been deposited to the ProteomeXchange Consortium *via* the Pride partner repository with the data set identifier PXD007517.

To assess the effect of Fe and Mn deficiencies in the protein profile of tomato xylem sap, we calculated the ratio of normalized protein abundance between the Fe-deficient or Mn-deficient and the control samples. Only changes with a $p \leq 0.05$ (ANOVA) and a normalized abundance ratio ≥ 2 or ≤ 0.5 were considered as statistically significant and biologically relevant, respectively. Multivariate statistical analysis (Principal Component Analysis; PCA) was carried out using SPSS Statistical software (v. 24.0), including only proteins showing statistically significant changes (ANOVA; $p \leq 0.05$) as a result of the Fe deficiency and Mn deficiency treatments.

We used the GO biological process annotation (http://www. geneontology.org) and domain annotations for classification of each individual protein identified into nine functional categories (proteolysis, protein synthesis, polysaccharide related, stress/oxido-reductases, lipid

metabolism, carbohydrate metabolism, signaling, unknown and a miscellaneous group containing functional categories not belonging to the previous groups). The presence of signal peptides in proteins was assessed using TargetP (www.cbs.dtu.dk/services/TargetP) (Emanuelsson et al., 2007), and SecretomeP (www.cbs.dtu.dk/services/SecretomeP) was used to assign proteins to secretory classical and non-classical classes (Bendtsen et al., 2004, 2005).

3.3.3. Results

Plant material and xylem sap collection

Tomato plants grown without Fe showed deficiency symptoms as soon as five days after the treatment onset. At sampling time (eight days) a marked chlorosis of the younger leaves was observed (Figures 3.4.1 and 3.4.2 in Chapter 3.4, *Data in Brief*), as indicated by the SPAD reading in these plants (13.6) which was significantly lower than that measured in control plants (42.4) (Table 3.3.1). Accordingly, the Fe concentration in the xylem sap of Fe-deficient plants was 15.5 μM, 68 % lower than that found in xylem sap from control plants, whereas no significant differences were observed in the concentrations of Mn, Cu and Zn (Table 3.3.1).

Table 3.3.1. *Xylem sap properties and leaf chlorophyll estimation. Xylem sap exudation rates (mL plant^{-1} h^{-1}), protein extraction yields (ng protein μL^{-1} xylem sap) and metal concentrations (μM), and leaf SPAD values from control, Fe-deficient and Mn-deficient plants. Values are means ± SD (n = 6). Different letters within the same row indicate statistically significant differences (Student's t-test, p ≤ 0.05).*

Xylem sap properties	Control	- Fe	- Mn
Exudation rates (mL plant^{-1} h^{-1})	0.8 ± 0.1 a	0.8 ± 0.2 a	1.1 ± 0.3 b
Protein extraction yield (ng protein μL^{-1} xylem sap)	9.0 ± 3.4 b	6.9 ± 1.7 b	4.2 ± 2.5 a
[Fe]	47.8 ± 12.5 c	15.5 ± 6.9 a	26.6 ± 4.2 b
[Mn]	6.5 ± 0.8 b	7.7 ± 3.2 b	0.7 ± 0.6 a
[Cu]	3.6 ± 0.8 a	3.6 ± 1.3 a	3.0 ± 0.5 a
[Zn]	9.5 ± 1.3 a	9.3 ± 4.7 a	7.0 ± 0.6 a
Leaf SPAD values	42.4 ± 4.1 c	13.6 ± 3.3 a	29.6 ± 4.9 b

To achieve Mn deficiency, plants were grown without Mn from germination. At sampling time, both old and young leaves in Mn-deficient plants showed interveinal chlorosis with a "checkered" pattern (Figures 3.4.1 and 3.4.2 in Chapter 3.4, *Data in Brief*). The SPAD value of Mn-deficient plants (29.6) was 30 % lower than those of control plants (Table 3.3.1). The concentration of Mn in xylem sap of deficient plants was almost 10 times lower than that in control plants (0.7 *vs.* 6.5 μM). The concentration of Fe in the xylem sap was also 44 % lower in Mn-deficient (26.6 μM) that in control plants (47.8 μM), but still significantly higher than that in Fe-deficient plants (Table 3.3.1). No significant changes were detected in the xylem sap concentrations of Cu and Zn (Table 3.3.1).

Xylem bleeding rates were similar in control and Fe-deficient plants (approximately 0.8 mL plant $^{-1}$ h $^{-1}$), whereas in the Mn-deficient plants this rate was 38 % higher (1.1 mL plant $^{-1}$ h $^{-1}$) (Table 3.3.1). Protein extraction yields were also similar in control and Fe-deficient plants, in the range from 6.9 to 9.0 ng protein μL $^{-1}$, whereas values in the Mn-deficient xylem sap were 53 % lower (4.2 ng protein μL $^{-1}$) than those in the controls (Table 3.3.1).

Identification of xylem sap proteins

The LC–MS/MS analysis detected 1,534 proteins in the tomato xylem sap, and 643 of them were reliably identified and quantified with at least two peptides and therefore considered in this study. The lists of peptides detected and proteins identified and quantified are shown in Tables 3.4.S1 and 3.4.S2 in Chapter 3.4, *Data in Brief*, respectively. The large majority of protein species identified and quantified (84 %; 542) were identified as pertaining to the *Solanum* genus, with 94 % of them (509) matching specifically to the species *S. lycopersicum* (Table 3.4.S2 in Chapter 3.4, *Data in Brief*).

The PCA analysis of the statistically significant changes (ANOVA; $p \leq 0.05$) showed a good separation between treatments, with the first and second components explaining approximately 74 and 11 % of the variation, respectively (Figure 3.4.3 in Chapter 3.4, *Data in Brief*).

The prediction programs TargetP and SecretomeP indicated that a high percentage (66 %; 425 proteins) of the 643 identified and quantified proteins can be assigned to the secretory pathway. Among these secretory proteins, 223 (35 % of the total identified in the xylem sap) were classified as classical secretory (CS) (containing peptide signals) whereas 202 (31 %) were classified as non-classical secretory (NCS). The remaining 218 proteins (34 %) were predicted as non-secretory, and therefore their presence in the xylem sap deserves further studies, since it possibly reflects some degree of contamination (see Rodríguez-Celma et al., 2016a for a discussion on this topic).

Effect of Fe deficiency on the xylem sap proteome

A volcano plot, showing the relationship between statistical significance [$-\log_{10}$ (p-value)] and biological significance [$\log_2$ (fold-change)], was used to describe the changes induced by Fe deficiency on the xylem sap proteome (Figure 3.3.1). Iron deficiency caused statistically significant (ANOVA, $p \leq 0.05$) and biologically relevant (fold ≥2 or fold ≤0.5) changes in 119 proteins (Figure 3.3.1). All these proteins are presented in Table 3.4.S3 in Chapter 3.4, *Data in Brief*, and those exhibiting large changes in abundance (fold > 5 or < 0.2) are shown in Table 3.3.2.

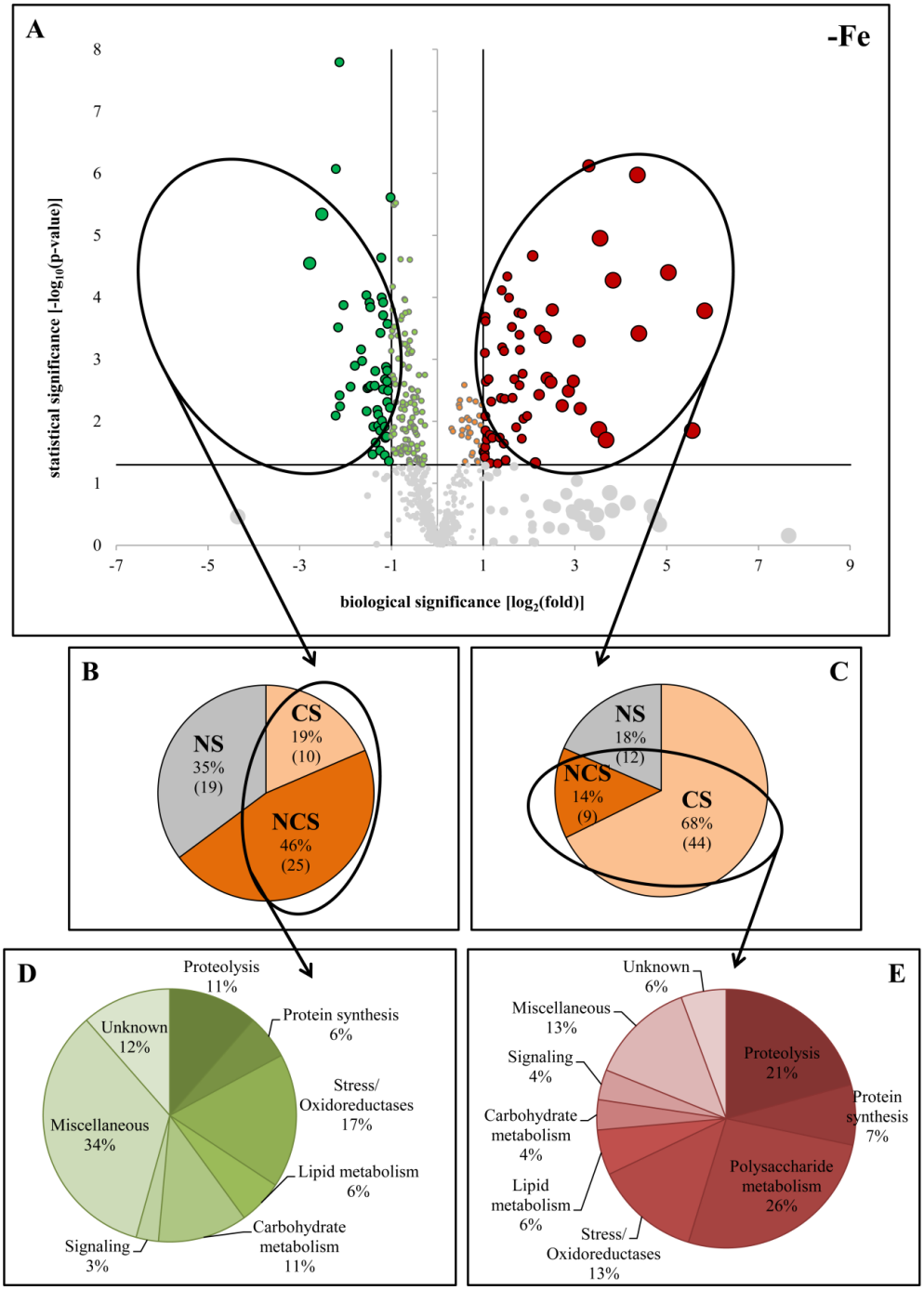

Figue 3.3.1. *Effect of Fe deficiency on the xylem protein profile as revealed by label-free shotgun analyses. Volcano scatter plot (A) showing the 643 identified and quantified proteins (peptides assigned to a protein and used for quantification ≥ 2) where proteins unaffected by Fe deficiency are depicted in grey and proteins changing as a result of Fe deficiency (ANOVA, p ≤ 0.05) are depicted green (decreasing) or red (increasing). Light colors are used for those proteins meeting only the statistical threshold (ANOVA, p ≤ 0.05) and bright colors where used when the statistical and biological (fold change ≤ 0.5 or ≥ 2) thresholds were met. The size of the dots is proportional to the fold changes. Pie chart depicting subcellular classification (NS: non-secretory, CS: classical secretory and NCS: non-classical secretory) as revealed by SignalP and SecretomeP prediction tools of proteins showing decreased (B) and increased (C) abundances. Functional classification based on GO biological process and domain annotations of secretory proteins showing decreased (D) and increased (E) abundances as a result of Fe deficiency.*

Among them, 54 proteins showed relative decreases (green dots in Figure 3.3.1A), and from these 35 were classified as secretory (10 CS and 25 NCS; Figure 3.3.1B; Table 3.4.S3 in Chapter 3.4, *Data in Brief*). The remaining 19 proteins (35 %) were classified as non-secretory and therefore excluded from the biological interpretation (Table 3.4.S3 in Chapter 3.4, *Data in Brief*).

***Table 3.3.2**. Proteins showing the large changes in abundance (fold > 5 or < 0.2) among the secretory proteins affected by Fe deficiency (ANOVA, $p \leq 0.05$ and fold ≥ 2 or ≤ 0.5). Accession indicates protein UniProt database entry. Pep_c/Pep_q indicates the number of peptides assigned to a protein and number of peptides used for quantification. Abundance changes (fold -Fe/control) were calculated by dividing the relative mean abundances in Fe-deficient (mean -Fe) by that of control samples (mean control). SecretomeP column indicates results from subcellular classification as classical (CS) and non-classical secretory (NCS) protein. Detailed information about functional classification, subcellular localization, identification and quantification is given in Table 3.4.S3 in Chapter 3.4, Data in Brief.*

Accession	Pep_c/ Pep_q	Mean Control	Mean -Fe	Fold -Fe/Control	Description	Secretome P
			Proteolysis			
K4B033	12 / 12	2448669	13965079	5.70	Predicted protein aspartic protease in guard cell 2-like (MEROPS A1)	CS
O82777	10 / 6	21221	140320	6.61	Subtilisin-like protease 3 (MEROPS S8)	NCS
K4CYB7	4 / 4	5979	59119	9.89	Predicted protein aspartic protease in guard cell 1 (MEROPS A1)	CS
K4C8U3	11 / 10	1400622	19995731	14.28	Predicted miraculin-like (MEROPS inhibitor I3, clan IC)	CS
K4AXP3	4 / 4	6188	128020	20.69	Predicted basic 7S globulin-like (MEROPS A1)	CS
			Polysaccharide metabolism			
K4CAY1	6 / 6	150109	769252	5.12	Predicted chitinase (GH-18)	CS
B5M9E5	3 / 3	2681	56597	21.11	β-Glucosidase 8 precursor (GH-17)	CS
			Oxido-reductases			
K4D7T6	10 / 9	535353	93758	0.18	Predicted peroxidase 44-like isoform 1 (AtPER44-like)	CS
K4C5I8	5 / 3	12142	88166	7.26	Predicted peroxidase 4-like (AtPER52-like)	CS
K4BFP3	3 / 2	7041	82696	11.75	Predicted peroxidase 72-like (AtPER72-like)	CS
			Lipid metabolism			
K4DD79	4 / 4	454	21484	47.32	Predicted GDSL esterase/lipase At1g28590-like	CS
			Signaling/regulation			
K4B2Y3	3 / 3	2622	86415	32.96	Probable LRR receptor-like serine/threonine-protein kinase	CS
K4D0Y5	19 / 18	51184	2924595	57.14	LRR receptor-like protein kinase	CS
			Phosphatases			
K4C6W9	3 / 3	9599	75298	7.84	Similar to predicted acid phosphatase 1-like	CS
K4CPW9	16 / 14	227820	1945258	8.54	Predicted probable inactive purple acid phosphatase 1	CS
			Unassigned/Unknown			
K4CP48	6 / 2	2243	25827	11.51	Similar to conglutin (*M. truncatula*)	CS
K4BDM8	2 / 2	22624	119293	5.27	Uncharacterized protein	CS

Functional classification of the 35 secretory proteins decreasing in abundance revealed that protein metabolism (17 %) and stress/oxido-reductases (17 %) were the most represented categories, whereas the remaining proteins were classified into a wide variety of miscellaneous categories (Figure 3.3.1D; Table 3.4.S3 in Chapter 3.4, *Data in Brief*). Interestingly, proteins involved in polysaccharide metabolism were not found among those decreasing in abundance (Figure 3.3.1D; Figure 3.3.3B). Overall, decreases were moderate (between 50 and 70 %) and only one CS protein, a peroxidase (AtPER44-like; K4D7T6) decreased > 80 % as a result of Fe deficiency (Table 3.3.2; Table 3.4.S3 in Chapter 3.4, *Data in Brief*).

Iron deficiency caused relative increases in the abundance of 65 proteins (red dots in Figure 3.3.1A) and from these 53 were classified as secretory proteins (44 CS and 9 NCS; Figure 3.3.1C; Table 3.4.S3 in Chapter 3.4, *Data in Brief*). The remaining 12 proteins (18 %) were classified as non-secretory and therefore excluded from the biological interpretation (Table 3.4.S3 in Chapter 3.4, *Data in Brief*). Functional classification of the 53 secretory proteins increasing in abundance revealed that protein metabolism (proteolysis and protein synthesis; 28%), polysaccharide metabolism (26 %), and stress/oxido-reductase proteins (13 %) were the most represented categories (Figure 3.3.1E; Figure 3.3.3B). Remarkable increases in abundance (higher than 10-fold) were observed in eight proteins classified as CS. Three of them increased > 30-fold, including two leucine rich-repeat (LRR) receptor-like kinases (K4B2Y3 and K4D0Y5) involved in regulation and a GDSL esterase/ lipase (K4DD79) classified in the lipid metabolism category (Table 3.3.2; Table 3.4.S3 in Chapter 3.4, *Data in Brief*). Five of them increased between 10- and 20-fold, including a protease inhibitor similar to miraculin (K4C8U3), a predicted basic 7S globulin with an aspartic peptidase domain (K4AXP3), a β-glucosidase 8 from the glycoside hydrolase (GH) family 17 (B5M9E5), a peroxidase (AtPER72-like; K4BFP3), and a nutrient reservoir protein similar to conglutin (K4CP48) (Table 3.3.2; Table 3.4.S3 in Chapter 3.4, *Data in Brief*). Furthermore, eight more proteins, mostly involved in catabolic processes, presented 5- to 10-fold increases, and these included three proteases (two aspartic proteases and a MEROPS family S8 peptidase), two acid phosphatases, a GH-18 family protein, a peroxidase-52 like protein, and an uncharacterized protein (Table 3.3.2). Except for the NCS MEROPS family S8 peptidase (O82777), all were classified as CS proteins (Table 3.3.2).

Effect of Mn deficiency on the xylem sap proteome

Manganese deficiency caused significant (ANOVA, $p \leq 0.05$) and biologically relevant (fold ≥ 2 or fold ≤ 0.5) changes in 118 proteins of the xylem sap proteome (Figure 3.3.2). All these proteins are presented in Table 3.4.S4 in Chapter 3.4, *Data in Brief*, and those exhibiting large changes in abundance (fold > 5 or < 0.2) are shown in Table 3.3.3.

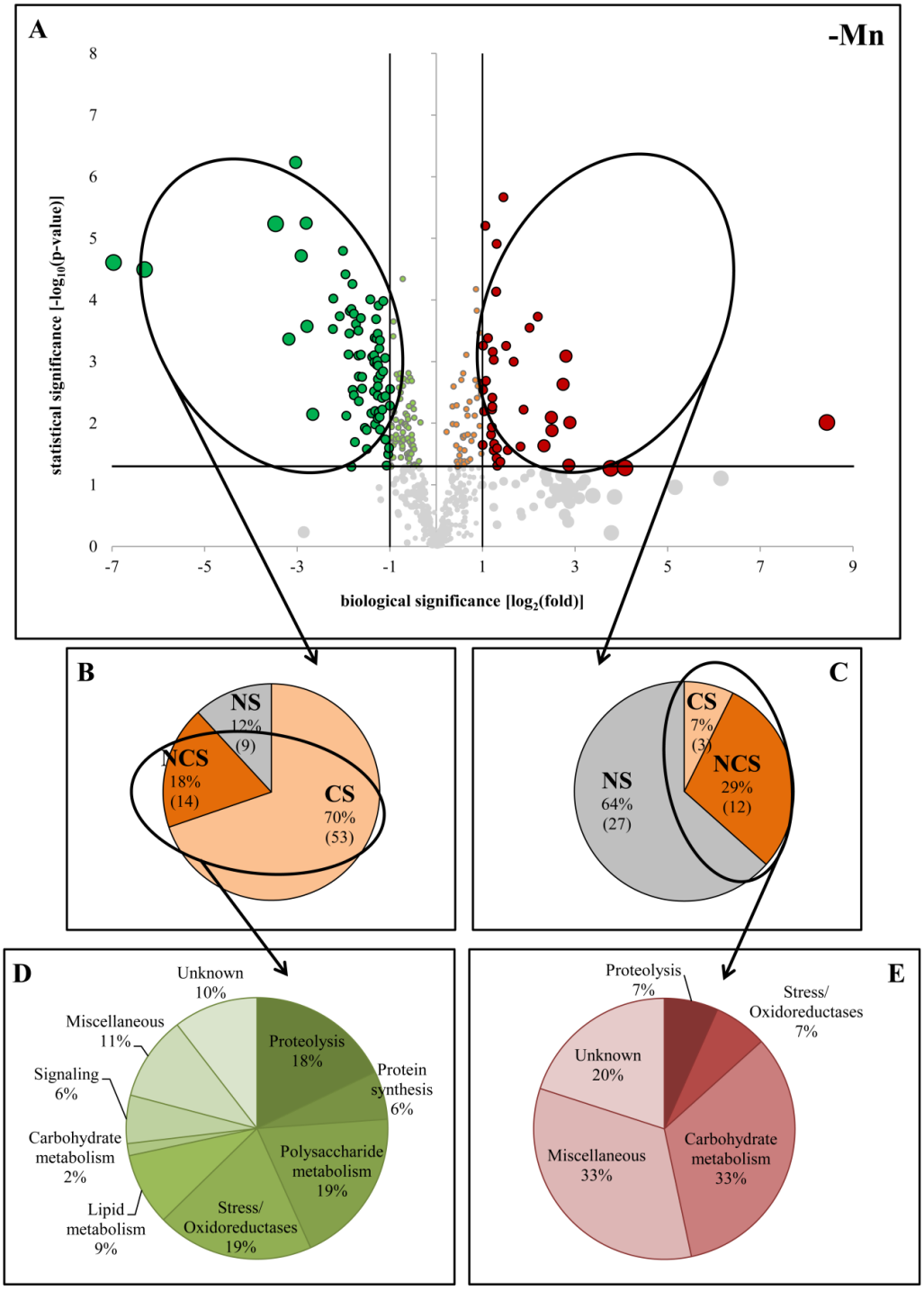

Figure 3.3.2. *Effect of Mn deficiency on the xylem protein profile as revealed by label-free shotgun analyses. Volcano scatter plot (A) showing the 643 identified and quantified proteins (peptides assigned to a protein and used for quantification ≥ 2) where proteins unaffected by Mn deficiency are depicted in grey and proteins changing as a result of Mn deficiency (ANOVA, p ≤ 0.05) are depicted green (decreasing) or red (increasing). Light colors are used for those proteins meeting only the statistical threshold (ANOVA, p ≤ 0.05) and bright colors where used when the statistical and biological (fold change ≤ 0.5 or ≥ 2) thresholds were met. The size of the dots is proportional to the fold changes. Pie chart depicting subcellular classification (NS: non-secretory, CS: classical secretory and NCS: non-classical secretory) as revealed by SignalP and SecretomeP prediction tools of proteins showing decreased (B) and increased (C) abundances. Functional classification based on GO biological process and domain annotations of secretory proteins showing decreased (D) and increased (E) abundances as a result of Mn deficiency.*

Among them, 76 proteins showed relative decreases in abundance (green dots in Figure 3.3.2A), and from these 67 were classified as secretory (53 CS and 14 NCS; Figure 3.3.2B; Table 3.4.S4 in Chapter 3.4, *Data in Brief*). Only 9 proteins (12 %) decreasing in abundance were classified as non-secretory and therefore excluded from the biological interpretation (Table 3.4.S4 in Chapter 3.4, *Data in Brief*). Functional classification of the secretory proteins decreasing in abundance with Mn deficiency revealed that protein metabolism (proteolysis and protein synthesis; 24 %), polysaccharide metabolism (19 %) and stress (19 %) were the most represented categories (Figure 3.3.2D; Figure 3.3.3B). Among them, the largest decrease (99 %) was found in two CS proteins, the endonuclease 1 (G3XKQ7) and a predicted LRR receptor-like kinase (K4B2Y3) (Table 3.3.3; Table 3.4.S4 in Chapter 3.4, *Data in Brief*). Interestingly, both proteins increased in Fe-deficient xylem sap, with the latter being among those proteins showing the largest increases (Table 3.3.2; Table 3.4.S3 in Chapter 3.4, *Data in Brief*).

Table 3.3.3. *Proteins showing the large changes in abundance (fold > 5 or < 0.2) among the secretory proteins affected by Mn deficiency (ANOVA, $p \leq 0.05$ and fold ≥ 2 or ≤ 0.5). Accession indicates protein UniProt database entry. Pep_c/Pep_q indicates the number of peptides assigned to a protein and number of peptides used for quantification. Abundance changes (fold -Mn/control) calculated by dividing the relative mean abundances in Mn-deficient (mean -Mn) by that of control samples (mean control). SecretomeP column indicates results from subcellular classification as classical (CS) and non-classical secretory (NCS) protein. Detailed information about functional classification, subcellular localization, identification and quantification is given in Table 3.4.S4 in Chapter 3.4, Data in Brief.*

Accession	Pep_c/ Pep_q	Mean Control	Mean -Mn	Fold -Mn/Control	Description	Secretome P
Protein metabolism (proteolysis and protein synthesis)						
K4D3L8	10 / 8	429869	57130	0.13	Predicted subtilisin-like protease-like (MEROPS S8)	CS
K4CUW3	2 / 2	25208	2787	0.11	Similar to 60S ribosomal protein L17	CS
Signaling/regulation						
K4B2Y3	3 / 3	2622	21	0.01	Probable LRR receptor-like Ser/Thr-kinase	CS
ATP Hydrolysis coupled to proton transport						
Q2MIB5	6 / 6	20384	142383	6.99	Similar to ATP synthase CF1 α chain	NCS
Phosphatases						
K4DC68	3 / 3	31485	4507	0.14	Predicted bifunctional purple acid phosphatase 26	CS
K4D9N7	4 / 4	95980	11757	0.12	Native purple acid phosphatase 29-like	CS
Unassigned/Unknown						
G3XKQ7	2 / 2	4416	56	0.01	Endonuclease 1	CS
K4CGQ4	4 / 4	300874	43580	0.14	Predicted uncharacterized protein LOC101247939	CS
K4D0G7	2 / 2	17572	2780	0.16	Predicted uncharacterized protein At4g06744-like	CS
K4B0S2	4 / 4	4651	33934	7.30	Similar to NAD(P)-binding Rossmann-fold protein	NCS
K4CHI8	2 / 2	851	11666	13.71	Uncharacterized protein	CS

Six more CS proteins presented considerable decreases (between 80 and 90 %) including two purple acid phosphatases (K4D9N7 and K4DC68), a predicted subtilisin from the MEROPS peptidase family S8 (K4D3L8), the subunit L17 of the 60S ribosomal complex (K4CUW3) and two uncharacterized proteins (K4CGQ4, K4D0G7) (Table 3.3.3; Table 3.4.S4 in Chapter 3.4, *Data in Brief*).

Manganese deficiency caused relative increases in the abundance of 42 proteins (red dots in Figure 3.3.2A) and from these only 15 were classified as secretory proteins (3 CS and 12 NCS; Figure 3.3.2C; Table 3.4.S4 in Chapter 3.4, *Data in Brief*). The remaining 27 proteins, accounting for a high percentage (64 %) of the identified proteins, were classified as non-secretory and therefore excluded from the biological interpretation (Table 3.4.S4 in Chapter 3.4, *Data in Brief*). Functional classification of the 15 secretory proteins showing increases in abundance revealed that carbohydrate metabolism (33 %, 5 proteins) was the most represented category (Figure 3.3.2E). The remaining proteins were distributed among unknown (three proteins), proteolysis and stress with one protein each, and in a miscellaneous group (five proteins involved in amino acid metabolism and ATP hydrolysis coupled to proton transport) (Figure 3.3.2E; Figure 3.3.3B). Most increases were moderate, ranging between 2- and 3-fold (Table 3.4.S4 in Chapter 3.4, *Data in Brief*). The most remarkable increases measured in Mn-deficient xylem sap (> 5 fold) corresponded to a regulatory subunit of the chloroplastic ATP synthase (7-fold; Q2MIB5) and to two uncharacterized proteins containing LRR (14-fold; K4CHI8) and NAD(P)-NAD(P) binding Rossmann (7-fold; K4B0S2) domains (Table 3.3.3).

Comparison of the changes observed in secretory proteins in both nutrient deficiencies

The comparison between secretory proteins showing significant and biologically relevant changes in Fe- and Mn-deficient conditions (88 and 82 proteins, respectively; Figure 3.3.3A) revealed that there were metabolic categories, including protein and polysaccharide metabolisms and stress/oxido-reductases, which clearly followed a different trend depending on the specific nutrient deficiency (Figure 3.3.3B). When considering the 24 secretory proteins changing in relative abundance in both nutrient deficiencies (20 CS and 4 NCS) (Table 3.3.4; Figure 3.3.3A and C), all of them decreased as a result of Mn deficiency, whereas in Fe-deficient xylem sap only eight of them decreased (Figure 3.3.3C, Table 3.3.4). Proteins in the protein and polysaccharide metabolism categories followed opposite trends (as occurred when all proteins changing in abundance were compared; Figure 3.3.3B), with most proteins increasing in Fe-deficient and decreasing in Mn-deficient xylem sap (Figure 3.3.3C). A similar behavior was observed in the miscellaneous group of proteins. On the other hand, the categories of lipid- and stress/oxido-reductase showed a similar behavior in both deficiencies, with the majority of proteins decreasing (Figure 3.3.3C).

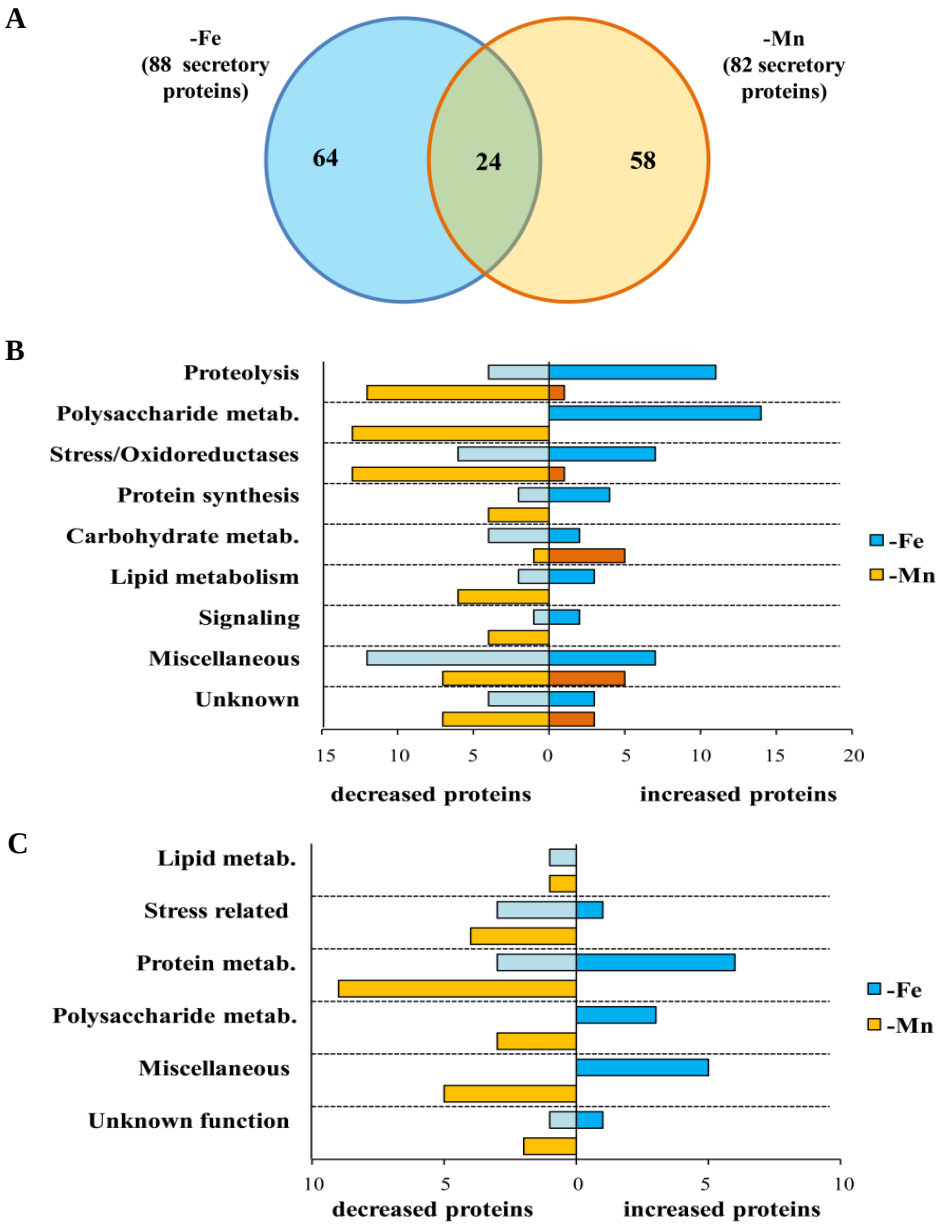

Figure 3.3.3. *A) Venn diagram comparing the number of secretory proteins changing as a result of Fe and Mn deficiency ($p \leq 0.05$, number of peptides for identification and quantification ≥ 2 and fold ≤ 0.5 or ≥ 2). B) Functional classification of all secretory proteins showing changes in Fe and Mn deficiencies. Proteins showing significant changes in both comparisons ($p \leq 0.05$), identified and quantified with at least two peptides, and above the threshold level (fold change ≥ 2 or ≤ 0.5) were classified according to their functions. Blue and orange bars indicate number of proteins decreasing and increasing in relative abundance in Fe deficiency and Mn deficiency, respectively. C) Functional classification of the 24 common secretory proteins showing changes in both treatments. Proteins showing significant changes in both comparisons ($p \leq 0.05$), identified and quantified with at least two peptides, and above the threshold level (fold change ≥ 2 or ≤ 0.5) were classified according to their functions. Blue and orange bars indicate number of proteins decreasing and increasing in relative abundance in Fe deficiency and Mn deficiency, respectively.*

Proteins showing opposite changes in abundance included three structural components of the ribosome and two aspartic proteases in the protein metabolism category, two hydrolases from families GH16 and 17, a SGN-hydrolase and a pectin esterase inhibitor in the polysaccharide metabolism category, and a miscellaneous group containing seven proteins

(three acid phosphatases, a LRR receptor-like kinase, a nectarin-1, an endonuclease 1 and an uncharacterized protein) (Table 3.3.4). The most remarkable change in these groups was measured in the LRR receptor-like kinase which, as commented above, was highly increased (33-fold) in Fe-deficient xylem sap and almost disappeared in Mn-deficient conditions.

Table 3.3.4*. List of the 24 secretory proteins (identified and quantified with at least two unique peptides) affected by both deficiencies (ANOVA, $p \leq 0.05$ and fold ≥ 2 or ≤ 0.5). Accession (UniProt identifiers) and protein description are shown in the first two columns, fold changes induced by Fe (-Fe/C) and Mn (-Mn/C) deficiencies were calculated by dividing the relative mean abundances in deficient by that of control samples. SecretomeP column indicates results from subcellular classification as classical (CS) and non-classical secretory (NCS) protein. Detailed information about functional classification, subcellular localization, identification and quantification is given in Tables S3 and S4 in Chapter 3.4, Data in Brief.*

Accession	Description	-Fe/C	-Mn/C	SecretomeP
K4D7T6	Predicted peroxidase AtPER44-like isoform 1 (AtPER44-like)	0.18	0.21	CS
K4BTH7	Predicted peroxidase AtPER12-like	0.32	0.41	CS
K4C1C0	Predicted cationic peroxidase 1 (AtPER52-like)	0.35	0.43	CS
K4ATR4	Predicted serine carboxypeptidase-like 45. (MEROPS S10)	0.22	0.30	CS
K4D3L8	Predicted subtilisin-like protease (MEROPS S8)	0.36	0.13	CS
K4C895	Predicted protein aspartic protease in guard cell 1 (MEROPS A1)	0.48	0.43	NCS
K4B315	Predicted PI-PLC X domain-containing protein; At5g67130-like (phosphatidylinositol-specific phospholipase C)	0.37	0.29	CS
K4CGQ4	Predicted uncharacterized protein LOC101247939	0.42	0.14	CS
K4CG62	Similar to ribosomal protein L11-like (*N. tabacum*)	2.01	0.35	NCS
K4BA70	Similar to 40S ribosomal protein S15-like (*S. tuberosum*)	2.07	0.31	NCS
K4CUW3	Similar to 60S ribosomal protein L17 (*A. thaliana*)	2.49	0.11	CS
B5M9E5	β-Glucosidase 8 precursor (GH-17)	21.11	0.28	CS
K4D4J5	Predicted cell wall / vacuolar inhibitor of fructosidase 2-like (pectinesterase_inhib_dom)	3.09	0.47	CS
K4B1G1	Rhamnogalacturonan acetylesterase-At4g34215-like (SGNH-hydro)	3.22	0.44	CS
Q6RHX9	Xyloglucan endotransglucosylase-hydrolase XTH6 precursor (GH-16)	3.59	0.34	CS
K4CBX5	Predicted probable inactive purple acid phosphatase 27	2.74	0.42	CS
K4CPW9	Predicted probable inactive purple acid phosphatase 1	8.54	0.41	CS
K4DC68	Predicted bifunctional purple acid phosphatase 26	3.20	0.14	CS
K4DGL5	Predicted protein aspartic protease in guard cell 1 (MEROPS A1)	3.89	0.32	CS
K4CYB7	Predicted protein aspartic protease in guard cell 1 (MEROPS A1)	9.89	0.24	CS
K4B2Y3	Probable LRR receptor-like Ser/Thr- kinase	32.96	0.01	CS
G3XKQ7	Endonuclease 1	2.57	0.01	CS
K4B1G7	Predicted nectarin-1 (MnSOD-like)	3.30	0.29	NCS
K4BE45	Predicted uncharacterized protein LOC101253159	3.64	0.38	CS

Proteins decreasing in both treatments included three peroxidases (AtPER14, 12- and 52-like), three proteases from the MEROPS peptidase families S8, 10 and A1, a lipid domain (PI-PLC X) containing protein and an uncharacterized protein (Table 3.3.4).

3.3.4. Discussion

The proteomic approach used in this study has allowed for the reliable identification and quantification of a large set of proteins in the xylem sap (643). This number is slightly higher than those found in other xylem sap studies with LC–MS/MS (Ligat et al., 2011; Zhang et al., 2015) and considerably higher than those found with 2-DE (100–200 proteins) (Rodríguez-Celma et al, 2016a), highlighting the sensitivity of the methodological approach used. Approximately 67 % of the identified xylem proteins (425) were classified as secretory using prediction tools, a percentage lower than those reported, using a similar shotgun approach, in *Brassica oleracea* (87 %) (Ligat et al., 2011) and *Gossypium hirsutum* (90 %) (Zhang et al., 2015). Approximately one third of the identified and quantified proteins were not considered in the biological interpretation of the results, since they were classified as non-secretory and thus could reflect cytoplasmic contamination. The higher percentage of non-secretory proteins found here may also be ascribed to the high sensitivity of the LC–MS/MS approach utilized, although their unequivocal assignment to the xylem sap proteome would require further studies.

Both micronutrient deficiencies caused significant and biologically relevant changes in a similar number of secretory proteins, accounting for approximately 20 % of the secretory xylem sap proteome. This percentage is within the ranges reported for the effects of Fe deficiency on other sub-proteomes (López-Millán et al., 2013) and somewhat higher than those reported for Mn-deficient plants (Li et al., 2015; Zargar et al., 2015). Manganese deficiency caused decreases in abundance in most of the xylem secretory proteins changing in abundance (82 %; 67 proteins), whereas only 40 % (35 proteins) decreased in abundance as a result of Fe deficiency (Figure 3.3.3B).

Overall, these results, along with the protein concentration changes observed (Table 3.3.1) indicate that Fe and Mn shortage increased and decreased, respectively, the xylem sap protein load. This would be in agreement with the opposite changes observed with both stresses in ribosomal proteins and certain proteases that can putatively be involved in protein maturation (Table 3.3.4). Since the xylem protein extraction yield in Mn-deficient plants was lower than those in Fe-deficient and control plants, the Mn deficiency-induced decreases in protein abundances would be even more marked if changes were compared on a xylem sap volume basis instead of on a protein basis.

The xylem sap proteome of manganese-deficient plants is less proteolytic than that of iron deficient plants

Among the secretory proteins affected in abundance by Fe and Mn deficiencies (88 and 82 proteins, respectively) a large number (15 and 13 proteins, respectively) were related to proteolysis. However, whereas the large majority of proteins affected by Fe deficiency (11 proteins) increased in abundance (Table 3.4.S3 in Chapter 3.4, *Data in Brief*; Figure 3.3.3B), Mn deficiency caused decreases in the relative abundance of all but one of these proteins (Figure 3.3.3B). Proteins increasing upon Fe deficiency included five aspartic proteases (MEROPS family A1), three subtilisin-like serine peptidases (MEROPS family S8), one serine carboxypeptidase (MEROPS family S10) and two protease inhibitors (MEROPS inhibitor family I3 and I20). Five of these proteins (Table 3.3.2) presented abundance increases among the largest measured in this study (between 5- and 21- fold). The peptidases decreasing with Mn deficiency were similar to those found in Fe-deficient xylem sap and included four aspartic proteases (MEROPS family A1), four subtilisin-like serine peptidases (MEROPS family S8), three serine carboxypeptidase (MEROPS family S10) and a glycopeptide hydrolase (PNGase A). The only protease increasing with Mn deficiency was a non-classical secretory processing metalloprotease (MEROPS family M16) that is likely to be mitochondrial. Among these proteins, a subtilisin-like protein (K4D3L8) showed one of the largest decreases measured (87%). These specific groups of proteases have been consistently found in xylem sap, where they play roles in the degradation of damaged proteins and signaling, and also constitute a defense mechanism against pathogen infection (Rodríguez-Celma et al., 2016a).

The increases in proteases abundance upon Fe deficiency may suggest that they are needed to mediate degradation of ROS-damaged proteins, since it is known that Fe deficiency increases oxidative stress (Lan et al., 2011; Zaharieva and Abadía, 2003). On the other hand, the decreases measured in Mn-deficient plants support that the environment of Mn-deficient xylem sap is less proteolytic and therefore it can be hypothesized that damaged proteins are less abundant under Mn deficiency than under Fe deficiency or control conditions. However, not all the proteases increased upon Fe shortage (four of them decreased) and protease inhibitors significantly increased in abundance, suggesting that creating a proteolytic environment for damaged protein degradation or defense is not the only role of the proteins found in this category in the Fe-deficient xylem sap, with other additional roles being likely. For instance, proteases may be needed for maturation of cell wall proteins (Schaller, 2004), and in *Arabidopsis* it has been described that some extracellular aspartic proteases can generate peptide elicitors, mediating a signaling system involved in the activation of local and systemic defense responses against biotic stresses (Xia et al., 2004). Indeed, three aspartic proteases were affected

by both nutrient deficiencies (one decreasing in both cases and two increasing or decreasing with Fe or Mn deficiency, respectively; Table 3.3.4). Taken together with the changes of LRR-RLKs (commented below), it is tempting to speculate that a similar peptide signaling system may also occur in nutrient deficiencies. Finally, the decrease in proteases upon Mn shortage could also indicate that maturation of secreted proteins is not needed, in line with the very low percentage (18 %) of secretory proteins increasing under Mn deficiency.

The xylem sap proteome of iron-deficient plants shows more protection against oxidative stress than that of manganese-deficient plants

The stress category (including oxido-reductases and defense proteins) was largely affected by Fe and Mn deficiencies (13 and 14 proteins, respectively). However, while Fe deficiency caused both increases and decreases in protein abundance (seven and six proteins, respectively), Mn deficiency caused decreases in abundance in all but one protein. Most of the proteins in this category corresponded to oxido-reductases, but the subcategories affected were slightly different depending on the specific nutrient stress, with Fe deficiency inducing changes mostly in class III heme-binding peroxidases (five decreasing and four increasing), and Mn deficiency causing decreases in Cu oxidases (five proteins) and peroxidases (three proteins).

The peroxidases decreasing in abundance in both deficiencies were similar, and among them we found orthologues of the *Arabidopsis* AtPrx 12, 44, 52 (in both deficiencies) and AtPrx 53 (only in the case of Fe deficiency) (Tables 3.4.S3 and 3.4.S4 in in Chapter 3.4, *Data in Brief*). All but AtPrx 44, which has an unknown specificity, are known to be involved in lignin formation and their activities affect lignin content, structure and composition (Fernández-Pérez et al., 2015a; Shigeto et al., 2014, 2016). Therefore, these decreases support that the lignin composition of the secondary cell wall is affected similarly by both nutrient deficiencies. However, four more peroxidases also increased in Fe-deficient xylem sap, and they were similar to AtPrx 21, 52, 63 and 72. Two of them (AtPrx 52 and 72) are involved in lignin synthesis, one has an unknown specificity and one (AtPrx 21) has been described as a defense protein (Chassot et al., 2007). These results indicate that the effect of Fe deficiency on the secondary cell wall *via* peroxidase activity is more marked than that of Mn deficiency, and furthermore reveal the complexity of the changes, since some lignin-related peroxidases increased and some decreased. It is remarkable that the availability of Fe does not seem to play a direct role in the abundance of these heme-binding peroxidases. In addition, the peroxidases increasing in abundance can also have a role protecting from Fe deficiency induced oxidative stress. The existence of oxidative stress is also supported by the increase measured in a predicted nectarin-1, (K4B1G7), a Mn binding germin likely having MnSOD activity (Carter and Thornburg, 2000), which is likely to

protect from oxidative stress while providing the substrate for the peroxidases. In the Mn-deficient xylem sap this nectarin decreased in abundance, reflecting the Mn shortage.

Manganese deficiency also caused decreases in five Cu-oxidases, including three blue-copper proteins of unknown function, with one cupredoxin and one phytocyanin domain, as well as two multi-copper oxido-reductases. These decreases might indicate changes in the redox state of the xylem sap towards a less oxidative environment, although the decrease in the predicted laccase (K4C1R5), which plays a role in lignin polymerization (Turlapati et al., 2011), may also affect the structure of the secondary cell wall. Two more proteins decreasing upon Mn deficiency were a predicted γ-glutamyltranspeptidase 3-like (K4DBV2), whose *Arabidopsis* orthologue has been described as a cell wall associated protein that prevents oxidative stress by removing oxidized glutathione (Ferretti et al., 2009; Ohkama-Ohtsu et al., 2007), and a L-gulonolactone oxidase-like, which catalyzes the synthesis of ascorbic acid (Maruta et al., 2010). These decreases in antioxidant enzymes also support that the environment in the Mn-deficient xylem is less oxidative than in control plants.

Overall, the changes in abundance of oxidative and proteolytic enzymes, which increase in Fe deficiency and decrease in Mn deficiency (Figure 3.3.3B), indicate that Fe deficiency elicits more stress responses in the xylem sap than Mn deficiency. In addition, changes in oxido-reductases related to lignin metabolism (which are similar to those measured in GHs) suggest differences in the secondary cell wall composition between Mn-deficient and Fe-deficient plants that could be mainly attributed to peroxidases in the case of Fe deficiency, and peroxidase, copper-oxidase and fasciclin-like arabinogalactan proteins in the case of Mn deficiency.

Iron and manganese deficiencies affect primary cell wall metabolism in an opposite manner

Iron and Mn deficiencies elicited a marked activation and deactivation, respectively, of the primary cell wall metabolism. A large number of proteins (14) involved in polysaccharide metabolism increased in abundance with Fe deficiency (Figure 3.3.3B), including 10 glycoside hydrolases (GH; families GH-5, 16, 17, 18, 19 and 20), two pectic modifying enzymes (K4D4J5 and K4D0N0), a rhamnogalacturonan acetylesterase (K4B1G1) and an expansin precursor (A7X331) (Table 3.4.S3 in Chapter 3.4, *Data in Brief*). Two of the GHs, belonging to families 17 (B5M9E5; β-glucosidase 8 precursor) and 18 (K4CAY1; a predicted chitinase), showed increases among the largest measured in this study (21- and 5- fold, respectively), whereas the others increased markedly (between 2- and 5-fold). All these proteins are extracellular and participate in the hydrolysis and/or rearrangement of glycoside bonds in cell wall polysaccharides (Minic, 2008). Five of the GHs belong to families 5 and 17, which are mainly

endo-glucanases (CAZy description) and in conjunction with the two pectin-esterases, could participate in primary cell wall degradation. In line with this hypothesis, it has been described that Fe deficiency causes a reduction in the xylem vessel size in leaves (Eichert et al., 2010; Fernández et al., 2008), as well as changes in the lignification pattern in roots (Donnini et al., 2009) and in the lignin/ protein ratio in stem tissues (Rodríguez-Celma et al., 2016c). Also, several GHs have been described as Fe-responsive in different sub-proteomes of Fe-deficient plants (López-Millán et al., 2013), with some increasing in abundance in the leaf apoplastic fluid (Ceballos-Laita et al., 2015). Iron deficiency-induced modifications in the primary cell wall may affect sap flow and composition by altering permeability, although it has also been speculated that the increases in abundance of GHs may lead to an extra C supply to complement the low photosynthetic rates of Fe-deficient plants (Donnini et al., 2010). Additionally, four GHs belonging to families 18, 19 and 20 are N-acetyl-hexosaminidases, mainly involved in N-glycan degradation, and therefore their increases may indicate a decrease in N-glycosylation, which is assumed to be a major post-translational modification of secreted proteins.

Conversely, Mn deficiency led to a down regulation of primary cell wall metabolism. Thirteen polysaccharide-related proteins decreased in abundance, with nine of them being GHs, two being pectic-modifying enzymes and two more being related to rhamnogalacturonan metabolism (a lyase and an acetylesterase) (Table 3.4.S4 in Chapter 3.4, *Data in Brief*). Among the GHs decreasing in abundance, two belong to GH families 10 and 17 (xylanases and endoglucanases) involved in cellulose and xylan degradation whereas three more belong to GH-19, 20 and 35 (N-acetylglucosaminidase, N-acetyl-galactosaminidase, and β-galactosidase) which hydrolyze C-N bonds. These decreases suggest that processes involving cell wall and N-glycan degradation may be reduced in the xylem sap of Mn-deficient plants, conversely to what was observed in the case of Fe deficiency. Likewise, the decreases in two pectin esterases and in three proteins affecting galacturonate residues (a rhamnogalacturonate lyase, the polygalacturonase GH-28 and a rhamnogalacturonate acetylesterase), which are very abundant in pectic polysaccharides, support that primary cell wall degradation is reduced upon Mn deficiency. Overall, the changes induced by Mn deficiency could lead to modifications in the rigidity of the primary cell wall, following the opposite direction than those observed with Fe deficiency.

Several xylem signaling pathways seem to play a role in the response to nutrient deficiencies

Data suggest that a CLE (CLAVATA3/EMBRYO SURROUNDING REGION-RELATED; CLV3/ESR-related) signaling pathway could be elicited in the xylem in response of Fe deficiency. The largest increases in abundance with Fe deficiency were measured in two leucine

rich repeat-receptor like kinases (LRR-RLK), K4D0Y5 and K4B2Y3 (57- and 33-fold increases, respectively), with K4B2Y3 showing one of the largest decreases in abundance (> 99%) upon Mn deficiency. The function of K4B2Y3 is unknown, but it is likely that this LRR-RLK is involved in a signaling pathway induced under Fe deficiency but repressed under Mn-deficient conditions. An antagonistic regulation of Mn and Fe acquisition has been recently proposed to occur in a genomics and proteomics study on whole *Arabidopsis* roots (Rodríguez-Celma et al., 2016b). The *Arabidopsis* orthologue of K4D0Y5 (AtSKM1, At2g25790) participates in the CLE45 signaling pathway (Endo et al., 2013; Kang et al., 2016). CLE45 mitigates heat stress by binding with SKM1/SKM2 to sustain pollen growth under high temperatures (Endo et al., 2013). Members of the CLE peptide family are xylem borne, composed of 12 or 13 amino acids and play crucial roles in xylem developmental processes (Hirakawa et al., 2008, 2010; Ito et al., 2006; Ohyama et al., 2009; Stahl et al., 2009). Furthermore, members of the CLE family are involved in N and P stress signaling pathways that regulate plant growth and development (Wang et al., 2015). Therefore, it is tempting to speculate that a xylem CLE signaling pathway is also involved in the response to Fe deficiency *via* K4D0Y5, and that this pathway may regulate Fe-induced changes in xylem growth processes.

Data also suggest that a lipid-based signaling system exists in the xylem sap that is tuned differently in the Fe and Mn deficiencies. In the phloem, lipids have been proposed as long-distance signals in response to abiotic stress in a mechanism that involves a putative GDSL-motif lipase, PIG-P-like protein, with a possible receptor-like function, and a lipid transfer protein (Barbaglia et al., 2016; Benning et al., 2012). Proteins involved in lipid metabolism were affected by both nutrient deficiencies (five and six proteins in Fe and Mn deficiency, respectively). The second largest increase in Fe-deficient xylem sap was measured in a GDSL-motif lipase (K4DD79; 47- fold). The exact role that this lipase plays in the Fe deficiency response is not clear. However, the presence of four more proteins related to lipid metabolism (two increasing and two decreasing), and especially the 3-fold increase of a lipid transfer protein (K4BFV4) could support the existence of a lipid-based signaling system in the xylem sap (Carella et al., 2016). Interestingly, upon Mn shortage, significant decreases were measured in all six proteins related to lipid metabolism, including a GDSL motif lipase and two lipid transfer proteins. The fact that these proteins decreased upon Mn deficiency could indicate that this signaling pathway is repressed under Mn stress, different to what occurs with Fe deficiency. However, one of them, a phosphatidylinositol-specific phospholipase C (PI-PLC) domain-containing protein (K4B315) decreased in both treatments (Table 3.3.4). PI-PLCs often play important roles in various signaling cascades (Hicks et al., 2008; Meldrum et al., 1991) and

therefore its decrease might indicate a common regulatory control point occurring in both deficiencies.

It is also worth mentioning that signaling-related fasciclin-like arabinogalactan proteins decreased in abundance in the xylem sap of plants affected by both nutrient deficiencies, including three in Mn-deficient (FLA-2, 11- and 12-like) and one in Fe-deficient (FLA-9-like) xylem sap. The FLA-11- and 12-like proteins belong to a subset of FLAs (groupA) that appear to contribute to the biomechanical properties (strength and elasticity) of stems through their impact on the synthesis and architecture of the secondary cell wall (Zhang et al., 2015; MacMillan et al., 2010).

Iron and Mn deficiencies also affect phosphorylation and glycosylation processes, as judged by changes in PAPs abundances, with modifications generally following an opposite pattern. Upon Fe deficiency, four purple acid phosphatases (PAPs) showed abundance increases ranging between 3 and 9-fold. These increases may account for changes in the phosphorylation status of the xylem sap, in line with the proposed existence of an extracellular phosphorylation network (Ndimba et al., 2003). It is generally thought that a main role for PAPs is to provide P to overcome P starvation conditions (Del Vecchio et al., 2014; Robinson et al., 2012), but some PAPs are extracellular and can also dephosphorylate GHs, thus modulating their activities in the cell walls (Kaida et al., 2010). Given that PAPs are Fe-containing proteins, their increases in abundance upon Fe starvation denote important roles. Having this in mind, and since a human PAP can act as an Fe transporter in combination with ascorbate (Nuttleman and Roberts, 1990), it is tempting to speculate that these proteins may also somehow participate in the transport of Fe in the xylem sap. In Mn-deficient xylem sap, considerable decreases (60–90 %) were measured in the PAPs abundances, opposite to what was observed upon Fe deficiency. This supports that in Mn limiting conditions proteins would likely remain phosphorylated when compared to control and/or Fe-deficient xylem sap, thus revealing a different tuning of phosphorylation in Fe and Mn stresses. A similar situation was observed for N-glycosylation, since, as commented in previous Section, GHs hydrolyzing C-N bonds increased in abundance in xylem sap of Fe-deficient plants but decreased in Mn-deficient ones.

Synthesis of proteins associated to the xylem sap is elicited by Fe deficiency and decreased by Mn deficiency

Interestingly, four structural components of the ribosome increased in abundance in Fe-deficient xylem sap whereas four decreased in Mn-deficient xylem sap, one of them showing one of the largest decreases observed (89 %). Since most of these proteins were classified as NCS, this suggests that Fe deficiency causes an increase in the abundance of ribosomes located in cells

having a close proximity to the xylem vessels, therefore being easily leaked upon cell rupture during xylem sampling. This is in line first with the large number of proteins increasing (60 %) and decreasing (82 %) in abundance in Fe- and Mn-deficient conditions, respectively, which would imply that *de novo* synthesis of proteins is not needed in Mn deficiency, and second with the opposite changes observed in certain proteases that can be involved in protein maturation (Table 3.3.4).

3.4. Data on xylem sap proteins from Mn- and Fe-deficient tomato plants obtained using shotgun proteomics

Laura Ceballos-Laita [a], Elain Gutierrez-Carbonell [a], Daisuke Takahashi [b,c], Anunciación Abadía [a], Matsuo Uemura [c], Javier Abadía [a], Ana Flor López-Millán [d]

[a] *Department of Plant Nutrition, Aula Dei Experimental Station, Consejo Superior de Investigaciones Científicas (CSIC), Zaragoza, Spain*

[b] *United Graduate School of Agricultural Sciences, Iwate University, Morioka, Japan*

[c] *Cryobiofrontier Research Center, Faculty of Agriculture, Iwate University, Morioka, Japan*

[d] *USDA-ARS Children's Nutrition Research Center, Department of Pediatrics, Baylor College of Medicine, Houston, TX, USA*

Published in Data in Brief (2018) 17, 512-516 (*doi.org/10.1016/j.dib.2018.01.034*)

ABSTRACT

This article contains consolidated proteomic data obtained from xylem sap collected from tomato plants grown in Fe- and Mn-sufficient control, as well as Fe-deficient and Mn-deficient conditions. Data presented here cover proteins identified and quantified by shotgun proteomics and Progenesis LC-MS analyses: proteins identified with at least two peptides and showing changes statistically significant (ANOVA; $p \leq 0.05$) and above a biologically relevant selected threshold (fold ≥ 2) between treatments are listed. The comparison between Fe-deficient, Mn-deficient and control xylem sap samples using a multivariate statistical data analysis (Principal Component Analysis, PCA) is also included. Data included in this article are discussed in depth in the research article entitled "Effects of Fe and Mn deficiencies on the protein profiles of tomato (*Solanum lycopersicum)* xylem sap as revealed by shotgun analyses" (Ceballos-Laita et al., 2018, Chapter 3.3). This dataset is made available to support the cited study as well to extend analyses at a later stage.

3.4.1. Specifications table

Subject area	Biology
More specific subject area	Plant Physiology
Type of data	Tables, figures and images (pictures of plant material)
How data was acquired	Shotgun mass spectroscopy approach using an ADVANCE UHPLC system
Data format	Raw, statistical uni- and multi-variate analysis

Experimental factors	Proteins were directly isolated from the xylem sap of Fe-deficient, Mn-deficient and control (Fe- and Mn-sufficient) plants
Experimental features	Plants grown in nutrient solution under control, Fe- and Mn-deficient conditions were analyzed and xylem sap collected by de-topping. Xylem sap proteins were precipitated, resuspended and analyzed by label free LCMS/MS (Ceballos-Laita et al., 2018, Chapter 3.3)
Data source location	Tomato (*Solanum lycopersicum*, cv. Tres Cantos) plants were grown hydroponically in a controlled environment chamber
Data accessibility	The MS proteomics data have been deposited to the ProteomeXchange Consortium *via* the Pride partner repository with the data set identifier PXD007517

3.4.2. Value of the data

- Tomato xylem sap proteins identified and quantified using a shotgun approach are presented herein, providing data on the protein composition of this fluid and facilitating comparisons with other plant species and different plant stresses.
- Statistically significant and biologically relevant changes in the xylem sap protein composition upon Fe and Mn deficiencies provide information to assess the effects of these nutritional deficiencies on the metabolic pathways of tomato plants growing in controlled environmental conditions, and results could be compared to those found in other nutritional constraints.
- Data would allow other researchers to assess the companion paper (Ceballos-Laita et al., 2018, Chapter 3.3), extend analyses at a later stage and facilitate the study of target proteins in tomato xylem sap.

3.4.3. Data

The proteome data presented herein were collected from xylem sap fluid of tomato plants grown in two nutritional deficiencies that occur often in plants, Fe and Mn deficiency (Figures 3.4.1 and 3.4.2). A shotgun proteomic approach and data processing software were used to identify and quantify a large number of proteins in the xylem sap as well as to assess the changes induced in the proteome of this fluid by these nutritional stresses. The peptides used in the quantification and the protein profiling of the xylem sap proteome are shown in Tables 3.4.S1 and 3.4.S2, respectively. To assess the effects of Fe deficiency or Mn deficiency, the ratios of normalized protein abundances between nutrient-deficient and control samples were calculated, and proteins showing changes statistically significant (ANOVA; $p \leq 0.05$) and above a biologically relevant threshold (fold ≥ 2) are shown in Tables 3.4.S3 and 3.4.S4, respectively.

Multivariate statistical analyses (Principal Component Analysis, PCA) of proteins showing statistically significant changes (ANOVA; $p \leq 0.05$) are shown in Figure 3.4.3. The MS proteomics data have been deposited to the ProteomeXchange Consortium *via* the Pride partner repository with the data set identifier PXD007517.The full description of Materials and Methods, Results and Discussion for this data set are presented in the associated research article (Ceballos-Laita et al., 2018, Chapter 3.3).

3.4.4. Experimental design, materials and methods

For each of three treatments (Fe- and Mn-sufficient control, Fe-deficient and Mn-deficient conditions), the xylem sap fluid from six independent batches of plants were collected after eight days of treatment (Figures 3.4.1 and 3.4.2).

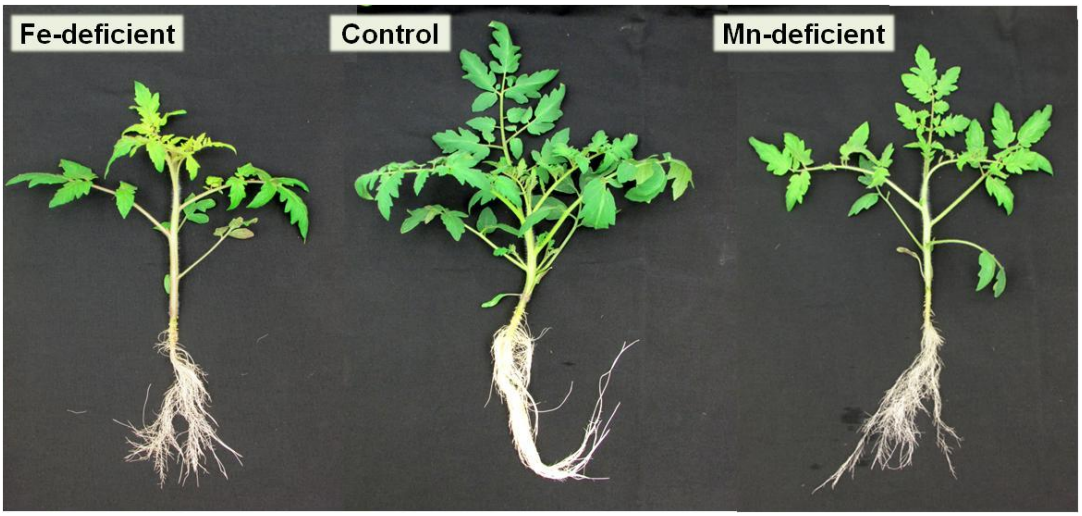

Figure 3.4.1: *Composite image depicting pictures of whole plants from Fe-deficient, control and Mn-deficient plants at the time of sampling.*

In each batch of plants, fluid from 16-18 plants was pooled together and considered as a biological replicate (total n = 6). Xylem sap proteins were precipitated, resuspended in the appropriated buffer (Ceballos-Laita et al., 2018, Chapter 3.3) and analyzed by shotgun proteomics. Mass spectrometry analysis was carried out on an LTQ Orbitrap XL (Thermo Fisher Scientific, Waltham, MA, USA) equipped with Xcalibur software (v. 2.0.7, Thermo Fisher Scientific). Parameters used were: peptide mass and MS/MS tolerances of ± 5 ppm and ± 0.6 Da, respectively; one missed cleavage, fixed modification carbamidomethylation (Cys) and variable modification oxidation (Met) allowed; and peptide charges +1 to +3. Data files obtained were processed (Progenesis QI) and all peptides identified and quantified are shown in Table 3.4.S1. Proteins identified (MASCOT v. 2.4.1 using the NCBI database) are shown in Table 3.4.S2. Data on abundance changes between treatments are provided after using two filters: ANOVA statistical significance ($p \leq 0.05$) and a biologically relevant threshold level

(fold ≥ 2) (Tables 3.4.S3 and 3.4.S4, for Fe and Mn deficiencies, respectively). Principal Component Analysis (PCA) analyses were carried out using SPSS Statistical software (v. 24.0) (Figure 3.4.3).

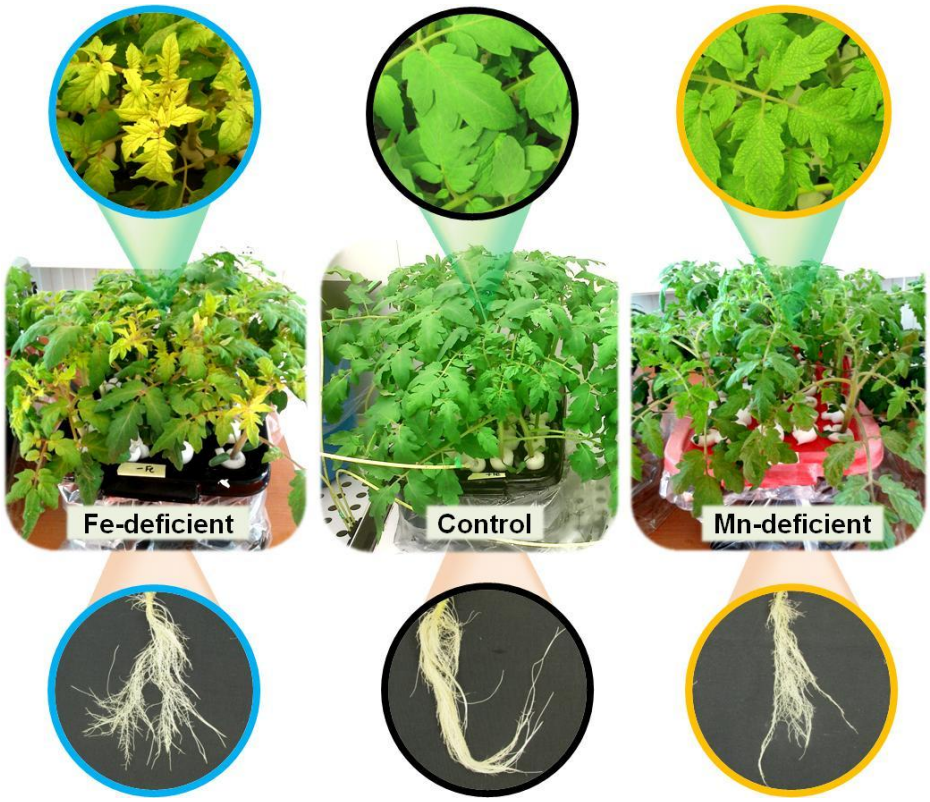

Figure 3.4.2: *Composite image showing pictures of the plant culture set up for Fe-deficient, control and Mn-deficient plants at the time of sampling, with insets showing close-ups of the leaves and roots of the same plants.*

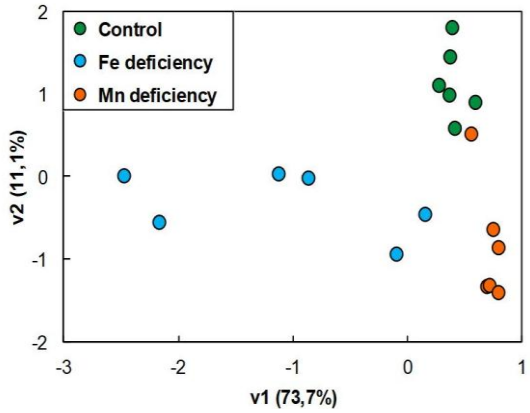

Figure 3.4.3: *Score scatter PCA (Principal Component Analysis) plot of nutrient-deficient samples when compared to controls. Principal component analysis was carried out using SPSS Statistical software (v. 24.0) and included proteins showing statistically significant changes (ANOVA; $p \leq 0.05$) as a result of the nutrient deficiency treatments. Fe-sufficient, Fe-deficient and Mn-deficient samples are depicted with green, blue and orange circles, respectively.*

Protein identification was carried out using the list of total peptides with the Mascot search engine (Ceballos-Laita et al., 2018, Chapter 3.3). Protein information was exported from Mascot .xml format and imported to Progenesis (Ceballos-Laita et al., 2018, Chapter 3.3), which then associates peptide and protein information.

Table 3.4.S1: *List of peptides identified and quantified by shotgun proteomics and Progenesis LC-MS analyses. (https://ars.els-cdn.com/content/image/1-s2.0-S2352340918300374-mmc2.xlsx)*

Table 3.4.S2: *List of proteins identified and quantified by shotgun proteomics and Progenesis LC-MS analyses. (https://ars.els-cdn.com/content/image/1-s2.0-S2352340918300374-mmc3.xlsx)*

Positive protein identification was assigned with at least two unique top-ranking peptides with scores above the statistical and biological threshold levels (ANOVA; $p \leq 0.05$ and fold ≥ 2). Proteins achieving these thresholds are shown in Tables 3.4.S3 and 3.4.S4 for Fe-and Mn-deficient samples, respectively.

Table 3.4.S3: *List of proteins showing significant changes (ANOVA; $p \leq 0.05$) above the biological relevance threshold (fold ≥ 2) and identified and quantified with at least two peptides when Fe-deficient xylem sap samples were compared to those of control conditions. (https://ars.els-cdn.com/content/image/1-s2.0-S2352340918300374-mmc3.xlsx)*

Table 3.4.S4: *List of proteins showing significant changes (ANOVA; $p \leq 0.05$) above the biological relevance threshold (fold ≥ 2) and identified and quantified with at least two peptides when Mn-deficient xylem sap samples were compared to those of control conditions. (https://ars.els-cdn.com/content/image/1-s2.0-S2352340918300374-mmc3.xlsx)*

Companyon article

Ceballos-Laita L., Gutierrez-Carbonell E., Takahashi D., Abadía A., Uemura M., Abadía J., López-Millán A.F. Effects of Fe and Mn deficiencies on the protein profiles of tomato (*Solanum lycopersicum*) xylem sap as revealed by shotgun analyses. J. Proteomics (2018) 170, 117-129.

3.5. Effects of manganese toxicity on the protein profile of tomato (*S. lycopersicum*) roots as revealed by two complementary proteomic approaches, two-dimensional electrophoresis and shotgun analysis

Laura Ceballos-Laita [a], Elain Gutierrez-Carbonell [a], Hiroyuki Imai [b,c], Anunciación Abadía [a], Matsuo Uemura [c], Javier Abadía [a], Ana Flor López-Millán [d]

[a] *Department of Plant Nutrition, Aula Dei Experimental Station, Consejo Superior de Investigaciones Científicas (CSIC), Zaragoza, Spain*

[b] *United Graduate School of Agricultural Sciences, Iwate University, Morioka, Japan*

[c] *Cryobiofrontier Research Center, Faculty of Agriculture, Iwate University, Morioka, Japan*

[d] *Department of Biological and Environmental Sciences. School of Science and Computer Engineering, University of Houston Clear Lake, Houston, TX, USA*

Sent to Journal of Proteomics (2018) *(accepted*)

ABSTRACT

The aim of this work was to assess the effects of manganese (Mn) toxicity on the proteome of tomato roots using two proteomic approaches, shotgun and two-dimensional electrophoresis. The shotgun approach yielded 367 reliable proteins, whereas the 2-DE approach detected 340 consistent spots. The 2-DE method found 54 proteins changing in relative abundance in the excess Mn treatment, whereas the shotgun detected changes in 118 proteins. Only 7 % of the differential proteins were found by both methods, illustrating their complementary nature. Metabolic pathways most affected were protein metabolism, oxido-reductases and signaling. Results support that Mn toxicity alters the protein turnover and impairs energy production in roots, leading to changes in glycolysis, pyruvate metabolism, TCA and oxidative phosphorylation. Excess Mn also induced changes in peroxidases and hydrolases participating in cell wall lignification and suberization and activated plant defense mechanisms, with changes occurring *via* pathogenesis-related proteins as well as peroxidases. Finally, Mn toxicity elicited regulatory mechanisms and affected the abundance of root nutrient reservoir proteins. The overall analysis of the differential root proteome upon Mn toxicity suggests a general slowdown of metabolic activities especially energy production, cell wall integrity and protein turnover which occurs in parallel with increases in stress related proteins.

Biological significance

The present work applies two dimensional electrophoresis and shotgun proteomic approaches to unravel the effects of Mn toxicity on the tomato root proteome. In spite of the well-known

sensitivity of the shotgun technique, the number of proteins detected exclusively by any of the two methods was relevant, confirming that both techniques are complementary. The overall analysis of the differential root proteome upon Mn toxicity suggests a general slowdown of metabolic activities, especially energy production, cell wall integrity and protein turnover which occurs in parallel with increases in stress related proteins. Mn toxicity seems to elicit changes in protein turnover, based on the decreases measured in the categories of protein synthesis and degradation. Metabolic pathways involved in energy production were heavily affected by Mn toxicity, showing a reduction in the production of ATP and reducing power. In addition, excess of Mn caused alterations in the root cell wall properties, associated to increases in several peroxidases and glycosyl-hydrolases involved in cell wall lignification and suberization, which probably affect cell wall stiffening and expansion, likely leading to the inhibition of root growth. Our results also suggest that exposure to excess Mn caused a high stress situation, increasing general and ROS defense related proteins. Finally, decreases in several proteins with RNA binding domains suggest that RNA regulatory mechanisms are relevant in the modulation of the cellular response to Mn toxicity.

3.5.1. Introduction

Manganese (Mn) is an essential micronutrient necessary for all living organisms, and in photosynthetic organisms it is a component of the O_2 evolving complex of the photosystem II that carries out water splitting (Pittman et al., 2005; Socha and Guerinot, 2014). In plants, Mn is also a cofactor of multiple enzymes participating in important physiological and biochemical processes such as the Krebs cycle and the biosynthesis of many cell components, including RNA, proteins, carbohydrates, acyl lipids, flavonoids and lignins (Lidon et al., 2004; Millaleo et al., 2010). In addition, Mn plays an important role in redox homeostasis and reactive oxygen species (ROS) physiology through the activity of MnSOD (Wang et al., 2007).

Manganese occurs in the soil in a wide range of oxidation states, with its solubility depending on soil pH and redox conditions, and is taken up by roots mainly as Mn(II) (Hernandez-Soriano et al., 2012; Marschner and Marschner, 2012). Since the amount of Mn(II) in soils increases when the pH decreases below 5.0 (Lynch and St. Clair, 2004; Watmough et al., 2007), Mn may become toxic for plants in acidic soils (Mukhopadhyay and Sharma, 1991), which includes 50 % of the arable lands in the world (Foy, 1984). The percentage of acid soils is progressively increasing due to use of intensive horticulture and acidifying fertilizers (Millaleo et al., 2010; Graham et al., 2002) and climate events such as elevated ozone levels, increased ambient temperatures and emission of acidic gases (Driscoll et al., 2001; Fernando and Lynch, 2015; Guo et al., 2010). Visual symptoms of Mn toxicity include brown spots, leaf chlorosis and necrosis of leaves, and they generally occur when leaf Mn concentrations are

higher than 100 mg Mn g^{-1} of dry weight (Millaleo et al., 2010; Epstein and Bloom, 2015). An excess of Mn also causes alterations in the correct function and structure of leaf cell organelles due to oxidative stress *via* ROS (González et al., 1998; Mittler, 2002; St. Clair and Lynch, 2005). In addition, Mn toxicity impairs photosynthesis, causes pigment degradation and alters hormone balances and enzyme activities (Durst, 1976; Millaleo et al., 2013; Srivastava and Singh, 2006; Yao et al., 2012). Finally, the genotoxic effects of this metal cause disturbances in the metabolism of carbohydrates, amino acids, proteins and nucleic acids, which ultimately affect cell division and therefore plant growth (Mukhopadhyay and Sharma, 1991; Yao et al., 2012; Durand et al., 2010; Führs et al., 2012; Zhou et al., 2013).

In spite of the importance of Mn, little is still known about the molecular mechanisms participating in its homeostasis. Several families of transporters are involved in Mn transport across membranes, including NRAMP (natural resistance associated macrophage protein), ZIP (ZRT/IRT1-related protein), YSL (yellow stripe-like), CAX (cation exchanger), CCX (Ca cation exchangers), CDF (cation diffusion/facilitator), P-type ATPases and VIT (vacuolar Fe transporter) (Pittman, 2005; Socha and Guerinot, 2014; Shao et al., 2017). Characterized members of these families participating in Mn transport into the cytosol include the Mn root plasma membrane uptake transporters AtNRAMP1, OsNRAMP5 and AtIRT1 (Cailliatte et al., 2010; Connolly et al., 2002; Curie et al., 2000; Ishimaru et al., 2012; Sasaki et al., 2012), the vacuolar exporters AtNRAMP3 and 4, AtZIP1 and OsYSL6 (Fecht-Christoffers et al., 2003; Milner et al., 2013; Thomine et al., 2003), the xylem unloading transporters AtZIP2 (Milner et al., 2013) and OsNRAMP3 (Yamaji et al., 2013), and the phloem unloading transporter OsYSL2 (Koike et al., 2004). Also, Ca-permeable channels can transport Mn in several plant species (Socha and Guerinot, 2014). Characterized transporters involved in Mn export from the cytosol include vacuolar CAX (AtCAX2, AtCAX4, AtCAX5, OsCAX1a, OsCAX3), CCX (AtCCX3), VIT (AtVIT1) and CDF importers (OsMPT8.1) (see Socha and Guerinot, 2014 for a review). In addition, two members of the P-type ATPases family, AtECA1 and AtECA3, have been described to export Mn from the cytosol into the endoplasmatic reticulum (ER) and Golgi, respectively, whereas AtMTP11 (the only characterized CDF Mn transporter so far) is localized in the Golgi apparatus and it is believed to participate in Mn vesicular trafficking and exocytosis (Peiter et al., 2007). The wide array of existing Mn transporters, their overlapping functions, and their ability to transport several micronutrients indicate the complexity of Mn homeostasis.

Physiological studies have revealed that plants can use several strategies to cope with excess Mn, including the regulation of the acquisition and distribution of Mn (Delhaize et al., 2003; Dou et al., 2009; Wu et al., 2002), a decreased translocation of Mn from roots to shoots (Zhou et al., 2013; Chen et al., 2016; You et al., 2014), and the complexation of free Mn ions into metabolically inactive chelates, either in the plant or in the rhizosphere (Pittman et al.,

2005; Chen et al., 2015; De la Luz Mora et al., 2009; Fernando et al., 2010; Horst and Maier, 1999). On the other hand, molecular studies characterizing Mn transporters have revealed that Mn sequestration in the vacuole or apoplast and mobilization into the ER and Golgi play important roles in the plant tolerance to Mn excess (Socha and Guerinot, 2014; Horst and Maier, 1999; Hirschi et al., 2000; Schaaf et al., 2002). It has been suggested that AtECA1 might play a major role in managing Mn toxicity in the cell (Wu et al., 2002), whereas AtECA3 and AtMTP11 participate in detoxification of Mn *via* the Golgi apparatus (Peiter et al., 2007; Wu et al., 2002; Li et al., 2008).

Proteomic approaches can be useful to understand the underling mechanisms used by plants to cope with Mn-toxicity on a whole plant basis. However, to date little proteomic information is available about plant responses to this nutritional stress. Proteomic studies to date have focused on the effect of Mn stress in leaves, which causes revealing major impairments in photosynthesis and large increases of reactive oxygen species (ROS) (Fecht-Christoffers et al., 2003; Führs et al., 2008). The only studies on the effects of Mn toxicity on root proteome were carried out by 2-DE using two Citrus species, *Citrus sinensis* and *Citrus grandis* (You et al., 2016) and *Glycine max* (Chen et al., 2016). These studies indicated the existence of an increased protein turnover as well as alterations in root cell wall structure and lignification, which are in line with the root growth inhibition observed with excess of Mn in several plant species (González et al., 1998; Fecht-Christoffers et al., 2003; Chen et al., 2015; 2016). Assessing the effects of Mn toxicity in roots of different plant species can provide new and complementary information about the plant responses elicited in the metabolic adaptation to this nutritional stress. Therefore, the aim of this work was to assess the effect of Mn toxicity on the root proteome of tomato (*Solanum lycopersicum*) using two proteomic approaches based on two-dimensional electrophoresis (2-DE) and mass spectrometry shotgun analyses.

3.5.2. Materials and methods

Plant material and sampling

Tomato (*Solanum lycopersicum*, cv. Tres Cantos) plants were grown hydroponically in a controlled environment chamber (Fitoclima 10.000 EHHF, Aralab, Lisbon, Portugal) with a photosynthetic photon flux density (PPFD) of 400 µmol m^{-2} s^{-1} photosynthetically active radiation, 80 % relative humidity and a photoperiod of 16 h, 23ºC/8 h, 18ºC day/night regime. Seeds were germinated in vermiculite for 13 days in half-strength Hoagland nutrient solution containing 4.6 µM $MnCl_2$. Seedlings were then transplanted to 10 L plastic buckets (16-18 plants per bucket) containing half-strength Hoagland nutrient solution and grown for an additional 13-day period. Iron was added as 45 µM Fe(III)-ethylenediamine tetraacetic acid

(EDTA). After this time, solutions were renewed and control (4.6 µM $MnCl_2$) and Mn-toxicity (300 µM $MnCl_2$) treatments imposed. Roots and leaf disks were collected eight days after treatment onset, frozen in liquid nitrogen and kept at -20ºC until analysis.

Experimental design

One independent experiment consisted in two buckets (one bucket per treatment) containing 16-18 plants each, with roots from two plants per bucket being pooled, used for protein extraction and considered as a biological replicate. This set up was repeated four times for the 2-D electrophoresis analysis (n = 4) and five times for the shotgun analysis (n = 5).

For mineral analysis, roots from two plants per treatment were sampled separately and mean values calculated, and the experiment was repeated at least three times (n = 3). Photosynthetic pigment analyses were performed in three plants per treatment (using two leaves in each plant and five disks per leaf) in at least three independent experiments (n = 3). For Fe reductase activity, measurements were performed in eight plants per treatment in a single experiment (n = 8).

Mineral analysis, chlorophyll estimation and photosynthetic pigment analysis

For nutrient analysis, roots were sampled, washed, dried and milled using standard procedures (Carrasco-Gil et al., 2016). Plant tissues (100 mg dry weight) were digested in a microwave system (Milestone Ethos Plus, Bergamo, Italy) with 6.4 mL HNO_3 (26 %, TraceSelect Ultra, Sigma-Aldrich, Madrid, Spain) and 1.6 mL H_2O_2 (30 %). The concentrations of micro- (Fe, Mn, Cu and Zn) and macronutrients (Ca, Mg and K) were determined by flame atomic absorption spectrometry (AAS) using a Solaar 969 apparatus (Unicam Ltd., Cambridge, UK).

Disks for pigment analysis were sampled using a calibrated 0.5-cm-diameter cork borer from young (L4-L5) and old (L1-L3) expanded leaves (Carrasco-Gil et al., 2016) at sampling time (eight days after treatment onset), wrapped in aluminum foil, frozen in liquid N_2 and stored at -20 °C until analysis. Leaf pigments were extracted with acetone in the presence of Na ascorbate and stored following the procedure described in (Abadía and Abadía, 1993). Pigment extracts were thawed on ice, filtered through a 0.22-µm polytetrafluoroethylene (PTFE) filter and analyzed by high-performance liquid chromatography using a Waters 600 pump and 996 photodiode array detector (Waters Co., Milford, MA, USA) (Larbi et al., 2004). The total concentrations of Chl (Chl *a* + Chl *b*), neoxanthin, violaxanthin (V), lutein epoxide (taraxanthin), antheraxanthin (A), lutein and zeaxanthin (Z). The ratios Chl *a*/Chl *b* and (A+Z)/(V+A+Z) were also calculated.

Root iron reductase activity

The root ferric reductase activity (FC-R) of intact, illuminated plants was determined by following the formation of the Fe(II)-BPDS complex from Fe(III)-EDTA (Bienfait et al., 1983). Eight days after the treatment onset, individual plants were transferred to 250 ml beakers containing 5 mM Mes-KOH pH 5.5 solution supplemented with 300 μM BPDS and 500 μM Fe(III)-EDTA. The beaker was fully covered with aluminum foil, and the solution was aerated continuously. Aliquots were collected 30 min after placing plants in the beakers and absorbance was measured at 535 nm with a spectrophotometer (UV2450, Shimadzu, Kyoto, Japan). An extinction coefficient of 22.14 mM^{-1} cm^{-1} was used for the estimation of reduced Fe. Blanks were made in the absence of plants to correct for any photoreduction and also in the presence of plants but adding Fe only at the end of the reaction to correct for Fe reduction caused by secreted substances.

Protein extraction

Approximately 0.5-1.0 g of root material (pooled from 2 plants of a given treatment) was ground in liquid N_2 with mortar and pestle, and then homogenized in 6 mL of phenol saturated with Tris-HCl 0.1 M (pH 8.0) containing 5 mM β-mercaptoethanol, by stirring for 30 min at 4 °C. After incubation, the homogenate was filtered (PVDF, 0.45 μm) and centrifuged at 5000 × *g* for 15 min. The phenol phase was re-extracted for 30 min with one volume of phenol saturated Tris-HCl 0.1 M (pH 8.0) containing 5 mM β-mercaptoethanol, and centrifuged as described above. The phenol phase was collected, and proteins precipitated by adding five volumes of cold 0.1 M ammonium acetate in methanol. Samples were kept overnight at -20ºC and then centrifuged at 20,000 × *g* for 20 min. The pellet was washed twice with cold methanol, dried with N_2 gas and solubilized in a sample rehydration buffer containing 8 M urea, 2 % (w/v) CHAPS, 50 mM DTT, 2 mM PMSF and 0.2 % (v/v) IPG buffer pH 3-10 (GE Healthcare, Uppsala, Sweden). After rehydration, samples were incubated in a Thermomixer Confort device (Eppendorf AG, Hamburg, Germany) at 42 ºC and 1,000 rpm during 3 h, then centrifuged at 10,000 × *g* for 10 min at room temperature and filtered (0.45 μm ultrafree-MC filters, Millipore, Bedford, USA). Protein concentration was quantified immediately with a Bradford kit (Sigma-Aldrich, St. Louis, MO, USA) method using microtiter plates in an Asys UVM 340 spectrophotometer (Biochrom Ltd., Cambridge, UK) and BSA as standard.

Label free liquid chromatography-tandem mass spectrometry (LC–MS/MS)

Sample preparation for label free LC–MS/MS shotgun analysis was carried out according to (Li et al., 2012). Briefly, 5 μg of total proteins were subjected to 1-DE to remove non-protein

compounds. The resulting gel bands were cut into six pieces, proteins were *in gel* digested with trypsin, and peptides were subsequently extracted.

Peptide solutions were concentrated in a trap column (Lcolumn Micro 0.3 x 5 mm; CERI, Japan) using an ADVANCE UHPLC system (Michrom Bioresources, Auburn, CA, USA). Elution was carried out with 0.1 % (v/v) formic acid in ACN and concentrated peptides were separated in a Magic C_{18} AQ nano column (0.1 x 150 mm; Michrom Bioresources) using a linear gradient of ACN (from 5 % to 45 %) and a flow rate of 500 nL min^{-1}. Peptide ionization was carried out with a spray voltage of 1.8 kV using an ADVANCE spray source (Michrom Bioresources). Mass spectrometry analysis was carried out on an LTQ Orbitrap XL (Thermo Fisher Scientific, Waltham, MA, USA) equipped with Xcalibur software (version 2.0.7, Thermo Fisher Scientific) and mass data acquisition parameters were set as described elsewhere (Gutierrez-Carbonell et al., 2016).

Mass data analysis was performed according to (Takahashi et al., 2013). Protein identification was carried out using the full peptide list with the Mascot search engine (version 2.5.1, Matrix Science, London, UK) and NCBI 20151004 database (72,195,234 sequences; 26,318,602,641 residues). Search parameters were: peptide mass tolerance ±5 ppm, MS/MS tolerance ±0.6 Da, one allowed missed cleavage, allowed fixed modification carbamidomethylation (Cys), and variable modification oxidation (Met) and peptide charges were set to +1, +2 and +3. Positive protein identification was assigned with at least two unique top-ranking peptides with scores above the threshold level ($p < 0.05$). The false discovery rate (FDR) for protein identification, based on a search of the Mascot decoy database, was less than 5%. Protein information was exported from Mascot .xml format and imported to Progenesis QI for proteomics software (v. 2.0, Nonlinear Dynamics, Newcastle upon Tyne, UK), which then associates peptide and protein information. The MS proteomics data have been deposited to the ProteomeXchange Consortium *via* the (Vizcaíno et al., 2016) partner repository, with the data set identifier PXD008326.

Proteins changing in relative abundance were selected using a paired Student *t*-test and a significance level of $p \leq 0.05$. Protein response ratios were defined as the normalized protein abundance in the treatment divided by the normalized abundance in the control. Only changes with a $p \leq 0.05$ (Student *t*-test) and a ratio ≥ 2 or ≤ 0.5 were considered as statistically significant and biologically relevant, respectively. Multivariate statistical analyses (Principal Component Analysis; PCA) were carried out using SPSS Statistical software (v. 24.0), including only proteins showing statistically significant changes (Student *t*-test; $p \leq 0.05$) as a result of the Mn toxicity treatment. We used the GO biological process annotation (http://www.geneontology.org) and domain annotations for classification of each individual protein identified into nine different functional categories (protein metabolism, signaling,

carbohydrate metabolism, oxido-reductases, polysaccharide metabolism, defense, lipid metabolism, unknown and a miscellaneous group containing functional categories not belonging to the previous groups).

Protein 2-DE separation of root samples

Preliminary 2-DE experiments were carried out in root samples using a first dimension IEF separation on 7 cm ReadyStrip IPG Strips (BioRad) with a linear pH gradient pH 5-8, using a Protean IEF Cell (BioRad, Hercules, CA, USA). Strips were rehydrated for 16 h at 20 °C in 125 μL of rehydration buffer containing 80 μg of root extract proteins and a trace of bromophenol blue, and then transferred onto a strip tray. IEF was run at 20 °C, for a total of 14000 V h (20 min with a 0 - 250 V linear gradient, 2 h with a 250 - 4000 V linear gradient and 4000 V until 10 000 V h). After IEF, strips were equilibrated for 15 min in equilibration solution I [6 M urea, 0.375 M Tris-HCl, pH 8.8, 2 % (w/v) SDS, 20 % (v/v) glycerol, 2 % (w/v) DTT] and for another 15 min in equilibration solution II [6 M urea, 0.375 M Tris-HCl pH 8.8, 2 % (w/v) SDS, 20 % (v/v) glycerol, 2.5 % (w/v) iodoacetamide]. For the second dimension SDS-PAGE, equilibrated IPG strips were placed on top of vertical 12 % SDS-polyacrylamide gels (8 × 10 × 0.1 cm) and sealed with melted 0.5 % agarose in 50 mM Tris HCl, pH 6.8, containing 0.1 % SDS. SDS-PAGE was carried out at 20 mA per gel for approximately 1.5 h, until the bromophenol blue reached the plate bottom, in a buffer containing 25 mM Tris, 192 mM glycine, and 0.1 % SDS, at 4°C. Gels were subsequently stained with Coomassie-blue R-250 (Sigma-Aldrich, St. Louis, MO, USA).

Gel image and statistical analysis

Stained gels were scanned with an Epson Perfection 4990 Photo Scanner (Epson Ibérica, Barcelona, Spain) at 600 dpi, previously calibrated using the SilverFast 8 software (LaserSoft Imaging AG, Kiel, Germany) and an IT8 reference card. Spot detection, gel matching and interclass analysis were performed with PDQuest 8.0 software (BioRad). First, normalized spot volumes based on total intensity of valid spots were calculated for each 2-DE gel and used for statistical calculations of protein abundance; for all spots present in the gels, pI, Mr, and normalized volumes (mean values and SD) were determined. Experimental Mr values were calculated by mobility comparisons with Precision Plus protein standard markers (BioRad) run in a separate lane on the SDS gel, and pI was determined by using a linear scale over the total dimension of the IPG strips. Only spots consistently present in 100 % of the replicates (four gels) from at least one class were considered and used in further analysis. The spots were also manually checked, and consistent reproducibility between normalized spot volumes was found in the different replicates.

Spots changing in relative abundance were selected using a paired Student *t*-test and a significance level of $p \leq 0.05$. Protein response ratios were defined as the relative abundance in the treatment divided by the relative abundance in the control.

Protein in gel digestion

Spots were excised automatically using an EXQuest spot cutter (BioRad), transferred to 500 µL Protein LoBind Eppendorf tubes, destained in 400 µL of 40 % [v/v] acetonitrile (ACN) and 60% [v/v] 200 mM NH_4HCO_3 for 30 min and dehydrated in 100 % ACN for 10 min. Gel pieces were dried at room temperature and then in gel digested with 15 µL Trypsin solution (Sequencing grade Modified Trypsin V511, Promega, Madison, WI, USA; 0.1 µg/µL in 40 mM NH_4HCO_3/ 9% ACN). After incubation overnight at 37 °C, the reaction was stopped by adding 1 µL of 1 % TFA. The peptide solution was then analyzed using mass spectrometry (MS).

Protein identification by nanoliquid chromatography-tandem mass spectrometry (nLC−ESI−MS/MS)

Peptides present in 6 µL of sample were preconcentrated on line onto a 300 µm i.d. × 5 mm, 5 µm particle size ZORBAX 300SB-C18 trap column (Agilent Technologies, Waldbronn, Germany), using a 100 µL min^{-1} flow rate of 3 % ACN, 0.1 % formic acid, in a nano-HPLC system 1200 series (Agilent Technologies). Backflow elution of peptides from the trap column was carried out, and separation was done with a 75 µm i.d. × 150 mm, 3.5 µm particle size ZORBAX 300SB-C18 column (Agilent Technologies), using a 300 nL min^{-1} nanoflow rate and a 55 min linear gradient from solution 97 % A (0.1 % formic acid) to 90 % of solution B (90 % ACN, 0.1 % formic acid). The nano-HPLC was connected to a HCT Ultra high-capacity ion trap (Bruker Daltoniks, Bremen, Germany) using a PicoTip emitter (50 µm i.d., 8 µm tip i.d., New Objective, Woburn, MA, USA) and an on line nanoelectrospray source. Capillary voltage was −1.8 kV in positive mode and a dry gas flow rate of 10 L min^{-1} was used with a temperature of 180 °C. The scan range used was from 300 to 1500 m/z. The mass window for precursor ion selection was ±0.2 Da and the rest of parameters were those recommended by the manufacturer for MS/MS proteomics work. Peak detection, deconvolution and processing were performed with Data Analysis 3.4 software (Bruker Daltoniks, Bremen, Germany).

Protein identification was carried out using the Mascot search engine (Matrix Science; London, UK) and the non-redundant databases NCBInr 20151004 (72195234 sequences; 26318602641 residues) and ITAG v2.3 20151015 (34727 sequences; 11956401 residues). Search parameters were: monoisotopic mass accuracy, peptide mass tolerance ± 0.3 Da, fragment mass tolerance ± 0.6 Da; one allowed missed cleavage; allowed fixed modification carbamidomethylation (Cys), and variable modification oxidation (Met). Positive identification

was assigned with Mascot scores above the threshold level ($p \leq 0.05$), at least 2 identified peptides with a score above homology and similar experimental and theoretical molecular weight and pI values. We used the GO biological process annotation (http://www.geneontology.org) and domain annotations for protein classification.

3.5.3. Results

Photosynthetic pigment analysis

Tomato plants grown with 300 μM Mn showed toxicity symptoms as soon as 6 days after the treatment onset. Visual toxicity symptoms at sampling time included brown spots in stems and along the main and secondary veins of all leaves and yellowing of younger leaves. Accordingly, total chlorophyll in old (L1-L3) and young (L4-L5) leaves decreased by approximately 50 % in plants affected by Mn toxicity, with the Chl *a*/Chl *b* ratio remaining constant (Table 3.5.1).

Table 3.5.1. *Concentrations of leaf photosynthetic pigments (in μmol m^{-2}) in Solanum lycopersicum plants grown in control and excess Mn conditions. Samples were taken at day 8 after treatment onset and data are means ± SE (n = 3). In the control plants there were no differences in leaf pigments between young and old leaves, and therefore the results presented are for the whole plant. Different letters within the same row indicate statistically significant differences (Student's t-test, p ≤ 0.05).*

Pigment (μmol·m^{-2})	**Control**	**+Mn Young leaves**	**+Mn Old leaves**
Neoxanthin	12.0 ± 0.6 a	5.3 ± 0.5 b	7.3 ± 0.9 b
Violaxanthin	17.6 ± 0.9 a	9.7 ± 0.7 b	8.4 ± 0.7 b
Taraxanthin	0.2 ± 0.1	n.d	n.d.
Antheraxanthin	0.8 ± 0.2 a	1.5 ± 0.3 b	3.1 ± 0.3 c
Lutein	44.8 ± 1.6 a	25.3 ± 2.1 b	30.9 ± 2.7 b
Zeaxanthin	0.2 ± 0.1 a	1.7 ± 0.5 b	4.6 ± 0.8 c
Total Chl (Chl a + Chl b)	323.9 ± 14.1 a	165.4 ± 15.3 b	162.8 ± 22.9 b
Chl a/Chl b ratio	3.0 ± 0.1 a	2.9 ± 0.1 a	2.7 ± 0.1 a
Violaxanthin cycle pigments (V + A + Z)	18.6 ± 0.8 a	12.9 ± 0.9 b	16.1 ± 1.0 ab
(A+Z)/(V + A + Z)	0.06 ± 0.01 a	0.22 ± 0.05 b	0.47 ± 0.04 c

The concentrations of A and Z were higher in young (2- and 8- fold, respectively) and old (4 and 21-fold, respectively) leaves of Mn-treated plants when compared to controls, whereas those of neoxanthin, V and lutein decreased between 43 and 56 % in young leaves and between 31 and 52 % in old leaves (Table 3.5.1). The concentration of taraxantin was always low and did not change with Mn toxicity. The total amount of violaxanthin cycle pigments (V+A+Z) was lower in young (31%) leaves from plants grown in excess Mn than in controls. The (A+Z)/(V+A+Z) ratio increased markedly with Mn toxicity from 0.06 to 0.22 and 0.47 in young and old leaves, respectively.

Mineral composition and root iron reductase activity

The Mn concentration in roots from plants grown in excess Mn was 17-fold higher than in the controls (Figure 3.5.1A) whereas no significant differences were measured in the concentrations of the other analyzed micro- (Fe, Cu and Zn) and macronutrients (Ca, Mg and K) (Table S1).

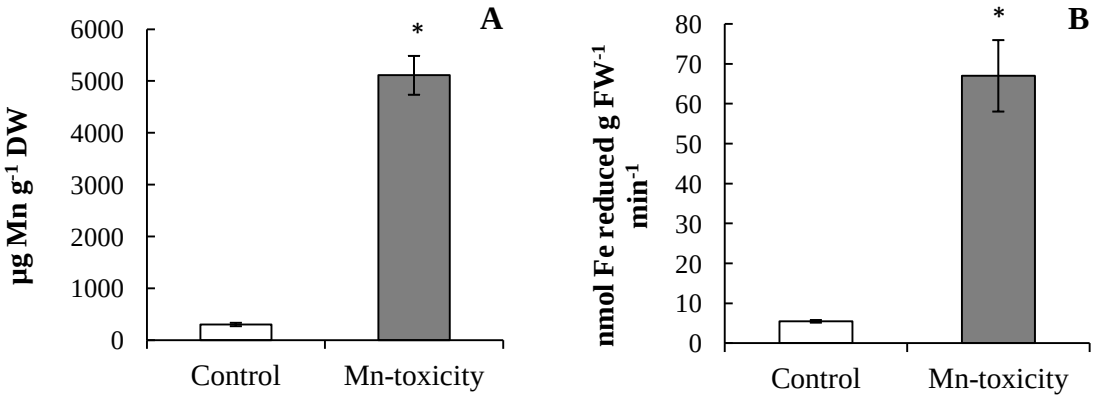

Figure 3.5.1. *(A) Concentration of Mn (A) and Fe reductase activity (B) in roots of Solanum lycopersicum plants grown in control and Mn-excess conditions after 8 days of treatment onset. Data correspond to means ± SE (n =3 for Mn concentration and n=8 for Fe reductase activity). Asterisks indicate statistically significant differences (Student's t- test, p ≤ 0.01).*

The Fe reductase activity in roots from plants treated with excess Mn was 12-fold higher than that measured in roots from control plants (Figure 3.5.1B).

Effect of Mn-toxicity on the root proteome

The shotgun proteomic approach detected 918 proteins in root extracts, and 367 of them were reliably identified and quantified with at least 2 peptides and considered in this study. The list of proteins detected is shown in Table S2 and the list of the corresponding peptides is available in the ProteomeXchange Consortium *via* the Pride partner repository with the data set identifier PXD008326. A large majority (88 %; 324 proteins) of the identified and quantified proteins are ascribed to the *Solanum* genus and 91 % of them (294 proteins) were matched specifically to the species *S. lycopersicum* (Table S2).

Changes induced by Mn toxicity on the root proteome using shotgun analysis are shown in a volcano plot, using the relationship between statistical significance [$-\log_{10}$ (p-value)] and biological significance [$\log_2$ (fold-change)] (Figure 3.5.2A). Manganese toxicity caused statisticallysignificant (Student *t*-test, $p \leq 0.05$) and biologically relevant (fold ≥ 2 or fold ≤ 0.5) changes in 118 proteins, with 79 of them showing relative decreases in abundance (green dots in Figure 3.5.2A, Table S3) and 39 showing relative increases in abundance (red dots in Figure 3.5.2A, Table S3).

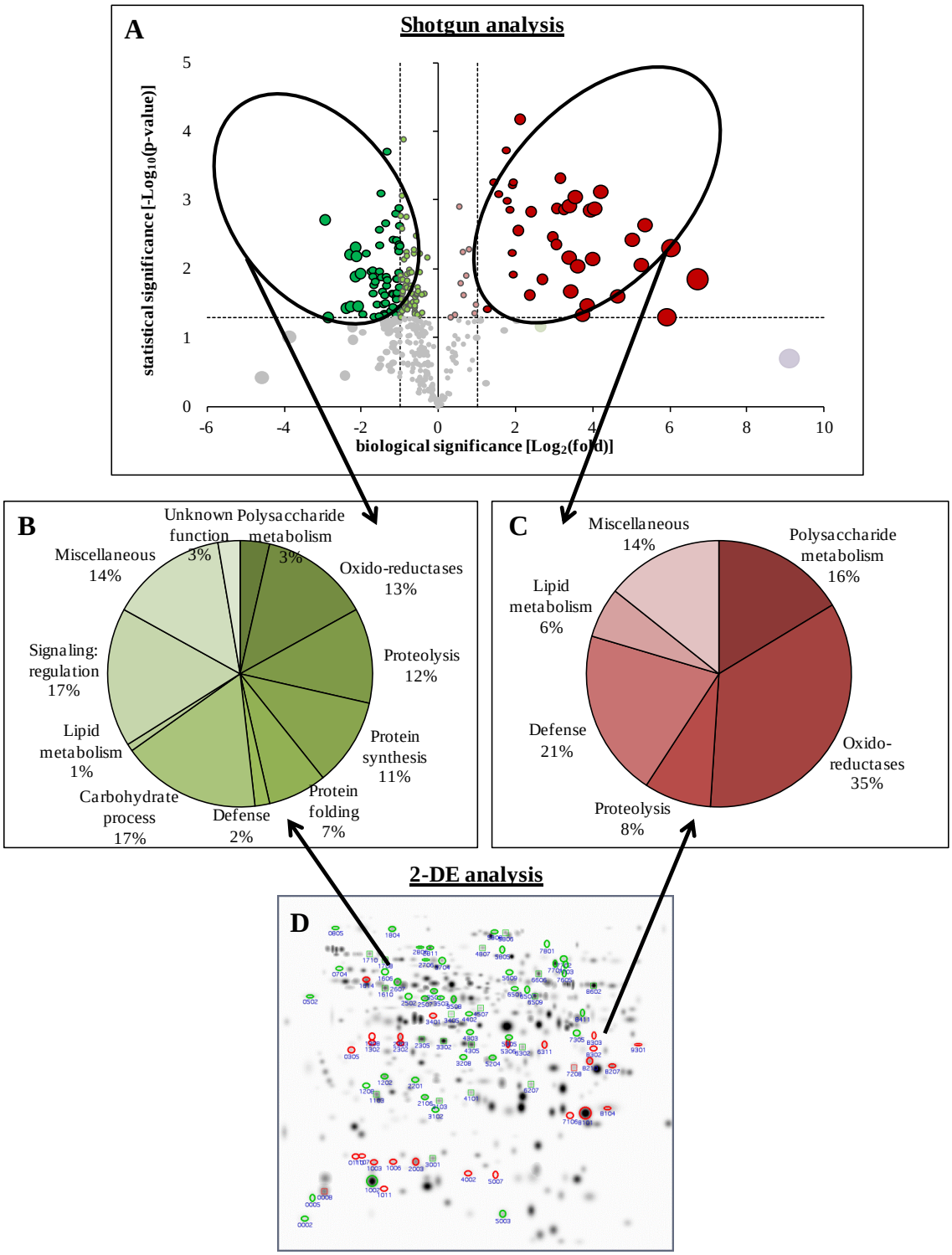

Figure 3.5.2. *Effect of Mn toxicity on the root protein profile as revealed by label-free shotgun analyses and bi-dimensional electrophoresis. (A) Volcano scatter plot showing the 367 identified and quantified proteins (peptides assigned to a protein and used for quantification ≥ 2) by shotgun analyses. Proteins unaffected by Mn toxicity are depicted in grey and proteins changing as a result of Mn toxicity (t-Student's, p ≤ 0.05) are depicted in green (decreasing) or red (increasing). Light colors are used for those proteins meeting only the statistical threshold (t-Student's, p ≤ 0.05) and bright colors where used when both statistical and biological (fold change ≤ 0.5 or ≥ 2) thresholds were met. The size of the dots is proportional to the fold changes. (B) and (C) Functional classification of proteins identified by shotgun and 2-DE analyses showing decreases and increases, respectively, in relative abundance as a result of*

Mn toxicity above the statistical and biological thresholds (fold change ≤ 0.5 or ≥ 2) . Classification was based on GO biological process and domain annotations. (D) Virtual composite 2-DE gel image showing the protein profile map of root extract preparations from Solanum lycopersicum plants. Spots showing changes in abundance above the biological and statistical thresholds (t-Student's, p ≤ 0.05 and fold ≥ 2 or ≤ 0.5) are depicted with green (decreases) and red (increases) circles whereas spots showing changes above the statistical threshold (t-Student's, p ≤ 0.05) but below the biological threshold (fold ≤ 2 or ≥0.5) are depicted with green (decreases) and red (increases) squares.

On the other hand, the 2-DE proteomic approach detected 340 consistent spots in extracts from tomato roots, with 87 of them showing statistically significant (*t*-Student's test; $p \leq 0.05$) changes; among those, 66 also showed biologically relevant (fold ≥ 2 or fold ≤ 0.5) changes as a result of Mn toxicity (Figure 3.5.2D; Table S4). Only spots showing statistically significant and biologically relevant changes in abundance as a result of Mn toxicity were analyzed by nLC ESIMS/MS, and 92 % of them (61 spots) were reliably identified, whereas two spots were not identified and in three spots several proteins were present and therefore they were not considered in further analyses. From the 61 differential spots reliably identified in the 2-DE approach, 37 of them corresponded to 36 proteins decreasing in abundance (green circles in Figure 3.5.2D, Table S4), whereas 24 spots corresponded to 18 protein species increasing in abundance (red circles in Figure 3.5.2D, Table S4), giving a total of 54 proteins changing in relative abundance.

In summary, a total of 161 proteins were found to show changes in relative abundance. Eleven of them (corresponding to 14 spots in 2-DE) were found with the two approaches used, whereas 107 proteins were detected only by the shotgun approach and 43 (corresponding to 47 spots) were identified only by the 2-DE approach (Figure 3.5.3). These 161 proteins are listed in Tables S5 and S6 (112 proteins decreasing and 49 increasing in relative abundance, see below), and those among them showing large changes in abundance (21 proteins having fold-changes > 25 or < 0.1) are listed in Table 3.5.2.

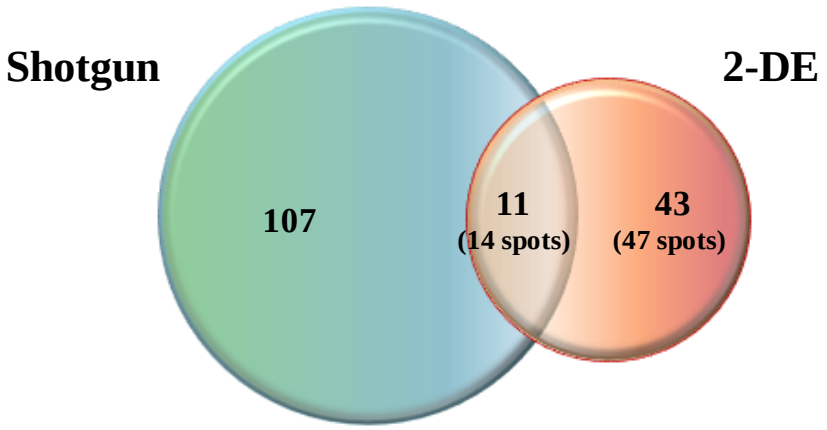

Figure 3.5.3. *Venn diagram comparing the number of root proteins changing as a result of Mn toxicity determined by shotgun and 2-DE methods (p ≤ 0.05, number of peptides for identification and quantification ≥ 2 and fold ≤ 0.5 or ≥ 2).*

Table 3.5.2. *Proteins showing large changes in abundance (fold-change > 25 or < 0.1) among the 161 root proteins affected by Mn toxicity (t-Student's, $p \leq 0.05$ and fold ≥ 2 or ≤ 0.5). Spot numbers correspond to spots depicted in Figure 3.5.2D. UniProt indicates UniProt database entry. Pepc and Pepq are the number of peptides used for identification and quantification. Mr/pI th and Mr/pI exp correspond to the theoretical and experimental molecular masses and pI, respectively. Fold-changes (Fold +Mn/C) were calculated by dividing the mean of normalized abundances (obtained with Progenesis QI v.2.5.1 in the case of shotgun) or the mean of normalized spot volumes (obtained with the PDQuest v.8 in the case of 2-DE) in plants affected by Mn toxicity by that of control samples. Detailed information about functional classification, identification and quantification is given in Tables S2-4.*

Nº Prot	Nº Spot	Uniprot	Description	Fold +Mn/C	Mr/pI th	Mr/pI exp	Pep_c	Pep_q
Decreased								
Oxido-reductases								
1	8411	Q07446	Predicted peroxidase 3-like	0.1	36.5/8.0	40.5/7.3	3	---
2	---	Q40131	Uncharacterized protein LOC544002	0.1	---	---	2	2
3	3102	K4CXJ6	Predicted probable NAD(P)H dehydrogenase (quinone) FQR1-like 1	0.1	21.7/5.7	21.7/6.2	6	---
Carbohydrate metabolism								
4	7703	K4CNR7	Acid β-fructofuranosidase	0.0	73.1/6.2	64.7/7.2	4	---
5	7305	K4BX34	Predicted fructose-bisphosphate aldolase 3	0.0	43.2/8.9	34.6/7.3	4	---
6	6507	K4B740	UDP-glucose 6-dehydrogenase	0.0	57.2/6.3	50.7/6.9	5	---
7	6501	K4B170	Dihydrolipoyl dehydrogenase 2	0.1	60.6/6.8	51.3/6.8	5	---
8	5609	Q8GT30	Dihydrolipoamide dehydrogenase precursor	0.1	53.1/6.9	60.2/6.8	12	---
Protein metabolism								
9	5305	Q2V9B2	Similar to eukaryotic translation initiation factor 2 subunit β (*S. tuberosum*)	0.0	30.1/6.1	33.6/6.8	2	---
Signaling:regulation								
10	2706	K4BZG0	Predicted switch-associated protein 70 isoform X2	0.0	55.6/5.6	67.8/6.2	4	---
11	---	K4D2D4	Predicted activator of 90 kDa heat shock protein ATPase homolog	0.1	---	---	2	2
Increased								
Polysaccharide metabolism								
12	---	Q01412	Glucan endo-1,3-β-glucosidase A	38.3	---	---	8	8
Oxido-reductases								
13	8210	Q4A3Y6	Peroxidase cevi16	New	32.2/7.7	29.2/7.4	11	---
Protein metabolism								
14	---	C9DFA6	Predicted subtilisin-like protease	41.0	---	---	6	3
15	---	K4BEU1	Predicted serine protease inhibitor 5-like	25.0	---	---	6	6
Defense								
16	---	Q53U35	Predicted pathogenesis-related protein STH-2	105.3	---	---	9	9
17	---	O24025	PR1a2 protein	60.6	---	---	3	2
18	110	K4CWC4	Pathogenesis-related protein STH-2-like	New	17.5/5.4	16.5/5.6	2	---
Lipid metabolism								
19	---	K4B6U4	Predicted patatin-like protein 1	65.2	---	---	3	2
Miscellaneous								
20	---	K4D0F3	Predicted uncharacterized protein LOC101254542	32.6	---	---	2	2
21	305	Q43633	Similar to phaseolin (*P. vulgaris*)	28.0	29.3/4.9	31.2/5.6	2	---

From the total 161 proteins changing in abundance with Mn toxicity, 112 decreased in relative abundance (79 by the shotgun approach and 36 with the 2-DE approach, with 3 being found with both techniques) (Table S5, Figure 3.5.2B). Functional classification of these proteins yielded nine functional categories, including protein metabolism (33 proteins, 30 % of the total), signaling (19 proteins, 17 %), carbohydrate metabolism (19 proteins, 17 %), oxido-reductases (15 proteins, 13 %), polysaccharide metabolism (4 proteins, 3 %), defense (2 proteins, 2 %), lipid metabolism (1 protein, 1 %), miscellaneous group (16 proteins, 14 %) and unknown proteins (3 proteins, 3 %). Decreases measured for most proteins (90 %) ranged between 50 and 80 % (Table S5), and only eleven proteins showed decreases in relative abundance above 90 %, with nine of them being identified by 2-DE (Table 3.5.2). Among these eleven proteins showing major decreases three were oxidoreductases, including a class III peroxidase (Q07446), an Fe(II) and 2- oxoglutarate (2OG)-dependent dioxygenase domain containing protein (Q40131) and a FMNreductase-like protein (K4CXJ6). Five more proteins decreasing strongly in abundance were ascribed to the carbohydrate category and included an acid β-fructofuranosidase (K4CNR7), a fructose-bisphosphate aldolase 3 (K4BX34), a dihydrolipoamide dehydrogenase precursor (Q8GT30) and a dihydrolipoyl dehydrogenase 2 (K4B170) and an UDP-glucose 6-dehydrogenase (K4B740) (Table 3.5.2). The remaining 3 proteins showing major decreases were an eukaryotic translation initiation factor (Q2V9B2) and two more proteins involved in signaling and regulation, a serine/threonine kinase (K4BZG0) and an ATPase activator (K4D2D4) (Table 3.5.2).

Forty-nine proteins increased in abundance as revealed by both techniques (39 by the shotgun approach and 18 with the 2-DE approach, with 8 found with both techniques) (Table S6, Figure 3.5.2C). Functional classification of these proteins only yielded six functional categories, including oxido-reductases (17 proteins, 35 % of the total), defense (10 proteins, 21%), polysaccharide metabolism (8 proteins, 16 %), protein metabolism (4 proteins, 8 %) and lipid metabolism (3 proteins, 6 %) and a miscellaneous group of 7 proteins (14 %) involved in amino acid metabolism and nutrient reservoir. Increases in the oxido-reductase and polysaccharide metabolism categories were moderate except for a glycoside hydrolase 17 (GH17) family protein (Q01412) which increased 38-fold and for a partial peroxidase (Q4A3Y6) which was detected *de novo* by the 2-DE approach (Table 3.5.2). Large increases were measured in a protein inhibitor (K4BEU1; 25-fold), a subtilisin-like protease (C9DFA6; 41-fold) belonging to the protein metabolism category, and in three pathogenesis related proteins (Q53U35, increasing 105-fold); O24025, increasing 61-fold; K4CWC4, detected *de novo* by the 2-DE approach) from the defense category and in a predicted patatin-like protein 1 (K4B6U4, 65-fold increase) involved in lipid metabolism (Table 3.5.2). Two more proteins, a phaseolin (Q43633) and a predicted protein involved in tryptophan catabolism (K4D0F3) also

presented remarkable (approximately 30-fold) increases (Table 3.5.2). The remaining 39 proteins showed increases between 2- and 18-fold (Table S6).

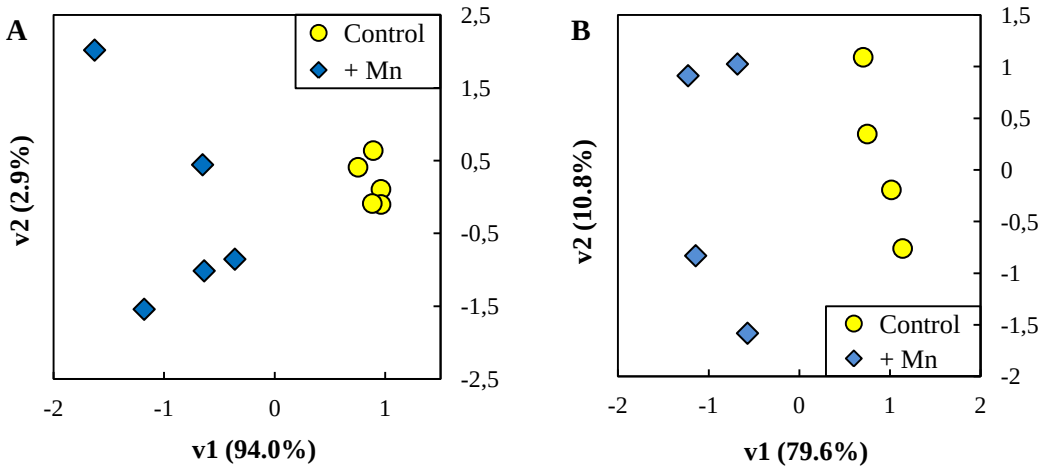

Figure 3.5.4. *Score scatter PCA (Principal Component Analysis) plot of differential proteins as revealed by shotgun (A) and 2-DE (B) as a result of Mn toxicity. Principal component analysis was carried out using SPSS Statistical software (v. 24.0) and included proteins showing statistically significant changes as a result of the Mn toxicity treatment (t-Student's; p ≤ 0.05). Control and Mn-treated samples are depicted by yellow dots and blue diamonds, respectively.*

The PCA analysis of the proteins showing statistically significant changes in the 2-DE and shotgun analyses (Student *t*-test; $p \leq 0.05$) showed a good separation between treatments, with the first and second components explaining approximately 94 and 3 % of the variation in the shotgun experiment (Figure 3.5.4A) and 80 and 11 % in the 2-DE one (Figure 3.5.4B).

Table 3.5.3. *List of proteins correlated to component 1 found by PCA in both experimental approaches. Fold changes (Fold +Mn/C) were calculated by dividing the mean of normalized abundances (obtained with Progenesis QI for shotgun) or the mean of normalized spot volumes (obtained with the PDQuest v.8 for 2-DE) in plants affected by Mn toxicity by that of control samples. Spot number corresponds to those in Table S4 and Figure 3.5.2D.*

Protein description	**UniProt Entry**	**Fold +Mn/C Shotgun**	**Spot**	**Fold +Mn/C 2-DE**
Suberization-associated anionic peroxidase 2-like	K4BE93	8.4	9301	6.6
Peroxidase 3 precursor	Q07446	0.7	8411	0.1
Glucan endo-1,3-β-glucosidase A	Q01412	38.3	5306	3.1
Glucan endo-1,3-β-glucosidase B precursor	Q01413	8.3	7106	5.1
			110	new
Pathogenesis-related protein STH-2-like	K4CWC4	10.5	2003	4.3
			1003	2.7
TSI-1 protein	O49881	16.0	1006	6.7
			1107	5.6
Lipoxygenase homology domain-containing protein 1-like	K4BJ74	3.8	8	1.9
			1011	10.7

In the 2-DE analysis, spots with large positive component 1 scores (27 spots) were mainly found in the carbohydrate (22 %, six spots) and protein metabolism (19 %, five spots)

categories, whereas those with large negative contributions (26 spots) were found in the redox (31 %, eight spots), defense (31 %, eight spots) and polysaccharide (15 %, four spots) categories (Table S7). Similar results were obtained in the shotgun PCA, where the category containing a larger number of proteins with positive component 1 scores (7 proteins) was protein metabolism (four proteins) whereas categories containing a larger number of proteins with negative component 1 scores (24 proteins) were also redox (25 %, six proteins), defense (29 %, seven proteins) and polysaccharide (17 %, four proteins) (Table S8). The comparison of the results obtained with each experimental approach yielded eight proteins with large contributions to the separation of the treatments, including two glycoside hydrolases subfamily 17 (Q01412 and Q01413), two Bet-V-I domain containing proteins from the defense category (K4CWC4 and O49881), two peroxidases (K4BE93 and Q07446) and a lipoxygenase domain containing protein (K4BJ74) (Table 3.5.3).

3.5.4. Discussion

Effects of Mn toxicity on the root proteome

The overall analysis of the differential root proteome upon Mn toxicity suggests a general slowdown of metabolic activities. Approximately 70 % of the proteins showing changes in relative abundance were found to decrease (112), and this set of proteins covered a wider range of functional categories than those of proteins increasing in abundance. A similar behavior has been previously described in roots of *Citrus sinensis* grown in excess Mn (You et al., 2014), as well as in *Beta vulgaris* exposed to Zn toxicity (Gutierrez-Carbonell et al., 2013) and *L. esculentum* grown under Cd toxicity (Rodríguez-Celma et al., 2010).

Mn toxicity alters protein turnover in roots

Protein metabolism was one of the most represented categories affected by Mn toxicity (33 proteins decreasing, four proteins increasing), and changes found in this category support an altered protein turnover. Results indicate that both protein synthesis and degradation of damaged proteins *via* the proteasome are diminished in roots of plants exposed to excess Mn. On one hand, the decreases in ten structural components of the ribosome indicate a lower number of ribosomes, and the decreases in one translation elongation factor and one initiation factor (one of the largest decreases measured) also suggest that translation is impaired. On the other hand, five regulatory units of the proteasome (mostly activating factors) and three subunits of the complex also decreased in abundance, suggesting a slowdown of protein degradation *via* the proteasome. Decreases in proteasome components were also found in *Citrus grandis* affected by Mn toxicity (You et al., 2014). In addition, five more proteases from MEROPS

families S8, A1, C1 and M16 decreased, whereas only two from the family S8 increased, and two protease inhibitors of the MEROPS family I3 increased also pointing towards a decrease in proteolysis. Increases in protease inhibitors were also found in soybean roots exposed to Mn toxicity (Chen et al., 2016). Overall, these results indicate that the decrease in protein synthesis might be balanced by a decrease in protein degradation, and this metabolic adjustment would lead to an accumulation of damaged proteins that could be behind some of the deleterious effects of Mn toxicity. Although it has been described that an excess of Mn can displace Mg and subsequently affect the correct assembly of the ribosomes (Cammarano et al., 1972), this competition does not necessarily lead to a decrease in ribosome components. Therefore, the decreases in ribosomal components measured in roots exposed to Mn toxicity suggest the existence of an additional toxicity mechanism affecting protein synthesis.

Further indications of an altered protein turnover were the decreases measured in eight chaperones, including two HSP70 (K4B2J4 and K4B2I9), four CPN60 (K4CWE4, P93570, K4C227 and K4C7I1), a predicted HSP70-HSP90 organizing protein 2 (A9NUH2) and a peptidyl-prolyl cis-trans isomerase (K4CAH4). Chaperones with a CPN60 domain usually assist folding of newly synthesized polypeptides (Hemmingsen et al., 1988; Kubota et al., 1995) and HSP70 proteins prevent partially synthesized peptides from aggregating (Mashaghi et al., 2016), whereas HSP70-HSP90 organizing proteins and peptidyl-prolyl cis-trans isomerases mediate the transfer of peptides (Wegele et al., 2004) and protein-protein interactions (D'Andrea and Regan, 2003), respectively, during the assembly of multiprotein complexes. Similar decreases in HSPs were found in *Citrus sinensis* roots affected by Mn toxicity (You et al., 2014). Heat shock proteins also play important roles in preventing aggregation of damaged or miss-folded proteins in stress situations including heavy metal stresses, although in such cases their abundance usually increases (Hossain and Komatsu, 2013). Therefore, decreases in these proteins likely suggest a less intense assembling of *de novo* synthesized proteins, in line with the proposed decrease in protein synthesis.

In addition, Mn toxicity also affected some proteins involved in amino acid metabolism processes, including an increase in a protein involved in tryptophan degradation (K4D0F3) and decreases in five proteins involved in GABA and glycine degradation (B1Q3F8 and K4B9V1, respectively) and in serine (K4BUB7, K4C261) and glutamine biosynthesis (A5A7P7). Decreases in free amino acids upon Mn toxicity have been described in leaves of *Brassica rapa* (Lee et al., 2011).

The importance of the protein metabolism category was further confirmed by the PCA which indicated that eight proteases, two translation related proteins, two chaperones and three amino acid related proteins were among those proteins greatly contributing to the separation of the treatments (Tables S7 and S8).

Mn toxicity impairs energy production in roots

Results in this study indicate that energy metabolism, including glycolysis, pyruvate metabolism, TCA and oxidative phosphorylation, was heavily affected by Mn toxicity. A large number (19) of proteins classified in the carbohydrate category decreased in abundance, including an invertase (K4CNR7), three proteins from the glycolysis pathway (one enolase, P26300 and two fructose-bisphosphate aldolases, K4D3E4 and K4BX34), four components of the pyruvate dehydrogenase complex (K4C8X8, B5LAW5, K4B170 and Q8GT30), four TCA proteins, including aconitase (K4CFD4), malate dehydrogenase (K4BLA1), and two succinato dehydrogenases (K4BB47 and M1CP34). Similar decreases were described in *Citrus sinensis* roots and in cowpea leaf apoplast upon Mn toxicity (Zhou et al., 2013; You et al., 2014; Führs et al., 2008), and altogether indicate a reduction in the production of ATP and reducing power.

The PCA of the 2-DE results revealed that proteins form the carbohydrate category including a component of the pyruvate dehydrogenase complex (M1CP34), two glycolysis-related (the enolase, K4BKV2, and the triosephosphate isomerase, K4B3X5), a fructokinase 2 (Q42896) involved in the synthesis of starch and a carbonic anhydrase (Q5NE21) had a large positive contribution to the separation of the treatments (Tables S7 and S8), supporting the effect of Mn toxicity in the carbohydrate metabolism.

Furthermore, the decreases in the relative abundance of a subunits of the complex I (K4D5V2), classified in the oxido-reductase category, and in the two succinate dehydrogenases (complex II) suggest a reduction in the electron transport activity, and therefore a decrease in energy production. Since the NADH:ubiquininone oxido-reductase (complex I) also contains a Fe-S cluster, the decreases measured might be associated to a decreased Fe availability caused by the competition between Mn and Fe at the molecular transporter level (Pittman et al., 2005; Socha and Guerinot, 2014; Williams and Pittman, 2010). Other Fe containing proteins such as a NADH-cytochrome b5 reductase (K4BZA6) and a dioxygenase (Q40131) also showed a similar behavior. This is in agreement with the increase in root Fe reductase activity measured in roots of plants grown in excess Mn (Figure 3.5.1B) that suggests some degree of Fe shortage, although the root Fe concentrations did not change and the decreases in leaf Fe concentrations were still higher than those typical of Fe-deficient plants (Table S1).

Mn toxicity modifies cell wall properties

Changes measured in peroxidases and GHs suggests that Mn toxicity causes alterations in the root cell wall properties. The second most represented category of differential proteins were oxido-reductases (17 proteins increasing and 15 decreasing). Although the number of proteins decreasing and increasing is similar, almost all of the proteins increasing (16) in abundance

were peroxidases, whereas only six peroxidases, a catalase and two ascorbate peroxidases decreased. Furthermore, most of the peroxidases increasing in abundance were orthologs of *Arabidopsis* peroxidases (AtPER12, 25, 52 and 72) involved in cell wall lignification and suberization (Andersson-Gunnerås et al., 2006; Fernández-Pérez et al., 2015a; 2015b; 2015c; Shigeto et al., 2014), indicating a Mn-induced increase in lignification which probably affects cell wall stiffening and expansion (Imberty et al., 1985; Kärkönen et al., 2002; Ros Barceló et al., 1987; Sato et al., 1995) and may ultimately lead to the inhibition of root growth (Chen et al., 2016). An induction of cell wall lignification by Mn toxicity has been previously described (Chen et al., 2016; Fecht-Christoffers et al., 2006; Lavres et al., 2009; Morita et al., 2006). On the other hand, peroxidases decreasing were orthologs of AtPER3, 27 and 70 and their changes might be related to redox homeostasis maintenance.

Accordingly, peroxidases accounted for a large percentage of the proteins explaining the separation between treatments in the PCA (seven in shotgun and ten in 2-DE) and furthermore, two of them PER52-K4BE93 (increasing and related to lignification) and PER3-Q07446 (decreasing and whose *Arabidopsis* ortolog is involved in stress response) were found in both treatments with opposite contributions to the separation (Table 3.5.3), suggesting their different roles in the response to Mn toxicity.

Changes in the polysaccharide related category (eight proteins increasing and four decreasing) also point towards alterations in the root cell wall. Proteins increasing included an expansin (K4CNF0) and seven GHs from families 17, 18 and 19, whereas proteins decreasing were two GHs from families 3 and 16 (K4B267 and Q6RHX9, respectively), a glycosyltransferase family 75 (Q6IV07) protein, and a probable cinnamyl alcohol dehydrogenase 1 involved in lignin formation. The increases in endo-hydrolyzing enzymes (GH 17, 18 and 19) and the decreases in glycosyl-forming enzymes (Q6RHX9 and Q6IV07) provide support for the existence of polysaccharide degradation, which in conjunction with the increase in expansin may alter the mechanical behavior of the cell wall. The expansin-like B1-like protein (K4CNF0) also increased in *Glycine max* roots exposed to Mn toxicity and was proposed to play a role in inhibiting root growth in Mn toxicity conditions by altering cell wall properties (Chen et al., 2016). The Mn-induced increase measured here in the same expansin protein is in line with this hypothesis. Since Mn is a cofactor of multiple peroxidases and of several enzymes involved in lignin biosynthesis (Morita et al., 2006; Huber and Graham, 1999; Malavolta, 2006; Thompson and Huber, 2007), changes observed in the abundance of these enzymes may be related to Mn availability.

Proteins in the polysaccharide category greatly contributed to the separation of treatments (four proteins in shotgun and five spots/four proteins in 2-DE) and two of them (GH17 Q01412

and GH17 Q01413) were found in both approaches (Tables S7, S8 and 3.5.3), supporting the importance of the endo-hydrolyzing enzymes in the response to Mn toxicity.

In addition, four proteins decreasing in the carbohydrate category were related to nucleotide sugar metabolism, including a dTDP-4-dehydrorhamnose reductase (K4CP14), an UTP-glucose-1-phosphate uridylyltransferase (P19595) and two UDP-glucose 6-dehydrogenases (Q9SQJ1 and K4B740). These proteins play central roles as glucosyl donors in cellular metabolic pathways, including the transfer of sugar nucleotides to cell wall polymers (Tenhaken and Thulke, 1996), and therefore their decreases also suggest Mn-induced changes in cell wall.

Excess Mn activates plant defense mechanisms

Changes in defense related proteins and in some oxido-reductases indicate that plants exposed to excess Mn are subjected to a high stress situation. Accordingly, these categories contained a significant number of proteins with large contributions to the separation of treatments in both PCAs (Tables S7 and S8). First, the increases measured in a large number of peroxidases, in addition to the role in lignification commented above, may also imply a higher level of protection in roots against oxidative damage. Furthermore, three enzymes from the ascorbategluthation cycle (ascorbate peroxidase 1, ascorbate peroxidase 2 and a dehydroascorbate reductase) decreased as a result of Mn excess, suggesting that this path for ROS protection is diminished, probably compensating the peroxidase increases. Second, a large number of defense related proteins (10) increased, whereas only two decreased as a result of Mn toxicity. Among proteins increasing, four were pathogenesis related (PR10) belonging to the Bet v I family (three predicted PR STH2, Q53U3, K4CWC6 and K4CWC4, and a TSI-1 protein, O49881), two were thaumatins (Q9M3X2 and Q84U62), two were PR2 with Barwin and RlpA-like domains (P32045 and O03994) and two more were PR1 proteins (B2LW68 and O24025) (Table S6). All these proteins have been involved in stress response in plants, but their specific roles remain unknown. Homologues of these proteins have been found in several species as a response to different biotic and abiotic stresses, including heavy metal toxicity (Chen et al., 2016; Li et al., 2013; Loukehaich et al., 2012; Udawat et al., 2014; Wang et al., 2013). Nevertheless, it is worth mentioning that two of them showed increases amongst the highest measured, a PR10 predicted STH-2 (Q53U35; 105-fold) and the small *cys* rich PR1a2 (O24025, 61-fold) (Table 3.5.2), whereas two more PR10, the STH-2 (KW4CWC4) and the TSI-1 (O49881), were found in both PCAs to have large contributions to the separation of the treatments (Table 3.5.3). PR10 proteins contain a hydrophobic pocket able to bind hormones and siderophores (Mogensen et al., 2002; Roth-Walter et al., 2014) and therefore they could be involved in hormone signaling. On the other hand the PR1a2 is a secretory *cys* rich protein that

has an unknown function, but members of this family have been reported to chelate Ca in mammals and therefore regulate the activity of some ion channels (Gibbs et al., 2006; Milne et al., 2003). Therefore, one may speculate that this secretory protein could sequester Mn in the apoplast as a detoxifying mechanism. Both proteins constitute good candidates for future studies.

Regulatory mechanisms elicited in Mn toxicity

The signaling-regulation category contained 19 proteins, all of them decreasing in abundance, and most of them (15 proteins) had RNA binding domains. Two of these RNA binding proteins presented significant contributions to the separation of treatments in the 2-DE PCA (Table S7). Although the specific functions of these proteins are still unknown, domains present include RRM (in seven proteins), KH (in three proteins), Zn finger (in two proteins), helicase C (in one protein), FDF (in one protein) and HABP4 (in one protein), which are usually involved in RNA stability, translation and regulation of alternative splicing (Ambrosone et al., 2015; Anantharaman and Aravind, 2004; Kenan et al., 1991; Lorkovic et al., 2009). Therefore, these decreases in RNA-binding proteins suggest that Mn toxicity might cause a decrease in RNA stability and also indicate that RNA regulatory mechanisms are important in the modulation of the cellular response to Mn toxicity as it occurs in other type of stresses such as salt or drought (Ambrosone et al., 2012; Nakaminami et al., 2012). The *Arabidopsis* ortholog of the HABP4 containing protein A9PDA1 (predicted plasminogen activator inhibitor 1) has already been described to play a key role in the tolerance to salt stress (Ambrosone et al., 2015), and the decrease found here suggests a role of this protein in general stress mechanisms.

In addition, this category had four more proteins with possible roles as activators and/or signal transducers. Two of them (Q94K24, K4BZG0) contained lipid binding-PH domains, suggesting that lipid-mediated regulation may also play a role in Mn toxicity as it has been proposed for Mn deficiency (Ceballos-Laita et al., 2018). The Ran-binding protein-1 (Q94K24) is a small GTPase that interacts with Ran, suppressing the Ran-mediated protein transport between the nucleus and the cytoplasm (Ki et al., 2001; 2003; Steggerda et al., 2002). A previous study in soybean roots exposed to Mn toxicity suggested that the suppressing action of GmRanBP1 over the delivery of the GmRan3 protein could contribute to the root growth inhibition upon Mn toxicity (Chen et al., 2016). The decrease measured in the putative G3BP-like protein isoform X1 (K4CAI5) involved in nuclear transport also supports an impairment of protein transport to the nucleus.

Further indications of an involvement of lipid-mediated signaling in Mn toxicity include the remarkable increase measured in a patatin-like protein (K4B6U4, 65-fold) and in two lipoxygenases (K4BJ73 and K4BJ74, ca. 5-fold). The latter lipoxygenase (K4BJ74) was found

in both PCAs as significantly contributing to explain differences between treatments whereas the first one was found only in the PCA of the shotgun results (Tables S7 and S8). Patatin is a root specific lipolytic acyl hydrolase that cleaves fatty acids from membrane lipids whereas lipoxygenases catalyze the dioxygenation of fatty acids into cell signaling oxylipins (Rydel et al., 2003). Both enzymes participate in signal transduction in stress situations (Baulande et al., 2010; Holk et al., 2002; La Camera et al., 2004; Wasternack et al., 2007; Weber, 2002), including nutrient stresses such as Fe and P deficiencies (Rietz et al., 2004; 2010).

Mn toxicity affects the abundance of nutrient reservoir proteins

It is also worth mentioning that five nutrient reservoir cupins were altered as a result of Mn toxicity (three increasing and two decreasing), with one of them (Q43633) showing a significant (28-fold) increase and three (Q43632, Q41115 and Q50JD8) having large component 1 scores in the 2-DE PCA (Table 3.5.2 and Table S7). Increases in these N storage proteins might be the result of the reduced protein synthesis and degradation. However, these proteins also contained RmlC and RmlC jelly roll domains, which are found in a dTDP-sugar isomerase enzyme involved in the synthesis of L-rhamnose, in Mn-binding proteins with oxalate oxidase or SOD activity and in auxin receptors (Interpro domain annotation), indicating that their changes in abundance may also be related to cell wall modifications or ROS defense. Interestingly, cupins increasing are annotated as vacuolar proteins, whereas one of the cupins decreasing (K4BKK9) is apoplastic, which makes tempting to speculate that upon Mn toxicity, Mn storage could occur in the root vacuoles in a process aided by cupins.

Comparison of 2-DE and shotgun

The experimental approach used, combining 2-DE and shotgun analysis, has been proven to be useful in the determination of the differential root proteome changes upon Mn toxicity, detecting a total of 161 proteins changing in relative abundance. Among those, only 54 proteins (34 % of the total; Figure 3.5.3) were detected by 2-DE, confirming the moderate sensitivity of this technique. This number is better than those found upon Mn toxicity in soybean (27; Chen et al., 2016), and *C. grandis* and *C. sinensis* (39-53; You et al., 2014), using in both cases a lower significance threshold (1.5- *vs.* the 2-fold change used here). The sensitivity of the shotgun technique was superior, not only confirming the changes in abundance in 11 of the proteins already found by 2-DE (7 % of the total; Figure 3.5.3), but also finding abundance changes not detected by 2-DE in 107 proteins more (66 % of the total; Figure 3.5.3). The PCA of the 2-DE and shotgun results revealed a similar number, 40 (53 spots) and 31 proteins, significantly contributing to the differences between treatments with seven of them found with both methods (Table 3.5.3). These numbers illustrate the complementarities of both techniques, since the

number of proteins detected exclusively by any of the two methods is relevant and are in agreement with previous studies also using both proteomic approaches (González-Fernández et al., 2013; Min et al., 2017). In addition, 2-DE allowed the identification of several spots corresponding to the same protein, which may allow us the study of isoforms or protein modifications occurring upon Mn toxicity in these specific cases. The complementarities of both proteomic approaches as well as the limitations and advantages described here have already been addressed in several reviews (Abdallah et al., 2012; Baggerman et al., 2005; Zargar et al., 2016) and clearly indicate that the combination of both approaches renders a more thorough description of differential proteomes.

Supplementary material

The supplementary data are included in the electronic version: **Table S1.** Concentrations of mineral nutrients in roots and leaves; **Table S2.** List of proteins identified and quantified in tomato roots by shotgun proteomics and Progenesis LC-MS analyses; **Table S3.** List of proteins that presented significant changes as a result of Mn toxicity; **Table S4.** 2-DE spots presenting significant changes in abundance as a result of Mn toxicity; **Table S5.** Proteins showing significant decreases in abundance as a result of Mn toxicity using both shotgun and 2-DE proteomic techniques; **Table S6.** Proteins showing significant increases in abundance as a result of Mn toxicity using both shotgun and 2-DE proteomic techniques. **Table S7.** Standardized component scores obtained in the principal component analysis of the differential proteins in the 2-DE experiment; **Table S8.** Standardized component scores obtained in the principal component analysis of the differential proteins of the shotgun experiment.

3.6. Effects of manganese toxicity on the protein profile of tomato (*Solanum lycopersicum*) xylem sap as revealed by shotgun analysis

Laura Ceballos-Laita [a], Elain Gutierrez-Carbonell [a,1], Hiroyuki Imai [b,c], Anunciación Abadía [a], Matsuo Uemura [c], Javier Abadía [a], Ana Flor López-Millán [d,*]

[a] *Department of Plant Nutrition, Aula Dei Experimental Station, Consejo Superior de Investigaciones Científicas (CSIC), Zaragoza, Spain*

[b] *United Graduate School of Agricultural Sciences, Iwate University, Morioka, Japan*

[c] *Cryobiofrontier Research Center, Faculty of Agriculture, Iwate University, Morioka, Japan*

[d] *Department of Biological and Environmental Sciences. School of Science and Computer Engineering, University of Houston Clear Lake, Houston, TX, USA*

ABSTRACT

The aim of this work was to study the effects of Mn toxicity on the xylem sap proteome of tomato using a shotgun proteomic approach. This approach yielded 641 proteins reliably identified and quantified with 66 % of them predicted as secretory proteins. Manganese toxicity caused statistically significant and biologically relevant changes in abundance in 217 proteins with more proteins decreasing than increasing (134 and 83 proteins, respectively), suggesting that this nutritional stress causes an overall deactivation of metabolic pathways. Metabolic pathways most affected by Mn toxicity were defense and polysaccharide and protein metabolisms. First, Mn toxicity induced changes in hydrolases and peroxidases involved in primary cell wall degradation and lignin formation indicate the existence of alterations in the cell wall. Excess Mn also affected protein turnover based on the decreases measured in proteolytic enzymes and in protein synthesis related proteins. Results also support that Mn toxicity modifies the redox environment of the xylem sap due to the several changes observed in the oxido-reductase category which together with changes observed in the defense category indicate a significant stress situation in the xylem sap. Finally, results suggest the existence of several signaling pathways including fasciclin arabinogalactans and lipids which overall seem to be repressed since most of the changes in the signaling category were decreases.

3.6.1. Introduction

Manganese (Mn) is an essential micronutrient which plays important roles in physiological processes in plants (Marchner, 1995). As a constituent of the oxygen evolving complex of the photosystem II, Mn is essential for photosynthesis; Mn also acts as a cofactor of several enzymes in important metabolic pathways such as the Krebs cycle or in redox homeostasis

through the action of Mn SOD (Millaleo et al., 2010; Pittman et al., 2005; Socha and Guerinot, 2014; Wang et al., 2007). However, when in excess Mn can be toxic for plants. Manganese is mainly taken up from the soil in the form of Mn (II). The amount of Mn in the soil is influenced by soil parameters such as pH, soil porosity, water contain or microbial activity. Nowadays, certain human activities including intensive horticulture and acidifying fertilizers (Millaleo et al. 2010; Graham et al., 2002) or climate events such as elevated ozone levels, increased ambient temperatures and emission of acidic gases (Fernando and Lynch, 2015; Driscoll et al., 2001; Guo et al. 2010), are increasing the percentage of acidic soils in the world (Foy 1984). In these soils, the prevalence of divalent Mn, highly available for plant roots, increases considerably and Mn toxicity can occur (Mukhopadhyay and Sharma 1991). High Mn concentrations increase the concentration of reactive oxygen species (ROS) and therefore cause oxidative stress and disturbances of the metabolisms of carbohydrates, amino acids, proteins and nucleic acids (Führs et al. 2010; Gangwar et al. 2010; Shi et al. 2006; Führs et al. 2012; Venkatesan et al. 2007; Yao et al. 2012; Zhou et al. 2013). Mn excess also alters photosynthesis and the contents of pigments and hormones (Durst, 1976; Millaleo et al., 2013; Srivastava and Singh, 2006). To cope with Mn toxicity, plants elicit several stress response mechanisms that include decreases in the translocation of the metal from roots to shoots (Zhou et al., 2013; Chen et al., 2016; You et al., 2014) and the regulation of the mechanisms involved in adquisition and distribution in the whole plant (Delhaize et al., 2003; Dou et al., 2009; Wu et al., 2002). The plant vascular system plays an essential role in these adaptive mechanisms since it constitutes the main conduit for the long distance delivery and distribution of Mn.

The vascular transport system is composed by phloem and xylem conduits with the apoplast compartment acting as an intracellular space between them and also between cells that controls the exchange of molecules, compounds and signals (Lucas et al., 2013; Oparka et al., 2000). The xylem is an essential component of the vascular transport system whose major role is the transport of nutrients, including Mn, and water from roots to shoots. Transport in the xylem occurs *via* the xylem sap, a fluid that flows trough the treachery elements that compose the xylem vessels and is driven by the negative pressure created by transpiration and/or by a positive root pressure created by the differences in water potential between the soil and the root system (Fisher, 2000). Altough the most abundant components of the xylem sap are water and mineral nutrients, this fluid also contains other compounds in low quantities including carbohydrates, hormones, secondary metabolites, peptides and proteins (Carella et al., 2016; Dickson, 1979; Escher et al., 2004; Friedman et al., 1986; López-Millán et al., 2000a; Rodrigues-Celma et al., 2016). The protein profile of xylem sap presents a characteristic composition and it is mainly composed by proteins containing N-terminal peptides that are synthetized in the roots and subsequently loaded in the xylem sap *via* the secretory pathway

(Rodríguez-celma et al., 2016; Alvarez et al., 2006; Fukuda et al., 1996; Ligat et al., 2011). However, the presence of proteins originated in neighboring tissues and indicating cytoplamic contamination is also commonly reported in the xylem sap proteome (Rodríguez-Celma et al., 2016).

Proteomic approaches are a powerful tool to understand the undelying mechanisms that plants elicit to respond to nutritional stresses including Mn toxicity. In spite of their advantages, limited information is available on the effects Mn toxicity exerts on the xylem sap proteome, which is an essential component in Mn homeostasis. Proteomic information on Mn toxicity to date is restricted to roots and leaves. Root proteomic analysis have been carried out by 2-DE using Citrus species and *Glycine max*, and by shotgun proteomics and 2-DE using *Solanum lycopersicum* (You et al., 2014; Chen et al., 2016; Ceballos-Laita et al., 2018, in second revision). These studies indicate that Mn toxicity causes alterations in the structure and lignin composition of root cell walls and an impairment of metabolic pathways involved in energy production, which are probably responsible for the growth inhibition observed in roots of plants grown in the presence of excess Mn (Chen et al., 2016; Ceballos-Laita et al., 2018, accepted). Other root alterations include changes in the protein turnover and an activation of plant defense and reactive oxygen species (ROS) protection mechanisms (Fecht-Christoffers et al., 2003; González et al., 1998; Chen et al., 2015; 2016). In leaves, proteomic studies have revealed that Mn toxicity causes a major impairment in photosynthesis and CO_2 fixation and important increases of ROS (You et al., 2014; Führs et al., 2008; Fecht-Christoffers et al., 2003). On the other hand, studies on xylem sap obtained from plants subjected to different biotic and abiotic stresses, including Mn deficiency, indicate the proteins in xylem sap might play important roles in nutrient stress signaling (Carella, 2016; Ceballos-Laita et al., 2018; Zhang et al., 2015; Del Vecchio et al., 2014; Kaida et al., 2010). Given the important role of xylem sap plays in Mn homeostasis and the advantages of proteomic approaches, the aim of this work was to assess the effect of Mn toxicity on the xylem sap proteome of tomato (*Solanum lycopersicum*) using a shotgun proteomic approach. Tomato was chosen as a model plant because the tomato genome has been published and the combination of root pressure and turgid stems allow for sufficient xylem sap collection by de-topping.

3.6.2. Materials and methods

Plant material and sampling

Tomato (*Solanum lycopersicum*, cv. Tres Cantos) plants were grown hydroponically in a controlled environment chamber (Fitoclima 10.000 EHHF, Aralab, Lisbon, Portugal) with a photosynthetic photon flux density (PPFD) of 400 µmol m^{-2} s^{-1} photosynthetically active

radiation, 80 % relative humidity and a photoperiod of 16 h, 23 ºC/8 h, 18 ºC day/night regime. Seeds were germinated in vermiculite for 13 days in half-strength Hoagland nutrient solution containing 4.6 µM $MnCl_2$. Seedlings were then transplanted to 10 L plastic buckets (16-18 plants per bucket) containing half-strength Hoagland nutrient solution and grown for an additional 13-day period. After this time, solutions were renewed and control (4.6 µM $MnCl_2$) and Mn-toxicity (300 µM $MnCl_2$) treatments imposed. Xylem sap were collected eight days after treatment onset. At this time, plants were de-topped approximately five mm above the mesocotyl using a carbon steel disposable scalpel (Nahita, Beriain, Spain) and the exuded fluid was collected from the cut surface. The initial sap collected during the first 5 min was discarded to minimize contamination with other plant fluids and broken cells, and the xylem sap was collected for 30 min using a micropipette tip. Samples were kept on ice during the entire collection period and immediately analyzed.

Experimental design

The experiment was repeated six times with independent sets of plants. Each batch of plants consisted of one 10 L bucket per treatment with 16-18 plants per bucket. In each batch of plants, xylem sap fluid from all plants in a given treatment was pooled together and considered as a biological replicate (n = 6).

Mineral analysis

Micronutrients (Fe, Mn, Cu and Zn) were measured in xylem sap obtained from 4 plants from each treatment. The concentrations of micronutrients in the collected fluid were determined by ICP-MS (Inductively Coupled Plasma Mass Spectrometry; model Agilent 7500 ce; Agilent Technologies, Tokyo, Japan) after digestion with 1 % HNO_3 (TraceSELECT Ultra, Sigma-Aldrich, Madrid, Spain).

Protein extraction

Proteins in the collected fluid were precipitated immediately by adding five volumes of cold 0.1M ammonium acetate in methanol containing 0.07 % β-mercaptoethanol, kept overnight at -20 ºC and then centrifuged at 20,000 x *g* for 20 min. The pellet was washed twice with cold methanol, dried with N_2 gas and solubilized in a sample rehydration buffer containing 8 M urea, 2 % (w/v) CHAPS, 50 mM DTT, 2 mM PMSF and 0.2 % (v/v) IPG buffer pH 3-10 (GE Healthcare, Uppsala, Sweden). After rehydration, samples were incubated in a Thermomixer Confort device (Eppendorf AG, Hamburg, Germany) at 42 ºC and 1,000 rpm during 3 h, then centrifuged at 10,000 x *g* for 10 min at RT and filtered (0.45 µm ultrafree-MC filters, Millipore, Bedford, USA). Protein concentration was quantified immediately with a Bradford kit (Sigma-

Aldrich, St. Louis, MO, USA) using microtiter plates in an Asys UVM 340 spectrophotometer (Biochrom Ltd., Cambridge, UK) and BSA as standard.

Label free liquid chromatography-tandem mass spectrometry (LC-MS/MS)

Sample preparation for label free LC-MS/MS shotgun analysis was carried out according to Li et al. (2012). Briefly, 5 µg of total proteins were subjected to 1-DE to remove non-protein compounds. The resulting gel bands were cut into six pieces, proteins were *in gel* digested with trypsin, and peptides were subsequently extracted. Peptide solutions were concentrated in a trap column (Lcolumn Micro 0.3 x 5 mm; CERI, Japan) using an ADVANCE UHPLC system (Michrom Bioresources, Auburn, CA, USA). Elution was carried out with 0.1 % (v/v) formic acid in ACN and concentrated peptides were separated in a Magic C_{18} AQ nano column (0.1 x 150 mm; Michrom Bioresources) using a linear gradient of ACN (from 5 % to 45 %) and a flow rate of 500 nL min^{-1}. Peptide ionization was carried out with a spray voltage of 1.8 kV using an ADVANCE spray source (Michrom Bioresources). Mass spectrometry analysis was carried out on an LTQ Orbitrap XL (Thermo Fisher Scientific, Waltham, MA, USA) equipped with Xcalibur software (version 2.0.7, Thermo Fisher Scientific) and mass data acquisition parameters were set as described elsewhere (Gutierrez-Carbonell et al., 2016).

Mass data analysis was performed according to Takahashi et al. (2014). Protein identification was carried out using the full peptide list with the Mascot search engine (version 2.4.1, Matrix Science, London, UK) and NCBI 20141009 database (50,750,890 sequences; 18,190,226,827 residues). Search parameters were: peptide mass tolerance ±5 ppm, MS/MS tolerance ±0.6 Da, one allowed missed cleavage, allowed fixed modification carbamidomethylation (Cys), and variable modification oxidation (Met) and peptide charges were set to + 1, + 2 and + 3. Positive protein identification was assigned with at least two unique top-ranking peptides with scores above the threshold level ($p < 0.05$). Protein information was exported from Mascot .xml format and imported to Progenesis QI for proteomics software (v. 2.0, Nonlinear Dynamics, Newcastle upon Tyne, UK), which then associates peptide and protein information. The MS proteomics data have been deposited to the ProteomeXchange Consortium *via* the Pride partner repository (Vizcaíno et al., 2016), with the data set identifier PXD007517.

To assess the effect of Mn toxicity in the protein profile of tomato xylem sap, we calculated the ratio of normalized protein abundance between treatment and control samples. Only changes with a $p \leq 0.05$ (ANOVA) and a ratio ≥ 2 or ≤ 0.5 were considered as statistically significant and biologically relevant, respectively. Multivariate statistical analyses (Principal Component Analysis; PCA) were carried out using SPSS Statistical software (v. 24.0), including only proteins showing statistically significant changes (ANOVA; $p \leq 0.05$) as a result

of the Mn toxicity treatment. We used the GO biological process annotation (http://www.geneontology.org) and domain annotations for classification of each individual protein identified into nine different functional categories (polysaccharide related, oxido-reductases, protein metabolism, carbohydrate metabolism, lipid metabolism, signaling, defense, nutrient reservoir, unknown and a miscellaneous group containing functional categories not belonging to the previous groups). The presence of a signal peptide in xylem sap proteins was assessed using TargetP (www.cbs.dtu.dk/services/TargetP) (Emanuelsson et al., 2007), and SecretomeP (www.cbs.dtu.dk/services/SecretomeP) was used to assign proteins to secretory classical and non-classical classes (Bendtsen et al., 2004, 2005).

3.6.3. Results

Xylem sap collection and mineral composition

Xylem bleeding rates were similar in control and Mn-treated plants (approximately 0.55 ml g^{-1} h^{-1}) whereas the protein extraction yield in xylem was 3 times higher in plants grown in the presence of high Mn concentration (27 ng protein μL^{-1}) than in the controls (9 ng protein μL^{-1}) (Table 3.6.1).

Table 3.6.1. *Exudation rates (mL $g^{-1}h^{-1}$), protein yield (ng prot μL^{-1}) and concentrations of mineral nutrients in xylem sap (in µM) of Solanum lycopersicum plants grown in control and excess Mn conditions after 8 days of treatment onset. Data correspond to means ± SE (n = 6 for collection parameters and n = 4 for micronutrient concentration). Statistically significant differences were determined with the Student's t-test, $^{*}p \leq 0.05$; $^{**}p \leq 0.01$; $^{***}p \leq 0.001$).*

	Control	**Mn-toxicity**
Collection parameters		
Exudation rates ($mLg^{-1}h^{-1}$)	0.56 ± 0.11	0.52 ± 0.21
Protein yield (ng prot μL^{-1} xylem)	9.0 ± 3.4	27.0 ± 12.5*
Micronutrient concentrations (µM)		
Mn	6.5 ± 0.8	385.7 ± 16.1***
Fe	47.8 ± 12.5	15.7 ± 2.5**
Zn	9.5 ± 1.3	8.0 ± 0.9
Cu	3.6 ± 0.8	3.1 ± 0.5

Manganese concentration in xylem sap from plants grown in excess Mn was approximately 60 times higher than in controls whereas the concentrations of Fe and Zn were 67% and 16 % lower and no significant differences were measured in the concentration of Cu (Table 3.6.1).

Effect of Mn-toxicity on the xylem sap proteome

The LC-MS/MS analysis detected 1534 proteins in tomato xylem sap, and 641 of them were reliably identified and quantified with at least 2 peptides and considered in this study. The list

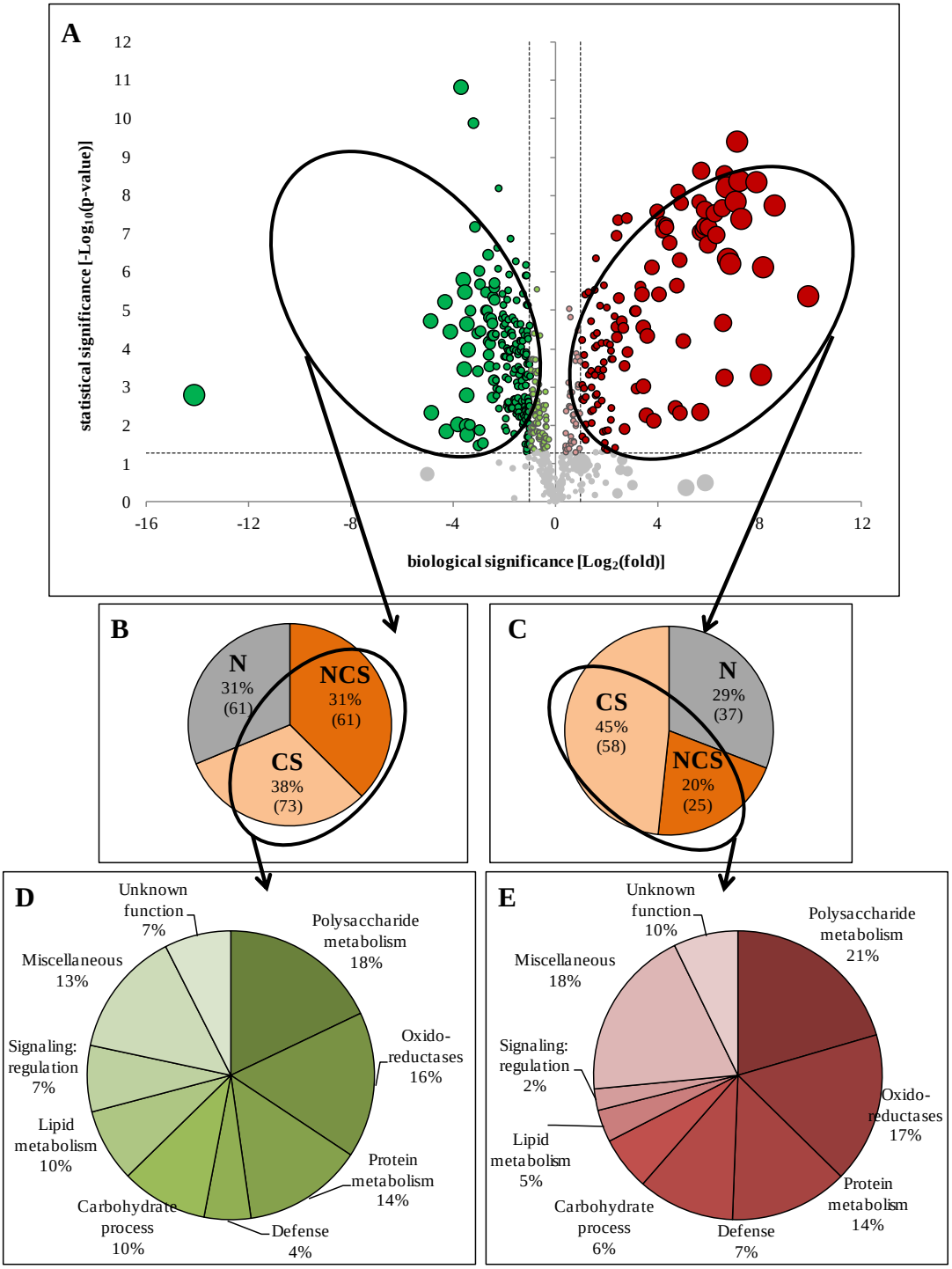

Figure 3.6.1. *Effect of Mn toxicity on the xylem protein profile as revealed by label-free shotgun analyses. Volcano scatter plot (A) showing the 641 identified and quantified proteins (peptides assigned to a protein and used for quantification ≥ 2) where proteins unaffected by Mn toxicity are depicted in grey and proteins changing as a result of Mn toxicity (ANOVA, p ≤ 0.05) are depicted green (decreasing) or red (increasing). Light colors are used for those proteins meeting only the statistical threshold (ANOVA, p ≤ 0.05) and bright colors where used when the statistical and biological (fold change ≤ 0.5 or ≥ 2) thresholds were met. The size of the dots is proportional to the fold changes. Pie chart depicting subcellular classification (NS: non-secretory, CS: classical secretory and NCS: non-classical secretory) as revealed by SignalP and SecretomeP prediction tools of proteins showing decreased (B) and increased (C) abundances. Functional classification based on GO biological process and domain annotations of secretory proteins showing decreased (D) and increased (E) abundances as a result of Mn toxicity.*

of proteins detected is shown in Table S1 and the list of the corresponding peptides is available in the ProteomeXchange Consortium *via* the Pride partner repository with the data set identifier PXD007517. A large majority (84 %; 542 proteins) of the identified and quantified proteins were ascribed to the *Solanum* genus and 94 % of them (508 proteins) where matched specifically to the species S. *lycopersicum* (Table S1).

Manganese toxicity caused significant (ANOVA, $p \leq 0.05$) and biologically relevant (fold ≥ 2 or fold ≤ 0.5) changes in 315 proteins of the xylem sap proteome (Tables S2 and S3). A volcano plot, showing the relationship between statistical significance [$-\log_{10}$(p-value)] and biological significance [$\log_2$(fold-change)], was used to visualize these changes (Figure 3.6.1A) and the prediction programs TargetP and SecretomeP were used to classify these proteins into the secretory pathway as classical secretory (CS), non-classical secretoy (NCS) and no secretory (NS) (Figure 3.6.1B, Tables S2 and S3).

Proteins decreasing in abundance

Among the 315 proteins showing changes above the statistical and biological thresholds, 195 proteins decreased in abundance (green dots in Figure 3.6.1A), and 134 of them were classified as secretory proteins (73 CS and 61 NCS; Figure 3.6.1B; Table S2). The remaining 61 proteins (31 %) were NS and since their unequivocal presence in xylem sap deserves further studies, they were excluded from the biological interpretation (Table S2). Polysaccharide metabolism (18 %, 24 proteins), oxido-reductases (16 %, 22 proteins) and protein metabolism (14 %, 19 proteins) were the most represented categories followed by carbohydrate metabolism (10 %, 13 proteins), lipid (10 %, 13 proteins) and signaling (7 %, 10 proteins) (Figure 3.6.1D, Table S2). Most (19 out of 24) of the proteins in the polysaccharide metabolism were glycoside hydrolases (GH) belonging to a wide variety of subfamilies (GH 3, 5, 10, 16, 17, 20, 28, 32, 35, 79 and 127) with GH17 (four proteins) and GH 28 (three proteins) being the most represented subfamilies. The remaining five proteins in this group included three pectin esterases (K4D4J5, K4CGQ4 and Q153F8) a glycosyl amidase (M1B8U3) and an UDP-N-acetylglucosamine pyrophosphorylase (K4B7I5) (Table S2). Only four proteins within this category were NCS (Table S2). The most represented families in the oxidoreductase category included peroxidases (five proteins), copper oxidases (seven proteins) and aldehyde/histidinol dehydrogenases (five proteins) (Table S2). The five remaining proteins in this category included two miscellaneous reductases (B1Q3F7 and K4D331), a superoxide dismutase (K4C5F4) and two miscellaneous oxidases (K4CM66 and A5BF85) (Table S2).The large majority of the oxidoreductases decreasing (68 %) were classified as CS (Table S2). In the protein metabolism category, decreases were measured in 14 proteins involved in proteolysis and in five structural components of the ribosomes (Table S2). Proteolytic proteins decreasing included four

subtilisins (MEROPS family S8), three serine carboxy-peptidases (MEROPS family S10), two cysteine proteases (MEROPS family C1), one aspartic peptidase (MEROPS family A1), one processing peptidase from the MEROPS family M16, a gamma-glutamyltranspeptidase (MEROPS family T3) and two regulatory subunits of 26 S proteasome (Table S2). The later five proteins were classified as NCS whereas the remaining ones were CS (Table S2).

Table 3.6.2. *Xylem sap proteins showing large changes in abundance (fold > 25 or < 0.1) among the 217 secretory proteins affected by Mn toxicity (ANOVA, $p \leq 0.05$ and fold ≥ 2 or ≤ 0.5). Accession indicates UniProt database entry. Pep_c and Pep_q are the number of peptides used for identification and quantification. Abundance changes (Fold +Mn/C) were calculated by dividing the mean of normalized abundances (obtained with Progenesis QI v.2.5.1) in plants affected by Mn toxicity by that of control samples. Description includes the protein name according to the UniProt database. SecretomeP column includes classification as classical secretory (CS) or non classical secretoty (NCS) as indicated by SecretomeP (www.cbs.dtu.dk/services/SecretomeP) software. Detailed information about functional classification, identification and quantification is given in Tables S2 and S3.*

Num.	Uniprot entry	Fold ++Mn/C	Description	SecretomeP
			Polysaccharide metabolism (13 proteins)	
1	F4ZE23	0,1	β-galactosidase STBG2	CS
2	K4CGQ4	0,1	Uncharacterized protein LOC101247939	CS
3	D2CGN7	276,6	Glucan endo-1,3-β-D-glucosidase precursor	CS
4	Q944C0	51,6	Glucan endo-1,3-β-D-glucosidase precursor	CS
5	Q01413	136,5	Glucan endo-1,3-β-glucosidase B precursor	CS
6	Q8GUR4	230,7	Glucan endo-1,3-β-glucosidase A precursor	CS
7	K4BBH7	48,8	Glucan endo-1,3-β-glucosidase-like	CS
8	K4CAY2	26,6	Chitotriosidase-1-like	CS
9	Q05538	102,9	Basic 30 kDa endochitinase precursor	CS
10	V9HZ13	56,9	Basic 30 kDa endochitinase-like	CS
11	K4D1H0	51,1	Endochitinase 3-like	CS
12	Q7Y0S1	91,3	Chitinase	CS
13	K4D4G1	28,8	Citrate-binding protein-like	CS
			Protein metabolism (8 proteins)	
19	K4ATR4	0,1	Predicted serine carboxypeptidase-like 45-like	CS
20	O22686	0,1	Similar to 60S ribosomal protein L17 (*Arabidopsis thaliana*)	CS
21	C9DFA6	57,0	Subtilisin-like serine protease	CS
22	O04678	74,3	Subtilisin-like protease precursor	CS
23	Q6TKT2	131,1	Miraculin-like	CS
24	D4IHB9	260,7	Miraculin-like, partial	NCS
25	K4BEU1	93,4	Serine protease inhibitor 1-like	CS
26	P20076	31,7	Ethylene-responsive proteinase inhibitor 1 precursor	CS
			Oxido-reductases (5 proteins)	
14	K4BU12	0,0	Blue copper protein-like	CS
15	K4CLQ0	0,1	Early nodulin-like protein 1-like	CS
16	A5BF85	0,1	Similar to hypothetical protein VITISV_044041 (*Vitis vinifera*)	NCS
17	K4BE93	27,6	Suberization-associated anionic peroxidase 2-like	CS
18	K4BTH6	62,7	Peroxidase 12-like	CS

(Continued)

Table 3.6.2: continued

Num.	Uniprot entry	Fold ++Mn/C	Description	SecretomeP
			Defense (5 proteins)	
19	K4CRT0	0,1	MLP-like protein 28-like	NCS
20	P32045	153,0	Pathogenesis-related protein P2 precursor	CS
21	O03994	29,8	Wound-induced protein	CS
22	B2LW68	61,8	PR1 protein precursor	CS
23	Q0H8U4	97,1	Pathogenesis-related protein	NCS
			Lipid metabolism (3 proteins)	
24	K4B315	0,1	PI-PLC X domain-containing protein At5g67130-like	CS
25	Q9LM08	377,9	Similar to pepper esterase (*Capsicum annuum*)	NCS
26	K4DD79	28,9	GDSL esterase/lipase At1g28590-like	CS
			Carbohydrate process (2 proteins)	
27	K4AW47	0,1	Galactokinase-like	NCS
28	Q10CK6	0,1	Probable UDP-glucose 6-dehydrogenase 1-like	NCS
			Signaling:regulation (1 proteins)	
29	Q8L7N0	0,1	Similar to TCP-1 chaperonin-like protein (*Arabidopsis thaliana*)	NCS
			Miscellaneous (2 proteins)	
30	K4C320	0,1	Actin-depolymerizing factor 2-like	NCS
31	K4CQI3	0,0	Adenosine kinase 2-like	NCS
			Unknown function (4 proteins)	
32	K4C4W2	0,1	Remorin-like	NCS
33	K4D0G7	0,1	Uncharacterized protein At4g06744-like	CS
34	K4BT79	77,7	Uncharacterized protein	CS
35	K4C3P2	50,4	Uncharacterized protein LOC101247825	NCS

Proteins decreasing in abundance as a result of Mn toxicity in the carbohydrate category were involved in glycolysis (three proteins; F1AHC9, P09043, A4ZGB6), TCA (four proteins; K4DHU7, K4CHF9, B5LAW5, B9GPX3), pentose phosphate shunt (two proteins; A2YRB6, A5B7A4) and in monosaccharide metabolism including galactose (two proteins; Q1EMR1, K4AW47), rhamnose (K4CP14), and manose (Q10CK6) (Table S2). All of these proteins but the 6-phosphogluconate dehydrogenase (A5B7A4) were classified as NCS (Table S2). In the lipid category, most of the proteins decreasing were esterases and lipases (nine out of 10 proteins and five of them being NCS) whereas three were lipid-transfer proteins (K4CLX6, C5YG98, B6TLU5) and one more CS was a lipoxygenase (K4BSP6) (Table S2). Half of the proteins (five) decreasing in the signaling category were CS fasciclin-like arabinogalactan proteins, whereas two NCS were chaperones (B6UBL7, Q8L7N0), two were receptors (the CS, K4DFQ3 and the NCS, K4CN56) and one NCS was a regulator of ribonuclease activity (I3SFU5) (Table S2). Proteins decreasing (five) as a result of Mn toxicity in the defense category including three CS osmotins belonging to the pathogenesis-related family 5 (PR-5) (V4S9T2, K4BVN4, K4C1Y2), one CS cysteine-rich secretory protein (CRSP, K4CBP6) and a NCS PR-10 family protein (K4CRT0) (Table S2). One more protein decreasing was a NCS

nectarin (Q9SPV5) classified into the nutrient reservoir category. Finally, ten proteins (3 NCS and 7 CS) remained unassigned whereas 17 more (15 NCS and 2 CS) were classified in a miscellaneous category containing proteins involved in amino acid metabolism (four proteins), photosynthesis (five proteins), purine metabolism (two proteins), among others (Table S2).

Overall, deceases were moderated (88 % of the decreases ranged between 50 and 80 %) and only 16 proteins, scattered among the different metabolic categories, decreased more than 90 % as a result of Mn toxicity (Table 3.6.2).

Proteins increasing in abundance

Manganese toxicity caused relative increases above the biological and statistical thresholds in the abundance of 120 proteins (red dots in Figure 3.6.1A) and 83 of them were classified as secretory proteins (58 CS and 25 NCS; Figure 3.6.1C; Table S3). The remaining 37 proteins (31%) were NS and therefore excluded from the biological interpretation (Table S3). Functional classification of the 83 secretory proteins increasing in abundance revealed that polysaccharide metabolism (21 %, 17 proteins) and oxido-reductases (17 %, 14 proteins) were the most represented categories followed by protein metabolism (14 %, 12 proteins), nutrient reservoir (11 %, nine proteins) and defense (7 %, six proteins) (Figure 3.6.1E). Although the most represented categories were the similar to those found for decreasing proteins; proteins increasing in abundance belonged to different subfamilies. In the polysaccharide-related metabolic category, GHs were also the most represented families (15 out 17 proteins) but, in contrast with GHs decreasing, the most abundant subfamilies belonged mostly to three subfamilies GH17 (five proteins), 18 (three proteins) and 19 (four proteins) with two of the subfamiles GHs18 and 19 not found among GHs decreasing (Table S3). Other GH subfamilies increasing in this category were GH 3, GH5 and GH 20 with one protein each, whereas the remaining two proteins in this group were a pectinacetylesterase (B7FKL0) and a polysaccharide lyase family 7 protein (K4D4G1). All polysaccharide-related proteins increasing were classified as CS (Table S3). Subfamiles of proteins increasing in the oxido-reductase category (14) included peroxidases (six proteins) as described in decreasing proteins; however, thioredoxins (three proteins) also increased whereas no copper oxidases or aldehyde/histidinol dehydrogenases where found in this category (Table S3). The remaining oxido-reductases increasing (five proteins) were all NCS and included a monodehydroascorbate reductase (Q43497), a 3-dehydroquinate synthase (Q8RU74), a phenylacetaldehyde reductase (A6N6K8) and two dehydrogenases (Q2HTL8 and Q5NE18) (Table S3). With regard to the protein metabolism category, only one NCS elongation factor (K4DAS6) involved in protein synthesis increased, whereas as occurred in proteins decreasing the large majority (11) proteins in this group were proteolysis related and nine of them were CS. This later group contained proteins

belonging to the MEROPS subfamilies S8 (four proteins) and A1 (three proteins), also found among proteins decreasing; however four of them were protease inhibitors from the MEROPS families I3 and 13, not found among proteins decreasing in abundance (Table S3). Proteins increasing in the defense category included a osmotin belonging to the PR-5 family (A9PJD5) and five cysteine-rich secretory proteins (CRSP) with barwin (P32045, O03994), allergen V5 (B2LW68, Q0H8U4) and Gnk2 (K4DBB0) domains (Table S3). Only one of them, the allergen V5 (Q0H8U4) was classified as NCS.

The fourth most represented category among proteins increasing was the nutrient reservoir which accounted for a significant percentage of the changes (11 %, eight CS proteins and one NCS) and included eight CS proteins with a cupin-1 domain and one NCS oleosin (G7KPZ8), however increases presented were moderated and ranged from 3 to 14-fold (Table S3). Finally, other metabolic categories, which accounted for 30 % of the total proteins increasing, were carbohydrate metabolism (two proteins from the gycolytic pathway and three from pentose phosphate shunt), lipid metabolism (two esterase/lipases and two lipid-transfer proteins), amino acid metabolism (three amino transferases and a glutamine synthetase GS1), signaling (two protein folding related proteins), two acid phosphatases and eight proteins of unknown function (Table S3). Among these later categories, 15 proteins (65 %) were classified as NCS (Table S3).

The polysaccharide-related, protein metabolism and defense categories also had a large number of proteins (11, 6 and 4 proteins, respectively) showing remarkable (fold $\geq$ 25) increases in abundance (Table 3.6.2). These proteins included ten glyco-hydrolases (GHs) from families 17, 18 and 19 and an alginate lyase (K4D4G1) in the polysaccharide category; four protease inhibitors from the MEROPS families I3 and I13 and two subtilisin-like proteases (O04678 and C9DFA6) in the protein metabolism category, and four pathogenesis related proteins (Table 3.6.2). In the oxido-reductase category only two peroxidases (K4BTH6 and K4BE93) increased remarkably (above the 25-fold threshold) with the remaining 12 proteins (including four peroxidases and a group of eight oxido-reductases with miscellaneous activities) increasing between 2 and 11-fold (Tables 3.6.2 and S3). Although the lipid category only accounted for 2% (two proteins) of the proteins changing as a result of Mn toxicity, the most remarkable increase (377-fold) was observed in this category in a NCS pepper-like esterase protein (Q9LM08), while one more protein in this group, a GDSL esterase (K4DD79) showed a 29-fold increase upon Mn toxicity (Table 3.6.2 and S3). Two more uncharacterized proteins (K4BT79 and K4C3P2) also showed remarkable increases (78- and 51-fold, respectively) upon Mn toxicity (Table 3.6.2).

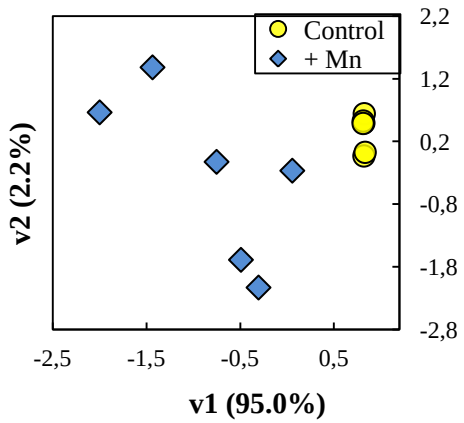

Figure 3.6.2. *Score scatter PCA (Principal Component Analysis) plot of Mn-treated samples when compared to controls. Principal component analysis was carried out using SPSS Statistical software (v. 24.0) and included proteins showing statistically significant changes (ANOVA, $p \leq 0.05$) when compared to controls. Yellow dots and blue diamonds depict control and Mn-treated samples, respectively.*

The PCA analysis of the statistically significant changes (ANOVA; $p \leq 0.05$) showed a good separation between treatments, with the first and second components explaining approximately 95 and 2.2 % of the variation, respectively (Figure 3.6.2; Table S4). Proteins with large positive component 1 scores (6 proteins) were mainly found in the oxido-reductases and lipid (8 %, 2 proteins in each), protein and carbohydrate (4 %, 1 protein in each) categories, whereas those with large negative contributions (20 proteins) were found in the polysaccharide (31 %, 8 proteins), defense (19 %, 5 proteins), oxido-reductases (11 %, 3 proteins), nutrient reservoir (8 %, 2 proteins) and protein (8 %, 2 proteins) categories (Table 3.6.3).

Table 3.6.3. *List of proteins correlated to component 1 in the PCA. Standarized component scores obtained in the principal component analysis of the differential proteins (ANOVA, $p \leq 0.05$). Accession and description correspond to the UniProt database identifier and name, respectively. Fold changes (Fold +Mn/C) were calculated by dividing the mean of normalized abundances (obtained with Progenesis QI v.2.5.1) in plants affected by Mn toxicity by that of control samples and p colum contains the p values of the ANOVA test. Proteins with an asterisks in the UniProt identifier are proteins not present in Tables S2 and S3 either for being out of the threshold range or for being Non secretory.*

Accession	Comp. 1 score	Comp. 2 score	Protein description	ANOVA (p)	Fold +Mn/C	Secretome P
Polysaccharide metabolism (8 proteins)						
Q01413	-0.379	-0.888	glucan endo-1,3-beta-glucosidase B precursor	0.00	136.53	CS
Q8GUR4	-0.019	0.088	glucan endo-1,3-beta-glucosidase A precursor	0.00	230.71	CS
Q944C0	-0.006	-0.015	glucan endo-1,3-beta-D-glucosidase precursor	0.00	51.62	CS
E0CRH7	-0.001	-0.063	glucan 1,3-beta-glucosidase-like	0.00	3.98	CS
K4D1H0	-0.003	-0.015	endochitinase 3-like	0.00	51.10	CS
K4C145	-0.002	0.003	acidic endochitinase-like	0.00	18.22	CS
K4BBH7	-0.001	-0.017	glucan endo-1,3-beta-glucosidase-like	0.00	48.76	CS
Q7Y0S1	-0.001	0.004	chitinase	0.00	91.25	CS

(Continued)

Table 3.6.3: continued

Accession	Comp. 1 score	Comp. 2 score	Protein description	ANOVA (p)	Fold +Mn/C	Secretome P
Protein metabolism (4 proteins)						
O04678	-0.009	0.042	subtilisin-like protease precursor	0.00	74.26	CS
C9DFA6	-0.32	1.52	subtilisin-like serine protease	0.00	57.00	CS
K4CLT6*	0.007	-0.018	aspartic protease in guard cell 1-like	0.01	0.51	CS
Q9LRJ9*	-0.001	-0.011	cysteine-rich repeat secretory protein 38-like	0.00	9.91	CS
Oxido-reductases (5 proteins)						
D2IX33	-0.001	0.001	protein disulfide-isomerase-like	0.00	10.71	CS
P46423*	-0.001	-0.001	glutathione S-transferase-like	0.00	2.59	NS
Q43497	-0.001	-0.003	monodehydroascorbate reductase	0.00	2.21	NCS
B5LST5	0.004	0.019	peroxidase 47-like	0.00	0.32	CS
Q2PYW5	0.007	0.122	catalase isozyme 1-like protein	0.00	0.15	NS
Defense (4 proteins)						
Q0H8U4	-0.232	-0.288	pathogenesis-related protein	0.00	97.14	NCS
K4CWC4	-0.005	-0.024	pathogenesis-related protein STH-2-like	0.00	19.80	NS
K4CWC6	-0.002	-0.007	pathogenesis-related protein STH-2-like	0.00	55.01	NS
P32045	-0.002	0.013	pathogenesis-related protein P2 precursor	0.00	153.03	CS
Lipid metabolism (2 proteins)						
K4CLX6	0.001	0.013	non-specific lipid-transfer protein 2-like isoform 1	0.00	0.17	CS
C5YG98	0.003	0.028	uncharacterized protein LOC101258342 isoform 1	0.00	0.43	CS
Nutrient reservoir (2 proteins)						
A0A072UDP2	-0.003	-0.493	legumin A2	0.04	3.78	CS
A0A072U3K0	-0.001	-0.195	legumin A2	0.04	4.98	CS
Carbohydrate process (1 proteins)						
Q42896*	0.001	0.015	fructokinase-2	0.04	0.72	NCS

Comparison of changes observed in xylem and root proteome in response to Mn toxicity

All proteins (S and NS) changing above the biological (fold ≥ 2 and ≤ 0.5) and statistical ($p \leq 0.05$) thresholds in xylem sap as a result of Mn toxicity were compared to those reported to change in roots of tomato plants grown in the same conditions using a combined 2-DE and shotgun proteomic approach (Ceballos Laita et al., accepted) (Figure 3.6.3). This comparison yielded 31 proteins in common between xylem sap and roots and most of them (29) followed the same changes in both tissues as a result of Mn toxicity (18 proteins increased and 11 decreased) whereas one non secretory catalase isoenzyme (Q2PYW5) decreased 90 % in xylem sap and increased 5-fold in roots and secretory GDSL esterase/lipase (K4DD79) followed the opposite behavior increasing almost 30-fold in xylem sap and decreasing 50 % in roots (Table 3.6.4).

Table 3.6.4. *List of proteins showing statistically significant (ANOVA, $p \leq 0.05$) and biologically relevant (fold ≥ 2 or ≤ 0.5) changes in abundance in both root and xylem sap proteomes when tomato plants grown in excess Mn were compared to controls. Proteins changing in abundance in roots as a result of Mn toxicity were obtained from Ceballos-Laita et al., accepted).*

			Secretome P	Xylem sap Fold +Mn/C	Root Fold +Mn/C
Proteins decreasing in both proteomes					
Oxido-reductase	Q07446	peroxidase 3-like	CS	0.5	0.1
	Q3I5C4	cytosolic ascorbate peroxidase 1	N	0.1	0.3
Carbohydrate metabolism	K4D3E4	fructose-bisphosphate aldolase cytoplasmic isozyme-like	N	0.4	0.3
	B5LAW5	similar to putative pyruvate dehydrogenase E3 subunit (*Capsicum annuum*)	N	0.5	0.5
	K4CP14	probable rhamnose biosynthetic enzyme 1-like	N	0.3	0.2
Polysaccharide metabolism	K4B2X5	probable cinnamyl alcohol dehydrogenase 2-like	N	0.2	0.3
Protein metabolism	K4DBV1	mitochondrial-processing peptidase subunit alpha-like	N	0.4	0.3
Defense	A9NNA0	similar to Universal Stress protein	N	0.1	0.5
Miscellaneous	K4C7I1	T-complex protein 1 subunit eta-like	N	0.3	0.2
	K4DHI9	probable voltage-gated potassium channel subunit beta-like	N	0.3	0.5
	K4ASJ4	formate--tetrahydrofolate ligase-like	N	0.4	0.3
Proteins increasing in both proteomes					
Polysaccharide metabolism	Q01413	glucan endo-1,3-beta-glucosidase B precursor (GH17)	CS	136.53	6.7
	Q05538	basic 30 kDa endochitinase precursor (GH19)	CS	102.91	3.5
	V9HZ13	basic 30 kDa endochitinase-like (GH19)	CS	56.95	9.5
	K4D1H0	endochitinase 3-like (GH19)	CS	51.1	3.6
	K4CAY2	chitotriosidase-1-like (GH18)	CS	26.58	3.4
Oxido-reductase	K4BTH6	peroxidase 12-like	CS	62.67	7.8
	K4BTH7	peroxidase 12-like	CS	2.74	6.3
	K4BE93	suberization-associated anionic peroxidase 2-like	CS	27.57	7.5
Protein metabolism	Q6TKT2	miraculin-like (MEROPS I3, clan IC)	CS	131.15	548.1
	C9DFA6	subtilisin-like serine protease (MEROPS S8/S53)	CS	57	41
	K4BEU1	serine protease inhibitor 1-like	CS	93.38	25
Defense	B2LW68	PR1 protein precursor	CS	61.84	4.3
	O03994	wound-induced protein	CS	29.84	16.6
	P32045	pathogenesis-related protein P2 precursor	CS	153.03	12.2
	Q53U35	pathogenesis-related protein STH-2-like	N	97.05	105.3
	K4CWC4	pathogenesis-related protein STH-2-like	N	19.8	5.8
	K4CWC6	pathogenesis-related protein STH-2-like	N	55.01	9
Miscellaneous	K4CBX5	probable inactive purple acid phosphatase 27-like	CS	2.6	3.3
Proteins with different response in root and xylem sap proteomes					
	Q2PYW5	similar to catalase isozyme 1-like protein	N	0.1	5.2
	K4DD79	GDSL esterase/lipase At1g28590-like	CS	28.95	0.5

The large majority of proteins decreasing in both tissues (10 proteins) were non secretory whereas the large majority of those increasing were secretory proteins (Table 3.6.4). The fold changes were very similar for decreasing proteins in roots and xylem sap whereas in general increases were more marked in xylem than in root samples (Table 3.6.4). Proteins increasing in abundance in both tissues were classified mainly in four metabolic categories (polysaccharide, defense, proteolysis and oxido-reductases) and included GHs (5 proteins), pathogenesis related proteins (six proteins), peroxidases (three proteins), proteolysis-related (three proteins) and a probable inactive purple acid phosphatase 27-like (K4CBX5) whereas those decreasing in abundance were scattered among different metabolic categories with carbohydrate metabolism being the most represented with three proteins (Table 3.6.4).

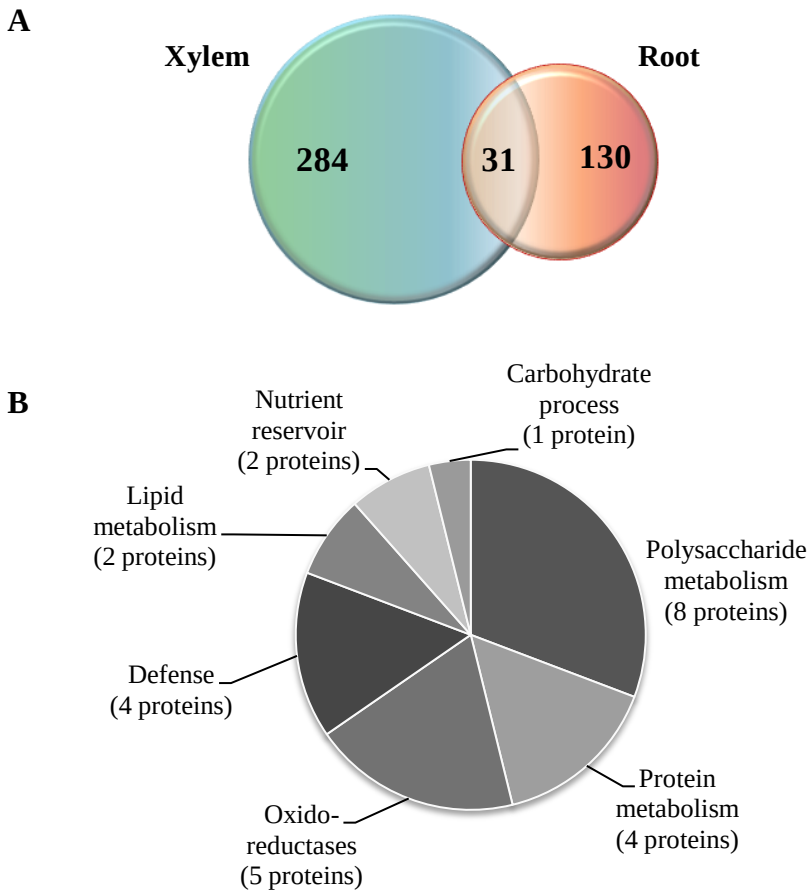

Figure 3.6.3. *A) Venn diagram comparing the number of proteins changing as a result of Mn-toxicity in roots and xylem sap of tomato plants. B) Functional classification of the 31 common proteins showing changes in xylem and root samples as a result of Mn toxicity. Proteins showing significant changes in both comparisons ($p \leq 0.05$), identified and quantified with at least two peptides, and above the threshold level (fold change ≥ 2 or ≤ 0.5) were classified according to their functions.*

3.6.4. Discussion

The proteomic approach used in this study has allowed for the reliable identification and quantification of a large set of proteins (641) in xylem sap and 66 % (424 proteins) of them

were classified as secretory proteins by several prediction tools, indicating that a significant percentage of the identified and quantified proteins in this study have an intracellular origin and thus may reflect some degree of cytoplasmic contamination. Manganese concentration in xylem sap was high compared to that reported in roots and leaves of similarly grown plants (Ceballos-Laita et al., 2018) indicating an active metal translocation from roots to shoots which in some plants has been related to their tolerance (Vose and Randall 1962; Zhou et al. 2013).

Effects of Mn toxicity on the secretory xylem sap proteome

Manganese toxicity caused significant and biological relevant changes in 217 proteins with more decreases in relative abundance than increases (134 and 83 proteins, respectively), suggesting that deactivation of metabolic pathways predominates in this nutritional stress.

Mn toxicity affects primary cell wall metabolism

Polysaccharide metabolism was the most represented category accounting for 19 % (41 proteins; 24 decreasing and 17 increasing) of the total changes observed in the xylem sap proteome upon Mn toxicity, indicating that this stress caused significant alterations in the xylem sap cell wall since most of these enzymes are extracellular and hydrolyze and/or rearrange glycoside bonds (Minic, 2008). Most of these proteins affected were GHs and except for two of them. Decreases in GHs were relatively moderated whereas increases measured in GHs were among the highest measured in this study (between 50- and 300-fold) suggesting that even though the number of proteins increasing and decreasing is similar, these later changes may play a more relevant role in the Mn toxicity response leading to an overall degradation of the primary cell wall. Proteins in the polysaccharide category greatly contributed to the separation of treatments (eight proteins) and five of them were endo-glucosidases including the highest increase in this category (Q8GUR4), supporting the importance of the endo-hydrolyzing enzymes in the response to Mn toxicity. This evidence was mentioned in root proteome upon Mn toxicity. Several subfamilies of GHs (GH 3, 5 and 17), which are mainly endo-glucanases acting in primary cell wall degradation, had members increasing and decreasing as a result of Mn toxicity. However, there were certain families which presented a distinct behavior. On one hand, subfamilies only presenting increases were GH 18 (three proteins) and 19 (four proteins), which are N-acetyl-hexosaminidases mainly involved in N-glycan degradation (Cazy database, www.cazy.org). Therefore, in addition to primary cell wall degradation, their large increases may also indicate a decrease in N-glycosylation, which is assumed to be a major post-translational modification of secreted proteins. Similar increases have been described in roots of tomato plants exposed to Mn toxicity (Ceballos-Laita et al., accepted). On the other hand, subfamilies with members only decreasing in abundance as a result of Mn toxicity had very

diverse catalytic and substrate specificities and included members from GH 10, 16, 28, 32, 35, 79 and 127 subfamilies, which are glycosylases acting in different residues including galactosides (GH28 and GH 35), fructosides (GH 32), glucuronic acid (GH 79), arabinofuranosides (GH127), or endoxylanases (GH10) and endoglucanases (GH16) (Cantarel et al., 2008) Overall, these decreases, although quantitatively less important than the increases in GHs, suggest that certain processes involving cell wall degradation may be reduced in the xylem sap of plants exposed to Mn toxicity and consequently lead to a modification of the cell wall composition. A similar situation has been described in the xylem sap of Mn-deficient plants (Ceballos-laita et al., 2018). These complex changes in GHs, in conjunction with the changes measured in pectin esterases (one increasing and three decreasing), indicate that Mn toxicity likely causes an increased degradation of the primary cell wall which occurs simultaneously with a re-arrangement of certain cell wall glycosides. A disorganization of the xylem vessels in soybean cultivars affected by Mn toxicity has been already been described by means of optical microscopy (Lavres et al., 2009). In line with this hypothesis, the protein concentration in xylem sap of plants exposed to Mn toxicity was 3-fold higher than in controls whereas the xylem flow rates were similar, indicating that an increased cell wall permeability in these plants.

Mn toxicity affects secondary cell wall metabolism

Almost 17 % (36 proteins) of the changes induced by Mn toxicity in the xylem sap proteome were classified in the oxido-reductase category and some of these changes could be associated to Mn-induced modifications in the secondary cell wall. Among them, ten were secretory peroxidases (four decreasing and six increasing). Peroxidases increasing were orthologues of the Arabidopsis AtPrx 12, 52 and 53 which are known to be involved in lignin formation and play a key role in controlling its deposition in the vascular tissue (Fernández-Pérez et al., 2015a, 2015b, 2015c; Shigeto et al., 2016; Freudenberg, 1959; Castillo and Greppin, 1986). However, four more peroxidases also decreased although less markedly, and they were similar to AtPrx 3, 10, 47 and 52. Two of them (AtPrx47 and 52) also involved in lignin synthesis, whereas the other two have been described as a stress-response proteins (Tokunaga et al., 2009; Kim et al., 2010; Kreps et al., 2002). These results indicate that Mn toxicity also affects the secondary cell wall *via* peroxidase activity and reveal the complexity of the changes, since some lignin-related peroxidases increased and some decreased. In addition, the peroxidases increasing in abundance can also have a ROS-protecting role by depleting hydrogen peroxide and therefore diminishing lipid peroxidation and protein oxidation (Shigeto and Tsutsumi, 2016; Santandrea, 2000). Increased peroxidase activity in cowpea leaf apoplasts has also been described to modulate Mn

oxidation and compartmentalization, and thus affect Mn tolerance (Fecht-Christoffers et al., 2006).

An alteration of lignin deposition in the secondary cell wall can also be hypothesized based on the decreases measured in seven Cu-oxidases, including six blue-copper proteins of unknown function, with one cupredoxin and one phytocyanin domain, and a multi-copper oxidoreductase, a laccase 3-like (K4CA83). Increases in blue copper and multicopper proteins have been previously related to increases in lignification (Dean et al., 1994; Ma et al; 2011; Ezaki et al., 2005) and therefore, decreases in these copper proteins may be reducing lignin deposition and affect the structure of the cell wall.

Mn toxicity alters protein turnover

Almost 14 % of the secretory proteins affected by Mn toxicity (31 proteins) were related to protein metabolism and their changes suggest a decrease in proteolysis in the xylem sap. Among proteins decreasing, twelve were proteolytic enzymes and two were regulatory subunits of the 26 S proteasome, indicating that both proteolytic pathways are affected by Mn toxicity. In addition, four of the increasing proteins were inhibitors of proteases (MEROPS inhibitor family I3) presenting fold increases amongst the largest measured in this study (30- to 290-fold). This deactivation of proteolytic processes is in agreement with the higher protein concentration measured in xylem sap of plants grown with high Mn concentrations. In addition, Mn toxicity caused decreases in five structural components of the ribosomes which indicate that protein synthesis might be compromised. Although four of them were NCS proteins, their decreases would be in agreement with the large number of proteins (62 %) decreasing in abundance in xylem sap as a result of Mn toxicity. Similar results have been described in the root proteome of tomato plants subjected to Mn toxicity and it was hypothesized that the decreased protein synthesis might be balanced with a less proteolytic environment, and that this altered protein turnover can lead to an accumulation of damaged proteins that could be behind some of the deleterious effects of Mn toxicity (Ceballos-Laita et al., accepted). However, seven proteases (four MEROPS S8B and three aspartic peptidases MEROPS A1) increased as a result of Mn toxicity, two of them greatly contributing to the separation of the treatments in the PCA (Table 3.6.3), indicating that some proteolytic events are induced upon Mn-toxicity. Increases in these peptidases might play roles in the degradation of ROS-damaged proteins as occurs in other nutritional stresses (Zaharieva et al., 2003; Lan et al., 2011), may be needed for maturation of cell wall proteins or act in a signaling system mediated by peptide elicitors (Schaller et al., 2004; Xia et al., 2004). An alteration in the protein turnover can also be inferred first from the changes observed in four chaperones (two increasing and two decreasing) involved in protein

folding and second by the increases measured in eight nitrogen storage cupins in the nutrient reservoir category.

Defense mechanisms elicited by Mn toxicity

As commented above, changes observed in the oxido-reductase category (14 proteins increasing and 22 proteins decreasing) can also alter the redox environment of the xylem sap which in conjunction with the elevated Mn concentration measured in this study, could potentially lead to oxidative stress. In line with this hypothesis, increases were measured in the abundance of several antioxidant proteins including monodehydroascorbate reductase (MDAR) and three thioredoxins. These later proteins act as antioxidants by reducing other proteins with disulfide bridges and have also been described to participate in redox signaling (Meng et al., 2010) whereas MDAR is active in the ascorbate-gluthahtione cycle that detoxifies hydrogen peroxide. In addition, the peroxidases increasing in abundance can also have a role protecting from Mn-toxicity by removing hydrogen peroxide; although in this process they can also generate ROS. Indeed ROS produced by extracellular peroxidases have been proposed to play a role in the IAA signaling pathway (Kawano, 2003). Increases in MDAR have also been previously described in *Citrus sinensis* roots (You et al., 2014); however in tomato roots, a decrease in the ascorbate-glutathione cycle was described indicating that thsi reponse to Mn toxicity may be species and tissue specific (Ceballos-Laita et al., accepted). It is worth mentioning, a decrease was measured in a Mn superoxide dismutase identified as the nutrient reservoir nectarin-1 (V4S9T2); however this protein was NCS with a mitochondrial localization. In addition to oxidative stress related proteins, eleven pathogenesis related proteins (six increasing and five decreasing) were affected by Mn toxicity with five of them (four increasing and one decreasing) having changes amongst the highest measured. These changes indicate that Mn tocicity elicits high stress in the xylem sap proteome. Increases of pathogenesis-related proteins have already been observed in other plant species such as tobacco or cowpea (Edreva, 1990; Fecht-Christoffers et al. 2003). All proteins increasing were cystein rich proteins with yet unknown function; however two of the ones showing large increases (P32045 and O03994) contained RlpA-like domains involved in lytic transglycolase activity (InterPro entry) suggesting a role in cell wall modification; and two more (B2LW68 and Q0H8U4) contained Tpx1 and CAP domains which have been described to regulate the activity of ion channels (Milne et al., 2003; Gibbs et al., 2006) suggesting an involvement in Mn homeostasis by sequestering Mn in xylem sap. The PCA of the shotgun results revealed that four proteins form the defense (two S and two NS) and two proteins from the oxido-reductases categories had a large positive contribution to the separation of the treatments (Tables S4), supporting the existence of a high stress environment in xylem sap of plants grown in excess Mn. The highest decrease in the defense category was measured in a PR-

10 protein (K4CRT0) containing a lipid-binding domain (START) found in signaling proteins which suggests the existence of a lipid based signaling system (see discussion below).

Signaling and regulation mechanisms occurring in Mn toxicity conditions

Changes in the xylem sap proteome induced by Mn toxicity suggest the existence of several regulatory and signaling mechanisms which overall seem to be repressed since most of the changes in the signaling category were decreases. Among the ten proteins decreasing in this category, fifty percent were fasciclin-like arabinogalactan (FLA) proteins (FLA-2, 9, 10 and 11). These proteins are a subclass of arabinogalactan proteins participating in cell-adhesion and involved in the regulation of stem development and response to abiotic stress (Zhang et al., 2015; MacMillan et al., 2010). FLAs affect stem biomechanics (strength and elasticity) by altering the cellulose deposition in the stem secondary cell wall (MacMillan et al., 2010; Lafarguette et al. 2004; Brown et al. 2005; Persson et al. 2005) and, therefore their decreases are in agreement with the changes in peroxidases and Cu-oxidases commented above. Similar decreases were observed in xylem sap of Mn-deficient plants (Ceballos-Laita et al., 2018) and indicate that alterations in Mn homeostasis have a strong impact in stem biomechanics and that alterations occur *via* FLAs.

Decreases were also observed in two receptor proteins including a strubbelig LRR receptor (K4DFQ3) and a PYL1 abscisic acid receptor (K4CN56). The *Arabidopsis* orthologue of the strubbelig receptor (SRF6; At1g53730) likely participates in stress-related processes and probably in the positive regulation of leaf size (Eyüboglu et al., 2007); the decrease in the first one would be in consonance with the smaller leaves of plants grown in the presence of Mn excess. The PYL1 receptor is required for ABA mediated responses such as stomatal closure (Miyazono et al., 2009; Zhang et al., 2013; Hao et al., 2011) and therefore a decrease would imply an inhibition of the ABA signaling pathway. This category also contained four chaperones (two increasing and two decreasing) involved in protein folding whose alterations are in line with the proposed alteration in the protein turnover.

Results also suggest the possible existence of a lipid-based signaling system as it has already been proposed to occur in the xylem sap of Mn-deficient tomato plants (Ceballos-Laita et al., 2018) and in phloem sap (Benning et al., 2012; Barbaglia et al., 2016). Changes in the abundance of lipases and lipid transfer proteins have been found in xylem of plants growing upon other nutritional deficiencies (Ceballos-Laita et al., 2018, Carella et al., 2016). Mn toxicity in tomato plants caused decreases in nine proteins with lipase, esterase or phospholipase activity, including one PI-PLC X domain containing lipase (K4B315) showing one of the largest decreases measured in this study (Table 3.6.2). However, two more lipases increased and one of them a NCS pepper-esterase-like (Q9LM08) presented the highest increase measured in

this study. The large number of lipases decreasing seems to suggest a reduction of lipid catabolism; however since lipases in conjunction with lipid-transfer proteins play important roles in signal transduction (Marshall et al., 2003; Ko, 2005), these changes may also indicate the existence of a lipid-based signal transduction pathway which may be repressed or induced depending on the specific lipase acting in the signaling cascade. Furthermore, changes in lipid transfer proteins (three decreasing and two increasing) and the above mentioned decrease in a PR-10 protein (K4CRT0) containing a lipid-binding domain (START) indicates that lipid metabolism plays an important role in the responses to Mn toxicity.

Finally, it should be noted that a large percentage of differential proteins (16 %) belonged to the oxido-reductase category and therefore we could not exclude the existence of a redox-based signaling mechanism as it has been proposed to occur in other stress situations (Suzuki et al., 2012).

Mn toxicity affects general metabolism

Mn toxicity affected a significant number of carbohydrate related proteins (18 proteins); however most of them were NCS (13 out of the 15 proteins in this category) and therefore their interpretation is difficult. Nevertheless, overall changes indicate a decrease in the TCA cycle which might imply a decrease in the production of reducing power and energy which has also been observed in roots of tomato plants exposed to excess Mn (Ceballos-Laita et al., 2018). The decreases in malate dehydrogenase and citrate synthase could also potentially lead to an accumulation of malate which has been described to chelate Mn (II) in Mn-hyperaccumulating species (Bidwell et al., 2002; Fernando et al. 2010). Other energy related pathways including glycolysis (three proteins decreasing and two increasing) and the pentose phosphate shunt (two proteins increasing and three decreasing) were also affected by Mn toxicity and their changes indicate the complexity of the metabolic regulation occurring upon Mn toxicity.

Two proteins in this category an UDP-glucose dehydrogenase (Q10CK6) and a galactokinase (K4AW47) which participates in galactose catabolism, presented remarkable decreases (> 90 %). UDP-glucose dehydrogenases are glucosyl donors which play an important role in carbon partitioning between sucrose synthesis and cell wall formation (Klinghammer et al., 2007; Tenhaken et al., 1996) and therefore this decrease also suggest Mn-induced changes in cell wall. Decreases in UDP-glucose dehydrogenases have also been observed in roots of tomato plants exposed to Mn toxicity (Ceballos-Laita et al., accepted).

Finally, as commented above, Mn toxicity also affected a large number of lipid-related proteins (17 proteins) and most of the changes were decreases in lipases (nine proteins) suggesting a decrease in lipid catabolism.

Comparison of changes induced by Mn toxicity in the root and xylem sap proteomes

Most of the common proteins increasing in abundance as a result of Mn toxicity were secretory proteins (15 out of 18 proteins) and were distributed in four metabolic categories including polysaccharide metabolism, oxido-reductase, protein metabolism and defense. These results indicate that these proteins are most likely participating in extracellular processes elicited by Mn toxicity that may be part of a non-tissue specific response. Proteins in the polysaccharide and oxido-reductase category were five endo-glycosilases and three suberization peroxidases (Table 3.6.4) which may be involved in cell wall modifications occurring upon Mn toxicity in both xylem sap and roots whereas common proteins in the defense category included a three STH2-like proteins, among others. One of them (Q53U35) showed increases amongst the highest measured in both proteomic studies. This STH2 is a PR10 protein containing a hydrophobic pocket able to bind hormones and siderophores (Mogensen et al., 2002) which could be involved in hormone signaling or even Mn sequestration and therefore constitutes a good candidate for future studies. Common proteins decreasing in abundance in both proteomes were mostly non secretory proteins (10 out of 11) which make difficult the interpretation of their changes. These proteins were distributed among a diverse array of metabolic functions with carbohydrate metabolism being the most represented category (three proteins); therefore suggesting that the impairment in energy production elicited by Mn toxicity in roots (Ceballos-Laita et al., accepted) could also take place in neighboring cells of the xylem sap.

Supplementary material

The supplementary data are included in the electronic version: **Table S1.** List of proteins identified and quantified in tomato xylem sap by shotgun proteomics and Progenesis LC-MS analyses; **Table S2.** List of proteins that presented significant decreases as revealed by shotgun analysis when Mn-treated samples were compared to controls; **Table S3.** List of proteins that presented significant increases as revealed by shotgun analysis when Mn-treated samples were compared to controls. **Table S4.** Standardized component scores obtained in the principal component analysis of the differential proteins of the shotgun experiment.

Capítulo 4

DISCUSIÓN GENERAL

En el año 2000 se publicó el genoma completamente secuenciado de *Arabidopsis*, convirtiéndose en un organismo óptimo para llevar a cabo estudios tanto proteómicos como genómicos (The Arabidopsis Genome Initiative, 2000). Sin embargo, la utilidad de *Arabidopsis* como especie modelo es limitada, ya que su genoma es entre 10 y 50 veces más pequeño que el de las especies de cultivo más importantes. Este hecho hace que su uso para el estudio de los procesos biológicos que ocurren en condiciones agrícolas presente limitaciones. En esta Tesis Doctoral se han utilizado dos especies como material vegetal, *Beta vulgaris* (remolacha) y *Solanum lycopersicum* (tomate), ambas ampliamente cultivadas a nivel agrícola. La especie *S. lycopersicum* resulta particularmente adecuada para la obtención del fluido de xilema debido a la elevada presión hidrostática en sus tallos y también a que posee un genoma secuenciado y ya disponible en las bases de datos. Por otro lado, *B. vulgaris* es una especie adecuada para la extracción del fluido apoplástico por el tamaño y semi-rigidez de sus hojas, que permiten el uso de protocolos basados en técnicas de centrifugación ya establecidos para la obtención de fluido apoplástico. Sin embargo, *B. vulgaris* presenta limitaciones a la hora de la identificación de proteínas, ya que su genoma está sólo descrito de forma incompleta. En esta Tesis Doctoral, esta limitación se resolvió mediante la creación de una base de datos que recoge tanto las secuencias de *B. vulgaris* anotadas en UniProt (www.uniprot.org) como la información contenida en cinco bases de datos disponibles hasta la fecha (http://bvseq.molgen.mpg.de/Genome/Download), correspondientes a modelos de genes de remolacha anotados a partir de febrero de 2013. Una vez eliminadas las secuencias redundantes se obtuvieron 82,368 secuencias de proteínas que nos permitieron llevar a cabo con éxito las identificaciones de nuestras proteínas de interés en esta especie.

A lo largo de los capítulos anteriores se han descrito los cambios inducidos por los estreses de Fe y Mn en dos proteomas que están involucrados en los procesos de transporte a larga y corta distancia en la planta, savia de xilema y fluido apoplástico, así como en el proteoma de la raíz, tejido responsable de la absorción de dichos metales.

En este apartado se lleva a cabo la discusión general de los resultados obtenidos y se compila el efecto global que dichos estreses nutricionales tienen en la planta, así como las ventajas e inconvenientes del uso de las técnicas de proteómica clásicas y avanzadas utilizadas en el desarrollo de la Tesis. De un modo general, se puede concluir que las categorías funcionales más afectadas en los estreses nutricionales estudiados son similares, aunque revelan diferentes comportamientos en función del tejido y de la alteración nutricional a la que la planta está sometida.

4.1. Efecto general de los estreses nutricionales sobre los proteomas estudiados

En términos generales, un 20 % del proteoma del fluido de xilema obtenido por "shotgun" sufrió cambios significativos ante las deficiencias nutricionales estudiadas (deficiencia de Fe y Mn). Estos porcentajes están dentro del rango encontrado en otros sub-proteomas, como por ejemplo el cloroplasto en estudios de deficiencia de Fe (López-Millán et al., 2013), y son algo superiores a los encontrados en los estudios de deficiencia de Mn en raíz de maíz y *Arabidopsis* (Li et al., 2015; Zargar et al., 2015). Sin embargo, sólo el 2,5 % de los spots consistentes del proteoma del fluido apoplástico obtenidos por 2D-IEF/SDS-PAGE cambiaron su abundancia de manera significativa ante la deficiencia de Fe, sugiriendo que, al contrario de lo que ocurre en el xilema, la homeostasis de proteínas en el apoplasto en condiciones de deficiencia de Fe está bien mantenida.

Si comparamos el efecto causado por las deficiencias de Fe y Mn sobre el perfil proteico del fluido de xilema, se observa que a pesar de causar cambios en aproximadamente el mismo número de proteínas (un 20 % del proteoma), la de Mn provocó descensos en la mayor parte de las proteínas que presentaron cambios significativos, mientras que la de Fe causó descensos en el 40 % de las proteínas e incrementos en el otro 60 %. Estos resultados fueron acordes con la cantidad de proteína extraída del xilema, inferior en las plantas crecidas en deficiencia de Mn, y con los cambios opuestos que se observaron tanto en proteínas del ribosoma (cuatro componentes estructurales del ribosoma aumentaron en deficiencia de Fe y cuatro disminuyeron en deficiencia de Mn) como en proteasas involucradas en la maduración de proteínas, que descendieron en condiciones de deficiencia de Mn, sugiriendo por tanto la existencia de una disminución de la síntesis proteica con este estrés.

De modo similar a lo que ocurre con la deficiencia de Mn en xilema, aunque con variaciones en las categorías afectadas, los efectos de la toxicidad del Mn sobre los perfiles proteicos de xilema y de raíz sugieren una ralentización general de las actividades metabólicas. Por un lado, el efecto de la toxicidad de Mn sobre el proteoma del xilema fue mayor que en el caso de las deficiencias nutricionales, con cambios significativos en aproximadamente el 50 % del proteoma, siendo descensos en el 62 % de los casos. Por otro lado, el proteoma de raíz presentó alteraciones en un porcentaje similar, un 44 %, con el 70 % de las proteínas afectadas mostrando descensos en su abundancia relativa y cubriendo un amplio rango de categorías funcionales, mucho mayor que en el caso de las proteínas que aumentaban. Un comportamiento similar ya había sido descrito en tejidos de raíz de *Citrus sinensis* expuestos a toxicidad de Mn (You et al., 2014), así como en raíces de plantas de *B. vulgaris* y *L. esculentum* cultivadas en condiciones de toxicidad de Zn (Gutierrez-Carbonell et al., 2013) y Cd (Rodríguez-Celma et al.,

2010), respectivamente. Estos resultados sugieren que un efecto común de la toxicidad de micronutrientes sería la prevalencia de disminuciones en la abundancia de muchas proteínas. El xilema de las plantas de tomate presentó mayores concentraciones de Mn en condiciones de toxicidad que la raíz o las hojas de estas mismas plantas, lo que indica una translocación activa del metal desde la raíz de la planta a la parte aérea.

A continuación se discuten los efectos de los distintos estreses nutricionales estudiados sobre las diferentes categorías metabólicas.

4.1.1 Pared celular

Los resultados descritos muestran que tanto el xilema como el fluido apoplástico son compartimentos altamente glicolíticos (Capítulo 3.1). Así, el 21 % del proteoma total del fluido apoplástico y el 28 % del proteoma del xilema están constituidos por proteínas relacionadas con el metabolismo de polisacáridos, siendo en su mayoría glucosidasas y galactosidasas que juegan importantes papeles en la modificación de la pared celular durante el desarrollo de la planta (Zhang et al., 2008; Witzel et al., 2011).

Un análisis global de los cambios inducidos por los estreses nutricionales estudiados sobre las proteínas relacionadas con la pared celular indica que este tipo de estreses causa modificaciones importantes, tanto en la composición de la pared celular primaria, *via* glicosidohidrolasas, como en la de la pared secundaria, *via* peroxidasas, cupro-oxidasas y/o fasciclin-arabinogalactanos, y que estos efectos varían dependiendo del tejido y tipo de estrés. Independientemente de los cambios específicos, todas estas alteraciones probablemente modifican las propiedades mecánicas de la pared celular y su porosidad, y por tanto pueden influir en el transporte de nutrientes en los tejidos en estudio.

<u>Pared celular primaria</u>

La categoría de metabolismo de polisacáridos resultó una de las más afectadas en la savia de xilema de plantas de tomate, crecidas tanto en condiciones de deficiencia de Fe y Mn (14 y 13 proteínas respectivamente) como en condiciones de toxicidad de Mn (12 proteínas), indicando que estos estreses nutricionales tienen un fuerte impacto sobre la pared celular. Sin embargo, tan solo 2 proteínas (una de ellas presentando 3 isoformas distintas) del proteoma diferencial del fluido apoplástico de plantas de remolacha crecidas en deficiencia de Fe pertenece a esta categoría metabólica.

La deficiencia de Fe indujo una fuerte activación del metabolismo de la pared celular primaria en la savia de xilema, puesto que causó aumentos en un gran número de endo-glicosidohidrolasas extracelulares, que participan en la hidrólisis de los enlaces glicosídicos de

los polisacáridos de la pared celular primaria (Minic, 2008), en pectin-esterasas, que participan en la degradación de pectina, y en N-glicosidohidrolasas implicadas en la degradación de los N-glicanos, modificación post-traduccional considerada como una de las más abundantes en las proteínas de secreción. En el apoplasto de hoja de remolacha, tan solo se observaron aumentos en un número reducido de quitinasas clasificadas como endo-glicosidohidrolasas, indicando en primer lugar que los efectos de la deficiencia de Fe en la pared celular primaria siguen la misma dirección en ambos fluidos, y en segundo lugar que la homeostasis de la pared celular del apoplasto de plantas deficientes en Fe está bien mantenida.

Por otro lado, la deficiencia de Mn causó una marcada desactivación del metabolismo de la pared celular primaria del xilema, efecto contrario al observado con la deficiencia de Fe, aunque las proteínas que presentaron alteraciones fueron similares a las observadas en la deficiencia de Fe (Capítulo 3.3). Así, la deficiencia de Mn causó descensos en la abundancia relativa de endo-glicosidohidrolasas, N-glicosidohidrolasas, pectin-esterasas y proteínas que actúan sobre residuos galacturonados, muy frecuentes en los polisacáridos péptidicos. Estos descensos indican que en la savia de xilema de las plantas crecidas en condiciones de deficiencia de Mn los procesos de degradación de la pared celular se encuentran reducidos.

La toxicidad de Mn en raíz produjo principalmente aumentos en endo-glicosidohidrolasas, sugiriendo que en estas condiciones también existe una degradación de la pared celular primaria. En savia de xilema, la toxicidad de Mn causó un número similar de aumentos y descensos de abundancia relativa en proteínas relacionadas con el metabolismo de los polisacáridos. Sin embargo, los descensos fueron moderados y los incrementos muy elevados, sugiriendo que la toxicidad de este nutriente también causa una degradación general de la pared celular primaria, al igual que en la raíz de las mismas plantas y a diferencia de lo que ocurre en condiciones de deficiencia de Mn (Capítulos 3.5 y 3.3, respectivamente). Sin embargo, los principales aumentos en abundancia causados por la toxicidad de Mn en xilema corresponden a N-acetil-hexosaminidasas involucradas en la degradación de los N-glicanos, las cuales disminuyen en el caso de la deficiencia de Mn. Estos resultados indican que la toxicidad de Mn produce un descenso en los procesos post-traduccionales de N-glicosilación en savia de xilema, lo que también se observa en raíz, y que por el contrario parecen aumentar en deficiencia de Mn. Estas evidencias, junto con el incremento en la concentración de proteínas encontrado en la savia de xilema de las plantas crecidas en condiciones de toxicidad de Mn, apuntan a que estas plantas presentan una pared celular más permeable que las plantas crecidas en condiciones control, lo que, como en el caso de las deficiencias, puede producir alteraciones en el flujo de Mn a través del xilema.

Una visión global de estos cambios en proteínas relacionadas con la pared celular primaria lleva a plantear que pueden estar produciéndose modificaciones en su composición que

podrían afectar su rigidez y/o porosidad como consecuencia de las deficiencias de Fe y Mn, y además, que estas modificaciones son distintas dependiendo del micronutriente y del tipo de estrés (deficiencia o toxicidad). Así, tanto la deficiencia de Fe como la toxicidad de Mn producirían en general un aumento de la degradación de la pared primaria en todos los tejidos analizados, mientras que la deficiencia de Mn produciría una disminución en su degradación. Se ha descrito que la deficiencia de Fe produce alteraciones en el tamaño de los vasos xilemáticos en hoja (Eichert et al., 2010; Fernández et al., 2008) que podrían estar relacionadas con estos cambios. En cualquier caso, los cambios en la rigidez y/o porosidad de la pared celular primaria pueden influir en el transporte de los micronutrientes a través de los vasos xilemáticos. Además, en el caso de la deficiencia de Fe se ha especulado que el incremento en las hidrolasas puede permitir un suministro de C anaplerótico que podría compensar las bajas tasas fotosintéticas que poseen las plantas con deficiencia de Fe (Zhang et al., 2008).

Pared celular secundaria

En el caso de las deficiencias de Fe y Mn, los cambios en los perfiles proteicos de la savia del xilema indican que el contenido, la estructura y la composición de lignina de la pared celular secundaria se encontraron alterados, mientras que en el caso el fluido apoplástico de remolacha deficiente en Fe no se encontraron diferencias (Capítulos 3.3 y 3.2, respectivamente). Los descensos en peroxidasas involucradas en la formación de lignina (Fernández-Pérez et al., 2015a; Shigeto et al., 2014, 2016) observados en la savia de xilema sugieren un efecto similar de ambas deficiencias sobre la composición de la pared celular secundaria. Sin embargo, el hecho de que la deficiencia de Fe también lleve a aumentos en la abundancia de otras peroxidasas también relacionadas con dichos procesos indica una mayor complejidad en este estrés nutricional. Además de los descensos observados para peroxidasas relacionadas con la suberización, la deficiencia de Mn también causó descensos en cupro-oxidasas y fasciclin-arabinogalactanos, proteínas implicadas en la formación de lignina y en la deposición de celulosa en la pared secundaria, respectivamente, sugiriendo que aunque ambas deficiencias afectan a la pared secundaria, el efecto es más intenso en la deficiencia de Mn. En línea con esta hipótesis, estudios previos han descrito que la deficiencia de Fe produce alteraciones en la composición de lignina en tallos de *Medicago truncatula* (Rodríguez-Celma et al., 2016c, Anexo I), así como cambios en el patrón de lignificación de la raíz de *Cucumis sativus* (Donnini et al., 2010).

La toxicidad de Mn también afecta a proteínas implicadas en la formación de la pared celular secundaria, tanto en xilema como en raíz. Sin embargo, el efecto de la toxicidad de Mn en la pared secundaria de xilema es más complejo que en el caso de la deficiencia de dicho nutriente y similar al observado en la deficiencia de Fe, ya que causó tanto aumentos (en seis

proteínas) como descensos (en cuatro) en la abundancia de peroxidasas de secreción relacionadas con procesos de lignificación. Hay que mencionar que debido a que la función exacta de estas peroxidasas es aún desconocida, podría ocurrir que las peroxidasas que aumentan en abundancia estuvieran relacionadas con procesos de homeostasis redox y no con modificaciones de la pared celular secundaria. En el caso de la raíz, la interpretación de los cambios inducidos por la toxicidad de Mn es más sencilla, puesto que la mayoría de la peroxidasas que incrementaron su abundancia relativa están involucradas en procesos de lignificación y suberización de la pared celular, sugiriendo que la toxicidad de Mn causa un aumento de la rigidez y una reducción de la expansión de la pared celular secundaria (Capítulo 3.5). Los resultados obtenidos con la savia de xilema de plantas sometidas a toxicidad de Mn contrastan con lo observado con la deficiencia de Mn, donde los descensos en peroxidasas, cupro-oxidasas y fasciclin-arabinogalactanos sugieren un descenso en la formación de lignina, y por tanto, de la rigidez de la pared celular secundaria. Las alteraciones observadas podrían ser las responsables de la inhibición del crecimiento de la raíz observado en las plantas sometidas a toxicidad de Mn (Chen et al., 2016).

Como conclusión, se puede decir que las deficiencias de Fe y Mn producirían una disminución en la lignificación de la pared secundaria en xilema mientras que la toxicidad de Mn llevaría a aumentos en la lignificación tanto en raíz como en xilema.

4.1.2. Metabolismo de proteínas

Los fluidos vegetales como la savia de xilema y el apoplasto de hoja se caracterizan por poseer una batería de proteínas con actividad proteolítica (un 12 % del proteoma en ambos casos; Capítulo 3.1), que participan principalmente en procesos de degradación de proteínas, señalización y defensa basal frente a la infección por patógenos (Xia et al., 2004; Shabab et al., 2008; Rodríguez-Celma et al., 2016a).

En el caso de la deficiencia de Fe, el análisis del proteoma diferencial del fluido apoplástico no mostró cambios significativos en la categoría de proteólisis (Capítulo 3.2). Por el contrario, tanto la deficiencia de Fe como la de Mn causaron cambios en la abundancia de un gran número de proteínas con actividad proteolítica en la savia de xilema. Sin embargo, la deficiencia de Fe produjo mayoritariamente aumentos en las abundancias (en 11 de 15 proteasas), mientras que la de Mn causó principalmente descensos (en 12 de 13 proteasas). Además, en ambos casos se midieron incrementos y descensos que se encontraban entre los mayores cambios observados en el xilema de las plantas sometidas a dichos estreses. En condiciones de deficiencia de Fe, el aumento de esta clase de proteínas puede estar relacionada con la degradación de proteínas dañadas por ROS, cuyos niveles son superiores debidos a la situación de escasez de este metal (Lan et al., 2011; Zaharieva et al., 2003). Sin embargo, el

hecho de que algunas proteasas disminuyeran su abundancia de forma significativa con la deficiencia de Fe indica que ese papel no es su única función, sugiriendo su posible implicación en otros procesos, como por ejemplo, su participación en la maduración de proteínas de la pared celular (Schaller et al., 2004) o en la generación de péptidos señal.

En contraposición a lo que ocurre con la deficiencia de Fe, los descensos en proteasas observados en condiciones de deficiencia de Mn sugieren que el proteoma de xilema en estas condiciones es menos proteolítico, y por tanto, que el número de proteínas que han sufrido daños no es elevado, siendo incluso menor que en las plantas crecidas en condiciones control. Además, el descenso en la abundancia de proteasas podría indicar que en condiciones de deficiencia de Mn la maduración de las proteínas de secreción es menor que en condiciones control, lo que estaría de acuerdo con el bajo porcentaje de proteínas de secreción que aumentan en condiciones de deficiencia de Mn (un 18 %). La hipótesis de que el xilema de plantas cultivadas en deficiencia de Mn refleja una situación de estrés menor que el de las plantas sometidas a deficiencia de Fe se ve reforzada por los cambios medidos en la abundancia de enzimas involucradas en la protección frente a estrés oxidativo, que siguen un comportamiento similar al de las proteasas, aumentando con la deficiencia de Fe y disminuyendo con la de Mn (ver apartado 4.1.3). Como se ha comentado anteriormente, los cambios en la abundancia de proteasas también pueden estar relacionados con procesos de señalización, en cuyo caso el sistema estaría más activado en condiciones de deficiencia de Fe y menos en condiciones de deficiencia de Mn.

También es interesante destacar la presencia de varias subunidades del proteasoma en el fluido apoplástico de *B. vulgaris* que están involucradas en la degradación de proteínas dañadas y mal plegadas mediante procesos de ubiquitinación (Van Der Hoorn and Jones, 2004; Xia et al., 2004; Pearce et al., 2010; Capítulo 3.2). Estos elementos del proteasoma se han observado hasta el momento únicamente en *B. vulgaris*, indicando que su presencia puede ser específica de la especie, aunque no hubo variaciones en su abundancia con la deficiencia de Fe, lo que sugiere que en dichas condiciones esta vía proteolítica no es de especial importancia.

La toxicidad de Mn ocasionó cambios en un gran número de proteínas relacionadas con el metabolismo proteico tanto en la savia de xilema (un 14% del proteoma diferencial) como en raíz (un 23 % del proteoma diferencial). Los cambios fueron similares en ambos tejidos, consistiendo, en primer lugar, en descensos en componentes estructurales del ribosoma, en segundo lugar, en aumentos de inhibidores de proteasas, y en tercer lugar, en descensos en proteínas con actividad proteolítica, tanto de secreción como pertenecientes al complejo del proteosoma. Estos cambios indican que la toxicidad de Mn causa disminuciones en los procesos de síntesis proteica y degradación de proteínas, cuyo resultado final alteraría la tasa de reposición proteica y podría causar una acumulación de proteínas dañadas. Esta acumulación

podría estar tras de algunos de los efectos nocivos de la toxicidad de Mn. El descenso de proteínas proteolíticas en raíz ya había sido descrito en *Citrus grandis* en condiciones de toxicidad de Mn (You et al., 2014), y también este descenso es acorde con la elevada concentración proteica observada en savia de xilema. Por otro lado, la acumulación de proteínas dañadas en el proteoma de raíz es acorde con los descensos observados para varias chaperonas e isomerasas, proteínas que desempeñan un papel importante en la prevención de la agregación de proteínas dañadas o mal plegadas en situaciones de estrés. Las disminuciones en estas proteínas probablemente sugieren, además de la disminución mencionada anteriormente en los procesos de síntesis, un ensamblaje menos intenso de las proteínas sintetizadas *de novo*.

Estos resultados son distintos a los observados en condiciones de deficiencia de Mn, ya que a pesar de observarse en ambos casos descensos en abundancias relativas, el xilema de las plantas deficientes en Mn presentó una concentración de proteínas muy inferior al observado en condiciones control, sugiriendo que no existe una acumulación de proteínas dañadas. Por último, es necesario comentar que aunque en menor número, varias proteasas (dos en raíz y siete en xilema), aumentaron en abundancia en plantas cultivadas en exceso de Mn, sugiriendo que algunos procesos proteolíticos se encuentran inducidos. Estos aumentos en proteasas, como se ha comentado anteriormente en el caso de la deficiencia de Fe, podrían estar involucrados en la degradación de proteínas dañadas por ROS (Zaharieva et al., 2003; Lan et al., 2011), ser necesarios para la maduración de proteínas de la pared celular o participar en procesos de señalización mediados por péptidos (Schaller et al., 2004; Xia et al., 2004).

Como conclusión, se puede decir que tanto la deficiencia de Fe como la toxicidad de Mn en los tejidos estudiados producen un ambiente más proteolítico que el observado con la deficiencia de Mn, sugiriendo la existencia de alteraciones en la tasa de recambio de proteico, en la maduración de proteínas y/o en procesos de señalización y defensa, lo que refleja la existencia de un mayor estrés en estas condiciones.

4.1.3. Protección contra estrés

La caracterización de los perfiles proteicos del fluido apoplástico de hoja y de la savia del xilema mostró una fracción importante de proteínas involucradas en mecanismos de defensa basales y de respuesta a estrés oxidativo cuando la planta no se encuentra sometida a condiciones de estrés (un 19% del proteoma del xilema y un 18% del proteoma del fluido apoplástico). Estos porcentajes, igual que en el caso de las proteasas, suponen la existencia de mecanismos de defensa constitutivos en los fluidos vegetales, creando un entorno hostil para prevenir la infección por patógenos (Delaunois et al., 2013; Pechanova et al., 2010).

Con las deficiencias de Fe y Mn las proteínas incluidas en la categoría de defensa no sufrieron grandes alteraciones (una proteína aumentando en abundancia relativa con la deficiencia de Fe en xilema y fluido apoplástico, y una aumentando y otra disminuyendo con la deficiencia de Mn), mientras que la toxicidad de Mn sí que provocó alteraciones importantes en las proteínas relacionadas con la defensa de la planta, tanto en el fluido xilemático como en la raíz. Así, en el xilema se observaron aumentos y descensos en un mismo número de proteínas (seis), mientras que en la raíz el número de proteínas que sufrieron aumentos en su abundancia relativa fue mayor (10) que el número de descensos (2). Estos datos sugieren que la alteración nutricional por toxicidad de Mn provoca mayor un estrés en la planta que el causado por las deficiencias de Fe o Mn.

El fluido apoplástico de *B. vulgaris* deficiente en Fe mostró aumentos en la abundancia relativa de una taumatina relacionada con la respuesta a estreses abióticos y bióticos. La misma proteína se vio también aumentada en xilema de tomate cultivado en condiciones de deficiencia y toxicidad de Mn y además, presenta aumentos tanto en en raíz como en tallo de *M. truncatula* cultivada en condiciones de deficiencia de Fe (Rodríguez-Celma et al., 2011), sugiriendo que participa de forma consistente en mecanismos de defensa si hay alteraciones nutricionales. Tras el suministro de Fe a plantas de *B. vulgaris* deficientes en Fe, esta proteína disminuyó su abundancia relativa en el fluido apoplástico, retornando de forma rápida (en 24 h) hacia valores similares a los valores control, lo que sin duda hace que esta proteína sea un buen candidato para futuros estudios.

La categoría de oxido-reducción también puede ser utilizada para inferir la situación de estrés, en este caso oxidativo, a la que se encuentra sometida la planta. Con la excepción del fluido apoplástico, donde no se observaron cambios en ninguna proteína de la categoría oxido-reducción, los estreses nutricionales estudiados indujeron mayores cambios en las proteínas de respuesta a estrés oxidativo que en las proteínas clasificadas en defensa. Además, los resultados indican que tanto la deficiencia de Fe como la toxicidad de Mn producen un mayor estrés oxidativo en los tejidos estudiados que la deficiencia de Mn, ya que esta última provocó descensos en abundancia relativa para la mayor parte de las proteínas que sufrieron cambios significativos dentro de la categoría, mientras que la deficiencia de Fe y la toxicidad de Mn causaron principalmente aumentos. Como ya se ha comentado anteriormente, la mayoría de las proteínas diferenciales en esta categoría son peroxidasas, algunas de ellas relacionadas con la lignificación (Fernández-Pérez et al., 2015a; Shigeto et al., 2014; 2016), con lo que sus cambios podrían implicar alteraciones en la pared celular. Sin embargo, no se puede descartar que los cambios de abundancia medidos en peroxidasas diferenciales también causen alteraciones en el estado redox del xilema inducidos por los estreses nutricionales estudiados. La deficiencia de Mn provocó también descensos en Cu-oxidasas y en enzimas antioxidantes que participan en la

regeneración del glutatión oxidado (Ferretti et al., 2009; Ohkama-Ohtsu et al., 2007) o catalizan la síntesis de ácido ascórbico (Maruta et al., 2010). Los descensos en estas últimas proteínas, junto con el papel dual que peroxidasas y proteasas juegan en la defensa y mantenimiento de la estructura de los vasos xilemáticos, sugieren que el proteoma de xilema de plantas deficientes en Mn no está sometido a un excesivo estrés, presentando un entorno menos oxidativo que el de las plantas control. Al contrario que la deficiencia de Mn, la deficiencia de Fe y la toxicidad de Mn parecen generar un mayor estrés oxidativo en xilema, debido no sólo al incremento en la abundancia relativa de un gran número de peroxidasas sino también a los aumentos medidos tanto en enzimas antioxidantes del ciclo glutation-ascorbato como en tioredoxinas. Como se ha comentado anteriormente, la toxicidad de Mn en raíz produjo aumentos en un gran número de proteínas de defensa así como en peroxidasas, sugiriendo que en este tejido la situación de estrés es elevada, tal y como como ocurre en xilema. Sin embargo, en este caso también se observaron descensos en abundancia relativa para tres enzimas antioxidantes del ciclo glutation-ascorbato, indicando que existen diferencias específicas en la respuesta dependiendo del tejido.

4.1.4. Señalización celular

Los perfiles proteicos del fluido apoplástico muestran algunas proteínas involucradas en procesos de señalización que se encuentran expresadas de forma constitutiva. Sin embargo, no se observaron cambios significativos en respuesta a la deficiencia de Fe, sugiriendo que los procesos de señalización en el apoplasto de hoja no tienen un papel importante en el mantenimiento de la homeostasis del metal.

Las deficiencias de Fe y Mn afectaron a proteínas involucradas en tres sistemas de señalización celular en el fluido del xilema, siendo antagónica la respuesta de la planta ante estas deficiencias. En primer lugar, la deficiencia de Fe provocó incrementos en proteínas relacionadas con la vía CLE (CLAVATA3/EMBRYO SURROUNDING REGION-RELATED; CLV3/ESR-related), mientras que la deficiencia de Mn mostró una represión de dicha vía. Esta ruta de señalización celular involucra péptidos señal que se originan en el xilema y participan en el control de los procesos de desarrollo de la planta (Hirakawa et al., 2008; 2010; Ito et al., 2006; Ohyama et al., 2009; Stahl et al., 2009). Estos péptidos ya han sido descritos como señalizadores en otros estreses nutricionales como los ocasionados por la carencia de N o P (Wang et al., 2015).

En segundo lugar, los cambios inducidos por ambas deficiencias en los perfiles proteicos del fluido de xilema indican la presencia de un sistema de señalización celular basado en lípidos (Carella et al., 2016). Este sistema también presentaría un comportamiento antagónico en función de la deficiencia, presentando una activación en el caso del estrés por Fe y un represión ante la deficiencia de Mn, si bien parece existir un punto de regulación común en ambas

deficiencias nutricionales, dada la disminución en la abundancia relativa de una PI-PLC que participa en varias cascadas de señalización celular. Por otro lado, la toxicidad de Mn, tanto en xilema como en raíz, también parece provocar alteraciones la vía de regulación mediada por lípidos, como sugieren los descensos en proteínas con actividades lipasa, esterasa y fosfolipasa. Los aumentos de una acil-hidrolasa lipolítica específica de la raíz, que participa en los procesos de liberación de ácidos grasos de los lípidos de membrana, y de dos lipoxigenasas, que catalizan la dioxigenación de los ácidos grasos en la señalización celular por oxilipinas (Rydel et al., 2003) ya habían sido descritas como proteínas con un papel activo en la transducción de señales en situaciones de estrés como las deficiencias de Fe y P (Rietz et al., 2004; 2010). Además, este tipo de regulación ya había sido descrito en el floema, donde fue propuesto como un modo de señalización a larga distancia en respuesta a estreses abióticos (Benning et al., 2012; Barbaglia et al., 2016). Por tanto, podemos concluir que el metabolismo lipídico parece jugar un papel importante en los procesos de señalización que participan en la respuesta a los estreses nutricionales estudiados, y que este sistema de señalización parece ser frecuente, puesto que se observa tanto en raíz como en xilema y tanto con Fe como con Mn.

En tercer lugar, el sistema de señalización basado en fasciclin-arabinogalactanos también parece estar involucrado en la regulación *via* xilema de los estreses nutricionales estudiados. Los descensos observados en fasciclin-arabinogalactanos en savia de xilema (tres proteínas en deficiencia de Fe, una en deficiencia de Mn y cinco en toxicidad de Mn) indican que este sistema de señalización se encontraría reprimido en xilema ante los estreses nutricionales estudiados. Esta represión afecta a la deposición de celulosa en la pared celular secundaria del tallo, alterando por tanto las propiedades biomecánicas de éste (MacMillan et al., 2010; Lafarguette et al. 2004; Brown et al. 2005; Persson et al. 2005). El hecho de que tanto la deficiencia como la toxicidad de Mn causen descensos en un mayor número de proteínas de esta ruta de señalización que la deficiencia de Fe sugiere que esta vía de señalización es más importante en el mantenimiento de la homeostasis del Mn que en la del Fe. También conviene comentar que en el proteoma de raíz de tomate crecido en exceso de Mn no se observaron cambios en fasciclin-arabinogalactanos, sugiriendo que su participación en la regulación es específica del tejido, limitándose al xilema.

Además de estas tres rutas de señalización comentadas anteriormente, los estreses nutricionales estudiados también afectaron en el fluido de xilema a dos de los mecanismos más importantes de modificación post-transduccional, como son los procesos de fosforilación y glicosilación. Por un lado, los cambios en abundancia relativa de ciertas fosfatasas ácidas púrpura (PAPs) indican la existencia de una red de fosforilación extracelular (Ndimba et al., 2003) que podría modular la actividad de las glicósidohidrolasas en la pared celular mediante procesos de desfosforilación. Dichas proteínas aumentaron en xilema de tomate deficiente en Fe

mientras que disminuyeron en condiciones de deficiencia de Mn, indicando que ambas alteraciones nutricionales provocan cambios antagónicos en el estado de fosforilación de las proteínas del xilema, con lo que esta red de fosforilación actuaría de un modo opuesto en ambas deficiencias, estando activada en la deficiencia de Fe y reprimida en la de Mn (Kaida et al., 2010). Este hecho es muy relevante en condiciones de deficiencia de Fe, ya que las fosfatasas contienen este metal. Por otro lado, la abundancia relativa de N-glicosilasas que actúan sobre enlaces C-N también aumentaron en el xilema de tomate deficiente en Fe y disminuyeron en condiciones de deficiencia de Mn, sugiriendo que el estado de glicosilación en xilema varía con la deficiencia nutricional, disminuyendo con la deficiencia de Fe y aumentando con la de Mn. En el xilema de tomate cultivado en toxicidad de Mn se observaron aumentos en N-glicosilasas pero no se observaron cambios en fosfatasas, sugiriendo que en este caso la presencia de glicosilaciones es menor que en condiciones control y que las fosforilaciones no juegan un papel relevante en condiciones de toxicidad de Mn.

Por último, como se ha comentado previamente, la toxicidad de Mn en raíz de tomate produce cambios en abundancia relativa en proteínas con dominios de unión a lípidos y en lipasas y lipooxigenasas, lo que parece indicar que en este caso también existe un mecanismo de señalización basado en el metabolismo lipídico. Sin embargo, la mayoría de las proteínas afectadas por la toxicidad de Mn en la categoría de señalización (15 de 19) contienen dominios de unión a RNA, sugiriendo que los procesos de regulación de la homeostasis del Mn no son los mismos en raíz y en savia de xilema. Así, la toxicidad de Mn produjo descensos en la abundancia relativa de proteínas con dominios RRM, KH, "Zn finger", helicasa C, FDF o HABP4, asociadas con procesos de traducción, mantenimiento y estabilidad del RNA y con mecanismos de regulación del ensamblaje alternativo del mismo (Ambrosone et al., 2015; Anantharaman et al., 2004; Kenan et al., 1991; Lorkovic, 2009). Estos resultados muestran la importancia de los mecanismos de regulación y estabilidad de RNA en la modulación de la respuesta celular ante esta toxicidad nutricional, participación que ya había sido descrita en estreses por salinidad y sequía (Ambrosone et al., 2012; Nakaminami et al., 2012). Además, la supresión del transporte de proteínas *vía* Ran en el proteoma de la raíz también sugiere una afectación del transporte de proteínas al núcleo.

4.1.5. Energía

Tanto la deficiencia de Fe como la de Mn tuvieron un efecto moderado en la fracción del proteoma del xilema relacionado con la obtención de energía, lo que concuerda con la naturaleza no secretoria de estas proteínas. En ambos casos, casi todas las proteínas afectadas (seis en cada deficiencia) fueron clasificadas, con una sola excepción, como NCS (non-classical secretory; proteínas secretorias no clásicas), por lo que su interpretación resulta compleja. De

forma general, en ambas deficiencias aumentaron proteínas relacionadas con la glicolisis (una en la deficiencia de Mn y dos en la de Fe), mientras que causaron efectos opuestos en la ruta de pentosas fosfato, con aumentos (dos proteínas) en la deficiencia de Mn y disminuciones (dos proteínas) en la de Fe. Del mismo modo, la deficiencia de Fe sólo afectó a dos proteínas pertenecientes a esta categoría en el apoplasto de remolacha. Por otro lado, aunque la toxicidad de Mn causó un gran número de alteraciones en la categoría relacionada con el metabolismo de carbohidratos en el proteoma del xilema, la mayor parte de estas proteínas se clasificaron nuevamente como NCS. A esto hay que añadir que tanto la ruta de la glicólisis como la de las pentosas fosfatos mostraron proteínas aumentadas y disminuidas, resaltando la dificultad para interpretar los cambios producidos en las proteínas NCS de xilema.

Por el contrario, la toxicidad de Mn sí que tuvo un claro efecto sobre las rutas metabólicas involucradas en los procesos de obtención de energía en el proteoma de raíz de plantas de tomate, incluyendo glicólisis, metabolismo del piruvato, ciclo de Krebs y fosforilación oxidativa. Los descensos en la abundancia relativa de proteínas implicadas en todas estas rutas metabólicas indican una reducción en la capacidad de obtención de ATP y poder reductor que también han sido descritos en raíz de *C. sinensis* cultivada con exceso de Mn (Zhou et al., 2013; You et al., 2014). Los descensos inducidos por la toxicidad de Mn en varias proteínas que contienen Fe, como la NADH:uniquininona oxidoreductasa, la dioxigenasa o la NADH-citocromo b5 reductasa se pueden asociar a la limitada disponibilidad de Fe en plantas crecidas en niveles tóxicos de Mn, debido a la competición entre Mn y Fe a nivel de transporte molecular. Estos resultados son acordes con el aumento de la actividad reductasa medido en las raíces de las plantas crecidas en condiciones de exceso de Mn, que también sugiere un cierto grado de escasez de Fe. Al mismo tiempo, aunque la concentración de Fe en la raíz no cambió, la concentración de Fe en hoja descendió pero sin llegar a alcanzar niveles considerados como deficientes.

Finalmente, es de destacar que la toxicidad de Mn en tomate también afectó a un elevado número de proteínas clasificadas como reservorios de nutrientes en los perfiles proteicos de la raíz (cinco proteínas) y el fluido de xilema (10), en contraposición con la deficiencia de Mn, que no presentó alteraciones en esta categoría. Los cambios en la abundancia relativa de estas proteínas pueden, por un lado, estar relacionados con la variación en la tasa de repuesto de proteínas anteriormente mencionado, ya que estas proteínas actúan como reservorios de N. Por otro lado, la gran mayoría de estas proteínas (tres en raíz y ocho en xilema) son cupinas con dominios RmlC y "RmlC jelly roll" que se encuentran normalmente en dTDP-isomerasas involucradas en la síntesis de L-ramnosa, en proteínas de unión a Mn (como la oxalato oxidasa o la MnSOD) y en receptores de auxina, indicando que sus cambios en abundancia podrían estar relacionados con modificaciones en la pared celular y/o en procesos de defensa frente a ROS.

Además, las cupinas que mostraron aumentos en el proteoma de raíz han sido descritas como proteínas vacuolares, mientras que las cupinas que presentaron descensos en dicho proteoma son extracelulares. Este hecho sugiere que en condiciones de toxicidad de Mn la planta almacena el metal en las vacuolas del tejido radicular en un proceso asistido por cupinas.

4.2. Comparación entre las técnicas de proteómica utilizadas

En esta Tesis Doctoral se ha utilizado la electroforesis bidimensional (2-DE), una técnica de proteómica clásica, junto con el "shotgun proteomics", una técnica de proteómica avanzada, para el estudio de los distintos proteomas de la planta. En la 2-DE, las proteínas de un extracto proteico se separan en función de su peso molecular y punto isoeléctrico mediante electroforesis en dos dimensiones, y a continuación los spots que presentan cambios significativos en abundancia relativa se digieren e identifican por espectrometría de masas (Figura 4.2.1). Durante varias décadas, este ha sido el método más comúnmente elegido para los estudios proteómicos.

Figura 4.2.1. *Flujo de trabajo utilizado en el estudio de los proteomas de la planta mediante electroforesis bidimensional.*

Sin embargo, la electroforesis en dos dimensiones no es la única plataforma para la separación de proteínas en la actualidad. El desarrollo de técnicas avanzadas basadas en el uso de cromatografía multidimensional, cuyo uso se ha incrementado recientemente, permite la digestión previa de muestras complejas de proteínas, el posterior fraccionamiento de los péptidos resultantes, su análisis e identificación mediante 2D-LC y la determinación mediante parámetros estadísticos de las variaciones significativas que van a determinar la respuesta biológica de la planta (Figura 4.2.2).

Figura 4.2.2. *Flujo de trabajo usado por las técnicas de proteómica avanzada en el estudio de los proteomas de la planta.*

En los estudios proteómicos se pueden distinguir dos aproximaciones generales. La primera sería la proteómica descriptiva, basada en la identificación del mayor número posible de proteínas dentro de un proteoma. La segunda sería la proteómica diferencial o comparativa,

centrada en el análisis de diferencias entre muestras. La proteómica descriptiva se ha utilizado en esta Tesis para describir proteomas de fluidos vegetales poco conocidos hasta la fecha, incluyendo la savia de xilema y floema y el fluido apoplástico, en una revisión de los estudios publicados sobre estos compartimentos vegetales (Capítulo 3.1). Este estudio refleja la dificultad del mapeo completo de un tejido y la importancia de establecer criterios claros, así como indicadores universales, para estimar la contaminación por componentes intracelulares en fluidos vegetales, que aparece frecuentemente debido la naturaleza invasiva de los métodos de obtención de estos fluidos. Junto con esta revisión, en el desarrollo de esta Tesis Doctoral se ha llevado a cabo el mapeo del fluido apoplástico de hoja de *Beta vulgaris* mediante el uso de 2-DE (Capítulo 3.2). Tanto el número de spots observados en este estudio (203 spots) como su identidad fueron consistentes con los reportados en otras especies vegetales, todos ellos basados en técnicas de electroforesis bidimensional. El proteoma del fuido apoplástico está compuesto por proteínas de carácter soluble, y probablemente contiene un mayor número de proteínas que los 200 spots que han sido identificados en estos estudios. Estos resultados muestran que la electroforesis bidimensional posee limitaciones inherentes a la técnica, como por ejemplo la visualización de proteínas que están presentes en bajas concentraciones en la muestra (Harry et al., 2000; Rabilloud, 2002). Este hecho sugiere que herramientas como el "shotgun" podrían ser de mayor utilidad en el mapeo de sub-proteomas, como los de los fluidos vegetales, en los que las proteínas se encuentran en baja abundancia.

En segundo lugar, la proteómica comparativa ha sido de gran utilidad para discernir los efectos de estreses abióticos como la deficiencia de Fe en el fluido apoplástico y la savia de xilema (descritos en los Capítulos 3.2 y 3.3, respectivamente), el efecto de la deficiencia de Mn en la savia de xilema (descrito en el Capítulo 3.3) y la toxicidad de Mn en la raíz y la savia de xilema (descritos en los Capítulos 3.5 y 3.6, respectivamente).

Los cambios en los perfiles proteicos con la toxicidad de Mn en los tejidos de raíz de tomate han sido analizados por ambas metodologías, para llevar a cabo una comparación entre la 2-DE clásica y la técnica de "shotgun". Los resultados obtenidos permiten concluir que la técnica de "shotgun", resulta más sensible para la identificación de proteínas, siendo la responsable de la identificación del 70% de las proteínas diferenciales totales. A pesar de esta sensibilidad, conviene destacar que tan sólo el 7% de las proteínas diferenciales en este estudio fueron identificadas mediante ambas técnicas, lo que sugiere que las dos metodologías, 2DE y "shotgun proteomics", presentan una gran complementariedad. Además, las nuevas técnicas de proteómica basadas en el análisis cromatográfico presentan desventajas para la detección de isoformas y modificaciones post-traduccionales, que resultan relativamente sencillas con la electroforesis basada en gel (véase Capítulo 3.2). Está claro que en los estudios de mapeo la 2-DE resulta limitada en comparación con las técnicas avanzadas, principalmente debido a la

mayor sensibilidad de estas nuevas metodologías. Sin embargo, en el caso de la proteómica comparativa, la 2-DE sigue siendo una herramienta de gran utilidad, ya que permite una visualización relativamente sencilla de los cambios, así como la detección de variaciones en isoformas y modificaciones post-traduccionales. Por ejemplo, el análisis por 2-DE del proteoma diferencial de apoplasto de remolacha deficiente en Fe reveló varias isoformas con distinto pI de una quitinasa, con una de ellas apareciendo *de novo*, lo que pone de manifiesto la utilidad de esta técnica. A pesar de estas ventajas, una de las mayores limitaciones de la 2-DE sigue siendo la dificultad en su automatización, que lleva a que el número de réplicas a analizar sea reducido, lo que resulta en una mayor variabilidad experimental, que además, se ve incrementada por la mayor intervención manual en este método (Quadroni and James, 1999; Lopez, 2000). Además, el número menor de réplicas conlleva a una menor robustez de los análisis estadísticos. Las técnicas no basadas en gel pueden reducir, por tanto, tanto costes como el tiempo invertido.

No toda la responsabilidad en la identificación de proteínas debe recaer sobre la tecnología utilizada, ya que junto a la elección de la metodología utilizada hay que tener en cuenta que la etapa más crítica se encuentra al inicio del proceso, que incluye tanto la extracción como la preparación de la muestra. Esta etapa es determinante para la posterior identificación de proteínas y adquiere gran importancia en los estudios sobre fluidos vegetales, ya que como se ha comentado anteriormente y se describe en los Capítulos 3.1 y 3.2, la naturaleza invasiva de los métodos de extracción puede llevar a que un alto porcentaje de las proteínas encontradas se pueda considerar como resultado de la contaminación por tejidos vecinos. Este hecho, unido a la alta sensibilidad de las técnicas de proteómica avanzada, lleva a que haya que replantearse los criterios de pureza utilizados y a la búsqueda de estrategias que permitan la distinción entre las proteínas propias del fluido y aquellas que sean contaminantes intracelulares. Por otro lado, la alta variabilidad de las muestras biológicas hace que se presenten variaciones en el tamaño molecular de los polipéptidos, en su carga e hidrofobicidad, en las modificaciones post-traduccionales o en su distribución celular, no existiendo un protocolo de extracción único ni un sistema de solventes capaz de extraer el proteoma completo de un tejido determinado. Este hecho se hace especialmente relevante en muestras de tejido, como es el caso de la raíz. En nuestros estudios se ha utilizado un protocolo de extracción para proteínas solubles basado en la solubilización de proteínas en fenol y su posterior precipitación en acetato de amonio en metanol (Hurkman and Tanaka, 1986; Meyer et al., 1988). Este protocolo genera extractos de calidad con una contaminación aparentemente mínima (Mijnsbrugge et al., 2000; Wang et al., 2003), minimizando también la proteolisis durante la extracción (Schuster and Davies, 1983), pero lleva a la pérdida selectiva de especies de proteínas con baja solubilidad, como son las proteínas hidrofóbicas.

Por último, hay que resaltar que los estudios proteómicos requieren generalmente la validación de resultados, que puede llevarse a cabo mediante una gran variedad de técnicas experimentales, incluyendo las de fisiología, bioquímica, metabolómica y genómica, lo que siempre incrementa la información y refuerza los datos obtenidos.

Capítulo 5

CONCLUSIONES

1. Los proteomas del fluido apoplástico y las savias de xilema y floema presentan categorías funcionales similares, si bien cada uno con proteínas específicas, existiendo no obstante un pequeño grupo que es común en los tres proteomas y que tiene funciones en el mantenimiento de pared celular y defensa.

2. La deficiencia de Fe tiene un mayor efecto sobre el perfil proteico de la savia de xilema que sobre el del fluido apoplástico, indicando que la homeostasis de proteínas es especialmente eficiente en último caso.

3. Las deficiencias de Fe y Mn afectan a un número similar de proteínas en el proteoma del xilema: la de Mn provoca descensos en la mayor parte de las proteínas y la de Fe causa descensos e incrementos casi por igual.

4. Los cambios causados por la toxicidad de Mn en los proteomas de xilema y de raíz muestran una ralentización general de las actividades metabólicas, siendo el efecto en el caso del xilema mayor que el originado por las deficiencias nutricionales.

5. Los proteomas del fluido apoplástico y la savia de xilema indican que son compartimentos altamente glicolíticos, siendo abundantes las proteínas relacionadas con el metabolismo de polisacáridos.

6. Tanto la deficiencia de Fe como la toxicidad de Mn llevan a cambios en los perfiles proteicos consistentes con aumentos de la degradación de la pared primaria, mientras que la deficiencia de Mn produce el efecto contrario, afectando dichos cambios a las propiedades biomecánicas y/o porosidad de la pared celular.

7. Las deficiencias de Fe y Mn producen una disminución en la lignificación de la pared secundaria en xilema, que es más intensa en el caso del Mn, mientras que la toxicidad de Mn produce el efecto contrario tanto en raíz como en xilema.

8. El proteoma del xilema muestra un entorno menos proteolítico con la deficiencia de Mn que con la de Fe, reflejando una situación de estrés menor, mientras que con la toxicidad de Mn disminuye tanto la actividad proteolítica del xilema como los procesos de síntesis y degradación de proteínas en la raíz.

9. La deficiencia de Fe y la toxicidad de Mn causan cambios en los perfiles proteicos que reflejan la existencia de estrés oxidativo, a diferencia de lo que ocurre con la deficiencia de Mn.

10. La toxicidad de Mn provoca grandes cambios en las abundancias relativas de proteínas relacionadas con defensa en el fluido xilemático y especialmente en la raíz, a diferencia de lo que ocurre con las deficiencias de Fe y Mn.

11. En cuanto a los sistemas de señalización celular, las deficiencias de Fe y Mn afectan de un modo antagónico a la vía CLE, el basado en lípidos y la red de fosforilación extracelular, mientras que el basado en fasciclin-arabinogalactanos se regula de forma análoga en ambas deficiencias. Por otro lado, la toxicidad de Mn provoca alteraciones en la vía de regulación mediada por lípidos.

12. La toxicidad de Mn tiene un claro efecto sobre los perfiles proteicos de la raíz, con disminuciones en los procesos de obtención de ATP, poder reductor y transporte electrónico.

13. Los resultados obtenidos permiten confirmar no sólo que las técnicas de proteómica avanzada resultan más sensibles que las clásicas en la identificación de proteínas, sino también que ambas aproximaciones resultan complementarias, teniendo las nuevas tecnologías una mayor sensibilidad y permitiendo la electroforesis 2-D una mejor visualización de los cambios y la detección de variaciones en cuanto a isoformas y modificaciones post-traduccionales.

BIBLIOGRAFÍA

Abadía J., Vázquez S., Rellán-Álvarez R., El-Jendoubi H., Abadía A., Álvarez-Fernández A., López-Millán A.F. Towards a knowledge-based correction of iron chlorosis. *Plant Physiol. Biochem.* 49 (2011) 471-482.

Abadía J., Álvarez-Fernández A., Rombolá A.D., Sanz M., Tagliavini M., Abadía A. Technologies for the diagnosis and remediation of Fe deficiency. *Soil Sci. Plant Nutr.* 50 (2004) 965-971.

Abadía J, Abadía A. Iron and pigments. In 'Iron chelation in plants and soil microorganisms'. (Eds L.L. Barton, B.C. Hemming) *Academic Press* (1993) 327–343.

Abdallah C., Dumas-Gaudot E., Renaut J., Sergeant K. Gel-based and gel-free quantitative proteomics approaches at a glance. *Int. J. Plant Genomics* (2012) 17.

Aki T., Shigyo M., Nakano R., Yoneyama T., Yanagisawa S. Nano scale proteomics revealed the presence of regulatory proteins including three FT-like proteins in phloem and xylem saps from rice. *Plant Cell Physiol.* 49 (2008) 767-790.

Albenne C.C., Canut H., Jamet E. Plant cell wall proteomics: the leadership of *Arabidopsis thaliana. Front. Plant Sci.* 4 (2013) 111.

Alejandro S., Cailliatte R., Alcon C., Dirick L., Domergue F., Correia D., Castaings L., Briat J.F., Mari S., Curie C. Intracellular distribution of manganese by the *trans*-Golgi network transporter NRAMP2 is critical for photosynthesis and cellular redox homeostasis. *Plant Cell* 29 (2017) 3068-3084.

Allen M.D., Kropat J., Tottey S., Del Campo J.A., Merchant S.S. Manganese deficiency in chlamydomonas results in loss of photosystem II and MnSOD function, sensitivity to peroxides, and secondary phosphorus and iron deficiency. *Plant Physiol.* 143 (2007) 263-277.

Alloway B.J. The origin of heavy metals in soils. In 'Heavy metals in soils'. (Ed. B.J. Alloway) *S.S.B.M.* (1995) 38-56.

Alvarez S., Goodger J.Q.D., Marsh E.L., Chen S., Asirvatham V.S., Schachtman D.P. Characterization of the maize xylem sap proteome. *J. Proteome Res.* 5 (2006) 963-972.

Álvarez-Fernández A., Díaz-Benito P., Abadía A., López-Millán A.F., Abadía J. Metal species involved in long distance metal transport in plants. *Front. Plant Sci.* 5 (2014) 105.

Álvarez-Fernández A. Abadía J., Abadía A. Iron deficiency, fruit yield and fruit quality. In: 'Iron nutrition in plants and rhizospheric microorganisms'. (Eds. L.L. Barton, J. Abadía) *Springer* (2006) 85-101.

Álvarez-Fernández A., Paniagua P., Abadía J., Abadía A. Effects of Fe deficiency chlorosis on yield and fruit quality in peach (*Prunus persica* L. Batsch). *J Agric Food Chem.* 51 (2003) 5738-5744.

Ambrosone A., Batelli G., Nurcato R., Aurilia V., Punzo P., Bangarusamy D.K., Ruberti I., Sassi M., Leone A., Costa A., Grillo S. The *Arabidopsis* RNA-binding protein AtRGGA regulates tolerance to salt and drought stress. *Plant Physiol.* 168 (2015) 292-306.

Ambrosone A., Costa A., Leone A., Grillo S. Beyond transcription: RNA-binding proteins as emerging regulators of plant response to environmental constraints. *Plant Sci.* 182 (2012) 12-18.

Anantharaman V., Aravind L. Novel conserved domains in proteins with predicted roles in eukaryotic cell-cycle regulation, decapping and RNA stability. *BMC Genomics* 5 (2004).

Andaluz S., López-Millán A.F., De las Rivas J., Aro E.-M., Abadía J., Abadía A. Proteomic profiles of thylakoid membranes and changes in response to iron deficiency. *Photosynth. Res.* 89 (2006) 141-155.

Andersson-Gunnerås S., Mellerowicz E.J., Love J., Segerman B., Ohmiya Y., Coutinho P.M., Nilsson P., Henrissat B., Moritz T., Sundberg B. Biosynthesis of cellulose-enriched tension wood in *Populus*: global analysis of transcripts and metabolites identifies biochemical and developmental regulators in secondary wall biosynthesis. *Plant J.* 45 (2006) 144-165.

Aoba K., Sekiya K. Microanalysis of leaves and fine roots of satsuma mandarin and twigs of apple absorbing excess manganese by electron microprobe X-ray analyzer. In: 'Studies on the minor metal elements in orchards'. *Fruit Tree Res. Sta.* 4 (1977) 25-35.

Atkins C.A., Smith P.M.C., Rodríguez-Medina C. Macromolecules in phloem exudates-a review. *Protoplasma* 248 (2011) 165-172.

Baggerman G., Vierstraete E., Loof A., Schoofs L. Gel-based versus gel-free proteomics: a review. *Comb. Chem High throughput Screen.* 8 (2005) 669-77.

Barbaglia A.M., Tamot B., Greve V., Hoffmann-Benning S. Phloem proteomics reveals new lipid-binding proteins with a putative role in lipid-mediated signaling. *Front. Plant Sci.* 7 (2016) 563.

Barber S.A. Soil nutrient bioavailability. A mechanistic approach, *John Wiley & Sons* (1995).

Barnes A., Bale J., Constantinidou C., Ashton P., Jones A., Pritchard J. Determining protein identity from sieve element sap in *Ricinus communis* L. by quadrupole time of flight (Q-TOF) mass spectrometry. *J. Exp. Bot.* 55 (2004) 1473-1481.

Barros J., Serk H., Granlund I., Pesquet E. The cell biology of lignification in higher plants. *Ann. Bot.* 115 (2015) 1053-1074.

Bashir K., Ishimaru Y., Nishizawa N.K. Identification and characterization of the major mitochondrial Fe transporter in rice. *Plant Signal. Behav.* 6 (2011) 1591-1593.

Baulande S., Langlois C. Proteins sharing PNPLA domain, a new family of enzymes regulating lipid metabolism. *Med. Sci.* 26 (2010) 177-184.

Becker R., Grün M., Scholz G. Nicotianamine and the distribution of iron into the apoplasm and symplasm of tomato (*Lycopersicon esculentum* Mill.). *Planta* 187 (1992) 48-52.

Bendtsen J., Kiemer L., Fausboll A., Brunak S. Non-classical protein secretion in bacteria. *BMC Microbiology* 5 (2005) 58.

Bendtsen J.D., Jensen L.J., Blom N., VonHeijne G., Brunak S. Feature-based prediction of non-classical and leader less protein secretion. *Protein Eng. Des. Sel.* 17 (2004) 349-356.

Benning U.F., Tamot B., Guelette B.S., Hoffmann-Benning S. New aspects of phloem-mediated long-distance lipid signaling in plants. *Front. Plant Sci.* 3 (2012).

Bernard C. Introduction à l'étude de la médecine expérimentale. *Paris: Éditions Garnier-Flammarion* (1865).

Bidwell S.D., Woodrow I.E., Batianoff G.N., Sommer-Knusden J. Hyperaccumulation of manganese in the rainforest tree *Austromyrtus bidwillii* (Myrtaceae) from Queensland, Australia. *Funct. Plant Biol.* 29 (2002) 899–905.

Bienfait H.F., Van den Briel W., Mesland-Mul N.T. Free space iron pools in roots*:* generation and mobilization. *Plant Physiol.* 78 (1985) 596-600.

Bienfait H.F., Bino R.J., van der Bliek A.M., Duivenboorden J.F., Fontaine J.M. Characterization of ferric reducing activity in roots of Fe-deficient *Phaseolus vulgaris*. *Plant Physiol.* 59 (1983) 196-202.

Bona E., Marsano F., Cavaletto M., Berta G. Proteomic characterization of copper stress response in *Cannabis sativa* roots. *Proteomics* 7 (2007) 1121-30.

Borlotti A., Vigani G., Zocchi G. Iron deficiency affects nitrogen metabolism in cucumber (*Cucumis sativus* L.) plants. *BMC Plant Biol.* 12 (2012) 189.

Boudart G., Jamet E., Rossignol M., Lafitte C., Borderies G., Jauneau A., Esquerré-Tugayé M.T., Pont-Lezica R. Cell wall proteins in apoplastic fluids of *Arabidopsis thaliana* rosettes: Identification by mass spectrometry and bioinformatics. *Proteomics* 5 (2005) 212-221.

Bowen G., Rovira A. The rhizosphere: the hidden half of the hidden half. In: 'Roots: The hidden half'. (Eds. Y. Waisel, A. Eshel, U. Kafkafi) *Marcel Dekker Inc.* (1992) 641-669.

Boyce C.K., Zwieniecki M.A., Cody G.D., Jacobsen C., Wirick S., Knoll A.H., Holbrook N.M. Evolution of xylem lignification and hydrogel transport regulation. *Proc. Natl. Acad. Sci. U.S.A.* 101 (2004) 17555-17558.

Briat J.F., Dubos C., Gaymard F. Iron nutrition, biomass production, and plant product quality. *Trends Plant Sci.* 20 (2015) 33-40.

Briat J.F., Lobreaux S., Grignon N., Vansuyt G. Regulation of plant ferritin synthesis: how and why. *Cell Mol. Life Sci.* 56 (1999) 155-166.

Broadley M., Brown P., Cakmak I., Rengel Z., Zhao F. Function of nutrients: Micronutrients A2. In: 'Marschner's mineral nutrition of higher plants'. *Academic Press* (2010) 191-248.

Broadley M.R., White P.J., Hammond J.P., Zelko I., Lux A. Zinc in plants. *New Phytol.* 173 (2007) 677-702.

Brown D.M., Zeef L.A.H., Ellis J., Goodacre R., Turner S.R. Identification of novel genes in *Arabidopsis* involved in secondary cell wall formation using expression profiling and reverse genetics. *Plant Cell.* 17 (2005) 2281–2295.

Brown P.H., Graham R.D., Nicholas D.J.D. The effects of manganese and nitrate supply on the levels of phenolics and lignin in young wheat plants. *Plant Soil* 81 (1984) 437-440.

Brumbarova T., Matros A., Mock H.P., Bauer P. A proteomic study showing differential regulation of stress, redox regulation and peroxidase proteins by iron supply and the transcription factor FER. *Plant J.* 54 (2008) 321-334.

Brune A.U.W., Dietz K.J. Compartmentation and transport of zinc in barley primary leaves as basic mechanisms involved in zinc tolerance. *Plant Cell Environ.* 17 (1994) 153–162.

Buhtz A., Kolasa A., Arlt K., Walz C., Kehr J. Xylem sap protein composition is conserved among different plant species. *Planta* 219 (2004) 610-618.

Burnell J.N. The biochemistry of manganese in plants. In: 'Manganese in soils and plants'. Proceedings of the international symposium on 'Manganese in soils and plants'. (Eds: R.D. Graham, R.J. Hannam, N.C Uren) *Springer* (1988) 125-137.

Busi M.V., Maliandi M.V., Valdez H., Clemente M., Zabaleta E.J., Araya A., Gomez-Casati D.F. Deficiency of *Arabidopsis thaliana* frataxin alters activity of mitochondrial Fe–S proteins and induces oxidative stress. *Plant J.* 48 (2006) 873-882.

Cailliatte R., Schikora A., Briat J.F., Mari S., Curie C. High-affinity manganese uptake by the metal transporter NRAMP1 is essential for *Arabidopsis* growth in low manganese conditions. *Plant Cell* 22 (2010) 904-917.

Cammarano P., Pons S., Romeo A., Galdieri M., Gualerzi C. Characterization of unfolded and compact ribosomal subunits from plants and their relationship to those of lower and higher animals: Evidence for physicochemical heterogeneity among eucaryotic ribosomes. *BBA Section Nucleic Acids and Protein Synthesis* 281 (1972) 571-596.

Cannon W.B. Physiological regulation of normal states: some tentative postulates concerning biological homeostatics. (Ed: A. Pettit) *Les Éditions Médicales* (1926) 91-93.

Cantarel B.L., Coutinho P.M., Rancurel C., Bernard T., Lombard V., Henrissat, B. The Carbohydrate-Active enZymes database (CAZy): an expert resource for Glycogenomics. *Nucleic Acids Res.* 37 (2009) 233–238.

Carella P., Wilson D.C., Kempthorne C.J., Cameron R.K. Vascular sap proteomics: Providing insight into long-distance signaling during stress. *Front. Plant Sci.* 7 (2016).

Carrasco-Gil S., Rios J.J., Álvarez-Fernández A., Abadía A., García-Mina J.M., Abadía J. Effects of individual and combined metal foliar fertilisers on iron- and manganese-deficient *Solanum lycopersicum* plants. *Plant Soil* 402 (2016) 27-45.

Carter C., Thornburg R.W. Tobacco Nectarin I: purification and characterization as a germin-like, manganese superoxide dismutase implicated in the defense of floral reproductive tissues. *J. Biol. Chem.* 275 (2000) 36726-36733.

Casasoli M., Spadoni S., Lilley K.S., Cervone F., De Lorenzo G., Mattei B. Identification by 2-D DIGE of apoplastic proteins regulated by oligogalacturonides in *Arabidopsis thaliana*. *Proteomics* 8 (2008) 1042-1054.

Castillo F.J., Greppin H. Balance between anionic and cationic extracellular peroxidase activities in *Sedum album* leaves after ozone exposure. Analysis by high-performance liquid chromatography. *Physiol. Plant.* 68 (1986) 201-208.

Ceballos-Laita L., Gutierrez-Carbonell E., Imai H., Abadía A., Uemura M., Abadía J., López-Millán A.F. Effects of manganese toxicity on the protein profile of tomato (*S. lycopersicum*) roots as revealed by two complementary proteomic approaches, two-dimensional electrophoresis and shotgun analysis. *J. Proteomics* (2018) accepted.

Ceballos-Laita L., Gutierrez-Carbonell E., Takahashi D., Abadía A., Uemura M., Abadía J., López-Millán A.F. Effects of Fe, Mn deficiencies on the protein profiles of tomato (*Solanum lycopersicum*) xylem sap as revealed by shotgun analyses. *J. Proteomics* 170 (2018) 117-129.

Ceballos-Laita L., Gutierrez-Carbonell E., Takahashi D., Abadía A., Uemura M., Abadía J., López-Millán A.F. Data on xylem sap from Mn- and Fe-deficient tomato plants. *J. Proteomics* 17 (2016) 512-516.

Ceballos-Laita L., Gutierrez-Carbonell E., Lattanzio G., Vázquez S., Contreras-Moreira B., Abadía A., Abadía J., López-Millán A.F. Protein profile of *Beta vulgaris* leaf apoplastic fluid and changes induced by Fe deficiency and Fe resupply. *Front. Plant Sci.* 6 (2015).

Cesco S., Neumann G., Tomasi N., Pinton R., Weisskopf L. Release of plant-borne flavonoids into the rhizosphere, their role in plant nutrition. *Plant Soil* 329 (2010) 1-25.

Chassot C., Nawrath C., Métraux J.P. Cuticular defects lead to full immunity to a major plant pathogen. *Plant J.* 49 (2007) 972-980.

Chelius D., Bondarenko P.V. Quantitative profiling of proteins in complex mixtures using liquid chromatography, mass spectrometry. *J. Proteome Res.* 1 (2002) 317-323.

Chen S., Sánchez-Fernández R., Lyver E.R., Dancis A., Rea P.A. Functional characterization of AtATM1, AtATM2, and AtATM3, a subfamily of *Arabidopsis* half-molecule ATP-binding cassette transporters implicated in iron homeostasis. *J. Biol. Chem.* 282 (2007) 21561-21571.

Chen Z., Yan W., Sun L., Tian J., Liao H. Proteomic analysis reveals growth inhibition of soybean roots by manganese toxicity is associated with alteration of cell wall structure, lignification. *J. Proteomics* 143 (2016) 151-160.

Chen Z., Sun L., Liu P., Liu G., Tian J., Liao H. Malate synthesis and secretion mediated by a manganese-enhanced malate dehydrogenase confers superior manganese tolerance in *Stylosanthes guianensis*. *Plant Physiol.* 167 (2015) 176-188.

Chen Z., Fujii Y., Yamaji N., Masuda S., Takemoto Y., Kamiya T., Yusuyin Y., Iwasaki K., Kato S.I., Maeshima M., Ma J.F., Ueno D. Mn tolerance in rice is mediated by MTP8.1, a member of the cation diffusion facilitator family. *J. Exp. Bot.* 64 (2013) 4375-4387.

Cheng N.H., Pittman J.K., Shigaki T., Hirschi K.D. Characterization of CAX4, an *Arabidopsis* H^+/cation antiporter. *Plant Physiol.* 128 (2002) 1245-1254.

Clark R.B. Plant genotype differences in the uptake, translocation, accumulation, and use of mineral elements required for plant growth. *Plant Soil* 72 (1983) 175-196.

Clemens S. Zn and Fe biofortification: The right chemical environment for human bioavailability. *Plant Sci.* 225 (2014) 52-57.

Colombo C., Palumbo G., He J.Z., Pinton R., Cesco S. Review on iron availability in soil: interaction of Fe minerals, plants,, microbes. *J. Soils Sediments* 14 (2014) 538-548.

Connolly E.L., Fett J.P., Guerinot M.L. Expression of the IRT1 metal transporter is controlled by metals at the levels of transcript, protein accumulation. *Plant Cell* 14 (2002) 1347-1357.

Connorton J.M., Balk J., Rodríguez-Celma J. Iron homeostasis in plants-a brief overview. *Metallomics* 9 (2017) 813-823.

Constantopoulos G. Lipid metabolism of manganese-deficient algae. I. Effect of manganese deficiency on the greening and the lipid composition of *Euglena gracilis* Z. *Plant Physiol.* 45 (1970) 76-80.

Conte S., Stevenson D., Furner I., Lloyd A. Multiple antibiotic resistance in *Arabidopsis* is conferred by mutations in a chloroplast-localized transport protein. *Plant Physiol.* 151 (2009) 559-573.

Conte S.S., Walker E.L. Transporters contributing to iron trafficking in plants. *Mol. Plant*, 4 (2011) 464-476.

Cordwell S.J., Nouwens A.S., Verrills N.M., Basseal D.J., Walsh B.J. Subproteomics based upon protein cellular location, relative solubilities in conjunction with composite two-dimensional electrophoresis gels. *Electrophoresis* 21 (2000) 1094-1103.

Corthals G., Rose K. Quantitation in proteomics. Proteome research: New frontiers in functional genomics. *Wilkins Springer-Verlag* (2007).

Coulombe B.A., Chaney R.L., Wiebold W.J. Bicarbonate directly induces iron chlorosis in susceptible soybean cultivars. *Soil Sci. Soc. Am. J.* 48 (1984) 1297-1301.

Covarrubias A.A., Ayala J.W., Reyes J.L., Hernandez M., Garciarrubio A. Cell-wall proteins induced by water deficit in bean (*Phaseolus vulgaris* L.) seedlings. *Plant Physiol.* 107 (1995) 1119-1128.

Cox B., Kislinger T., Wigle D., Kannan A., Brown K., Okubo T., Hogan B., Jurisica I., Frey B., Rossant J., Emili A. Integrated proteomic, transcriptomic profiling of mouse lung development and *Nmyc* target genes. *Mol. Syst. Biol.* 3 (2007) 8.

Curie C., Cassin G., Couch D., Divol F., Higuchi K., Le Jean M., Misson J., Schikora A., Czernic P., Mari S. Metal movement within the plant: contribution of nicotianamine and yellow stripe1-like transporters. *Ann. Bot.* 103 (2009) 1-11.

Curie C., Briat J.F. Iron transport and signaling in plants. *Annu. Rev. Plant Biol.* 54 (2003) 183-206.

Curie C.A., Briat J.F, Iron transport and signaling in plants. *Annu. Rev. Plant Biol.* 54 (2003) 183-206.

Curie C., Panaviene Z., Loulergue C., Dellaporta S.L., Briat J.F., Walker E.L. Maize yellow stripe1 encodes a membrane protein directly involved in Fe(III) uptake. *Nature* 409 (2001) 346-349.

Curie C., Alonso J.M., Jean M.L.E., Ecker J.R., Briat J.F. Involvement of NRAMP1 from *Arabidopsis thaliana* in iron transport. *Biochem. J.* 347 (2000) 749-755.

Cvjetko P., Zovko M., Balen B. Proteomics of heavy metal toxicity in plants. *Arh. Hig. Rada. Toksikol* 65 (2014) 1-18.

Dafoe N.J., Zamani A., Ekramoddoullah A.K.M., Lippert D., Bohlmann J.R., Constabel C.P. Analysis of the poplar phloem proteome and its response to leaf wounding. *J. Proteome Res.* 8 (2009) 2341-2350.

DalCorso G., Farinati S., Furini A. Regulatory networks of cadmium stress in plants. *Plant Signal. Behav.* 5 (2010) 663–667.

D'Andrea L.D., Regan L. TPR proteins: The versatile helix. *Trends Biochem. Sci.*, 28 (2003) 655-662.

Dani V., Simon W.J., Duranti M., Croy R.R. Changes in the tobacco leaf apoplast proteome in response to salt stress. *Proteomics* 5 (2005) 737-745.

Dannel F., Pfeffer H., Marschner H. Isolation of apoplasmic fluid from sunflower leaves and its use for studies on influence of nitrogen supply on apoplasmic pH. *J. Plant Physiol.* 146 (1995) 273-278.

De la Luz Mora M., Rosas A., Ribera A., Rengel Z. Differential tolerance to Mn toxicity in perennial ryegrass genotypes: involvement of antioxidative enzymes and root exudation of carboxylates. *Plant Soil* 320 (2009) 79-89.

De Varennes A., Carneiro J.P., Goss M.J. Characterization of manganese toxicity in two species of annual medics. *J. Plant Nutr.* 24 (2001) 1947-1955.

Dean J.F.D. and Eriksson K.E.L. Laccase and the deposition of lignin in vascular plants. *Holzforschung* 48 (1994) 21-33.

Del Vecchio H.A., Ying S., Park J., Knowles V.L., Kanno S., Tanoi K., She Y.M., Plaxton W.C. The cell wall-targeted purple acid phosphatase AtPAP25 is critical for acclimation of *Arabidopsis thaliana* to nutritional phosphorus deprivation. *Plant J.* 80 (2014) 569-581.

Delaunois B., Colby T., Belloy N., Conreux A., Harzen A., Baillieul F., Clement C., Schmidt J., Jeandet P., Cordelier S. Large-scale proteomic analysis of the grapevine leaf apoplastic fluid reveals mainly stress-related proteins and cell wall modifying enzymes. *BMC Plant Biology* 13 (2013) 24.

Delhaize E., Gruber B.D., Pittman J.K., White R.G., Leung H., Miao Y., Jiang L., Ryan P.R., Richardson A.E. A role for the AtMTP11 gene of *Arabidopsis* in manganese transport and tolerance. *Plant J.* 51 (2007) 198-210.

Delhaize E., Kataoka T., Hebb D.M., White R.G., Ryan P.R. Genes encoding proteins of the cation diffusion facilitator family that confer manganese tolerance. *Plant Cell* 15 (2003) 1131-1142.

Demura T., Tashiro G., Horiguchi G., Kishimoto N., Kubo M., Matsuoka N., Minami A., Nagata-Hiwatashi M., Nakamura K., Okamura Y., Sassa N., Suzuki S., Yazaki J., Kikuchi S., Fukuda H. Visualization by comprehensive microarray analysis of gene expression programs during transdifferentiation of mesophyll cells into xylem cells. *Proc. Natl. Acad. Sci. U.S.A.* 99 (2002) 15794-15799.

Di Toopi L., Gabrielli R. Response to cadmium in higher plants. *Environ. Exp. Bot.* 41 (1999) 105-30.

Dickson R.E. Xylem translocation of amino-acids from roots to shoots in cottonwood plants. *Can. J. For. Res.*, 9 (1979) 374-378.

DiDonato R.J., Roberts L.A., Sanderson T., Eisley R.B., Walker E.L. *Arabidopsis* Yellow Stripe-Like2 (YSL2): a metal-regulated gene encoding a plasma membrane transporter of nicotianamine–metal complexes. *Plant J.* 39 (2004) 403-414.

Dietz K.J., Sauter A., Wichert K., Messdaghi D., Hartung W. Extracellular beta-glucosidase activity in barley involved in the hydrolysis of ABA glucose conjugate in leaves. *J. Exp. Bot.* 51 (2000) 937-944.

Dietz K.J. Functions and responses of the leaf apoplast under stress. *Prog. Bot.* 58 (1997) 221–254.

Divol F., Couch D., Conéjéro G., Roschzttardtz H., Mari S., Curie C. The *Arabidopsis* Yellow Stripe Like4 and 6 transporters control iron release from the chloroplast. *Plant Cell* 25 (2013) 1040-1055.

Djordjevic M.A., Oakes M., Li D.X., Hwang C.H., Hocart C.H., Gresshoff P.M. The *Glycine max* xylem sap and apoplast proteome. *J. Proteome Res.* 6 (2007) 3771-3779.

Dodd I.C. Root-to-shoot signaling: assessing the roles of 'up' in the up and down world of long-distance signaling in plant. *Plant Soil* 274 (2005) 251-270.

Donnini S., Prinsi B., Negri A.S., Vigani G., Espen L., Zocchi G. Proteomic characterization of iron deficiency responses in *Cucumis sativus* L. roots. *BMC Plant Biology* 10 (2010) 268.

Donnini S., Castagna A., Ranieri A., Zocchi G. Differential responses in pear and quince genotypes induced by Fe deficiency and bicarbonate. *J. Plant Physiol.* 166 (2009) 1181-1193.

Dou C., Fu X., Chen X., Shi J., Chen Y. Accumulation and interaction of calcium and manganese in *Phytolacca americana*. *Plant Sci.* 177 (2009) 601-606.

Driscoll C.T., Lawrence G.B., Bulger A.J., Butler T.J., Cronan C.S., Eagar C., Lambert K.F., Likens G.E., Stoddard J.L., Weathers K.C. Acidic deposition in the northeastern United States: sources and inputs, ecosystem effects, and management strategies. *BioScience* 51 (2001) 180-198.

Ducic T., Polle A. Transport and detoxification of manganese and copper in plants. *Braz. J. Plant Physiol.* 17 (2005) 103-112.

Dunkley T.P.J., Dupree P., Watson R.B., Lilley K.S. The use of isotope-coded affinity tags (ICAT) to study organelle proteomes in *Arabidopsis thaliana. Biochem. Soc. Trans.* 32 (2004) 520-523.

Durand T.C., Sergeant K., Planchon S., Carpin S., Label P., Morabito D., Hausman J.F., Jenny R. Acute metal stress in *Populus tremula* × *P. alba* (717-1B4 genotype): leaf and cambial proteome changes induced by cadmium(2+). *Proteomics* 10 (2010) 349-368.

Durst F. Correlation of phenylalanine ammonia-lyase and cinnamic acid hydroxylase activity changes in Jerusalem artichoke tuber tissues. *Planta* 132 (1976) 221-227.

Duy D., Wanner G., Meda A.R., von Wirén N., Soll J., Philippar K. PIC1, an ancient permease in *Arabidopsis* chloroplasts, mediates iron transport. *Plant Cell* 19 (2007) 986-1006.

Edmond C., Shigaki T., Ewert S., Nelson M.D., Connorton J.M., Chalova V., Noordally Z., Pittman J.K. Comparative analysis of CAX2-like cation transporters indicates functional and regulatory diversity. *Biochem. J.* 418 (2009) 145-154.

Edreva A. Induction of 'pathogenesis-related' proteins in tobacco leaves by physiological (non-pathogenic) disorders. *J. Exp. Bot.* 41 (1990) 701-703.

Eichert T., Peguero-Pina J.J., Gil-Pelegrín E., Heredia A., Fernández V. Effects of iron chlorosis and iron resupply on leaf xylem architecture, waterrelations, gas exchange and stomatal performance offield-grown peach (*Prunus persica*). *Plant Physiol.* 138 (2010) 48-59.

Eide D., Broderius M., Fett J., Guerinot M.L. A novel iron-regulated metal transporter from plants identified by functional expression in yeast. *Proc. Natl. Acad. Sci. U.S.A.*, 93 (1996) 5624-5628.

El-Jendoubi H., Melgar J.C., Álvarez-Fernández A., Sanz M., Abadía A., Abadía J. Setting good practices to assess the efficiency of iron fertilizers. *Plant Physiol. Biochem.* 49 (2011) 483-488.

Emanuelsson O., Brunak S., von Heijne G., Nielsen H. Locating proteins in the cell using TargetP, SignalP and related tools. *Nat. Protocols* 2 (2007) 953-971.

Endo S., Shinohara H., Matsubayashi Y., Fukuda H. A novel pollen-pistil interaction conferring high-temperature tolerance during reproduction *via* CLE45 signaling. *Curr. Biol.* 23 (2013) 1670-1676.

Enstone D.E., Peterson C.A., Ma F. Root endodermis and exodermis: structure, function, and responses to the environment. *Plant Growth Regul.* 21 (2002) 335-351.

Ephritikhine G.V., Ferro M., Rolland N. Plant membrane proteomics. *Plant Physiol. Biochem.* 42 (2004) 943-962.

Epstein E., Bloom A.J. Mineral nutrition of plants: Principles and perspectives. *Sinauer Associates* (2005).

Eroglu S., Meier B., von Wirèn N., Peiter E. The vacuolar manganese transporter MTP8 determines tolerance to iron deficiency-induced chlorosis in *Arabidopsis. Plant Physiol.* 170 (2016) 1030-1045.

Escher P., Eiblmeier M., Hetzger I., Rennenberg H. Seasonal and spatial variation of carbohydrates in mistletoes (*Viscum album*) and the xylem sap of its hosts (*Populus x euamericana* and *Abies alba*). *Physiol. Plant.* 120 (2004) 212-219.

Eyüboglu B., Pfister K., Haberer G., Chevalier D., Fuchs A., Mayer K.F.X., Schneitz K. Molecular characterisation of the *STRUBBELIG-RECEPTOR FAMILY* of genes encoding putative leucine-rich repeat receptor-like kinases in *Arabidopsis thaliana. BMC Plant Biol.* 7 (2007) 16.

Fazekas S.G.S., Webster R., Datyner A. Two new staining procedures for quantitative estimation of proteins on electrophoretic strips. *BBA* 71 (1963) 377-391.

Fecht-Christoffers M.M., Führs H., Braun H.P., Horst W.J. The role of hydrogen peroxide-producing and hydrogen peroxide-consuming peroxidases in the leaf apoplast of cowpea in manganese tolerance. *Plant Physiol.* 140 (2006) 1451-1463.

Fecht-Christoffers M.M., Braun H.P., Lemaitre-Guillier C., VanDorsselaer A., Horst W.J. Effect of manganese toxicity on the proteome of the leaf apoplast in cowpea. *Plant Physiol.* 133 (2003) 1935-1946.

Fernández V., Orera I., Abadía J., Abadía A. Foliar iron fertilisation of fruit trees: present and future perspectives. *J. Hort. Sci. Biotechnol.* 84 (2009) 1-6.

Fernández V., Eichert T., Del Río V., López-Casado G., Heredia-Guerrero J.A., Abadía A., Heredia A., Abadía J. Leaf structural changes associated with iron deficiency chlorosis in field-grown pear and peach: physiological implications. *Plant Soil* 311 (2008) 161-172.

Fernández-García N., Hernandez M., Casado-Vela J., Bru R., Elortza F., Hedden P., Olmos E. Changes to the proteome and targeted metabolites of xylem sap in *Brassica oleracea* in response to salt stress. *Plant Cell Environ.* 34 (2011) 821-836.

Fernández-Pérez F., Vivar T., Pomar F., Pedreño M.A., Novo-Uzal E. Peroxidase 4 is involved in syringyl lignin formation in *Arabidopsis thaliana. J. Plant Physiol.* 175 (2015a) 86-94.

Fernández-Pérez F., Pomar F., Pedreño M.A., Novo-Uzal E. The suppression of AtPrx52 affects fibers but not xylem lignification in *Arabidopsis* by altering the proportion of syringyl units. *Physiol. Plant.* 154 (2015b) 395-406.

Fernández-Pérez F., Pomar F., Pedreño M.A., Novo-Uzal E. Suppression of *Arabidopsis* peroxidase 72 alters cell wall and phenylpropanoid metabolism. *Plant Sci.* 239 (2015c) 192-199.

Fernando D.R., Lynch J.P. Manganese phytotoxicity: new light on an old problem. *Ann. Bot.* 116 (2015) 313-319.

Fernando D.R., Mizuno T., Woodrow I.E., Baker A.J.M., Collins R.N. Characterization of foliar manganese (Mn) in Mn (hyper)accumulators using X-ray absorption spectroscopy. *New Phytol.* 188 (2010) 1014-1027.

Ferretti M., Destro T., Tosatto S.C.E., La Rocca N., Rascio N., Masi A. γ-glutamyl transferase in the cell wall participates in extracellular glutathione salvage from the root apoplast. *New Phytol.* 181 (2009) 115-126.

Ferro M., Brugière S., Salvi D., Seigneurin-Berny D., Court M., Moyet L., Ramus C., Miras S., Mellal M., Le Gall S., Kieffer-Jaquinod S., Bruley C., Garin J., Joyard J., Masselon C., Rolland N. AT_CHLORO, a comprehensive chloroplast proteome database with subplastidial localization and curated information on envelope proteins. *Mol. Cell. Proteomics*, 9 (2010) 1063-1084.

Fey S., Larsen P. 2D or not 2D. Two-dimensional gel electrophoresis. *Curr. Opin. Chem. Biol.* 5 (2001) 26-33.

Fiehn O. Metabolic networks of *Cucurbita maxima* phloem. *Phytochemistry* 62 (2003) 875-886.

Fisher D.B. Long-distance transport. In: 'Biochemistry and molecular biology of plants'. (Eds. B. Buchanan, W. Gruissem, R. Jones) *Am. Soc. Plant Physiol.* (2000) 729–784.

Flis P., Ouerdane L., Grillet L., Curie C., Mari S., Lobinski R. Inventory of metal complexes circulating in plant fluids: a reliable method based on HPLC coupled with dual elemental and high-resolution molecular mass spectrometric detection. *New Phytol.* 211 (2016) 1129-1141.

Floerl S., Majcherczyk A., Possienke M., Feussner K., Tappe H., Gatz C., Feussner I., Kues U., Polle A. *Verticillium longisporum* infection affects the leaf apoplastic proteome, metabolome, and cell wall properties in *Arabidopsis thaliana. PLoS ONE* 7 (2012) 31435.

Floerl S., Druebert C., Majcherczyk A., Karlovsky P., Kues U., Polle A. Defence reactions in the apoplastic proteome of oilseed rape (*Brassica napus* var. *napus*) attenuate *Verticillium longisporum* growth but not disease symptoms. *BMC Plant Biol.* 8 (2008) 129.

Fourcroy P., Sisó-Terraza P., Sudre D., Savirón M., Reyt G., Gaymard F., Abadía A., Abadía J., Álvarez-Fernández A., Briat J.F. Involvement of the ABCG37 transporter in secretion of scopoletin and derivatives by *Arabidopsis* roots in response to iron deficiency. *New Phytol.* 201 (2014) 155-167.

Fournier M., Gilmore J., Martin-Brown S., Washburn M. Multidimensional separations-based shotgun proteomics. *Chem. Rev*. 107 (2007) 3654-3686.

Fox T.C., Guerinot M.L. Molecular biology of cation transport in plants. *Annu. Rev. Plant Biol.* 49 (1998) 669-696.

Foy C.D. Physiological effects of hydrogen, aluminum and manganese toxicities in acid soils. In: 'Soil acidicity and liming' (Ed: J. Adams) *Am. Soc. Agron.* (1984) 57-97.

Freudenberg K. Biosynthesis and constitution of lignin. *Nature* 183 (1959) 1152–1155.

Friedman R., Levin N., Altman A. Presence and identification of polyamines in xylem and phloem exudates of plants. *Plant Physiol.* 82 (1986) 1154-1157.

Froechlich D.M., Fehr W.R. Agronomic performance of soybeans with differing levels of iron deficiency chlorosis on calcareous soil. *J. Trop. Crop Sci.* 21 (1981) 438-441.

Frohlich A., Gaupels F., Sarioglu H., Holzmeister C., Spannagl M., Durner J.R., Lindermayr C. Looking deep inside: detection of low-abundance proteins in leaf extracts of *Arabidopsis* and phloem exudates of pumpkin. *Plant Physiol.* 159 (2012) 902-914.

Fu J., Zhou Q., Liu J., Liu W., Wang T., Zhang Q., Jiang G. High levels of heavy metals in rice (*Oryza sativa* L.) from a typical E-waste recycling area in southeast China and its potential risk to human health. *Chemosphere* 71 (2008) 1269-75.

Führs H., Specht A., Erban A., Kopka J., Horst W.J. Functional associations between the metabolome and manganese tolerance in *Vigna unguiculata*. *J. Exp. Bot.* 63 (2012) 329-340.

Führs H., Behrens C., Gallien S., Heintz D., Van Dorsselaer A., Braun H.P., Horst W.J. Physiological and proteomic characterization of manganese sensitivity and tolerance in rice (*Oryza sativa*) in comparison with barley (*Hordeum vulgare*). *Ann. Bot.* 105 (2010) 1129-1140.

Führs H., Götze S., Specht A., Erban A., Gallien S.B., Heintz D., Van Dorsselaer A., Kopka J., Braun H.P., Horst W.J. Characterization of leaf apoplastic peroxidases and metabolites in *Vigna unguiculata* in response to toxic manganese supply and silicon. *J. Exp. Bot.* 60 (2009) 1663-1678.

Führs H., Hartwig M., Molina L.E., Heintz D., Van Dorsselaer A., Braun H., Horst W.J. Early manganese-toxicity response in *Vigna unguiculata* L. A proteomic and transcriptomic study. *Proteomics* 8 (2008) 149-159.

Fukao Y., Ferjani A., Tomioka R., Nagasaki N., Kurata R., Nishimori Y., Fujiwara M., Maeshima M. iTRAQ analysis reveals mechanisms of growth defects due to excess zinc in *Arabidopsis. Plant Physiol.* 155 (2011) 1893-1907.

Fukuda H. Xylogenesis: initiation, progression, and cell death. *Annu. Rev. Plant Biol.* 47 (1996) 199-325.

Ezaki B., Sasaki K., Matsumoto H., Nakashima S. Functions of two genes in aluminium (Al) stress resistance: repression of oxidative damage by the *AtBCB* gene and promotion of efflux of Al ions by the *NtGDI1*gene. *J. Exp. Bot.* 56 (2005) 2661–2671.

Furukawa J., Yamaji N., Wang H., Mitani N., Murata Y., Sato K., Katsuhara M., Takeda K., Ma J.F. An aluminum-activated citrate transporter in barley. *Plant Cell Physiol.* 48 (2007) 1081-1091.

Gangwar S., Singh V.P., Maurya J.N. Responses of *Pisum sativum* L. to exogenous indole acetic acid application under manganese toxicity. *Bull Environ Contam Toxicol.* 86 (2011) 605.

Gangwar S., Singh V.P., Prasad S.M., Maurya J.N. Modulation of manganese toxicity in *Pisum sativum* L. seedlings by kinetin. *Sci. Hort.* 126 (2010) 467–474.

Geilfus C.M., Mithöfer A., Ludwig-Müller J., Zörb C., Muehling K.H.C. Chloride-inducible transient apoplastic alkalinizations induce stomata closure by controlling abscisic acid distribution between leaf apoplast and guard cells in salt-stressed *Vicia faba. New Phytol.* 208 (2015) 803-816.

Gendre D., Czernic P., Conéjéro G., Pianelli K., Briat J.F., Lebrun M., Mari S. TcYSL3, a member of the YSL gene family from the hyper-accumulator *Thlaspi caerulescens*, encodes a nicotianamine-Ni/Fe transporter. *Plant J.* 49 (2007) 1-15.

George T.S., French A.S., Brown L.K., Karley A.J., White P.J., Ramsay L., Daniell T.J. Genotypic variation in the ability of landraces and commercial cereal varieties to avoid manganese deficiency in soils with limited manganese availability: is there a role for root-exuded phytases? *Physiol. Plant.* 151 (2014) 243-256.

Ghanem M.E., Albacete A., Smigocki A.C., Frébort I., Pospísilová H., Martínez-Andújar C. Acosta M., Sánchez-Bravo J., Lutts S., Dodd I.C., Pérez-Alfocea F. Root-synthesized cytokinins improve shoot growth and fruit yield in salinized tomato (*Solanum lycopersicum L.*) plants. *J. Exp. Bot.* 62 (2011) 125-140.

Gherardi M.J., Rengel Z. The effect of manganese supply on exudation of carboxylates by roots of lucerne (*Medicago sativa*). *Plant Soil* 260 (2004) 271-282.

Giavalisco P., Kapitza K., Kolasa A., Buhtz A., Kehr J. Towards the proteome of *Brassica napus* phloem sap. *Proteomics* 6 (2006) 896-909.

Gibbs G.M., Scanlon M.J., Swarbrick J., Curtis S., Gallant E., Dulhunty A.F., O'Bryan M.K. The cysteine-rich secretory protein domain of Tpx-1 is related to ion channel toxins and regulates ryanodine receptor Ca^{2+} signaling. *J. Biol. Chem.* 281 (2006) 4156-63.

Gilbert F.A. Mineral nutrition and the balance of life. *Soil Science* 85 (1958) 291.

Girard A.L., Mounet F., Lemaire-Chamley M., Gaillard C.D., Elmorjani K., Vivancos J., Runavot J.L., Quemener B., Petit J., Germain V.R., Rothan C., Marion D., Bakan B.N.D. Tomato GDSL1 is required for cutin deposition in the fruit cuticle. *Plant Cell* 24 (2012) 3119-3134.

Gollhofer J., Timofeev R., Lan P., Schmidt W., Buckhout T.J. Vacuolar-Iron-Transporter1-Like proteins mediate iron homeostasis in *Arabidopsis. PLOS ONE* 9 (2014) 110468.

Gómez G., Pallás V. A long-distance translocatable phloem protein from cucumber forms a ribonucleoprotein complex in vivo with hop stunt viroid RNA. *J. Virol.* 78 (2004) 10104-10110.

Gong X., Wang Y., Liu C., Wang S., Zhao X., Zhou M., Li N., Lu Y., Hong F. Effects of manganese deficiency on spectral characteristics and oxygen evolution in maize chloroplasts. *Biol. Trace Elem. Res.* 136 (2010) 372-382.

González A., Steffen K.L., Lynch J.P. Light and excess manganese. Implications for oxidative stress in common bean. *Plant Physiol.* 118 (1998) 493-504.

González-Fernández R., Aloria K., Arizmendi J.M., Jorrin-Novo J.V. Application of label-free shotgun nUPLC-MSE and 2-DE approaches in the study of *Botrytis cinerea Mycelium. J. Proteome Res.* 12 (2013) 3042-3056.

González-Vallejo E.B., Morales F., Cistué L., Abadía A., Abadía J. Iron deficiency decreases the Fe(III)-chelate reducing activity of leaf protoplasts. *Plant Physiol.* 122 (2000) 337-344.

Goodger J.Q.D., Sharp R.E., Marsh E.L., Schachtman D.P. Relationships between xylem sap constituents and leaf conductance of well-watered and water-stressed maize across three xylem sap sampling techniques. *J. Exp. Bot.* 56 (2005) 2389-2400.

Goshe M., Smith R. Stable isotope-coded proteomic mass spectrometry. *Curr. Opin. Biotechnol.* 14 (2003) 101-109.

Goulet C., Goulet C., Goulet M.C., Michaud D. 2-DE proteome maps for the leaf apoplast of *Nicotiana benthamiana*. *J. Proteomics* 10 (2010) 2536-2544.

Graham M.H., Haynes R.J., Meyer J.H. Changes in soil chemistry and aggregate stability induced by fertilizer applications, burning and trash retention on a long-term sugarcane experiment in South Africa. *Eur. J. Soil Sci.* 53 (2002) 589-598.

Green L.S., Rogers E.E. FRD3 controls iron localization in *Arabidopsis. Plant Physiol.* 136 (2004) 2523-2531.

Griffith M., Ala P., Yang D.S.C., Hon W.C., Moffatt B.A. Antifreeze protein produced endogenously in winter rye leaves. *Plant Physiol.* 100 (1992) 593-596.

Grotz N., Guerinot M.L. Molecular aspects of Cu, Fe and Zn homeostasis in plants. *BBA-Molecular Cell Research* 1763 (2006) 595-608.

Guerinot M.L. Improving rice yield-ironing out the details: Engineering crops to release more iron-solubilizing chelators may increase their yield in alkaline soils. *Nat. Biotechnol.* 19 (2001) 417-418.

Guerinot M.L., Yi Y. Iron: nutritious, noxious, and not readily available. *Plant Physiol.* 104 (1994) 815-820.

Guo J.H., Liu X.J., Zhang Y., Shen J.L., Han W.X., Zhang W.F., Christie P., Goulding K.W., Vitousek P.M., Zhang F.S. Significant acidification in major Chinese croplands. *Science* 327 (2010) 1008-1010.

Gutierrez-Carbonell E., Takahashi D., Lüthje S., González-Reyes J.A., Mongrand S., Contreras-Moreira B., Abadía A., Uemura M., Abadía J., López-Millán A.F. A shotgun proteomic approach reveals that Fe deficiency causes marked changes in the protein profiles of plasma membrane and detergent-resistant microdomain preparations from *Beta vulgaris* roots. *J. Proteome Res.* 15 (2016) 2510-2524.

Gutierrez-Carbonell E., Lattanzio G., Albacete A., Rios J.J., Kehr J., Abadía A., Grusak M.A., Abadía J., López-Millán A.F. Effects of Fe deficiency on the protein profile of *Brassica napus* phloem sap. *Proteomics* 15 (2015) 3835-3853.

Gutierrez-Carbonell E., Takahashi D., Lattanzio G., Rodríguez-Celma J., Kehr J., Soll J., Philippar K., Uemura M., Abadía J., López-Millán A.F. The distinct functional roles of the inner and outer chloroplast envelope of pea (*Pisum sativum*) as revealed by proteomic approaches. *J. Proteome Res.* 13 (2014) 2941-2953.

Gutierrez-Carbonell E., Lattanzio G., Sagardoy R., Rodríguez-Celma J., Ríos Ruiz J.J., Matros A., Abadía A., Abadía J., López-Millán A.F. Changes induced by zinc toxicity in the 2-DE protein profile of sugar beet roots, *J. Proteomics* 94 (2013) 149-161.

Gygi S., Rist B., Gerber S., Turecek F., Gelb M., Aebersold R. Quantitative analysis of complex protein mixtures using isotope-coded affinity tags. *Nat Biotechnol* 17 (1999) 994-999.

Hannam R.J., Ohki K. Detection of manganese deficiency and toxicity in plants. In: ‘ Manganese in soils and plants’. Proceedings of the international symposium on 'Manganese in soils and plants'. (Eds. R.D. Graham, R.J. Hannam, N.C.Uren) *Springer* (1988) 243-259.

Hansen N.C., Hopkins B.G., Ellsworth J.W., Jolley V.D. Iron nutrition in field crops. In: ‘Iron nutrition in plants and rhizospheric microorganisms’. (Eds. L.L. Barton, J. Abadía) *Springer* (2006) 23-59.

Hao Q., Yin P., Li W., Wang L., Yan C., Lin Z., Wu J.Z., Wang J., Yan S.F., Yan N. The molecular basis of ABA-independent inhibition of PP2Cs by a subclass of PYL proteins. *Mol. Cell.* 42 (2011) 62-672.

Harada E., Sugase K., Namba K., Iwashita T., Murata Y. Structural element responsible for the Fe(III)-phytosiderophore specific transport by HvYS1 transporter in barley. *FEBS Letters* 581 (2007) 4298-4302.

Hartung W.E., Radin J.W. Auxin and cytokinins in the apoplasmic solution of dehydrated cotton leaves. *J. Plant Physiol.* 140 (1992) 324-327.

Harry J.L., Wilkins M.R., Herbert B.R., Packer N.H., Gooley A.A., Williams K.L. Proteomics: capacity *versus* utility. *Electrophoresis* 21 (2000) 1071-1081.

Haydon M.J., Cobbett C.S. Transporters of ligands for essential metal ions in plants: Research review. *New Phytol.* 174 (2007) 499-506.

Heazlewood J.L., Tonti-Filippini J.S., Gout A.M., Day D.A., Whelan J., Millar A.H. Experimental analysis of the *Arabidopsis* mitochondrial proteome highlights signaling and regulatory components, provides assessment of targeting prediction programs, and indicates plant-specific mitochondrial proteins. *Plant Cell* 16 (2004) 241-256.

Hebbern C.A., Pedas P., Schjoerring J.K., Knudsen L., Husted S. Genotypic differences in manganese efficiency: field experiments with winter barley (*Hordeum vulgare* L.). *Plant Soil* 272 (2005) 233-244.

Heckman J.R. Can soil fertility influence tomato flavor? *New Jersey Annual Vegetable Meeting Proceedings* (2008) 11-13.

Hell R., Stephan U.W. Iron uptake, trafficking and homeostasis in plants. *Planta* 216 (2003) 541-551.

Hemmingsen S.M., Woolford C., Van Der Vies S.M., Tilly K., Dennis D.T., Georgopoulos C.P., Hendrix R.W., Ellis R.J. Homologous plant and bacterial proteins chaperone oligomeric protein assembly. *Nature* 333 (1988) 330-334.

Herbik A., Koch G., Mock H.P., Dushkov D., Czihal A., Thielmann J., Stephan U.W. Isolation, characterization and cDNA cloning of nicotianamine synthase from barley. *Eur. J. Biochem.* 265 (1999) 231-239.

Hernandez-Soriano M.C., Degryse F., Lombi E., Smolders E. Manganese toxicity in barley is controlled by solution manganese and soil manganese speciation. *Soil Sci. Soc. Am. J.* 76 (2012) 399-407.

Herren T., Feller U. Transfer of zinc from xylem to phloem in the peduncle of wheat. *J. Plant Nutr.* 17 (1994) 1587-1598.

Hicks S.N., Jezyk M.R., Gershburg S., Seifert J.P., Harden T.K., Sondek J. General and versatile autoinhibition of PLC isozymes. *Mol. Cell* 31 (2008) 383-394.

Higuchi K., Suzuki K., Nakanishi H., Yamaguchi H., Nishizawa N.K., Mori S. Cloning of nicotianamine synthase genes, novel genes involved in the biosynthesis of phytosiderophores. *Plant Physiol.* 119 (1999) 471-480.

Hirakawa Y., Kondo Y., Fukuda H. TDIF peptide signaling regulates vascular stem cell proliferation *via* the WOX4 homeobox gene in *Arabidopsis. Plant Cell* 22 (2010) 2618-2629.

Hirakawa Y., Shinohara H., Kondo Y., Inoue A., Nakanomyo I., Ogawa M., Sawa S., Ohashi-Ito K., Matsubayashi Y., Fukuda H. Non-cell-autonomous control of vascular stem cell fate by a CLE peptide/receptor system. *Proc. Natl. Acad. Sci. U.S.A.* 105 (2008) 15208-15213.

Hirose N., Takei K., Kuroha T., Kamada-Nobusada T., Hayashi H., Sakakibara H. Regulation of cytokinin biosynthesis, com-partmentalization and translocation. *J. Exp. Bot.* 59 (2008) 75-83.

Hirschi K.D., Korenkov V.D., Wilganowski N.L., Wagner G.J. Expression of *Arabidopsis* CAX2 in tobacco. Altered metal accumulation and increased manganese tolerance. *Plant Physiol.* 124 (2000) 125-133.

Holk A., Rietz S., Zahn M., Quader H., Scherer G.F.E. Molecular identification of cytosolic, patatin-related phospholipases a from *Arabidopsis* with potential functions in plant signal transduction. *Plant Physiol.* 130 (2002) 90-101.

Hopff D., Wienkoop S., Lüthje S. The plasma membrane proteome of maize roots grown under low and high iron conditions. *J Proteomics* 91 (2013) 605-618.

Horst W.J., Maier P. Compartmentation of manganese in the vacuoles and in the apoplast of leaves in relation to genotypic manganese leaftissue tolerance in *Vigna unguiculata* (L.) Walp. In: 'Plant nutrition-molecular biology and genetics'. (Eds. G Gissel-Nielsen, A Jensen) *Kluwer Academic Publishers* (1999) 223-234.

Horst W.J. The physiology of manganese toxicity. In: 'Manganese in soils and plants'. Proceedings of the international symposium on 'Manganese in soils and plants'. (Eds. R.D. Graham, R.J. Hannam, N.C. Uren) *Springer* (1988) 175-188.

Hoson T. Apoplast as the site of response to environmental signals. *J. Plant Res.* 111 (1998) 167-177.

Hossain Z., Khatoon A., Komatsu S. Soybean proteomics for unraveling abiotic stress response mechanism. *J. Proteome Res.* 12 (2013) 4670-4684.

Huang S., Jacoby R.P., Millar A.H., Taylor N.L. Plant mitochondrial proteomics. In: 'Plant proteomics: methods and protocols'. (Eds. J.V. Jorrin-Novo, S. Komatsu, W. Weckwerth, S. Wienkoop) *Humana Press* (2014) 499-525.

Huber D.M., Graham R.D. The role of nutrition in crop resistance and tolerance to disease. In: 'Mineral nutrition of crops fundamental mechanisms and implications'. (Ed. Z. Rengel) *Food Product Press* (1999) 205-226.

Hummel J., Niemann M., Wienkoop S., Schulze W., Steinhauser D., Selbig J., Walther D., Weckwerth W. ProMEX: a mass spectral reference database for proteins and protein phosphorylation sites. *BMC Bioinformatics* 8 (2007) 216.

Hurkman W.J., Tanaka C.K. Solubilization of plant membrane proteins for analysis by two-dimensional gel electrophoresis. *Plant Physiology* 81 (1986) 802-806.

Husted S., Laursen K.H., Hebbern C.A., Schmidt S.B., Pedas P., Haldrup A., Jensen P.E. Manganese deficiency leads to genotype-specific changes in fluorescence induction kinetics and state transitions. *Plant Physiol.* 150 (2009) 825-833.

Husted S., Schjoerring J.K. Apoplastic pH and ammonium concentration in leaves of *Brassica napus* L. *Plant Physiol.* 109 (1995) 1453-1460.

Imberty A., Goldberg R., Catesson A.M. Isolation and characterization of *Populus isoperoxidases* involved in the last step of lignin formation. *Planta* 164 (1985) 221-226.

Inoue H., Mizuno D., Takahashi M., Nakanishi H., Mori S., Nishizawa N.K. A rice FRD3-like (OsFRDL1) gene is expressed in the cells involved in long-distance transport. *J. Soil Sci. Plant Nutr.* 50 (2004) 1133-1140.

Irwin P.L., Sevilla M.D., Chamulitrat W. Homopolygalacturonan molecular size in plant cell wall matrices *via* paramagnetic ion and nitroxyl amide dipolar spin-spin interactions. *Biophys. J.* 54 (1988) 337-344.

Ishimaru Y., Takahashi R., Bashir K., Shimo H., Senoura T., Sugimoto K., Ono K., Yano M., Ishikawa S., Arao T., Nakanishi H., Nishizawa N.K. Characterizing the role of rice NRAMP5 in manganese, iron and cadmium transport. *Sci. Rep.* 2 (2012) 286.

Ishimaru Y., Suzuki M., Tsukamoto T., Suzuki K., Nakazono M., Kobayashi T., Wada Y., Watanabe S., Matsuhashi S., Takahashi M., Nakanishi H., Mori S., Nishizawa N. Rice plants take up iron as an Fe^{3+}-phytosiderophore and as Fe^{2+}. *Plant J* 45 (2006) 335-346.

Ishiwatari Y., Honda C., Kawashima I., Nakamura S.I., Hirano H., Mori S., Fujiwara T., Hayashi H., Chino M. Thioredoxin h is one of the major proteins in rice phloem sap. *Planta* 195 (1995) 456-463.

Islam E., Yang X., He Z., Mahmood Q. Assessing potential dietary toxicity of heavy metals in selected vegetables and food crops. *J. Zhejiang Univ. Sci. B* 8 (2007) 1-13.

Islas-Flores I., Alcocer-Alvarez C., Sánchez-Rodríguez Y.A., Canto-Canché B. Recovery of active pathogenesis-related enzymes from the apoplast of *Musa acuminata* infected by *Mycosphaerella fijiensis. Afr. J. Biotechnol*. 14 (2015) 1970-1981.

Ito Y., Nakanomyo I., Motose H., Iwamoto K., Sawa S., Dohmae N., Fukuda H. Dodeca-CLE peptides as suppressors of plant stem cell differentiation. *Science* 313 (2006) 842.

Jain A., Wilson G., Connolly E. The diverse roles of FRO family metalloreductases in iron and copper homeostasis. *Front. Plant Sci.* 5 (2014).

Jeong J., Connolly E.L. Iron uptake mechanisms in plants: Functions of the FRO family of ferric reductases. *Plant Sci.* 176 (2009) 709-714.

Jeong J., Cohu C., Kerkeb L., Pilon M., Connolly E.L., Guerinot M.L. Chloroplast Fe(III) chelate reductase activity is essential for seedling viability under iron limiting conditions. *Proc. Natl. Acad. Sci. U.S.A.* 105 (2008) 10619-10624.

Jiang W.Z. Mn use efficiency in different wheat cultivars. *Environmental and Experimental Botany* 57 (2006) 41-50.

Johansson A., Staal J., Dixelius C. Early responses in the *Arabidopsis-Verticillium longisporum* pathosystem are dependent on NDR1, JA- and ET-associated signals *via* cytosolic NPR1 and RFO1. *Mol. Plant-Microbe Interact.* 19 (2006) 958-969.

Joosten M.H., De Wit P.J. Identification of several pathogenesis-related proteins in tomato leaves inoculated with *Cladosporium fulvum* (syn. *Fulvia fulva*) as 1,3-beta-glucanases and chitinases. *Plant Physiol.* 89 (1989) 945-951.

Jorrín-Novo J.V., Pascual J., Sánchez-Lucas R., Romero-Rodríguez M.C., Rodríguez-Ortega M.J., Lenz C., Valledor L. Fourteen years of plant proteomics reflected in Proteomics: moving from model species and 2DE-based approaches to orphan species and gel-free platforms. *Proteomics* 15 (2015) 1089-1112.

Jorrín-Novo J., Maldonado A., Echevarría-Zomeño S., Valledor L., Castillejo M., Curto M., Valero J., Sghaier B., Donoso G., Redondo I. Plant proteomics update (2007-2008): Second-generation proteomic techniques, an appropriate experimental design, and data analysis to fulfill MIAPE standards, increase plant proteome coverage and expand biological knowledge. *J. Proteomics* 72 (2009) 285-314.

Jorrín-Novo J.V., Maldonado A.M., Castillejo M.A. Plant proteome analysis: A 2006 update. *Proteomics* 7 (2007) 2947-2962.

Joyard J., Ferro M., Masselon C., Seigneurin-Berny D., Salvi D., Garin J., Rolland N. Chloroplast proteomics highlights the subcellular compartmentation of lipid metabolism. *Prog. Lipid Res.* 49 (2010) 128-158.

Kaida R., Serada S., Norioka N., Norioka S., Neumetzler L., Pauly M., Sampedro J., Zarra I., Hayashi T., Kaneko T.S. Potential role for purple acid phosphatase in the dephosphorylation of wall proteins in tobacco cells. *Plant Physiol.* 153 (2010) 603-610.

Kamiya T., Akahori T., Maeshima M. Expression profile of the genes for rice cation/H^+ exchanger family and functional analysis in yeast. *Plant Cell Physiol.* 46 (2005) 1735-1740.

Kamiya T., Maeshima M. Residues in internal repeats of the rice cation/H^+ exchanger are involved in the transport and selection of cations. *J. Biol. Chem.* 279 (2004) 812-819.

Kang Y.H., Hardtke C.S. *Arabidopsis* MAKR5 is a positive effector of BAM3-dependent CLE45 signaling. *EMBO Reports* 17 (2016) 1145-1154.

Karhumaa P L.J., Parkkila S, Kaunisto K, Tapanainen J, Rajaniemi H. The identification of secreted carbonic anhydrase VI as a constitutive glycoprotein of human and rat milk. *Proc. Natl. Acad. Sci. U.S.A.* 98 (2001) 11604–8.

Kärkönen A., Koutaniemi S., Mustonen M., Syrjänen K., Brunow G., Kilpeläinen I., Teeri T.H., Simola L.K. Lignification related enzymes in picea abies suspension cultures. *Physiol. Plant.* 114 (2002) 343-353.

Karley A.J., White P.J. Moving cationic minerals to edible tissues: potassium, magnesium, calcium. *Curr. Opin. Plant Biol.* 12 (2009) 291-298.

Katoh H., Hagino N., Grossman A.R., Ogawa T. Genes essential to iron transport in the cyanobacterium *Synechocystis* sp. strain PCC 6803. *Journal of Bacteriology* 183 (2001) 2779-2784.

Kawano T. Roles of the reactive oxygen species-generating peroxidase reactions in plant defense and growth induction. *Plant Cell. Rep.* 21 (2003) 829-837.

Kehr J., Rep M. Protein extraction from xylem and phloem sap. In: 'Plant proteomics: methods and protocols' (Eds. H. Thiellement, M. Zivy, C. Damerval, V. Méchin) *Humana Press* (2007) 27-35.

Kehr J., Buhtz A., Giavalisco P. Analysis of xylem sap proteins from *Brassica napus. BMC Plant Biology* 5 (2005) 11.

Kenan D.J., Query C.C., Keene J.D. RNA recognition: towards identifying determinants of specificity. *Trends Biochem. Sci.* 16 (1991) 214-220.

Khandakar J., Haraguchi I., Yamaguchi K., Kitamura Y. A small-scale proteomic approach reveals a survival strategy, including a reduction in alkaloid biosynthesis, in *Hyoscyamus albus* roots subjected to iron deficiency. *Front. Plant Sci.* 4 (2013) 331.

Kieffer P., Planchon S., Oufir M., Ziebel J., Dommes J., Hoffmann L. Combining proteomics and metabolite analyses to unravel cadmium stress-response in poplar leaves. *J Proteome Res* 8 (2009) 400-17.

Kieffer P., Dommes J., Hoffmann L., Hausman J., Renaut J. Quantitative changes in protein expression of cadmium exposed poplar plants. *Proteomics* 8 (2008) 2514-30.

Kim J.Y., Wu J., Kwon S.J., Oh H., Lee S.E., Kim S.G., Wang Y., Agrawal G.K., Rakwal R., Kang K.Y., Ahn I.P., Kim B.-G., Kim S.T. Proteomics of rice and *Cochliobolus miyabeanus* fungal interaction: Insight into proteins at intracellular and extracellular spaces. *J. Proteomics* 14 (2014) 2307-2318.

Kim S.A., Guerinot M.L. Mining iron: Iron uptake and transport in plants. *FEBS Letters* 581 (2007) 2273-2280.

Kim S.A., Punshon T., Lanzirotti A., Li L., Alonso J.M., Ecker J.R., Kaplan J., Guerinot M.L. Localization of iron in *Arabidopsis* seed requires the vacuolar membrane transporter VIT1. *Science* 314 (2006) 1295-1298.

Kim S.G., Wang Y., Lee K.H., Park Z.-Y., Park J., Wu J., Kwon S.J., Lee Y.H., Agrawal G.K., Rakwal R., Kim S.T., Kang K.Y. In-depth insight into in vivo apoplastic secretome of rice-*Magnaporthe oryzae* interaction. *J. Proteomics* 78 (2013) 58-71.

Kim S.H., Roux S.J. An *Arabidopsis* Ran-binding protein, AtRanBP1c, is a co-activator of Ran GTPase-activating protein and requires the C-terminus for its cytoplasmic localization. *Planta* 216 (2003) 1047-1051.

Kim S.H., Arnold D., Lloyd A., Roux S.J. Antisense expression of an *Arabidopsis* Ran binding protein renders transgenic roots hypersensitive to auxin and alters auxin-induced root growth and development by arresting mitotic progress. *Plant Cell* 13 (2001) 2619-2630.

Kim S.Y., Kim B.H., Lim C.J., Lim C.O., Nam K.H. Constitutive activation of stress-inducible genes in a brassinosteroid-insensitive 1 (*bri1*) mutant results in higher tolerance to cold. *Physiol. Plant.* 138 (2010) 191-204.

Kirk G.J.D. Rice root properties for internal aeration and efficient nutrient acquisition in submerged soil. *New Phytol.* 159 (2003) 185-194.

Klinghammer M., Tenhaken R. Genome-wide analysis of the UDP-glucose dehydrogenase gene family in *Arabidopsis*, a key enzyme for matrix polysaccharides in cell walls. *J. Exp. Bot.* 58 (2007) 3609-3621.

Klose J. Protein mapping by combined isoelectric focusing and electrophoresis of mouse tissues. A novel approach to testing for induced point mutations in mammals. *Humangenetik*, 26 (1975) 231-43.

Ko, M.K., Jeon, W.B., Kim, K.S. Lee H.H., Seo H.H., Kim Y.S., Oh B.J. A *Colletotrichum gloeosporioides*-induced esterase gene of nonclimacteric pepper (*Capsicum annuum*) fruit during ripening plays a role in resistance against fungal infection. *Plant Mol. Biol.* 58 (2005) 529.

Koike S., Inoue H., Mizuno D., Takahashi M., Nakanishi H., Mori S., Nishizawa N.K. OsYSL2 is a rice metal-nicotianamine transporter that is regulated by iron and expressed in the phloem. *Plant J.* 39 (2004) 415-424.

Koller A., Washburn M.P., Lange B.M., Andon N.L., Deciu C., Haynes P.A., Hays L., Schieltz D., Ulaszek R., Wei J., Wolters D., Yates J.R. Proteomic survey of metabolic pathways in rice. *Proc. Natl. Acad. Sci. U.S.A.* 99 (2002) 11969-11974.

Korcak R.F. Satisfying and altering edaphic requirements for acidophilic plants. *J. Plant Nutr.* 10 (1987) 1071-1078.

Kosová K., Vítámvás P., Prásil I.T., Renaut J. Plant proteome changes under abiotic stress - Contribution of proteomics studies to understanding plant stress response. *J. Proteomics* 74 (2011) 1301-1322.

Kranzler C., Lis H., Finkel O.M., Schmetterer G., Shaked Y., Keren N. Coordinated transporter activity shapes high-affinity iron acquisition in cyanobacteria. *The ISME Journal* 8 (2014) 409-417.

Kreps J.A., Wu Y., Chang H.S., Zhu T., Wang X., Harper J.F. Transcriptome changes for *Arabidopsis* in response to salt, osmotic, and cold stress. *Plant Physiol.* 230 (2002) 2129-2141.

Kriedemann P.E., Graham R.D., Wiskich J.T. Photosynthetic dysfunction and *in vivo* changes in chlorophyll a fluorescence from manganese-deficient wheat leaves. *Aust. J. Agric. Res.* 36 (1985) 157-169.

Krishnan H.B., Natarajan S.S., Bennett J.O., Sicher R.C. Protein and metabolite composition of xylem sap from field-grown soybeans (*Glycine max*). *Planta* 233 (2011) 921-931.

Krüger C., Berkowitz O., Stephan U.W., Hell R. A metal-binding member of the Late Embryogenesis Abundant protein family transports iron in the phloem of *Ricinus communis* L. *J. Biol. Chem.* 277 (2002) 25062-25069.

Kubota H., Hynes G., Willison K. The chaperonin containing t-complex polypeptide 1 (TCP-1): Multisubunit machinery assisting in protein folding and assembly in the eukaryotic cytosol. *Eur. J. Biochem.* 230 (1995) 3-16.

Kurepa J., Smalle J.A. Structure, function and regulation of plant proteasomes. *Biochimie* 90 (2008) 324-335.

Kushnir S., Babiychuk E., Storozhenko S., Davey M.W., Papenbrock J., De Rycke R., Engler G., Stephan U.W., Lange H., Kispal G., Lill R., Van Montagu M. A mutation of the mitochondrial ABC transporter Sta1 leads to dwarfism and chlorosis in the *Arabidopsis* mutant starik. *Plant Cell* 13 (2001) 89-100.

La Camera S., Gouzerh G., Dhondt S., Hoffmann L., Fritig B., Legrand M., Heitz T. Metabolic reprogramming in plant innate immunity: The contributions of phenylpropanoid and oxylipin pathways. *Immunol. Rev.* 198 (2004) 267-284.

Lafarguette F., Leple J.C., Dejardin A., Laurans F., Costa G., Lesage-Descauses M.C., Pilate G. Poplar genes encoding fasciclin-like arabinogalactan proteins are highly expressed in tension wood. *New Phytol.* 164 (2004) 107-121.

Lan P., Li W., Wen T.N., Shiau J.Y., Wu Y.C., Lin W., Schmidt W. iTRAQ protein profile analysis of *Arabidopsis* roots reveals new aspects critical for iron homeostasis. *Plant Physiol.* 155 (2011) 821-834.

Lanquar V., Ramos M.S., Lelievre F.O., Barbier-Brygoo H.L.N., Krieger-Liszkay A., Kramer U., Thomine S.B. Export of vacuolar manganese by AtNRAMP3 and AtNRAMP4 is required for optimal photosynthesis and growth under manganese deficiency. *Plant Physiol.* 152 (2010) 1986-1999.

Lanquar V., Lelievre F.O., Bolte S., Hames C.C., Alcon C., Neumann D., Vansuyt G.R., Curie C., Schroder A., Kramer U., Barbier-Brygoo H.L.N., Thomine S. Mobilization of vacuolar iron by AtNRAMP3 and AtNRAMP4 is essential for seed germination on low iron. *EMBO J.* 24 (2005) 4041-4051.

Larbi A., Abadía A., Morales F., Abadía J. Fe resupply to Fe-deficient sugar beet plants leads to rapid changes in the violaxanthin cycle and other photosynthetic characteristics without significant *de novo* chlorophyll synthesis. *Photosynth. Res.* 79 (2004) 59-69.

Lattanzio G., Andaluz S., Matros A., Calvete J.J., Kehr J., Abadía A., Abadía J., López-Millán A.F. Protein profile of *Lupinus texensis* phloem sap exudates: Searching for Fe- and Zn-containing proteins. *Proteomics* 13 (2013) 2283-2296.

Lavres J., Malavolta E., Nogueira N.L., Moraes M.F., Reis A.R., Rossi M.L. and Cabral C.P. Changes in anatomy and root cell ultrastructure of soybean genotypes under manganese stress. *Rev. Bras. Cienc. Solo* 33 (2009) 395-403.

Lee T.J., Luitel B.P., Kang W.H. Growth and physiological response to manganese toxicity in Chinese cabbage (*Brassica rapa* L. ssp. campestris). *Hortic. Environ. Biotechnol.* 52 (2011) 252-258.

Leinonen J P.S., Kaunisto K, Koivunen P, Rajaniemi H. Secretion of carbonic anhydrase isoenzyme VI (CA VI) from human and rat lingual serous von Ebner's glands. *J. Histochem. Cytochem.* 49 (2001) 657–62.

Lewandowska D., ten Have S., Hodge K., Tillemans V., Lamond A.I., Brown J.W.S. Plant SILAC: stable-isotope labelling with amino acids of *Arabidopsis* seedlings for quantitative proteomics. *PLOS ONE* 8 (2013) 72207.

Li B., Takahashi D., Kawamura Y., Uemura M. Comparison of plasma membrane proteomic changes of *Arabidopsis* suspension-cultured cells (T87 Line) after cold and ABA treatment in association with freezing tolerance development. *Plant Cell Physiol.* 53 (2012) 543-554.

Li G., Peng X., Xuan H., Wei L., Yang Y., Guo T., Kang G. Proteomic analysis of leaves and roots of common wheat (*Triticum aestivum* L.) under copper-stress conditions. *J. Proteome Res.* 12 (2013) 4846-4861.

Li J., Wu X.D., Hao S.T., Wang X.J., Ling H.Q. Proteomic response to iron deficiency in tomato root. *Proteomics* 8 (2008) 2299-2311.

Li L., Chen O.S., Ward D.M., Kaplan J. CCC1 is a transporter that mediates vacuolar iron storage in yeast. *J. Biol. Chem.* 276 (2001) 29515-29519.

Li T., Xu S.L., Oses-Prieto J.A., Putil S., Xu P., Wang R.J., Li K.H., Maltby D.A., An L.H., Burlingame A.L., Deng Z.P., Wang Z.Y. Proteomics analysis reveals post-translational mechanisms for cold-induced metabolic changes in *Arabidopsis. Mol. Plant* 4 (2011) 361-374.

Li Z., Phillip D., Neuhäuser B., Schulze W.X., Ludewig U. Protein dynamics in young maize root hairs in response to macro- and micronutrient deprivation. *J. Proteome Res.* 14 (2015) 3362-3371.

Liang C., Tian J., Liao H. Proteomics dissection of plant responses to mineral nutrient deficiency. *Proteomics* 13 (2013) 624-636.

Liao C., Liu R., Zhang F., Li C., Li X. Nitrogen under- and oversupply induces distinct protein responses in maize xylem sap. *J. Integr. Plant Biol.* 54 (2012) 374-387.

Lidon F.C., Barreiro M., Ramalho J.C. Manganese accumulation in rice: implications for photosynthetic functioning. *J. Plant Physiol.* 161 (2004) 1235-1244.

Ligat L., Lauber E., Albenne C., Clemente H.S., Valot B., Zivy M., Pont-Lezica R., Arlat M., Jamet E. Analysis of the xylem sap proteome of *Brassica oleracea* reveals a high content in secreted proteins. *Proteomics* 11 (2011) 1798-1813.

Lin M.K., Lee Y.J., Lough T.J., Phinney B.S., Lucas W.J. Analysis of the pumpkin phloem proteome provides insights into angiosperm sieve tube function. *Mol. Cell. Proteomics* 8 (2009) 343-356.

Lin S., Cianzio S., Shoemaker R. Mapping genetic loci for iron deficiency chlorosis in soybean. *Mol. Breed.* 3 (1997) 219-229.

Lindsay W.L., Schwab A.P. The chemistry of iron in soils and its availability to plants. *J. Plant Nutr.* 5 (1982) 821-840.

Ling H.Q., Koch G., Bäumlein H., Ganal M.W. Map-based cloning of *chloronerva*, a gene involved in iron uptake of higher plants encoding nicotianamine synthase. *Proc. Natl. Acad. Sci. U.S.A.* 96 (1999) 7098-7103.

Liu H., Sadygov R.G., Yates J.R. A model for random sampling and estimation of relative protein abundance in shotgun proteomics. *Anal. Chem.* 76 (2004) 4193-4201.

Lohaus G., Pennewiss K., Sattelmacher B., Hussmann M., Hermann Muehling K. Is the infiltration-centrifugation technique appropriate for the isolation of apoplastic fluid? A critical evaluation with different plant species. *Physiol. Plant* 111 (2001) 457-465.

Loneragan J.F. Distribution and movement of manganese in plants. In: 'Manganese in soils and plants'. (Eds. R.D. Graham, R.J. Hannam, N.C. Uren) *Springer* (1988) 113-124.

López M.F. Better approaches to finding the needle in a haystack: optimizing proteome analysis through automation. *Electrophoresis* 21 (2000) 1082-1093.

López-Millán A.F., Grusak M.A., Abadía A., Abadía J. Iron deficiency in plants: an insight from proteomic approaches. *Front. Plant Sci.* 4 (2013) 254.

López-Millán A.F., Morales F., Abadía A., Abadía J. Effects of iron deficiency on the composition of the leaf apoplastic fluid and xylem sap in sugar beet. Implications for iron and carbon transport. *Plant Physiol.* 124 (2000a) 873-884.

López-Millán A.F., Morales F., Andaluz S., Gogorcena Y., Abadía A., Rivas J.D.L., Abadía J. Responses of sugar beet roots to iron deficiency. Changes in carbon assimilation and oxygen use. *Plant Physiol.* 124 (2000b) 885-898.

Lorkovic Z.J. Role of plant RNA-binding proteins in development, stress response and genome organization. *Trends Plant Sci.* 14 (2009) 229-236.

Loukehaich R., Wang T., Ouyang B., Ziaf K., Li H., Zhang J., Lu Y., Ye Z. SpUSP, an annexin-interacting universal stress protein, enhances drought tolerance in tomato. *J. Exp. Bot.* 63 (2012) 5593-5606.

Lucas W.J., Groover A., Lichtenberger R., Furuta K., Yadav S.R., Helariutta Y., He X.Q., Fukuda H., Kang J., Brady S.M., Patrick J.W., Sperry J., Yoshida A., López-Millán A.F. Grusak M.A., Kachroo P. The plant vascular system: evolution, development and functions. *J. Integr. Plant Biol.* 55 (2013) 294-388.

Lucas W.J., Yoo B.C., Kragler F. RNA as a long-distance information macromolecule in plants. *Nat. Rev. Mol. Cell Biol.* 2 (2001) 849-57.

Lucena J.J. Effects of bicarbonate, nitrate and other environmental factors on iron deficiency chlorosis. A review. *J. Plant Nutr.* 23 (2000) 1591-1606.

Lynch J., StClair S. Mineral stress: the missing link in understanding how global climate change will affect plants in real world soils. *Fields Crops Res.* 90 (2004) 101-115.

Ma J.F., Zhang Z., Yang G., Mao J., Xu F. Ultrastructural topochemistry of cell wall polymers in populus nigra by transmission electron microscopy and raman imaging. *BioResources* 6 (2011) 4.

Ma J.F., Nomoto K. Effective regulation of iron acquisition in graminaceous plants. The role of mugineic acids as phytosiderophores. *Physiol. Plant.* 97 (1996) 609-617.

Ma J.F., Shinada T., Matsuda C., Nomoto K. Biosynthesis of phytosiderophores, mugineic acids, associated with methionine cycling. *J. Biol. Chem.* 270 (1995) 16549-16554.

MacMillan C.P., Mansfield S.D., Stachurski Z.H., Evans R., Southerton S.G. Fasciclin-like arabinogalactan proteins: specialization for stem biomechanics and cell wall architecture in *Arabidopsis* and Eucalyptus. *Plant J.* 62 (2010) 689-703.

MacNicol R.D., Beckett P.H.T. Critical tissue concentrations of potentially toxic elements. *Plant Soil* 85 (1985) 107-129.

Magalhaes J.V., Liu J., Guimaraes C.T., Lana U.G.P., Alves V.M.C., Wang Y.H., Schaffert R.E., Hoekenga O.A., Piñeros M.A., Shaff J.E., Klein P.E., Carneiro N.P., Coelho C.M., Trick H.N., Kochian L.V. A gene in the multidrug and toxic compound extrusion (MATE) family confers aluminum tolerance in sorghum. *Nat. Genet.* 39 (2007) 1156.

Mai H.J., Bauer P. From the proteomic point of view: Integration of adaptive changes to iron deficiency in plants. *Curr. Plant Biol.* 5 (2016) 45-56.

Majeran W., Cai Y., Sun Q., van Wijk K.J. Functional differentiation of bundle sheath and mesophyll maize chloroplasts determined by comparative proteomics. *Plant Cell* 17 (2005) 3111-3140.

Malavolta E. Manual de nutriçao mineral de plantas. *Agronômica Ceres* (2006).

Mangeon A., Junqueira R.M., Sachetto-Martins G. Functional diversity of the plant glycine-rich proteins superfamily. *Plant Signal Behav.* 5 (2010) 99-104.

Mano S., Miwa T., Nishikawa S.I., Mimura T., Nishimura M. The plant organelles database (PODB): a collection of visualized plant organelles and protocols for plant organelle research. *Nucleic Acids Res.* 36 (2008) 929-937.

Mansfeldt T. Redox potential of bulk soil and soil solution concentration of nitrate, manganese, iron, and sulfate in two Gleysols. *J. Plant Nutr. Soil Sci.* 167 (2004) 7-16.

Marmagne A., Rouet M.A., Ferro M., Rolland N., Alcon C., Joyard J., Garin J.R., Barbier-Brygoo H.L.N., Ephritikhine G.V. Identification of new intrinsic proteins in *Arabidopsis* plasma membrane proteome. *Mol. Cell Proteomics* 3 (2004) 675-691.

Marschner H. Mineral nutrition of higher plants. *Academic Press* (1995)

Marschner H., Römheld V., Kissel M. Localization of phytosiderophore release and of iron uptake along intact barley roots. *Physiol. Plant.* 71 (1987) 157-162.

Marschner P. Marschner's mineral nutrition of higher plants. *Academic Press* (2012) 315-330.

Martin A.C., Del Pozo J., Iglesias J., Rubio V., Solano R., De La Pena A., Leyva A., Paz-Ares J. Influence of cytokinins on the ex-pression of phosphate starvation responsive genes in *Arabidopsis*. *Plant J.* 24 (2000) 559-567.

Maruta T., Ichikawa Y., Mieda T., Takeda T., Tamoi M., Yabuta Y., Ishikawa T., Shigeoka S. The contribution of *Arabidopsis* homologs of L-gulono-1,4-lactone oxidase to the biosynthesis of ascorbic acid. *Biosci. Biotechnol. Biochem.* 74 (2010) 1494-1497.

Mashaghi A., Bezrukavnikov S., Minde D.P., Wentink A.S., Kityk R., Zachmann-Brand B., Mayer M.P., Kramer G., Bukau B., Tans S.J. Alternative modes of client binding enable functional plasticity of Hsp70. *Nature* 539 (2016) 448.

Marshall S.D.G., Putterill J.J., Plummer K.M., Newcomb R.D. The carboxylesterase gene family from *Arabidopsis thaliana. J. Mol. Evol.* 57 (2003) 487-500.

Masuda S., Sakuta C., Satoh S. cDNA cloning of a novel lectin-like xylem sap protein and its root-specific expression in cucumber. *Plant Cell Physiol.* 40 (1999) 1177-1181.

Masui M., Nukaya A., Ishida A., Ogura T. Studies on the manganese excess of muskmelon. VI. Manganese distribution in the plant parts. *J. Jpn. Soc. Hortic. Sci.*, 49 (1980) 79-84.

May D., Fitzgibbon M., Liu Y., Holzman T., Eng J., Kemp C.J., Whiteaker J., Paulovich A., McIntosh M. A platform for accurate mass and time analyses of mass spectrometry data. *J. Proteome Res.* 6 (2007) 2685-2694.

McHargue J.S. The role of manganese in plants. *J. Am. Chem. Soc.* 44 (1922) 1592-1598.

Mei H., Cheng N.H., Zhao J., Park S., Escareno R.A., Pittman J.K., Hirschi K.D. Root development under metal stress in *Arabidopsis thaliana* requires the H^+/cation antiporter CAX4. *New Phytol.* 183 (2009) 95-105.

Meisinger C., Sickmann A., Pfanner N. The mitochondrial proteome: from inventory to function. *Cell* 134 (2008) 22-24.

Meisrimler C.N., Planchon S., Renaut J., Sergeant K., Lüthje S. Alteration of plasma membrane-bound redox systems of iron deficient pea roots by chitosan. *J. Proteomics* 74 (2011) 1437-1449.

Meldrum E., Parker P.J., Carozzi A. The PtdIns-PLC superfamily and signal transduction. *BBA* 1092 (1991) 49-71.

Memon A.R., Chino M., Hara K., Yatazawa M. Microdistribution of manganese in the leaf tissues of different plant species as revealed by X-ray microanalyzer. *Physiol. Plant.* 53 (1981) 225-232.

Mendoza-Cózatl D.G., Butko E., Springer F., Torpey J.W., Komives E.A., Kehr J., Schroeder J.I. Identification of high levels of phytochelatins, glutathione and cadmium in the phloem sap of *Brassica napus*. A role for thiol-peptides in the long-distance transport of cadmium and the effect of cadmium on iron translocation. *Plant J.* 54 (2008) 249-259.

Meng L., Wong J.H., Feldman L.J., Lemaux P.G., Buchanan B.B. A membrane-associated thioredoxin required for plant growth moves from cell to cell, suggestive of a role in intercellular communication. *Proc. Natl. Acad. Sci. U.S.A.* 107 (2010) 3900-3905.

Mengel K., Kosegarten H., Kirkby E.A. Principles of plant nutrition. *S.S.B.M.* (2001).

Mengel K., Geurtzen G. Iron chlorosis on calcareous soils. Alkaline nutritional condition as the cause for the chlorosis. *J. Plant Nutr.* 9 (1986) 161-173.

Meyer Y., Grosset J., Chartier Y., Cleyet-Marel J.C. Preparation by two-dimensional electrophoresis of proteins for antibody production: antibodies against proteins whose synthesis is reduced by auxin in tobacco mesophyll protoplasts. *Electrophoresis* 11 (1988) 704-712.

Migocka M., Papierniak A., Maciaszczyk-Dziubinska E., Pozdzik P., Posyniak E., Garbiec A., Filleur S. Cucumber metal transport protein MTP8 confers increased tolerance to manganese when expressed in yeast and *Arabidopsis thaliana*. *J. Exp. Bot.* 65 (2014) 5367-5384.

Mijnsbrugge K.V., Meyermans H., Van Montagu M., Bauw G., Boerjan W. Wood formation in poplar: identification, characterization and seasonal variation of xylem proteins. *Planta* 210 (2000) 589-598.

Millaleo R., Reyes-Díaz M., Alberdi M., Ivanov A.G., Krol M., Huner N.P. Excess manganese differentially inhibits photosystem I versus II in *Arabidopsis thaliana*. *J. Exp. Bot.* 64 (2013) 343-354.

Millaleo R., Reyes-Díaz M., Ivanov A.G., Mora M.L., Alberdi M. Manganese as essential and toxic element for plants: transport, accumulation and resistance mechanisms. *J. Soil Sci. Plant Nutr.* 10 (2010) 470-481.

Miller G.A.D., Suzuki N., Ciftci-Yilmaz S., Mittler R.O.N. Reactive oxygen species homeostasis and signalling during drought and salinity stresses. *Plant Cell Environ.* 33 (2009) 453-467.

Miller I., Crawford J., Gianazza E. Protein stains for proteomic applications: Which, when, why? *Proteomics* 6 (2006) 5385-5408.

Milne T.J., Abbenante G., Tyndall J.D.A., Halliday J., Lewis R.J. Isolation and characterization of a cone snail protease with homology to CRISP proteins of the pathogenesis-related protein superfamily. *J. Biol. Chem.* 278 (2003) 31105-31110.

Milner M.J., Seamon J., Craft E., Kochian L.V. Transport properties of members of the ZIP family in plants and their role in Zn and Mn homeostasis. *J. Exp. Bot.* 64 (2013) 369-381.

Mimmo T., Del Buono D., Terzano R., Tomasi N., Vigani G., Crecchio C., Pinton R., Zocchi G., Cesco S. Rhizospheric organic compounds in the soil–microorganism–plant system: their role in iron availability. *Eur. J. Soil Sci.* 65 (2014) 629-642.

Min C.W., Lee S.H., Cheon Y.E., Han W.Y., Ko J.M., Kang H.W., Kim Y.C., Agrawal G.K., Rakwal R., Gupta R., Kim S.T. In-depth proteomic analysis of *Glycine max* seeds during controlled deterioration treatment reveals a shift in seed metabolism. *J. Proteomics* 169 (2017).

Min Y., boqing T., Meizhen T., Aoyama I. Accumulation and uptake of manganese in a hyperaccumulator *Phytolacca americana*. *Miner. Eng.* 20 (2007) 188-190.

Minic Z. Physiological roles of plant glycoside hydrolases. *Planta* 227 (2008) 723-740.

Mira H., Martínez-García F., Peñarrubia L. Evidence for the plant-specific intercellular transport of the *Arabidopsis* copper chaperone CCH. *Plant J.* 25 (2001) 521-528.

Mittler R. Oxidative stress, antioxidants and stress tolerance. *Trends Plant Sci.* 7 (2002) 405-410.

Miwa K., Kamiya T., Fujiwara T. Homeostasis of the structurally important micronutrients, B and Si. *Curr. Opin. Plant Biol.* 12 (2009) 307-311.

Miyazono K., Miyakawa T., Sawano Y., Kubota K., Kang H.J., Asano A., Miyauchi Y., Takahashi M., Zhi Y., Fujita Y., Yoshida T., Kodaira K.S., Yamaguchi-Shinozaki K., Tanokura M. Structural basis of abscisic acid signalling. *Nature* 462 (2009) 609-614.

Mogensen J.E., Wimmer R., Larsen J.N., Spangfort M.D., Otzen D.E. The major birch allergen, Bet_v_1, shows affinity for a broad spectrum of physiological ligands. *J. Biol. Chem.* 277 (2002) 23684-23692.

Moog P.R., van der Kooij T.A.W., Bruggemann W., Schiefelbein J.W., Kuiper P.J.C. Responses to iron deficiency in *Arabidopsis thaliana*: The Turbo iron reductase does not depend on the formation of root hairs and transfer cells. *Planta* 195 (1995) 505-513.

Morales F., Warren C.R. Photosynthetic responses to nutrient deprivation and toxicities. In: 'Terrestrial photosynthesis in a changing environment: a molecular, physiological and ecological approach' (Ed. J. Flexas) *Cambridge University Press* (2012) 312-330.

Morales F., Grasa R., Abadía A., Abadía J. Iron chlorosis paradox in fruit trees. *J. Plant Nutr.* 21 (1998) 815-825.

Morgan M.J., Lehmann M., Schwarzländer M., Baxter C.J., Sienkiewicz-Porzucek A., Williams T.C.R., Schauer N., Fernie A.R., Fricker M.D., Ratcliffe R.G., Sweetlove L.J., Finkemeier I. Decrease in manganese superoxide dismutase leads to reduced root growth and affects tricarboxylic acid cycle flux and mitochondrial redox homeostasis. *Plant Physiol.* 147 (2008) 101-114.

Morita A., Yokota H., Ishka M.R., Ghanati F. Changes in peroxidase activity and lignin content of cultured tea cells in response to excess manganese. *J. Soil Sci. Plant Nutr.* 52 (2006) 26-31.

Morris J., Tian H., Park S., Sreevidya C.S., Ward J.M., Hirschi K.D. AtCCX3 is an *Arabidopsis* endomembrane H^+-dependent K^+ transporter. *Plant Physiol.* 148 (2008) 1474-1486.

Morrissey J., Baxter I.R., Lee J., Li L., Lahner B., Grotz N., Kaplan J., Salt D.E., Guerinot M.L. The ferroportin metal efflux proteins function in iron and cobalt homeostasis in *Arabidopsis. Plant Cell* 21 (2009) 3326-3338.

Msilini N., Zaghdoudi M., Govindachary S., Lachaâl M., Ouerghi Z., Carpentier R. Inhibition of photosynthetic oxygen evolution and electron transfer from the quinone acceptor QA to QB by iron deficiency. *Photosynth. Res.* 107 (2011) 247-256.

Muchuweti M., Birkett J.W., Chinyanga E., Zvauya R., Scrimshaw M.D., Lester J.N. Heavy metal content of vegetables irrigated with mixtures of wastewater and sewage sludge in Zimbabwe: Implications for human health. *Agric. Ecosyst. Environ.* 112 (2006) 41-48.

Mueller L.N., Rinner O., Schmidt A., Letarte S., Bodenmiller B., Brusniak M.Y., Vitek O., Aebersold R., Müller M. SuperHirn–a novel tool for high resolution LC-MS-based peptide/protein profiling. *Proteomics* 7 (2007) 3470-3480.

Mukherjee I., Campbell N.H., Ash J.S., Connolly E.L. Expression profiling of the *Arabidopsis* ferric chelate reductase (FRO) gene family reveals differential regulation by iron and copper. *Planta* 223 (2006) 1178-1190.

Mukhopadhyay M., Sharma A. Manganese in cell metabolism of higher plants. *Bot. Rev.* 57 (1991) 117-149.

Murata Y., Ma J.F., Yamaji N., Ueno D., Nomoto K., Iwashita T. A specific transporter for iron(III)–phytosiderophore in barley roots. *Plant J.* 46 (2006) 563-572.

Nable R.O., Loneragan J.F. Translocation of manganese in subterranean clover (*Trifolium subterraneum* L. Cv. Seaton Park) I. Redistribution during vegetative growth. *Funct. Plant Biol.* 11 (1984) 101-111.

Nahnsen S., Bielow C., Reinert K., Kohlbacher O. Tools for label-free peptide quantification. *Mol. Cell. Proteomics* 12 (2013) 549-556.

Nakaminami K., Matsui A., Shinozaki K., Seki M. RNA regulation in plant abiotic stress responses. *BBA-Gene Regul. Mech.* 1819 (2012) 149-153.

Ndimba B.K., Chivasa S., Hamilton J.M., Simon W.J., Slabas A.R. Proteomic analysis of changes in the extracellular matrix of *Arabidopsis* cell suspension cultures induced by fungal elicitors. *Proteomics* 3 (2003) 1047-1059.

Nechushtai R., Conlan A.R., Harir Y., Song L., Yogev O., Eisenberg-Domovich Y., Livnah O., Michaeli D., Rosen R., Ma V., Luo Y., Zuris J.A. Paddock M.L., Cabantchik Z.I., Jennings P.A., Mittler R., Characterization of *Arabidopsis* NEET reveals an ancient role for NEET proteins in iron metabolism. *Plant Cell* 24 (2012) 2139-2154.

Neumann K.H., Steward F.C. Investigations on the growth and metabolism of cultured explants of *Daucus carota*. I. Effects of iron, molybdenum and manganese on growth. *Planta* 81 (1968) 333-350.

Nguyen-Kim H., San Clemente H., Balliau T., Zivy M., Dunand C., Albenne C., Jamet E. *Arabidopsis thaliana* root cell wall proteomics: Increasing the proteome coverage using a combinatorial peptide ligand library and description of unexpected Hyp in peroxidase amino acid sequences. *Proteomics* 16 (2016) 491-503.

Nickelsen J., Rengstl B. Photosystem II assembly: From cyanobacteria to plants. *Annu. Rev. Plant Biol.* (2013) 609-635.

Nikolic M., Römheld V. The apoplast of higher plants: compartment of storage, transport and reactions. The dynamics of iron in the leaf apoplast. (Eds. B.Sattelmacher, W.J. Horst) *Springer* (2007) 353-371.

Nikolic M., Römheld V. Mechanism of Fe uptake by the leaf symplast: Is Fe inactivation in leaf a cause of Fe deficiency chlorosis? *Plant Soil* 215 (1999) 229-237.

Nishiyama R., Kato M., Nagata S., Yanagisawa S., Yoneyama T. Identification of Zn-Nicotianamine and Fe-2'-Deoxymugineic acid in the phloem sap from rice plants (*Oryza sativa* L.). *Plant Cell Physiol.* 53 (2012) 381-390.

Nomata T., Kabeya Y., Sato N. Cloning and characterization of glycine-rich RNA-binding protein cDNAs in the moss *physcomitrella patens. Plant Cell Physiol.* 45 (2004) 48-56.

Norbeck A., Monroe M., Adkins J., Anderson K., Daly D., Smith R. The utility of accurate mass and LC elution time information in the analysis of complex proteomes. *J. Am. Soc. Mass Spectrom.* 16 (2005) 1239-1249.

Nozoye T., Nagasaka S., Kobayashi T., Takahashi M., Sato Y., Sato Y., Uozumi N., Nakanishi H., Nishizawa N.K. Phytosiderophore efflux transporters are crucial for iron acquisition in Graminaceous plants. *J. Biol. Chem.* 286 (2011) 5446-5454.

Numan M., Bhosle N. alfa-l-Arabinofuranosidases: the potential applications in biotechnology. *J. Ind. Microbiol. Biotechnol.* 33 (2006) 247-260.

Nuttleman P.R., Roberts R.M. Transfer of iron from uteroferrin (purple acid phosphatase) to transferrin related to acid phosphatase activity. *J. Biol. Chem.* 265 (1990) 12192-12199.

Ohkama-Ohtsu N., Radwan S., Peterson A., Zhao P., Badr A.F., Xiang C., Oliver D.J. Characterization of the extracellular γ-glutamyl transpeptidases, GGT1 and GGT2, in *Arabidopsis. Plant J.* 49 (2007) 865-877.

Ohyama K., Shinohara H., Ogawa-Ohnishi M., Matsubayashi Y. A glycopeptide regulating stem cell fate in *Arabidopsis thaliana*. *Nat. Chem. Biol.* 5 (2009) 578-580.

Old W.M., Meyer-Arendt K., Aveline-Wolf L., Pierce K.G., Mendoza A., Sevinsky J.R., Resing K.A., Ahn N.G. Comparison of label-free methods for quantifying human proteins by shotgun proteomics. *Mol. Cell. Proteomics* 4 (2005) 1487-1502.

Ong S., Mann M. Mass spectrometry-based proteomics turns quantitative. *Nat. Chem. Biol.* 1 (2005) 252-262.

Ong S.E., Blagoev B., Kratchmarova I., Kristensen D.B., Steen H., Pandey A., Mann M. Stable isotope labeling by amino acids in cell culture, SILAC, as a simple and accurate approach to expression proteomics. *Mol. Cell. Proteomics* 1 (2002) 376-386.

Oparka K.J., Cruz S.S. The great escape: phloem transport and unloading of macromolecules. *Annu. Rev. Plant Biol.* 51 (2000) 323-347.

Orera I., Rodríguez-Castrillón J.A., Moldovan M., García-Alonso J.I., Abadía A., Abadía J., Álvarez-Fernández A. Using a dual-stable isotope tracer method to study the uptake, xylem transport and

distribution of Fe and its chelating agent from stereoisomers of an Fe(III)-chelate used as fertilizer in Fe-deficient Strategy I plants. *Metallomics* 2 (2010) 646-657.

Pallotta M.A., Graham R.D., Langridge P., Sparrow D.H.B., Barker S.J. RFLP mapping of manganese efficiency in barley. *Theor. Appl. Genet.* 101 (2000) 1100-1108.

Park S.K., Venable J.D., Xu T., Yates J.R. A quantitative analysis software tool for mass spectrometry-based proteomics. *Nat. Methods* 5 (2008) 319.

Parkhurst D. Stereological methods for measuring internal leaf structural variables. *Am. J. Bot.* 69 (1982) 31–39.

Pearce G., Yamaguchi Y., Barona G., Ryan C.A. A subtilisin-like protein from soybean contains an embedded, cryptic signal that activates defense-related genes. *Proc. Natl. Acad. Sci. U.S.A.* 107 (2010) 14921-14925.

Pechanova O., Hsu C.-Y., Adams J.P., Pechan T., Vandervelde L., Drnevich J., Jawdy S., Adeli A., Suttle J.C., Lawrence A.M., Tschaplinski T.J., Séguin A., Yuceer C. Apoplast proteome reveals that extracellular matrix contributes to multistress response in poplar. *BMC Genomics* 11 (2010) 1-22.

Pedas P., Schiller Stokholm M., Hegelund J.N., Ladegärd A.H., Schjoerring J.K., Husted S.R. Golgi localized barley MTP8 proteins facilitate Mn transport. *PLOS ONE* 9 (2014) 113759.

Pedas P., Ytting C.K., Fuglsang A.T., Jahn T.P., Schjoerring J.K., Husted S.R. Manganese efficiency in barley: identification and characterization of the metal ion transporter HvIRT1. *Plant Physiol.* 148 (2008) 455-466.

Peiter E., Montanini B., Gobert A., Pedas P., Husted S., Maathuis F.J.M., Blaudez D., Chalot M., Sanders D. A secretory pathway-localized cation diffusion facilitator confers plant manganese tolerance. *Proc. Natl. Acad. Sci. U.S.A.* 104 (2007) 8532-8537.

Persson S., Wei H.R., Milne J., Page G.P., Somerville C.R. Identification of genes required for cellulose synthesis by regression analysis of public microarray data sets. *Proc. Natl. Acad. Sci. U.S.A.* 102 (2005) 8633-8638.

Petriccione M., Salzano A.M., Di Cecco I., Scaloni A., Scortichini M. Proteomic analysis of the *Actinidia deliciosa* leaf apoplast during biotrophic colonization by *Pseudomonas syringae* pv. *actinidiae. J. Proteomics* 101 (2014) 43-62.

Pich A., Manteuffel R., Hillmer S., Scholz G., Schmidt W. Fe homeostasis in plant cells: does nicotianamine play multiple roles in the regulation of cytoplasmic Fe concentration? *Planta* 213 (2001) 967-76.

Pierce A., Unwin R., Evans C., Griffiths S., Carney L., Zhang L., Jaworska E., Lee C.F., Blinco D., Okoniewski M.J., Miller C.J., Bitton D.A., Spooncer E., Whetton A.D. Eight-channel iTRAQ enables comparison of the activity of six leukemogenic tyrosine kinases. *Mol. Cell. Proteomics* 7 (2008) 853-863.

Pilon M., Cohu C.M., Ravet K., Abdel-Ghany S.E., Gaymard F. Essential transition metal homeostasis in plants. *Curr. Opin. Plant Biol.* 12 (2009) 347-357.

Pittman J. Managing the manganese: molecular mechanisms of manganese transport and homeostasis. *New Phytol*. (2005) 733-742.

Pittman J.K., Shigaki T., Marshall J.L., Morris J.L., Cheng N.H., Hirschi K.D. Functional and regulatory analysis of the *Arabidopsis thaliana* CAX2 cation transporter. *Plant Mol. Biol.* 56 (2004) 959-971.

Puig S., Peñarrubia L. Placing metal micronutrients in context: transport and distribution in plants. *Curr. Opin. Plant Biol.* 12 (2009) 299-306.

Pulford I.D., Watson C. Phytoremediation of heavy metal-contaminated land by trees-a review. *Environ. Int.* 29 (2003) 529-540.

Quadroni M., James P. Proteomics and automation. *Electrophoresis* 20 (1999) 664-677.

Rabilloud T. Two-dimensional gel electrophoresis in proteomics: Old, old fashioned, but it still climbs up the mountains. *Proteomics* 2 (2002) 3-10.

Rahayu Y.S., Walch-Liu P., Neumann G., Römheld V., von Wirén N., Bangerth F. Root-derived cytokinins as long-distance signalsfor NO^{-3}-induced stimulation of leaf growth. *J. Exp. Bot.* 56 (2005) 1143-1152.

Raven J.A., Evans M.C.W., Korb R.E. The role of trace metals in photosynthetic electron transport in O_2-evolving organisms. *Photosynth. Res.* 60 (1999) 111-149.

Rellán-Álvarez R., Andaluz S., Rodríguez-Celma J., Wohlgemuth G., Zocchi G., Álvarez-Fernández A., Fiehn O., López-Millán A.F., Abadía J. Changes in the proteomic and metabolic profiles of *Beta vulgaris* root tips in response to iron deficiency and resupply. *BMC Plant Biol.* 10 (2010a) 1-15.

Rellán-Álvarez R., Giner-Martínez-Sierra J., Orduna J., Orera I., Rodríguez-Castrillón J.A., García-Alonso J.I., Abadía J., Álvarez-Fernández A. Identification of a tri-iron (III), tri-citrate complex in the xylem sap of iron-deficient tomato resupplied with iron: new insights into plant iron long-distance transport. *Plant Cell Physiol.* 51 (2010b) 91-102.

Rellán-Álvarez R., Abadía J., Álvarez-Fernández A. Formation of metal-nicotianamine complexes as affected by pH, ligand exchange with citrate and metal exchange. A study by electrospray ionization time-of-flight mass spectrometry. *Rapid Commun. Mass Spectrom.* 22 (2008) 1553-1562.

Rengel Z. Availability of Mn, Zn and Fe in the rhizosphere. *J. Soil Sci. Plant Nutr.* 15 (2015) 397-409.

Rengel Z. Manganese uptake and transport in plants. *Met Ions Biol Syst* 37 (2000) 57-87.

Rengel Z., Graham R.D., Pedler J.F. Manganese nutrition and accumulation of phenolics and lignin as related to differential resistance of wheat genotypes to the take-all fungus. *Plant Soil* 151 (1993) 255-263.

Rep M., Dekker H.L., Vossen J.H., de Boer A.D., Houterman P.M., de Koster C.G., Cornelissen B.J.C. A tomato xylem sap protein represents a new family of small cysteine-rich proteins with structural similarity to lipid transfer proteins. *FEBS Letters* 534 (2003) 82-86.

Reuter D.J. Temperate and tropical crops. In: 'Plant analysis: an interpretation manual'. (Eds. D.J. Reuter, J.B. Robinson) *S.B.S.* (1997) 83-278.

Reuter D.J., Heard T.G., Alston A.M. Correction of manganese deficiency in barley crops on calcareous soils. 1. Manganous sulphate applied at sowing and as foliar sprays. *Aust. J. Exp. Agr.* 13 (1973) 434-439.

Rezaul K., Wu L., Mayya V., Hwang S.I., Han D. A systematic characterization of mitochondrial proteome from human T leukemia cells. *Mol. Cell. Proteomics* 4 (2005) 169-181.

Rietz S., Dermendjiev G., Oppermann E., Tafesse F.G., Effendi Y., Holk A., Parker J.E., Teige M., Scherer G.F.E. Roles of *Arabidopsis* patatin-related phospholipases a in root development are related to auxin responses and phosphate deficiency. *Mol. Plant* 3 (2010) 524-538.

Rietz S., Holk A., Scherer G.F.E. Expression of the patatin-related phospholipase A gene AtPLA IIA in *Arabidopsis thaliana* is up-regulated by salicylic acid, wounding, ethylene, and iron and phosphate deficiency. *Planta* 219 (2004) 743-753.

Righetti P.G., Boschetti E. The ProteoMiner and the FortyNiners: searching for gold nuggets in the proteomic arena. *Mass Spectrom. Rev.* 27 (2008) 596-608.

Righetti P.G., Castagna A., Antonioli P., Boschetti E. Prefractionation techniques in proteome analysis: The mining tools of the third millennium. *Electrophoresis* 26 (2005) 297-319.

Rios J.J., Carrasco-Gil S., Abadía A., Abadía J. Using perls staining to trace the iron uptake pathway in leaves of a *Prunus* rootstock treated with iron foliar fertilizers. *Front. Plant Sci.* 7 (2016) 893.

Roberts L.A., Pierson A.J., Panaviene Z., Walker E.L. Yellow stripe1. Expanded roles for the maize iron-phytosiderophore transporter. *Plant Physiol.* 135 (2004) 112-120.

Robinson N.J., Procter C.M., Connolly E.L., Guerinot M.L. A ferric-chelate reductase for iron uptake from soils. *Nature* 397 (1999) 694-697.

Robinson W.D., Carson I., Ying S., Ellis K., Plaxton W.C. Eliminating the purple acid phosphatase AtPAP26 in *Arabidopsis thaliana* delays leaf senescence and impairs phosphorus remobilization. *New Phytol.* 196 (2012) 1024-1029.

Rodríguez-Celma J., Ceballos-Laita L., Grusak M.A., Abadía J., López-Millán A.F. Plant fluid proteomics: delving into the xylem sap, phloem sap and apoplastic fluid proteomes. *BBA-Proteins Proteom.* 1864 (2016a) 991–1002

Rodríguez-Celma J., Tsai Y.H., Wen T.N., Wu Y.C., Curie C., Schmidt W. Systems-wide analysis of manganese deficiency-induced changes in gene activity of *Arabidopsis* roots. *Sci. Rep.* 6 (2016b) 35846.

Rodríguez-Celma J., Lattanzio G., Villarroya D., Gutierrez-Carbonell E., Ceballos-Laita L., Rencoret J., Gutiérrez A., Del Río J.C., Grusak M.A., Abadía A., Abadía J., López-Millán A.F. Effects of Fe deficiency on the protein profiles and lignin composition of stem tissues from *Medicago truncatula* in absence or presence of calcium carbonate. *J. Proteomics* 140 (2016c) 1-12.

Rodríguez-Celma J., Lin W.D., Fu G.M., Abadía J., López-Millán A.F., Schmidt W. Mutually exclusive alterations in secondary metabolism are critical for the uptake of insoluble iron compounds by *Arabidopsis* and *Medicago truncatula. Plant Physiol.* 162 (2013a) 1473-1485.

Rodríguez-Celma J., Lattanzio G., Jiménez S., Briat J.F., Abadía J., Abadía A., Gogorcena Y., López-Millán A.F. Changes induced by Fe deficiency and Fe resupply in the root protein profile of a peach-almond hybrid rootstock. *J. Proteome Res.* 12 (2013b) 1162-1172.

Rodríguez-Celma J., Lattanzio G., Grusak M.A., Abadía A., Abadía J., López-Millán A.F. Root responses of *Medicago truncatula* plants grown in two different iron deficiency conditions: changes in root protein profile and riboflavin biosynthesis. *J. Proteome Res.* 10 (2011) 2590-2601.

Rodríguez-Celma J., Rellán-Álvarez R., Abadía A., Abadía J., López-Millán A.F. Changes induced by two levels of cadmium toxicity in the 2-DE protein profile of tomato roots. *J. Proteomics* 73 (2010) 1694-1706.

Rodríguez-Medina C., Atkins C.A., Mann A.J., Jordan M.E., Smith P.M.C. Macromolecular composition of phloem exudate from white lupin (*Lupinus albus* L.). *BMC Plant Biol.* 11 (2011) 36.

Rogers S., Girolami M., Kolch W., Waters K., Liu T., Thrall B., Wiley H. Investigating the correspondence between transcriptomic and proteomic expression profiles using coupled cluster models. *Bioinformatics* 24 (2008) 2894-900.

Rombolà A.D., Tagliavini M. Iron nutrition of fruit tree crops. In: 'Iron nutrition in plants and rhizospheric microorganisms'. (Eds. L.L. Barton, J. Abadía) *Springer* (2006) 61-83.

Römheld V. The chlorosis paradox: Fe inactivation as a secondary event in chlorotic leaves of grapevine. *J. Plant Nutr.* 23 (2000) 1629-1643.

Römheld V., Marschner H. Evidence for a specific uptake system for iron phytosiderophores in roots of grasses. *Plant Physiol.* 80 (1986) 175-180.

Römheld V., Marschner H. Iron deficiency stress induced morphological and physiological changes in root tips of sunflower. *Physiol. Plant.* 53 (1981) 354-360.

Ros Barceló A., Muñoz R., Sabater F. Lupin peroxidases. I. Isolation and characterization of cell wall-bound isoperoxidase activity. *Physiol. Plant.* 71 (1987) 448-454.

Rose J.K.C., Lee S.J. Straying off the highway: trafficking of secreted plant proteins and complexity in the plant cell wall proteome. *Plant Physiol.* 153 (2010) 433-436.

Ross G.S., Wegrzyn T., MacRae E.A., Redgwell R.J. Apple β-galactosidase. Activity against cell wall polysaccharides and characterization of a related cDNA clone. *Plant Physiol.* 106 (1994) 521-528.

Ross P., Huang Y., Marchese J., Williamson B., Parker K., Hattan S., Khainovski N., Pillai S., Dey S. Daniels S., Purkayastha S., Juhasz P., Martin S., Bartlet-Jones M., He F., Jacobson A., Pappin D.J. Multiplexed protein quantitation in *Saccharomyces cerevisiae* using amine-reactive isobaric tagging reagents. *Mol. Cell. Proteomics* 3 (2004) 1154-1169.

Roth-Walter F., Gómez-Casado C., Pacios L., Mothes-Luksch N., Roth G., Singer J., Díaz-Perales A., Jensen-Jarolim E. Bet v 1 from birch pollen is a lipocalin-like protein acting as allergen only when devoid of iron by promoting Th2 lymphocytes. *J. Biol. Chem.* 289 (2014) 17416-17421.

Rouached H., Stefanovic A., Secco D., Bulak A.A., Gout E., Bligny R., Poirier Y. Uncoupling phosphate deficiency fromits major effects on growth and transcriptome *via* PHO1 expressionin *Arabidopsis. Plant J.* 65 (2011) 557-570.

Rudella A., Friso G., Alonso J.M., Ecker J.R., Van Wijk K.J. Downregulation of ClpR2 leads to reduced accumulation of the ClpPRS protease complex and defects in chloroplast biogenesis in *Arabidopsis. Plant Cell* 18 (2006) 1704-1721.

Ruffel S., Krouk G., Ristova D., Shasha D., Birnbaum K.D., Coruzzi G.M. Nitrogen economics of root foraging: Transitive closure of the nitrate-cytokinin relay and distinct systemic signaling for N supply *vs.* demand. *Proc. Natl. Acad. Sci. U.S.A.* 108 (2011) 18524-18529.

Rydel T.J., Williams J.M., Krieger E., Moshiri F., Stallings W.C., Brown S.M., Pershing J.C., Purcell J.P., Alibhai M.F. The crystal structure, mutagenesis, and activity studies reveal that patatin is a lipid acyl hydrolase with a Ser-Asp catalytic dyad. *Biochemistry* 42 (2003) 6696-6708.

Sakurai N. Dynamic function and regulation of apoplast in the plant body. *J. Plant Res.* 111 (1998) 133-148.

Sakuta C., Satoh S. Vascular tissue-specific gene expression of xylem sap glycine-rich proteins in root and their localization in the walls of metaxylem vessels in cucumber. *Plant Cell Physiol.* 41 (2000) 627-638.

Salomé P.A. Manganese is a plant's best friend: Intracellular Mn transport by the transporter NRAMP2. *Plant Cell* 29 (2017) 2953-2954.

Salt D.E., Blaylock M., Kumar N.P.B.A., Dushenkov V., Ensley B.D., Chet I., Raskin I. Phytoremediation: a novel strategy for the removal of toxic metals from the environment using plants. *Bio/Technology* 13 (1995) 468.

Salvador V.H., Lima R.B., dos Santos W.D., Soares A.R., Böhm P.A.F., Marchiosi R., Ferrarese M.L.L., Ferrarese-Filho O. Cinnamic acid increases lignin production and inhibits soybean root growth. *PLOS ONE* 8 (2013) 69105.

Sampedro J., Sieiro C., Revilla G., González-Villa T., Zarra I. Cloning and expression pattern of a gene encoding an alfa-xylosidase active against xyloglucan oligosaccharides from *Arabidopsis. Plant Physiol.* 126 (2001) 910-920.

Sánchez-Rodríguez A.R., Cañasveras J.C., del Campillo M.C., Barrón V., Torrent J. Iron chlorosis in field grown olive as affected by phosphorus fertilization. *Eur. J. Agron.* 51 (2013) 101-107.

Santandrea G., Pandolfini T., Bennici A. A physiological characterization of Mn-tolerant tobacco plants selected by in vitro culture. *Plant Sci.* 150 (2000) 163-170.

Santi S., Schmidt W. Dissecting iron deficiency-induced proton extrusion in *Arabidopsis* roots. *New Phytol.* 183 (2009) 1072-1084.

Santi S., Schmidt W. Laser microdissection-assisted analysis of the functional fate of iron deficiency-induced root hairs in cucumber. *J. Exp. Bot.* 59 (2008) 697-704.

Santi S., Cesco S., Varanini Z., Pinton R. Two plasma membrane H(+)-ATPase genes are differentially expressed in iron-deficient cucumber plants. *Plant Physiol. Biochem.* 43 (2005) 287-92.

Sanz M., Cavero J., Abadía J. Iron chlorosis in the Ebro River basin, Spain. *J. Plant Nutr.* 15 (1992) 1971-1981.

Sasaki A., Yamaji N., Yokosho K., Ma J.F. Nramp5 is a major transporter responsible for manganese and cadmium uptake in rice. *Plant Cell* 24 (2012) 2155-2167.

Sasaki A., Yamaji N., Xia J., Ma J.F. OsYSL6 is involved in the detoxification of excess manganese in rice. *Plant Physiol.* 157 (2011) 1832-1840.

Sato Y., Sugiyama M., Komamine A., Fukuda H. Separation and characterization of the isoenzymes of wall-bound peroxidase from cultured *Zinnia* cells during tracheary element differentiation. *Planta* 196 (1995) 141-147.

Satoh S. Organic substances in xylem sap delivered to above-ground organs by the roots. *J. Plant Res.* 119 (2006) 179-187.

Satoh S., Iizuka C., Kikuchi A., Nakamura N., Fujii T. Proteins and carbohydrates in xylem sap from squash root. *Plant Cell Physiol.* 33 (1992) 841-847.

Sattelmacher B., Mühling K.H., Pennewiß K. The apoplast — its significance for the nutrition of higher plants. *Zeitschrift für Pflanzenernährung und Bodenkunde* 161 (1998) 485-498.

Savino G., Briat J.F., Lobréaux S. Inhibition of the iron-induced ZmFer1 maize ferritin gene expression by antioxidants and serine/threonine phosphatase inhibitors. *J. Biol. Chem.* 272 (1997) 33319-33326.

Schaaf G., Catoni E., Fitz M., Schwacke R., Von Wiren N., Frommer W.B. A putative role for the vacuolar calcium/manganese proton antiporter AtCAX2 in heavy metal detoxification. *Plant Biol.* 4 (2002).

Schaller A. A cut above the rest: the regulatory function of plant proteases. *Planta* 220 (2004) 183-197.

Schirle M., Heurtier M.A., Kuster B. Profiling core proteomes of human cell lines by one-dimensional PAGE and liquid chromatography-tandem mass spectrometry. *Mol. Cell. Proteomics* 2 (2003) 1297-1305.

Schmid N.B., Giehl R.F.H., Döll S., Mock H.P., Strehmel N., Scheel D., Kong X., Hider R.C., von Wirèn N. Feruloyl-CoA 6'-hydroxylase1-dependent coumarins mediate iron acquisition from alkaline substrates in *Arabidopsis. Plant Physiol.* 164 (2014) 160-172.

Schmidke I., Krüger C., Frömmichen R., Scholz G., Stephan U.W. Phloem loading and transport characteristics of iron in interaction with plant-endogenous ligands in castor bean seedlings. *Physiol. Plant.* 106 (1999) 82-89.

Schmidt O., Pfanner N., Meisinger C. Mitochondrial protein import: from proteomics to functional mechanisms. *Nat. Rev. Mol. Cell Biol.* 11 (2010) 655.

Schmidt S.B., Jensen P.E., Husted S.R. Manganese deficiency in plants: the impact on photosystem II. *Trends Plant Sci.* 21 (2016) 622-632.

Schmidt W. Mechanisms and regulation of reduction-based iron uptake in plants. *New Phytol.* 141 (1999) 1-26.

Schneider A., Steinberger I., Herdean A., Gandini C., Eisenhut M., Kurz S., Morper A., Hoecker N., Rühle T., Labs M., Flügge U.I., Geimer S., Schmidt S.B., Husted S., Weber A.P., Spetea C., Leister D. The evolutionarily conserved protein photosynthesis affected mutant71 is required for efficient manganese uptake at the thylakoid membrane in *Arabidopsis. Plant Cell* 28 (2016) 892-910.

Schobert C., Gottschalk M., Kovar D.R., Staiger C.J., Yoo B.C., Lucas W.J. Characterization of *Ricinus communis* phloem profilin, RcPRO1. *Plant Mol. Biol.* 42 (2000) 719-730.

Scholz G., Schlesier G., Seifert K. Effect of nicotianamine on iron uptake by the tomato mutant '*chloronerva*'. *Physiol. Plant.* 63 (1985) 99-104.

Schuler M., Rellán-Álvarez R., Fink-Straube C., Abadía J., Bauer P. Nicotianamine functions in the phloem-based transport of iron to sink organs, in pollen development and pollen tube growth in *Arabidopsis. Plant Cell* 24 (2012) 2380-2400.

Schurr U. Xylem sap sampling - new approaches to an old topic. *Trends Plant Sci.* 3 (1998) 293-298.

Schuster A., Davies E. Ribonucleic acid and protein metabolism in pea epicotyls: III. Response to auxin in aged tissue. *Plant Physiology* 73 (1983) 822-827.

Schützendübel A., Polle A. Plant responses to abiotic stresses: heavy metal-induced oxidative stress and protection by mycorrhization. *J. Exp. Bot.* 53 (2002) 1351-1365.

Schwarzländer M., König A.C., Sweetlove L.J., Finkemeier I. The impact of impaired mitochondrial function on retrograde signalling: a meta-analysis of transcriptomic responses. *J. Exp. Bot.* 63 (2012) 1735-1750.

Sergeant K., Spieß N., Renaut J., Wilhelm E., Hausman J.F. One dry summer: A leaf proteome study on the response of oak to drought exposure. *J. Proteomics* 74 (2011) 1385-1395.

Serra-Soriano M., Navarro J.A., Genoves A., Pallás V. Comparative proteomic analysis of melon phloem exudates in response to viral infection. *J. Proteomics* 124 (2015) 11-24.

Shabab M., Shindo T., Gu C., Kaschani F., Pansuriya T., Chintha R., Harzen A., Colby T. Kamoun S., van der Hoorn R.A.L. Fungal effector protein AVR2 targets diversifying defense-related cys proteases of tomato. *Plant Cell* 20 (2008) 1169-1183.

Shao J.F., Yamaji N., Shen R.F., Ma J.F. The key to Mn homeostasis in plants: regulation of Mn transporters. *Trends Plant Sci.* 22 (2017) 215-224.

Sharma C.P., Sharma P.N., Chatterjee C., Agarwala S.C. Manganese deficiency in maize affects pollen viability. *Plant Soil* 138 (1991) 139-142.

Shenton M., Berberich T., Kamo M., Yamashita T., Taira H., Terauchi R. Use of intercellular washing fluid to investigate the secreted proteome of the rice-*Magnaporthe* interaction. *J. Plant Res.* 125 (2012) 311-316.

Shi J., Chen Y., Xu Y., Ji D., Chen C., Xie C. Differential proteomic analysis by iTRAQ reveals the mechanism of *Pyropia haitanensis* responding to high temperature stress. *Sci. Rep.* 7 (2017) 44734.

Shi Q., Zhu Z., Xu M., Qian Q., Yu J. Effect of excess manganese on the antioxidant system in *Cucumis sativus* L. under two light intensities. *Environ. Exp. Bot.* 58 (2006) 197–205.

Shigaki T., Pittman J.K., Hirschi K.D. Manganese specificity determinants in the *Arabidopsis* metal/H^+ antiporter CAX2. *J. Biol. Chem.* 278 (2003) 6610-6617.

Shigeto J., Tsutsumi Y. Diverse functions and reactions of class III peroxidases. *New Phytol.* 209 (2016) 1395-1402.

Shigeto J., Nagano M., Fujita K., Tsutsumi Y. Catalytic profile of *Arabidopsis* peroxidases, AtPrx-2, 25 and 71, contributing to stem lignification. *PLoS ONE* 9 (2014).

Shimoni-Shor E., Hassidim M., Yuval-Naeh N., Keren N.I.R. Disruption of Nap14, a plastid-localized non-intrinsic ABC protein in *Arabidopsis thaliana* results in the over-accumulation of transition metals and in aberrant chloroplast structures. *Plant Cell Environ.* 33 (2010) 1029-1038.

Shojima S., Nishizawa N.K., Fushiya S., Nozoe S., Irifune T., Mori S. Biosynthesis of phytosiderophores: *in vitro* biosynthesis of 2´-deoxymugineic acid from L-methionine and nicotianamine. *Plant Physiol.* 93 (1990) 1497-1503.

Sinha S., Mukherji S., Dutta J. Effect of manganese toxicity on pigment content, Hill activity and photosynthetic rate of *Vigna radiata* L. Wilczek seedlings. *J. Environ. Biol.* 23 (2002) 253-257.

Sisó-Terraza P., Luis-Villarroya A., Fourcroy P., Briat J.F., Abadía A., Gaymard F., Abadía J., Álvarez-Fernández A. Accumulation and secretion of coumarinolignans and other coumarins in *Arabidopsis thaliana* roots in response to iron deficiency at high pH. *Front. Plant Sci. 7* (2016a).

Sisó-Terraza P., Rios J.J., Abadía J., Abadía A., Álvarez-Fernández A. Flavins secreted by roots of iron-deficient *Beta vulgaris* enable mining of ferric oxide *via* reductive mechanisms. *New Phytol.* 209 (2016b) 733-745.

Soares N.C., Francisco R., Vielba J.M., Ricardo C.P., Jackson P.A. Associating wound-related changes in the apoplast proteome of *Medicago* with early steps in the ROS signal-transduction pathway. *J. Proteome Res.* 8 (2009) 2298-2309.

Soares N.C., Francisco R., Ricardo C.P., Jackson P.A. Proteomics of ionically bound and soluble extracellular proteins in *Medicago truncatula* leaves. *J. Proteomics* 7 (2007) 2070-2082.

Socha A.L., Guerinot M.L. Mn-euvering manganese: The role of transporter gene family members in manganese uptake and mobilization in plants. *Front. Plant Sci.* 5 (2014).

Solti Á., Müller B., Czech V., Sárvári É., Fodor F.C. Functional characterization of the chloroplast ferric chelate oxido-reductase enzyme. *New Phytol.* 202 (2014) 920-928.

Solti Á., Kovács K., Basa B., Vértes A., Sárvári E., Fodor F. Uptake and incorporation of iron in sugar beet chloroplasts. *Plant Physiol. Biochem.* 52 (2012) 91-97.

Srivastava A.K., Singh S. Biochemical Markers and Nutrient Constraints Diagnosis in Citrus: A Perspective. *J. Plant Nutr.* 29 (2006) 827-855.

St. Clair S.B., Lynch J.P. Differences in the success of sugar maple and red maple seedlings on acid soils are influenced by nutrient dynamics and light environment. *Plant Cell Environ.* 28 (2005) 874-885.

Stahl Y., Wink R.H., Ingram G.C., Simon R. A signaling module controlling the stem cell niche in *Arabidopsis* root meristems. *Curr. Biol.* 19 (2009) 909-914.

Starrach N M.W. Changes of the apoplasmic pH and K^+ concentration in the *Phaseolus pulvinus* in situ in relation to rhythmic leaf movements. *J. Exp. Bot.* 40 (1989) 865–873.

Steggerda S.M., Paschal B.M. Regulation of nuclear import and export by the GTPase ran. *Int. Rev. Cytol.* 217 (2002) 41-91.

Stephan U.W., Schmidke I., Stephan V., Scholz G. The nicotianamine molecule is made-to-measure for complexation of metal micronutrients in plants. *Biometals* 9 (1996) 84-90.

Stephan U.W., Schmidke I., Pich A. Phloem translocation of Fe, Cu, Mn, and Zn in *Ricinus* seedlings in relation to the concentrations of nicotianamine, an endogenous chelator of divalent metal ions, in different seedling parts. *Plant Soil* 165 (1994) 181-188.

Stephan U.W., Scholz G. Nicotianamine: mediator of transport of iron and heavy metals in the phloem? *Plant. Physiol.* 88 (1993) 522-529.

Steudle E., Smith J.A.C., Lüttge U. Water-relation parameters of individual mesophyll cells of *Kalanchöe daigremontiana. Plant Physiol.* 66 (1980) 1155–1163.

Sturm M., Bertsch A., Gröpl C., Hildebrandt A., Hussong R., Lange E., Pfeifer N., Schulz-Trieglaff O., Zerck A., Reinert K., Kohlbacher O. OpenMS-An open-source software framework for mass spectrometry. *BMC Bioinformatics* 9 (2008) 163.

Sun Q., Zybailov B., Majeran W., Friso G., Olinares P., van Wijk K. PPDB, the Plant Proteomics Database at Cornell. *Nucleic Acids Res.* 37 (2009) 2.

Suzuki N., Koussevitzky S., Mittler R., Miller G. ROS and redox signaling in the response of plants to abiotic stress. *Plant Cell. Environ*. 35 (2012) 259-270.

Switzer R., Merril C., Shifrin S. A highly sensitive silver stain for detecting proteins and peptides in polyacrylamide gels. *Anal. Biochem.* 98 (1979) 231-237.

Tachi H., Fukuda-Yamada K., Kojima T., Shiraiwa M., Takahara H. Molecular characterization of a novel soybean gene encoding a neutral PR-5 protein induced by high-salt stress. *Plant Physiol. Biochem.* 47 (2009) 73-79.

Tagliavini M., Abadía J., Rombolà A.D., Abadía A., Tsipouridis C., Marangoni B. Agronomic means for the control of iron deficiency chlorosis in deciduous fruit trees. *J. Plant Nutr.* 23 (2000) 2007-2022.

Takahashi D., Li B., Nakayama T., Kawamura Y., Uemura M. Shotgun proteomics of plant plasma membrane and microdomain proteins using nano-LC–MS/MS. In: 'Plant proteomics: methods and protocols'. (Eds. J.V. Jorrin-Novo, S. Komatsu, W. Weckwerth, S. Wienkoop) *Humana Press* (2014) 481-498.

Takahashi D., Kawamura Y., Uemura M. Changes of detergent-resistant plasma membrane proteins in oat and rye during cold acclimation: association with differential freezing tolerance. *J. Proteome Res.* 12 (2013) 4998-5011.

Takei K., Takahashi T., Sugiyama T., Yamaya T., Sakakibara H. Multiple routes communicating nitrogen availability from roots to shoots: A signal transduction pathway mediated by cytokinin. *J. Exp. Bot.* 53 (2002) 971-977.

Tanz S.K., Castleden I., Hooper C.M., Vacher M., Small I., Millar H.A. SUBA3: a database for integrating experimentation and prediction to define the SUBcellular location of proteins in *Arabidopsis. Nucleic Acids Res.* 41 (2012) 1185-1191.

Tarantino D., Morandini P., Ramirez L., Soave C., Murgia I. Identification of an *Arabidopsis* mitoferrin like carrier protein involved in Fe metabolism. *Plant Physiol. Biochem.* 49 (2011) 520-529.

Tarantino D., Casagrande F., Soave C., Murgia I. Knocking out of the mitochondrial AtFer4 ferritin does not alter response of *Arabidopsis* plants to abiotic stresses. *J. Plant Physiol.* 167 (2010) 453-460.

Taylor S.W., Fahy E., Zhang B., Glenn G.M., Warnock D.E., Wiley S., Murphy A.N., Gaucher S.P., Capaldi R.A., Gibson B.W., Ghosh S.S. Characterization of the human heart mitochondrial proteome. *Nat. Biotechnol.* 21 (2003) 281.

Tenhaken R., Thulke O. Cloning of an enzyme that synthesizes a key nucleotide-sugar precursor of hemicellulose biosynthesis from soybean. UDP-glucose dehydrogenase. *Plant Physiol.* 112 (1996) 1127-1134.

The Arabidopsis Genome Initiative. Analysis of the genome sequence of the flowering plant *Arabidopsis thaliana. Nature* 408 (2000) 796-815.

Thomine S., Lelièvre F., Debarbieux E., Schroeder J.I., Barbier-Brygoo H. AtNRAMP3, a multispecific vacuolar metal transporter involved in plant responses to iron deficiency. *Plant J.* 34 (2003) 685-695.

Thomine S.b., Wang R., Ward J.M., Crawford N.M., Schroeder J.I. Cadmium and iron transport by members of a plant metal transporter family in *Arabidopsis* with homology to *Nramp* genes. *Proc. Natl. Acad. Sci. U.S.A.* 97 (2000) 4991-4996.

Thompson G.A., Schulz A. Macromolecular trafficking in the phloem. *Trends Plant Sci.* 4 (1999) 354-360.

Thompson I.A., Huber D.M. Manganese and plant disease. In: 'Mineral nutrition and plant disease'. (Eds. L.E. Datnoff, W.H. Elmer, D.M. Huber) *APS Press* (2007) 139-153.

Timperio A.M., Egidi M.G., Zolla L. Proteomics applied on plant abiotic stresses: role of heat shock proteins (HSP). *J. Proteomics* 71 (2008) 391-411.

Tokunaga N., Kaneta T., Sato S., Sato Y. Analysis of expression profiles of three peroxidase genes associated with lignification in *Arabidopsis thaliana*. *Physiol. Plant*. 136 (2009) 237-249.

Tonge R., Shaw J., Middleton B., Rowlinson R., Rayner S., Young J., Pognan F., Hawkins E., Currie I., Davison M. Validation and development of fluorescence two-dimensional differential gel electrophoresis proteomics technology. *Proteomics* 1 (2001) 377-396.

Tottey S., Block M.A., Allen M., Westergren T., Albrieux C., Scheller H.V., Merchant S., Jensen P.E. *Arabidopsis* CHL27, located in both envelope and thylakoid membranes, is required for the synthesis of protochlorophyllide. *Proc. Natl. Acad. Sci. U.S.A.* 100 (2003) 16119-16124.

Turgeon R., Oparka K. The secret phloem of pumpkins. *Proc. Natl. Acad. Sci. U.S.A.* 107 (2010) 13201-13202.

Turlapati P.V., Kim K.W., Davin L.B., Lewis N.G. The laccase multigene family in *Arabidopsis thaliana*: towards addressing the mystery of their gene function(s). *Planta* 233 (2011) 439-470.

Udawat P., Mishra A., Jha B. Heterologous expression of an uncharacterized universal stress protein gene (SbUSP) from the extreme halophyte, *Salicornia brachiata*, which confers salt and osmotic tolerance to *E. coli. Gene* 536 (2014) 163-170.

Vakhmistrov D.B. Localization of the free space in the barley roots. *Fiziol. Rast.* 14 (1967) 397-404.

Van Bel A.J.E. The phloem, a miracle of ingenuity. *Plant Cell Environ.* 26 (2003) 125-149.

Van den Ende W., De Coninck B., Van Laere A. Plant fructan exohydrolases: a role in signaling and defense? *Trends Plant Sci.* 9 (2004) 523-528.

Van der Hoorn R.A.L., Jones J.D.G. The plant proteolytic machinery and its role in defence. *Curr. Opin. Plant Biol.* 7 (2004) 400-407.

Van Goor B.J., Wiersma D. Chemical forms of manganese and zinc in phloem exudates. *Physiol. Plant.* 36 (1976) 213-216.

van Wijk K. Challenges and prospects of plant proteomics. *Plant Physiol.* 126 (2001) 501-508.

Vatansever R., Filiz E., Ozyigit I.I. In silico analysis of Mn transporters (NRAMP1) in various plant species. *Mol. Biol. Rep.* 43 (2016) 151-163.

Vazzola V., Losa A., Soave C., Murgia I. Knockout of frataxin gene causes embryo lethality in *Arabidopsis. FEBS Letters* 581 (2007) 667-672.

Venkatesan S., Hemalatha K.V., Jayaganesh S. Characterization of manganese toxicity and its influence on nutrient uptake, antioxidant enzymes and biochemical parameters in tea. *Res. J. Phytochem.* 1 (2007) 52–60.

Vert G., Grotz N., Dédaldéchamp F., Gaymard F., Guerinot M.L., Briat J.F., Curie C. IRT1, an *Arabidopsis* transporter essential for iron uptake from the soil and for plant growth. *Plant Cell* 14 (2002) 1223-1233.

Vigani G., Zocchi G., Bashir K., Philippar K., Briat J.F. Signals from chloroplasts and mitochondria for iron homeostasis regulation. *Trends Plant Sci.* 18 (2013) 305-311.

Vigani G. Discovering the role of mitochondria in the iron deficiency-induced metabolic responses of plants. *J. Plant Physiol.* 169 (2012) 1-11.

Vigani G. Maffi D., Zocchi G. Iron availability affects the function of mitochondria in cucumber roots. *New Phytol.* 182 (2009) 127-136.

Vizcaíno J.A., Csordas A., del-Toro N., Dianes J.A., Griss J., Lavidas I., Mayer G., Perez-Riverol Y., Reisinger F., Ternent T., Xu Q.W., Wang R., Hermjakob H. 2016 update of the PRIDE database and related tools. *Nucleic Acids Res.* 44 (2016) 447-456.

Vollmer M., Van de Goor T. HPLC-Chip/MS technology in proteomic profiling. *Methods Mol. Biol.* 544 (2009) 3-15.

von Wirén N., Klair S., Bansal S., Briat J.-F., Khodr H., Shioiri T., Leigh R.A., Hider R.C. Nicotianamine chelates both Fe-III and Fe-II. Implications for metal transport in plants. *Plant Physiol.* 119 (1999) 1107-1114.

Vose P.B., Randall P.J. Resistance to aluminum and manganese toxicities in plants related to variety and cation exchange capacity. *Nature* 196 (1962) 85–86.

Walton G.H. The effect of manganese on seed yield and the split seed disorder of sweet and bitter phenotypes of *Lupinus angustifolius* and *L. cosentinii. Aust. J. Agric. Res.* 29 (1978) 1177-1189.

Walz C., Giavalisco P., Schad M., Juenger M., Klose J., Kehr J. Proteomics of curcurbit phloem exudate reveals a network of defence proteins. *Phytochemistry* 65 (2004) 1795-1804.

Wang C.Y., Shen R.F., Wang C., Wang W. Root protein profile changes induced by Al exposure in two rice cultivars differing in Al tolerance. *J. Proteomics* 78 (2013) 281-293.

Wang G., Zhang G., Wu M. CLE peptide signaling and crosstalk with phytohormones and environmental stimuli. *Front. Plant Sci.* 6 (2015) 1211.

Wang W., Zhou H., Lin H., Roy S., Shaler T.A., Hill L.R., Norton S., Kumar P., Anderle M., Becker C.H. Quantification of proteins and metabolites by mass spectrometry without isotopic labeling or spiked standards. *Anal. Chem.* 75 (2003) 4818-4826.

Wang Y., Wang H., Yang C.H., Wang Q., Mei R. Two distinct manganese-containing superoxide dismutase genes in *Bacillus cereus*: Their physiological characterizations and roles in surviving in wheat rhizosphere. *FEMS Microbiology Letters* 272 (2007) 206-213.

Washburn M., Wolters D., Yates J. Large-scale analysis of the yeast proteome by multidimensional protein identification technology. *Nat. Biotechnol.* 19 (2001) 242-247.

Wasternack C. Oxylipins: biosynthesis, signal transduction and action. *Annual Plant Reviews* (2007) 185-228.

Waters B.M., Chu H.H., DiDonato R.J., Roberts L.A., Eisley R.B., Lahner B., Salt D.E., Walker E.L. Mutations in *Arabidopsis* yellow stripe-like1 and yellow stripe-like3 reveal their roles in metal ion homeostasis and loading of metal ions in seeds. *Plant Physiol.* 141 (2006) 1446-1458.

Watmough S.A., Eimers M.C., Dillon P.J. Manganese cycling in central Ontario forests: Response to soil acidification. *Appl. Geochem.* 22 (2007) 1241-1247.

Watson B.S., Lei Z., Dixon R.A., Sumner L.W. Proteomics of *Medicago sativa* cell walls. *Phytochemistry* 65 (2004) 1709-1720.

Weber G., von Wirén N., Hayen H. Investigation of ascorbate-mediated iron release from ferric phytosiderophores in the presence of nicotianamine. *BioMetals* 21 (2008) 503-513.

Weber H. Fatty acid-derived signals in plants. *Trends Plant Sci.* 7 (2002) 217-224.

Wedepohl K.H. Chemical composition and fractionation of the continental crust. *Geol. Rundsch.* 80 (1991) 207-223.

Wegele H., Müller L., Buchner J. Hsp70 and Hsp90-a relay team for protein folding. *Rev. Physiol. Biochem. Pharmacol.* 151 (2004) 1-44.

White M.C., Decker A.M., Chaney R.L. Metal complexation in xylem fluid: I. Chemical composition of tomato and soybean stem exudate. *Plant Physiol.* 67 (1981) 292-300.

White P.J., Brown P.H. Plant nutrition for sustainable development and global health. *Ann. Bot.* 105 (2010) 1073-1080.

White P.J., Bowen H.C., Demidchik V., Nichols C., Davies J.M. Genes for calcium-permeable channels in the plasma membrane of plant root cells. *BBA-Biomembranes* 1564 (2002) 299-309.

Whitelegge J.P. Plant proteomics: Blasting out of a MudPIT. *Proc. Natl. Acad. Sci. U.S.A.* 99 (2002) 11564-11566.

Wilkins M.R. 2D electrophoresis: from protein maps to genomes. *First Siena conference, Siena* (1994)

Williams L.E., Pittman J.K. Dissecting pathways involved in manganese homeostasis and stress in higher plant cells. In: 'Cell biology of metals and nutrients' (Eds. R. Hell, R.R. Mendel) *Springer* (2010) 95-117.

Wissemeier A.H., Horst W.J. Callose deposition in leaves of cowpea (*Vigna unguiculata* [L.] Walp.) as a sensitive response to high Mn supply. *Plant Soil* 102 (1987) 283-286.

Witzel K., Shahzad M., Matros A., Mock H.P., Mühling K.H. Comparative evaluation of extraction methods for apoplastic proteins from maize leaves. *Plant Methods* 7 (2011) 48.

Wolf O., Munns R., Tonnet M.L., Jeschke W.D. Concentrations and transport of solutes in xylem and phloem along the leaf axis of NaCl-treated *Hordeum vulgare*. *J. Exp. Bot.* 41 (1990) 1133–1141.

Wolters D., Washburn M., Yates J. An automated multidimensional protein identification technology for Shotgun Proteomics. *Anal. Chem.* 73 (2001) 5683-5690.

Wout B., John R., Marie B. Lignin Biosynthesis. *Annu. Rev. Plant Biol.* 54 (2003) 519-546.

Wu D., Yamaji N., Yamane M., Kashino-Fujii M., Sato K., Feng Ma J. The HvNramp5 transporter mediates uptake of cadmium and manganese, but not iron. *Plant Physiol.* 172 (2016) 1899-1910.

Wu H., Li L., Du J., Yuan Y., Cheng X., Ling H.Q. Molecular and biochemical characterization of the Fe(III) chelate reductase gene family in *Arabidopsis thaliana. Plant Cell Physiol.* 46 (2005) 1505-1514.

Wu Z., Liang F., Hong B., Young J.C., Sussman M.R., Harper J.F., Sze H. An endoplasmic reticulum-bound Ca^{2+}/Mn^{2+} pump, ECA1, supports plant growth and confers tolerance to Mn^{2+} stress. *Plant Physiol.* 130 (2002) 128-137.

Xia Y., Suzuki H., Borevitz J., Blount J., Guo Z., Patel K., Dixon R.A., Lamb C. An extracellular aspartic protease functions in *Arabidopsis* disease resistance signaling. *EMBO J.* 23 (2004) 980-988.

Xiong H., Kakei Y., Kobayashi T., Guo X., Nakazono M., Takahashi H., Nakanishi H., Shen H., Zhang F., Nishizawa K., Zuo Y. Molecular evidence for phytosiderophoreinduced improvement of iron nutrition of peanut intercropped with maize in calcareou soil. *Plant Cell Environ.* 36 (2013) 1888-1902.

Xu X., Yang J., Zhao X., Zhang X., Li R. Molecular binding mechanisms of manganese to the root cell wall of *Phytolacca americana* L. using multiple spectroscopic techniques. *J. Hazard. Mater.* 296 (2015) 185-191.

Xue S.G., Chen Y.X., Reeves R.D., Baker A.J.M., Lin Q., Fernando D.R. Manganese uptake and accumulation by the hyperaccumulator plant *Phytolacca acinosa* Roxb. (Phytolaccaceae). *Environ. Pollut.* 131 (2004) 393-399.

Yamaji N., Ma J.F. The node, a hub for mineral nutrient distribution in graminaceous plants. *Trends Plant Sci.* 19 (2014) 556-563.

Yamaji N., Sasaki A., Xia J.X., Yokosho K., Ma J.F. A node-based switch for preferential distribution of manganese in rice. *Nat. Commun.* 4 (2013) 2442.

Yao Q., Ge H., Wu S., Zhang N., Chen W., Xu C., Gao J., Thelen J.J., Xu D. P3DB 3.0: From plant phosphorylation sites to protein networks. *Nucleic Acids Res.* 42 (2014) 1206-1213.

Yao Y., Xu G., Mou D., Wang J., Ma J. Subcellular Mn compartation, anatomic and biochemical changes of two grape varieties in response to excess manganese. *Chemosphere* 89 (2012) 150-157.

Yi E.C., Li X.J., Cooke K., Lee H., Raught B., Page A., Aneliunas V., Hieter P., Goodlett D.R., Aebersold R. Increased quantitative proteome coverage with $^{13}C/^{12}C$-based, acid-cleavable isotope-coded affinity tag reagent and modified data acquisition scheme. *Proteomics* 5 (2005) 380-387.

Yokosho K., Yamaji N., Ueno D., Mitani N., Ma J.F. OsFRDL1 is a citrate transporter required for efficient translocation of iron in rice. *Plant Physiol.* 149 (2009) 297-305.

Yoo B.C., Kragler F., Varkonyi-Gasic E., Haywood V., Archer-Evans S., Lee Y.M., Lough T.J., Lucas W.J. A systemic small RNA signaling system in plants. *Plant Cell* 16 (2004) 1979-2000.

You X., Yang L.T., Lu Y.-B., Li H., Zhang S.Q., Chen L.S. Proteomic changes of *Citrus* roots in response to long-term manganese toxicity. *Trees* 28 (2014) 1383-1399.

Young T.F., Terry N. Transport of iron into leaves following iron resupply to iron-stressed sugar beet plants. *J. Plant Nutr.* 5 (1982) 1273-1283.

Zaharieva B.T., Abadía J. Iron deficiency enhances the levels of ascorbate, glutathione, and related enzymes in sugar beet roots. *Protoplasma* 221 (2003) 269-275.

Zargar S.M., Gupta N., Mir R.A., Rai V. Shift from gel based to gel free proteomics to unlock unknown regulatory network in plants: a comprehensive review. *J. Adv. Res. Biotech.* 1 (2016) 19.

Zargar S.M., Fujiwara M., Inaba S., Kobayashi M., Kurata R, Ogata Y, Fukao Y. Correlation analysis of proteins responsive to Zn, Mn, or Fe deficiency in Arabidopsis roots based on iTRAQ analysis. *Plant Cell Rep.* 34 (2015) 157-166.

Zhang C., Yu X., Ayre B.G., Turgeon R. The origin and composition of cucurbit "phloem" exudate. *Plant Physiol.* 158 (2012) 1873-1882.

Zhang F., Römheld V., Marschner H. Role of the root apoplasm for iron acquisition by wheat plants. *Plant Physiol.* 97 (1991) 1302-1305.

Zhang J., Ma H., Feng J., Zeng L., Wang Z., Chen S. Grape berry plasma membrane proteome analysis and its differential expression during ripening. *J. Exp. Bot.* 59 (2008) 2979-2990.

Zhang L., Tian L.H., Zhao J.F., Song Y., Zhang C.J., Guo Y. Identification of an apoplastic protein involved in the initial phase of salt stress response in rice root by two-dimensional electrophoresis. *Plant Physiol.* 149 (2009) 916-928.

Zhang Y., Xu Y.H., Yi H.Y., Gong J.M. Vacuolar membrane transporters OsVIT1 and OsVIT2 modulate iron translocation between flag leaves and seeds in rice. *Plant J.* 72 (2012) 400-410.

Zhang Z., Chao M., Wang S., Bu J., Tang J., Li F., Wang Q., Zhanga B. Proteome quantification of cotton xylem sap suggests the mechanisms of potassium deficiency-induced changes in plant resistance to environmental stresses. *Sci. Rep.* 6 (2016) 21060.

Zhang Z., Xin W., Wang S., Zhang X., Dai H., Sun R., Frazier T., Zhang B., Wang Q. Xylem sap in cotton contains proteins that contribute to environmental stress response and cell wall development. *Funct. Integr. Genomics* 15 (2015) 17-26.

Zhang X., Jiang L., Wang G., Yu L., Zhang Q., Xin Q., Wu W., Gong Z., Chen Z. Structural insights into the abscisic acid stereospecificity by the ABA receptors PYR/PYL/RCAR. PLoS ONE 8 (2013) 67477.

Zhou C.P., Qi Y.P., You X., Yang L.T., Guo P., Ye X., Zhou X.X., Ke F.J., Chen L.S. Leaf cDNA-AFLP analysis of two citrus species differing in manganese tolerance in response to long-term manganese-toxicity. *BMC Genomics* 14 (2013) 621.

Zhou L., Bokhari S.A., Dong C.J., Liu J.Y. Comparative proteomics analysis of the root apoplasts of rice seedlings in response to hydrogen peroxide. *PLoS ONE* 6 (2011) 16723.

Zocchi G. Metabolic changes in iron-stressed dicotyledonous plants. In: 'Iron nutrition in plants and rhizospheric microorganisms'. (Eds. L.L. Barton, J. Abadía) *Springer* (2006) 359–370.

ANEXOS

Anexo I. Effects of Fe deficiency on the protein profiles and lignin composition of stem tissues from *Medicago truncatula* in absence or presence of calcium carbonate

Jorge Rodríguez-Celma [a,1], Giuseppe Lattanzio [a], Dido Villarroya [a], Elain Gutierrez-Carbonell [a], Laura Ceballos-Laita [a], Jorge Rencoret [b], Ana Gutiérrez [b], José C. del Río [b], Michael A. Grusak [c], Anunciación Abadía [a], Javier Abadía [a], Ana-Flor López-Millán [c]

[a] *Plant Nutrition Department, Aula Dei Experimental Station (CSIC), P.O. Box 13034, E-50080, Zaragoza, Spain*

[b] *Instituto de Recursos Naturales y Agrobiología de Sevilla (CSIC), Reina Mercedes 10, E-41012 Sevilla, Spain*

[c] *USDA-ARS Children's Nutrition Research Center, Department of Pediatrics, Baylor College of Medicine, 1100 Bates Street, Houston, TX 77030, USA*

Published in Journal of Proteomics (2016) 140, 1-12 (*doi: 10.1016/j.jprot.2016.03.017*)

ABSTRACT

Iron deficiency is a yield-limiting factor with major implications for crop production, especially in soils with high $CaCO_3$. Because stems are essential for the delivery of nutrients to the shoots, the aim of this work was to study the effects of Fe deficiency on the stem proteome of *Medicago truncatula*. Two-dimensional electrophoresis separation of stem protein extracts resolved 276 consistent spots in the whole experiment. Iron deficiency in absence or presence of $CaCO_3$ caused significant changes in relative abundance in 10 and 31 spots, respectively, and 80% of them were identified by mass spectrometry. Overall results indicate that Fe deficiency by itself has a mild effect on the stem proteome, whereas Fe deficiency in the presence of $CaCO_3$ has a stronger impact and causes changes in a larger number of proteins, including increases in stress and protein metabolism related proteins not observed in the absence of $CaCO_3$. Both treatments resulted in increases in cell wall related proteins, which were more intense in the presence of $CaCO_3$. The increases induced by Fe deficiency in the lignin per protein ratio and changes in the lignin monomer composition, assessed by pyrolysis-gas chromatography–mass spectrometry and microscopy, respectively, further support the existence of cell wall alterations.

Biological significance

In spite of being essential for the delivery of nutrients to the shoots, our knowledge of stem responses to nutrient deficiencies is very limited. The present work applies 2-DE techniques to

unravel the response of this understudied tissue to Fe deficiency. Proteomics data, complemented with mineral, lignin and microscopy analyses, indicate that stems respond to Fe deficiency by increasing stress and defense related proteins, probably in response of mineral and osmotic unbalances, and eliciting significant changes in cell wall composition. The changes observed are likely to ultimately affect solute transport and distribution to the leaves.

A.I.1. Introduction

Many environmental conditions, including the high pH of calcareous soils, can result in scarce Fe availability in farmlands, resulting in Fe deficiency chlorosis and marked reductions in agricultural produce yield and quality (Abadía et al., 2011; Álvarez-Fernández et al., 2003; Mengel, 1994). Iron deficiency associated with soils rich in $CaCO_3$ is a major constraint for yield in economically relevant crops such as soybean grown in the upper Midwest areas of the U.S. (Coulombe et al.,1984; Froelichet al., 1981; Lin et al., 1997) and fruit tree crops in Mediterranean climate areas (Álvarez-Fernández et al., 2011; Rombolà and Tagliavini, 2006). When facing low soil Fe availability, plants respond by inducing root morphological and physiological changes aimed to increase the Fe uptake capacity, which vary depending on the taxonomical group (Romheld, 1987). Efforts have been devoted to deciphering this complex network in plants at the transcriptomic, proteomic and metabolomic levels (Hindt and Guerinot, 1823; Lan et al., 2011; López-Millán et al., 2013; Rellán-Álvarez et al., 2010a; 2011; Rodríguez-Celma et al., 2013a; Schmidt and Buckhout, 2011). In dicotyledonous plants, root responses include an induction of the Fe-reduction based uptake machinery (Eide et al., 1996; Robinson et al., 1999), an enhanced proton extrusion capacity (Santi and Schmidt, 2009), the excretion of organic compounds including carboxylates, phenolics and flavins (Cesco et al., 2010; Fourcroy et al., 2014; Rodríguez-Celma et al., 2011a; 2013a; Schmid et al., 2014), and a reprogramming of general metabolic pathways such as the tricarboxylic acid cycle (TCA) and glycolysis to fuel the high energy requirements for Fe uptake (López-Millán et al., 2009; Zocchi, 2006). Being an essential micronutrient, Fe must be translocated to the shoots, where it plays important roles in respiration and chlorophyll synthesis among others (Marschner, 1995). In the xylem pathway, complexation with citrate plays a determinant role (Durrett et al., 2007; Rellán-Álvarez et al., 2010b; Roschzttardtz et al., 2011).

The effects of Fe deficiency are not restricted to roots and leaves, and low soil Fe availability also results in plants with reduced stem length and mass (Vasconcelos et al., 2014). Plant stems provide mechanical support to the plant and are essential for the delivery of water and nutrients (e.g., minerals, sugars amino acids) to the various plant organs (Lucas et al., 2013). In addition, the vascular systems within the stem act as long distance communication channels between roots and shoots, in which hormones, micro-RNAs, peptides and proteins act

as signaling molecules (Hossain and Komatsu, 2013). The dual role of these systems, including delivery of nutrients as well as signaling, makes stems crucial for the coordination of responses to nutritional stresses at the whole plant level. However, very little information is available to date about the effects of Fe deficiency in stem tissues.

Proteomic profiling using 2-DE is an excellent tool to provide a holistic picture of changes induced by nutritional stresses (Hossain and Komatsu, 2013; Jorrín-Novo et al., 2009; Liang et al., 2013). Indeed, changes in the protein profiles in response to Fe deficiency have already been studied in different plant tissues, mainly roots and thylakoids, using model plant species such as barrel medic (*Medicago truncatula*) (López-Millán et al., 2013). This plant species has a small diploid genome that yields manageable genetic tools, it is autogamous, has a short generation time and a prolific seed production that makes it useful as a model legume (Benedito et al., 2008; Colditz and Braun, 2010; Watson et al., 2003). Among the resources for *M. trucatula*, several reference proteomes, including that of stems, are currently available (Watson et al., 2003).

In the present study, we have examined the effects of Fe deficiency on the stem protein profiles of *M. truncatula* plants submitted to Fe deficiency, and used pyrolysis-gas chromatography–mass spectrometry and microscopy to assess changes in the lignin composition of these tissues. Legumes are valuable agricultural and commercial crops that serve as important nutrient sources for both humans and animals, and a better understanding of the effects of Fe deficiency in stems, essential for the long distance transport of Fe, may strengthen our ability to enhance Fe-efficiency responses. Two different treatments have been used to impose Fe deficiency in nutrient solution, with or without $CaCO_3$, with the aim to know whether the presence of $CaCO_3$, which is often found in Fe-deficient soils, causes additional effects to those of a direct Fe shortage alone.

A.I.2. Material and methods

Plant material and growth conditions

Medicago truncatula cv. 'Jemalong' plants were grown in a controlled environment chamber with a photosynthetic photon flux density at leaf height of 350 μmol m^{-2} s^{-2} photosynthetically active radiation, 80 % relative humidity and at a 16 h-23 °C/8 h-19 °C, day/night regime. Seeds were scarified by nicking the seed coat, then imbibed overnight in distilled water and germinated on filter paper for three days in darkness with full humidity. Seedlings were grown for an additional two-week period in half-strength Hoagland nutrient solution (pH 5.5) with 45 μM Fe(III)-EDTA (Terry, 1980). Plants were then transplanted to 10 L plastic buckets (six plants per bucket) containing half-strength Hoagland nutrient solution and treatments were

imposed. Control plants were grown with 45 μM Fe(III)-EDTA (pH 5.5) and Fe-deficient plants were grown with no added Fe (0 μM Fe), with (pH 7.7) or without (pH 5.5) 1 g L^{-1} $CaCO_3$. After six days, stem tissues (including main stems and petioles but excluding cotyledons and leaves; Supplementary Figure S1) were harvested, frozen in liquid N_2 and stored at −80 °C. Five independent batches of plants were grown and sampled for proteomic analysis. Tissues for mineral (stems including petioles, roots and leaves) and lignin (stems and petioles separately) analyses were also harvested six days after treatment onset from three plants per treatment in two independent batches of plants.

Protein extraction

For protein extraction, approximately 0.5–1 g of tissue (pooled from two plants of a given treatment), containing whole stems (including the main stems and petioles, see Supplementary Figure S1) but excluding cotyledons and leaves, was ground in liquid N_2 with mortar and pestle. The tissue was homogenized in 6 mL of phenol saturated with 0.1 M Tris-HCl (pH 8.0) and containing 5 mM β-mercaptoethanol, by stirring for 30 min at 4 °C. Then, the homogenate was filtered (PVDF, 0.45 μm) and centrifuged at 5000 ×g for 15 min. The phenol phase was reextracted for 30 min with one volume of phenol-saturated 0.1 M TrisHCl (pH 8.0) containing 5 mM β-mercaptoethanol, and centrifuged as described above. Proteins in the phenol phase were precipitated by adding four volumes of 0.1 M ammonium acetate in cold methanol, followed by overnight incubation at −20 °C. Samples were then centrifuged at 5000 ×g for 15 min, and the pellet was washed three times with cold methanol, dried with N_2 gas and resuspended in sample rehydration buffer containing 8 M urea, 2 % (w/v) CHAPS, 50 mM DTT, 2 mM PMSF and 0.2 % (v/v) 3–10 ampholytes (Amersham, Uppsala, Sweden). After rehydration, samples were incubated at 38 °C for 1.5 h and then centrifuged at 15,000 ×g for 10 min at 20 °C. Samples were analyzed immediately by 2-DE. Protein concentration was measured with the Bradford method (BioRad kit), using microtiter plates in an Asys UVM 340 (Biochrom Ltd., Cambridge, UK) spectrophotometer and BSA as standard.

Protein 2-DE separation

Preliminary 2-DE experiments were carried out using a first dimension IEF separation with a linear pH gradient 3–10; in these conditions most of the spots were concentrated in the central region of the 2-DE gel (results not shown); therefore, to prevent protein comigration and improve resolution a narrower pH gradient was chosen. A first dimension IEF separation was carried out on 7 cm ReadyStrip IPG Strips (BioRad) with a linear pH gradient pH 5–8 using a Protean IEF Cell (BioRad, Hercules, CA, USA). Strips were passively rehydrated for 16 h at 20 °C in 125 μL of rehydration buffer containing 60 μg of root extract proteins and a trace of

bromophenol blue, and then transferred onto a strip tray. IEF was run at 20 °C, for a total of 14,000 V h (20 min with a 0–250 V linear gradient, 2 h with a 250–4000 V linear gradient and 4000 V until 10,000 V h). After IEF, strips were equilibrated for 10 min in equilibration solution I [6 M urea, 0.375 M Tris-HCl, pH 8.8, 2 % (w/v) SDS, 20 % (v/v) glycerol, 2 % (w/v) DTT] and for another 10 min in equilibration solution II [6 M urea, 0.375 M Tris-HCl pH 8.8, 2% (w/v) SDS, 20 % (v/v) glycerol and, 2.5 % (w/v) iodoacetamide]. For the second dimension SDS-PAGE, equilibrated IPG strips were placed on top of vertical 12 % SDS-polyacrylamide gels (8 × 10 × 0.1 cm) and sealed with melted 0.5 % agarose in 50 mM Tris HCl, pH 6.8, containing 0.1 % SDS. SDS-PAGE was carried out at 20 mA per gel for approximately 1.5 h, until the bromophenol blue reached the plate bottom, in a buffer containing 25 mM Tris, 192 mM glycine, and 0.1 % SDS, at 4 °C. Gels were subsequently stained with colloidal Coomassie-blue G-250 (Serva, Barcelona, Spain). For each treatment, gels were made from independent whole stem samples (including petioles) preparations obtained from five different batches of plants (n = 5).

Gel image and statistical analysis

Stained gels were scanned with an Epson Perfection 4990 Photo Scanner (Epson Ibérica, Barcelona, Spain) at 600 dpi, previously calibrated using the SilverFast 6 software (LaserSoft Imaging AG, Kiel, Germany) and an IT8 reference card. Spot detection, gel matching and interclass analysis were performed with PDQuest 8.0 software (BioRad). First, normalized spot volumes based on total intensity of valid spots were calculated for each 2-DE gel and used for statistical calculations of protein abundance; for all spots present in the gels, pI, Mr, and normalized volumes (mean values and SD) were determined. Experimental MR values were calculated by mobility comparisons with Precision Plus protein standard markers (BioRad) run in a separate lane on the SDS gel, and pI was determined by using a linear scale over the total dimension of the IPG strips. Only spots consistently present in at least 80 % of the replicates (four out of five gels) from at least one class were considered and used in further analysis; missing spot volumes were estimated from the data set by a sequential K-Nearest Neighbor algorithm using an R 2.7.0 environment. After the input of missing values, a second normalization based on total intensity of valid spots per gel was used to compensate for gel replicate variations, and resulting data were used for statistical analyses. The spots were also manually checked, and consistent reproducibility between normalized spot volumes was found in the different replicates (Supplementary Table S1).

Univariate and multivariate statistical analyses were carried out. Spots changing in relative abundance were selected using a paired Studentt-test and a significance level of $p<0.05$. Protein response ratios were defined as the relative abundance in a given treatment divided by

the relative abundance in the controls. Only proteins with mean response ratios above 2.0 or below 0.5 were considered as physiologically relevant and are discussed in this study. Principal component analysis (PCA) was carried out using Excel ad-in Multibase 2014.

Protein identification by nano-liquid chromatography-tandem mass spectrometry (nLC-ESI-MS/MS)

Consistent spots showing statistically significant differences in accumulation were excised automatically using a spot cutter EXQuest (BioRad), proteins in spots digested, and peptides separated by nanoHPLC (n-HPLC system 1200 series, Agilent Technologies, Waldbronn, Germany) as described in (Gutierrez-Carbonell et al., 2013). The nano-HPLC was connected to a HCT Ultra high-capacity ion trap (Bruker Daltonics, Bremen, Germany) using a PicoTip emitter (50 μm i.d., 8 μm tip i.d., New Objective, Woburn, MA, USA) and an online nano-electrospray source. Capillary voltage was −1.8 kV in positive mode and a dry gas flow rate of 10 L min^{-1} was used with a temperature of 180 °C. MS data were acquired automatically using Hystar 3.2 software following a MS survey scan from 50 to 3000 m/z at a resolution of 5500. The mass window for precursor ion selection was ±0.15 m/z with an active exclusion after two spectra and release after 1.2 min for the one most intense peptide. MS/MS spectra were sequentially and dynamically acquired in a scan from 300 to 1500 m/z with a maximum accumulation time of 750 ms depending on sample concentration. The fragmentation amplitude for MS/MS was 1 V. Singly charged ions and trypsin peptides were excluded from MS/MS analysis. Peak detection, deconvolution and processing were performed with Data Analysis 3.4 (Bruker Daltonics). Protein identification was carried out using the Mascot search engine (version 2.3.02, Matrix Science; London, UK) and the non-redundant databases NCBInr 20,120,303 (17,378,729 sequences; 5,967,463,365 residues). Search parameters were: monoisotopic mass accuracy, peptide mass tolerance ±0.2 Da, fragment mass tolerance ±0.6 Da; one allowed missed cleavage; allowed fixed modification carbamidomethylation (Cys), and variable modification oxidation (Met). Positive identification was assigned with Mascot scores above the threshold level ($p \leq 0.05$) and at least two identified peptides with a score above homology. The list of peptides identified is shown in Supplementary Table S2. We used the GO biological process annotation (http://www.geneontology.org) of the individual identified proteins and UniProt database information for manual classification into functional categories.

Mineral analysis

Roots, whole stems (including petioles) and leaves were harvested from three plants per treatment, dried in a conventional oven at 60 °C and ground in a stainless steel mill. Subsamples (ca. 0.15 g dry weight) of each ground sample were digested and processed for elemental

analysis as described elsewhere (García and Grusak, 2015). Elemental analysis (Ca, Cu, Fe, K, Mg, Mn, Mo, Na, P, S, and Zn) was carried out using inductively coupled plasma-optical emission spectroscopy (CIROS ICP Model FCE12; Spectro, Kleve, Germany); the instrument was calibrated daily with certified standards. Tomato leaf standards (SRM 1573 A; National Instituteof Standards and Technology, Gaithersburg, MD, USA) were digested and analyzed along with the *M. truncatula* samples to ensure accuracy.

Microscopy

For microscopy analysis, sections from both petioles and stems of *M. truncatula* plants grown for 6 d in the control conditions or with 0 μM Fe in the presence or absence of $CaCO_3$, were excised with a razor blade and embedded in 5 % agar. Eight different petiole and stem sections from eight different plants for each treatment were analyzed. Stem and petiole transversal sections (60 μM thick) were obtained using a vibrating blade microtome (VT1000 S, Leica Microsystems GmbH). Cell walls were stained using phloroglucinol (SIGMA), and bright field and auto-fluorescence images of the transversal slices were taken with an inverted microscope (DM IL LED, Leica Microsystems GmbH) equipped with a fluorescence kit (340–380 excitation wavelength and 425 nm cut-off filter; A1 filter cube, Leica Microsystems GmbH) and a CCD camera (DFC 240C, Leica Microsystems GmbH).

Lignin analysis

Lignin analysis was carried out by pyrolysis-gas chromatography–mass spectrometry (Py-GC–MS) using separately petioles and stems harvested from three *M. truncatula* plants per treatment. Pyrolysis of the samples (approximately 7 mg) was performed with a 3030 μ-furnace pyrolyzer (Frontier Laboratories Ltd.) connected to an Agilent 7820 A GC using a DB-1701 fused-silica capillary column (60 m × 0.25 mm i.d., 0.25 μm film thickness) and an Agilent 5975 mass selective detector (EI at 70 eV). The pyrolysis was performed at 500 °C. The oven temperature was programmed from 45 °C (4 min) to 280 °C (10 min) at 4 °C min^{-1}. Helium was the carrier gas (2 mL min^{-1}). Compounds were identified by comparing their mass spectra with those in the Wiley and NIST libraries and those reported in the literature (Ralph and Hatfield, 1991). Peak molar areas were calculated for the main lignin-degradation products using their characteristic mass fragment ions, the summed areas were normalized, and data from four biological replicates were averaged and expressed as percentages. The main lignin compounds and the mass fragment ions used for quantitation were: guaiacol (m/z 124), 4-methylguaiacol (m/z 138), 4-ethylguaiacol (m/z 137), 4-vinylguaiacol (m/z 150), eugenol (m/z 164), cis-isoeugenol (m/z 164) and trans-isoeugenol (m/z 164) as guaiacyllignin markers, and syringol (m/z 154), 4-methylsyringol (m/z 168), 4-ethylsyringol (m/z 167), 4-vinylsyringol (m/z 180), 4-

allylsyringol (m/z 194), cis-4-propenylsyringol (m/z 194), and trans-4-propenylsyringol (m/z 194) as syringyl-lignin markers. The compounds used for quantitation of proteins and their characteristic fragment ions were phenylacetonitrile (m/z 117), indole (m/z 117), and 3-methylindole (m/z 130).

A.I.3. Results

Symptoms of Fe deficiency in *M. truncatula* plants included a yellowing of young leaves and a reduction of biomass, which were more intense in the treatment that included $CaCO_3$; these symptoms were described in detail in a parallel study focused to root proteomic changes (Rodríguez-Celma et al., 2011b).

Protein profiles

Changes in the protein profile of extracts of stems (including petioles) from Fe-deficient *M. truncatula* plants grown in the absence (pH 5.5) or presence of $CaCO_3$ (pH 7.7) were studied by 2-D IEF-SDS PAGE electrophoresis. Typical real scans of 2-DE gels obtained from root protein extracts of Fe-sufficient and Fe-deficient (pH 5.5 or 7.7) plants are shown in Figure A.I.1A-C, respectively.

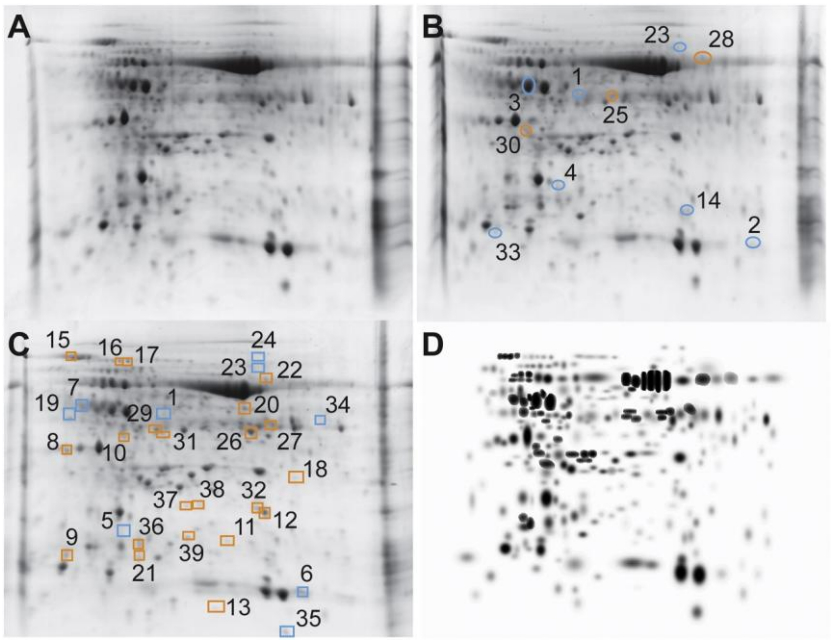

Figure A.I.1. *2-DE IEF-SDS PAGE protein profile maps of stem extracts from Medicago truncatula plants. Scans of typical gels from the stems of Fe-sufficient and Fe-deficient plants grown in the absence and presence of $CaCO_3$ are shown in A, B and C, respectively. To facilitate visualization of the studied spots, a virtual composite image (D) was created containing all spots present in the real gels A, B and C. In B (−Fe) and C (−Fe + $CaCO_3$), spots whose intensities decreased or increased when compared to control maps are marked with blue and orange symbols, respectively. Identified spots are labeled in B and C with the corresponding number assigned in Table A.I.1.*

The average number of detected spots (mean ± SD) was 265 ± 2, 261 ± 2 and 267 ± 2 in gels from plants grown with 45 μM Fe and 0 μM Fe in the absence or presence of $CaCO_3$; approximately 95 % of spots were consistently found in all five replicates within each treatment (Supplementary Table S3). The total number of spots consistently detected in the whole experiment (present in at least 80 % of the gels of one treatment) was 276 (Supplementary Tables S1 and S3). A composite averaged virtual map containing all spots present in all 15 gels (5 per treatment) is shown in Figure A.I.1D.

When compared to the control plants, four and 11 % of the consistent spots (10 and 31 spots, respectively) showed changes in relative abundances that were statistically significant at $p<0.05$ and above the cut-off values for fold-change (≥ 2 or ≤ 0.5) in the 0 μM Fe treatments in the absence or presence of $CaCO_3$, respectively (these spots are marked in bold and with an asterisk in Table A.I.1). Two of these changes (decreases in the relative abundance of spots 1 and 23) occurred irrespectively of the presence of $CaCO_3$ (Table A.I.1 and Figure A.I.2B). From the total 39 spots showing physiologically relevant changes, 80 % (31 spots) were reliably identified (Table A.I.1).

Table A.I.1. *Proteins identified in 2-D IEF-SDS PAGE gels. In the −Fe vs +Fe and −Fe + $CaCO_3$ vs + Fe columns, spots showing statistically significant changes (t-Student's test, $p < 0.05$) and above the biological relevant cut-off values (fold ≥ 2 or fold ≤ 0.5) are marked in bold with an asterisk, and spots showing significant changes in relative abundance but with fold-changes outside the cut-off values are marked only in bold. For some spots, fold changes outside the threshold cut off values ($p < 0.05$ and/or fold ≥ 2 or fold ≤ 0.5) are indicated in normal typeface in a given treatment when they were significant in the other treatment. Spots were analyzed by LC–MS/MS and positive identification was retained with Mascot scores (Sc) above the threshold levels ($p < 0.05$) and at least two identified peptides with a ion score above homology (ion/pep). Function was inferred from GO and UniProt entry annotation. "new" and "lost" indicate spots that have been newly detected or no longer detected in the −Fe treatments.*

Spot	UniProt	Protein description	Sc/ion /pep	Sq (%)	Mw/pI_{th} Mw/pI_{exp}	−Fe *vs* +Fe	−Fe+ $CaCO_3$ *vs* +Fe	GO:BP
Photosynthesis								
1	Q40073	Rubisco activase A (*H. vulgare*)	162/2 /2	8	47/8.6 44/6.2	**0.2***	**0.1***	Photosynthesis (GO:0015979); ATP binding (GO:0005524)
2	B7FMC2	Rubisco small chain 3A (*M. truncatula*)	343/10 /6	44	20/8.7 16/7.3	**0.2***	**0.7**	Photosynthesis (GO:0015979); C fixation (GO:0015977)
3	A0A072UZ59	Rubisco activase (*M. truncatula*)	975/53 /15	45	48.0/6.9 43/5.7	**0.5***	**0.6**	Photosynthesis (GO:0015979); reductive pentose-phosphate cycle (GO:0019253)
4	P28459	Rubisco large chain *(V. acerifolium)*	62/2 /2	4	53/6.1 25/5.9	**lost***	0.7	Photosynthesis (GO:0015979); reductive pentose-phosphate cycle (GO:0019253)

(Continued)

Table A.I.1: continued

Spot	UniProt	Protein description	Sc/ion /pep	Sq (%)	Mw/pI_{th} Mw/pI_{exp}	−Fe *vs* +Fe	−Fe+ $CaCO_3$ *vs* +Fe	GO:BP
5	B7FGU7	Cytochrome b6-f complex iron-sulfur (*M. truncatula*)	156/2 /2	11	24/7.6 23/5.9	0.3	**lost***	Photosynthetic electron transport chain (GO:0,009,767)
6	KEH21532	Rubisco small chain (*M. truncatula*)	275/14 /6	37	20.4/8.7 16/7.6	0.2	**0.2***	Photosynthesis (GO:0015979); C fixation (GO:0015977)
7	Q8GTY4	Rubisco activase (*M. sativa*)	480/10 /6	39	30/5.6 43/5.4	1.8	**0.5***	Photosynthesis (GO:0015979); ATP binding (GO:0005524)
8	P14226	Oxygen-evolving enhancer protein 1 (*P. sativum*)	141/3 /3	13	35/6.2 30/5.2	**1.5**	**2.2***	Photosynthesis (GO:0015979); photosystem II stabilization (GO:0042549)
					Defense/response to oxidative stress			
9	B7FKA0	Polyketide cyclase/ dehydrase/lipid transporter (*M. truncatula*)	148/3 /3	24	18/5.1 20/5.5	0.9	**2.1***	Defense response (GO:0006952); mRNA modification (GO:0016556)
10	A6XJ26	Thioredoxin reductase (*M. truncatula*)	155/2 /2	7	40/6.9 34/5.8	1.4	**2.8***	Removal of superoxide radicals (GO:0019430)
11	Q56VU1	Glutathione peroxidase 1 (*L. japonicus*)	125/3 /2	9	26/8.8 22/6.7	2.9	**3.7***	Response to oxidative stress (GO:0006979)
12	B6ZHC0	PR-5b protein (*G. max*)	159/3 /2	17	27/6.3 27/7.0	2.8	**12.4***	Phatogenesis related
13	A0A072TXU3	Glutaredoxin C4 (*M. truncatula*)	108/2 /2	34	11.4/6.5 14/6.6	new	**new***	Cell redox homeostasis (GO:0045454)
					Protein-related process			
14	B7FF81	Ubiquitin-conjugating enzyme (*M. truncatula*)	77/2 /2	14	17/6.2 20/7.1	**0.4***	0.9	Protein ubiquitination (GO:0016567)
15	P49118	78 kDa glucose regulated protein (*S.lycopersicum*)	367/5 /4	13	41/8.5 74/5.4	**1.4**	**2.1***	Protein folding (GO:0006457)
16	G7JU14	HSP 70 kDa (*M. truncatula*)	887/16 /13	24	72/5.9 70/5.8	1.2	**2.3***	Protein folding (GO:0006457)
17	P37900	HSP 70 kDa. mitochondrial (*P. sativum*)	241/6 /4	8	72/5.8 70/5.8	1.2	**2.5***	Protein folding (GO:0006457)
18	P38548	GTP-binding nuclear protein Ran/TC4 (*V. faba*)	175/5 /4	19	25.6/6.4 29/7.3	lost	**6.1***	Small GTPase mediated signal transduction (GO:0007264); protein transport (GO:0015031)
19	XM_ 003594608	30S ribosomal protein S1 (*M. truncatula*)	297/5 /5	18	44.9/5.2 44/5.3	1.0	**lost***	Translation (GO:0006412)
20	D7KCE2	Elongation factor Tu (*A. lyrata*)	366/10 /6	15	49/6.6 43/6.8	1.1	**2.8***	Translational elongation (GO:0006414)

(Continued)

Table A.I.1: continued

Spot	UniProt	Protein description	Sc/ion /pep	Sq (%)	Mw/pI_{th} Mw/pI_{exp}	−Fe *vs* +Fe	−Fe+ $CaCO_3$ *vs* +Fe	GO:BP
21	G7LE33	40S ribosomal protein S12 (*M. truncatula*)	218/6 /5	51	15.6/5.5 20/6.0	0	**22.9***	Translation (GO:0006412)
Oxidation/reduction process								
22	O81413	Ferric leghemoglobin reductase-2 (*G. max*)	278/7 /6	14	53/6.9 51/7.0	nd	**new***	Cell redox homeostasis (GO:0045454)
23	G7JL79	Ferredoxin-nitrite reductase (*M. truncatula*)	223/4 /4	9	65.8/6.5 64/7.0	**0.2***	**0.3***	Nitrate transport (GO:0015706); cysteine biosynthetic process (GO:0019344); oxidation-reduction process (GO:0055114)
24	G7J8R4	NADH-ubiquinone oxido-reductase 75 kDa subunit (*M. truncatula*)	310/5 /5	8	82/7.1 74/7.0	0.7	**0.4***	Respiratory chain complex I (GO:0045271); proteasome core complex assembly (GO:0080129); oxidation-reduction process (GO:0055114); ATP synthesis coupled electron transport (GO:0042773); response to oxidative stress (GO:0006979)
Metabolism								
25	Q9FT00	Malate dehydrogenase 2 (*C. arietinum*)	71/2 /2	8	36/5.9 43/6.4	**4.8***	2.5	TCA (GO:0006099); carbohydrate metabolic process (GO:0005975)
26	O48904	Malate dehydrogenase precursor (*M. sativa*)	541/12 /7	24	36/8.8 36/6.9	1.0	**2.6***	TCA (GO:0006099); carbohydrate metabolic process (GO:0005975)
27	B7FJQ4	Malate dehydrogenase (*M. truncatula*)	351/11 /5	13	36/6.1 42/7.1	2.2	**2.7***	TCA (GO:0006099); carbohydrate metabolic process (GO:0005975)
28	A9YWS0	Serine-hydroxymethyl-transferase (*M. truncatula*)	87/2 /2	7	58/8.4 52/7.2	**3.1***	**1.5**	Serine (GO:0006563) and glycine (GO:0006544) metabolic process; one C metabolism (GO:0006730); methylation (GO:0032259)
Secondary metabolism								
29	B7FHV0	Phenylcoumaran benzylic ether reductase-like protein Fi1 (*M. truncatula*)	358/6 /6	27	33.9/5.6 42/6.1	nd	**new***	Oxidation-reduction process (GO:0055114); phenylpropanoid metabolic process (GO:0009698)
30	B7FIC1	Putative *O*-methyl-transferase (*M. truncatula*)	114/4 /4	23	28/5.4 30/5.7	**3.8***	4.6	Methylation (GO:0032259); phenylpropanoid metabolic process (GO:0009698); cysteine biosynthetic process (GO:0019344)

(Continued)

Table A.I.1: continued

Spot	UniProt	Protein description	Sc/ion /pep	Sq (%)	Mw/pI_{th} Mw/pI_{exp}	−Fe *vs* +Fe	−Fe+ $CaCO_3$ *vs* +Fe	GO:BP
31	Q45FF2	pyridoxal biosynthesis protein PDX1.3 (*M. truncatula*)	334/8 /4	16	34/5.6 35/6.2	nd	**new***	Pyridoxal phosphate biosynthetic process (GO:0042823)
				Not identified				
32		Not identified			27/6.9	**1.4**	**2.3***	
33		Not identified			17/5.5	**lost***	1.1	
34		Not identified			43/7.5	0.4	**lost***	
35		Not identified			13/7.1	0.7	**0.4***	
36		Not identified			22/5.9	1.0	**2.0***	
37		Not identified			28/6.3	1.7	**2.3***	
38		Not identified			28/6.5	1.0	**2.4***	
39		Not identified			23/6.4	1.2	**3.2***	

When a PCA analysis was run using all consistent spots, the samples from Fe-deficient plants in the presence of $CaCO_3$ were well separated, whereas those from Fe-sufficient plants and Fe-deficient plants grown without $CaCO_3$ overlapped (Figure S2A). However, when the PCA analysis was run using only those spots showing significant differences in relative abundance, samples from the three treatments were clearly separated (Figure S2B).

The statistical analysis of averaged maps indicated that the Fe deficiency treatment in absence of $CaCO_3$ caused significant increases ($p < 0.05$; fold-change ≥ 2) in relative abundance of three spots (spots 25, 28 and 30 in Table A.I.1; orange ellipses in Figure A.I.1B). All of them matched reliably to known proteins and were manually classified by their GO: BP (Biological Process) annotation to general metabolism (spots 25 and 28) and phenylpropanoid metabolism (spot 30) (Figure A.I.2A). Five spots (spots 1–3, 14 and 23) showed significant decreases in relative abundance and two more (spots 4 and 33) were no longer detected in the 0 μM Fe treatment when compared to controls ($p < 0.05$; fold-change ≤ 0.5; blue ellipses in Figure A.I.1B), and six of them were reliably identified (spots labeled 1–4, 14 and 23 in Table A.I.1); they were assigned to photosynthesis (spots 1–4), protein modification (spot 14) and oxidation/reduction process (spot 23) (Figure A.I.2A).

Changes in the whole stem protein profile were more marked when Fe deficiency was imposed in the presence of $CaCO_3$. Eighteen spots showed significant increases in relative abundance (spots 8–12, 15–18, 20, 21, 26, 27, 32, and 36–39 in Table 1) and four more were detected de novo (spots 13, 22, 29 and 31 in Table 1) in the Fe-deficient treatment in the presence of $CaCO_3$ when compared with the controls ($p < 0.05$; fold-change ≥ 2; orange rectangles in Figure A.I.1C). Among them, 17 were reliably identified and manually classified

in the following functional categories: photosynthesis (spot 8), defense and oxidative stress (spots 9–13), protein metabolism (spots 15–18, 20 and 21), oxidation/ reduction processes (spot 22), general metabolism (spots 26 and 27) and secondary metabolism (spots 29 and 31) (Table 1, Figure A.I.2A). Six spots showed significant decreases in relative abundance (spots 1, 6, 7, 23, 24 and 35 in Table A.I.1) and three more (spots 5, 19 and 34 in Table A.I.1) were no longer detected ($p < 0.05$; fold-change ≤ 0.5; blue rectangles in Figure A.I.1C). Among them, seven spots were identified and assigned to photosynthesis (spots 1 and 5–7), translation (spot 19), and oxidation-reduction process (spots 23 and 24) (Figure A.I.2A).

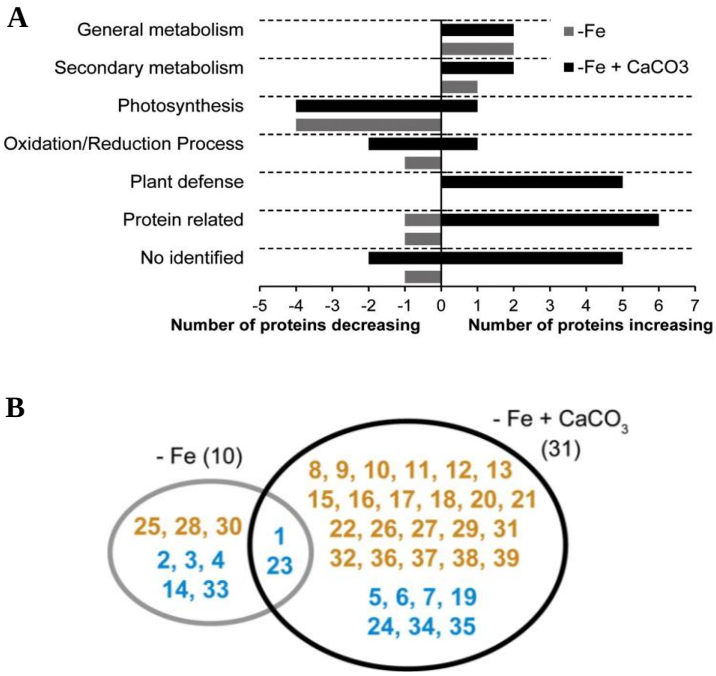

Figure A.I.2. A. *Number of identified spots changing as a result of Fe deficiency, organized in metabolic pathways. Pathways related to the identified proteins were integrated according to the UniProt database and GO annotation.* ***B.*** *Venn diagram depicting proteins with changes in abundance as a result of the Fe deficiency treatments. Numbers indicate spots as in Table 1. Orange and blue color numbers indicate increases (including new appearances) and decreases (including disappearances) in spot abundance as a result of Fe deficiency, respectively.*

The information on the significant changes ($p < 0.05$; fold-change ≥ 2 or ≤ 0.5) in protein abundance as a result of both Fe deficiency treatments is summarized in a Venn diagram (Figure A.I.2B), using the same color code than that used in Figure A.I.1 (orange and blue numbers for increases and increases in relative abundance, respectively). Two spots (spots 1 and 23 in Table 1) changed significantly and above the cut-off values in both Fe deficiency treatments.

Mineral analysis

Mineral analysis was carried out in whole stem samples (including stems and petioles). The stem dry weights from Fe-deficient plants grown in both conditions were approximately 24%

lower than that of the Fe-sufficient controls (Figure A.I.3A). Iron concentration in stems of Fe-deficient plants grown in the absence of $CaCO_3$ did not change when compared to controls, whereas in Fe-deficient plants grown in the presence of $CaCO_3$ the Fe concentration was 54 % lower than in Fe-sufficient controls (Figure A.I.3B).

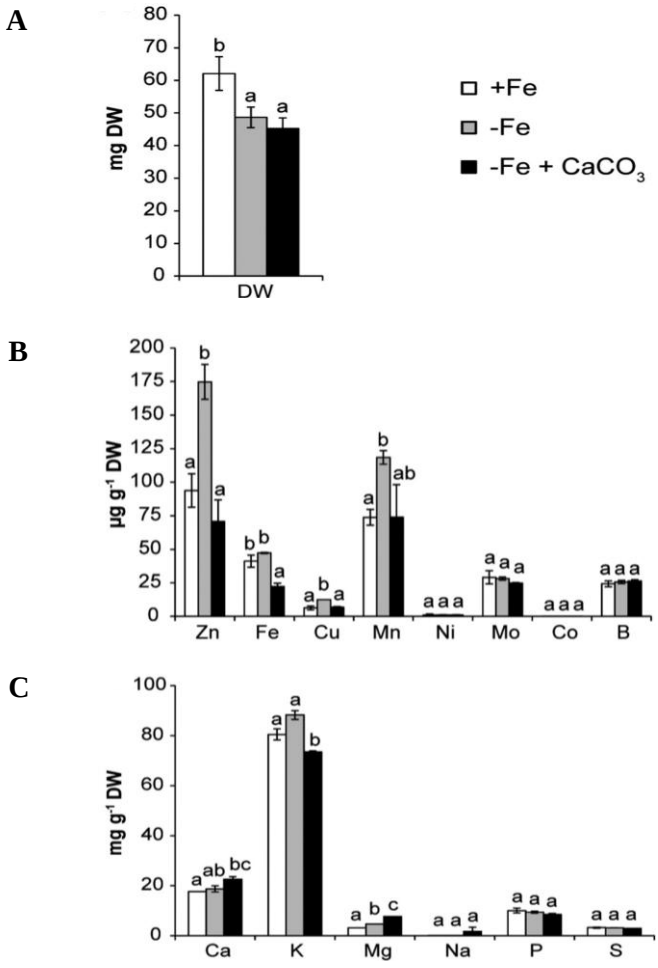

Figure A.I.3. *Mineral composition of stems, including petioles, as affected by Fe deficiency.* ***A:*** *dry mass (DW, in mg per plant);* ***B:*** *micronutrient concentrations (in µg g^{-1} DW), and* ***C:*** *macronutrient concentrations (in mg g^{-1} DW) of stems (including petioles) of Medicago truncatula plants grown for six days in Fe-sufficient (white columns) and Fe-deficient conditions (grey columns for plants grown in the absence of $CaCO_3$ and black columns for plants grown in the presence of $CaCO_3$). Data are means ± SE (n = 3; from one batch of plants with three samples per treatment). Columns marked with the same letter are not significantly different at the $p \leq 0.05$ probability level.*

The total Fe content in stems was lower in both Fe deficiency treatments when compared to controls, due to the lower stem dry weights in the absence of Fe (Supplementary Figure S3). Stem concentrations of Zn, Cu and Mn from Fe-deficient plants grown in the absence of $CaCO_3$ were 90, 100 and 60 % higher, respectively, than those in the Fe-sufficient controls, whereas the concentrations of Ni, Mo, Co and B did not change significantly (Figure A.I.3B). The presence of $CaCO_3$ in the zero-Fe solution did not lead to significant changes in the concentrations of Zn, Cu, Mn, Ni, Mo Co and B when compared to the Fe-sufficient controls (Figure A.I.3B). With

regard to macronutrient concentrations, in whole stems of Fe-deficient plants grown in the absence of $CaCO_3$ the only significant change was a 50 % increase in Mg concentration when compared to Fe-sufficient controls (Figure A.I.3C). In the presence of $CaCO_3$, increases in Mg (140 %), and Ca (28 %) concentrations and a decrease in K concentration (10 %) were found when compared to those in Fe-sufficient controls (Figure A.I.3C).

The mineral composition of leaves and roots was also determined (Supplementary Figure S4). In roots, Fe concentration was lower than in controls in both Fe deficiency treatments, whereas Zn and Cu concentrations increased in the absence of $CaCO_3$ and Ni concentration increased in the presence of $CaCO_3$. In leaves, Fe concentration only decreased in the presence of $CaCO_3$. Regarding other micronutrients in leaves, results were similar to those described above for stems, with Zn, Cu, Mn and also Ni concentrations being higher in the Fe deficiency treatment in the absence of $CaCO_3$ than in Fe-sufficient controls, and similar to controls or only slightly higher in the presence of $CaCO_3$ (Supplementary Figure S4). The trends observed for changes in macronutrient concentrations in leaves and roots as a result of both Fe deficiency treatments were quite similar to those observed in stems (Supplementary Figure S4). The only significant changes in macronutrient root concentrations occurred in Fe-deficient plants in the presence of $CaCO_3$, and included an increase in Ca and decreases in P and S concentrations (Supplementary Figure S4). In leaves, Fe deficiency increased Ca and Mg concentrations, with the increases being larger in the presence of $CaCO_3$.

Microscopy of petiole and stem sections

In order to study possible cell wall changes, lignin was localized in sections of stems and petioles using autofluorescence and phloroglucinol staining. In Fe-sufficient petioles, the blue autofluorescence signal was mainly detected in xylem vessels and sclerenchyma tissue (Figure A.I.4A). When compared to controls, Fe-deficient petioles from plants grown in the absence of $CaCO_3$ showed a slightly lower autofluorescence intensity in both xylem vessel and sclerenchyma tissue (Figure A.I.4B), whereas in petiole sections from Fe-deficient plants grown in the presence of $CaCO_3$, the autofluorescence signal intensity decreased in xylem vessels when compared to both sclerenchyma and controls (Figure A.I.4C). This decrease in autofluorescence occurred especially in the innermost part of xylem vessels, where blue autofluorescence was barely observed and instead a greenish color was detected (Figure A.I.4C). When phloroglucinol staining was used, lignin distribution in Fe-sufficient petioles was similar to that found using autofluorescence, but the staining was more intense in the sclerenchyma (deep red) than in xylem vessels (almost black) (Figure A.I.4D). Phloroglucinol staining of Fe-deficient petioles from plants grown in the absence of $CaCO_3$ yielded an intense coloration in xylem vessels similar to that observed in Fe-sufficient controls and little staining

in the sclerenchyma (Figure A.I.4E). In petiole sections from Fe-deficient plants grown in the presence of $CaCO_3$, phloroglucinol staining was intense and even higher than that observed in controls in both xylem vessels and sclerenchyma (Figure A.I.4F).

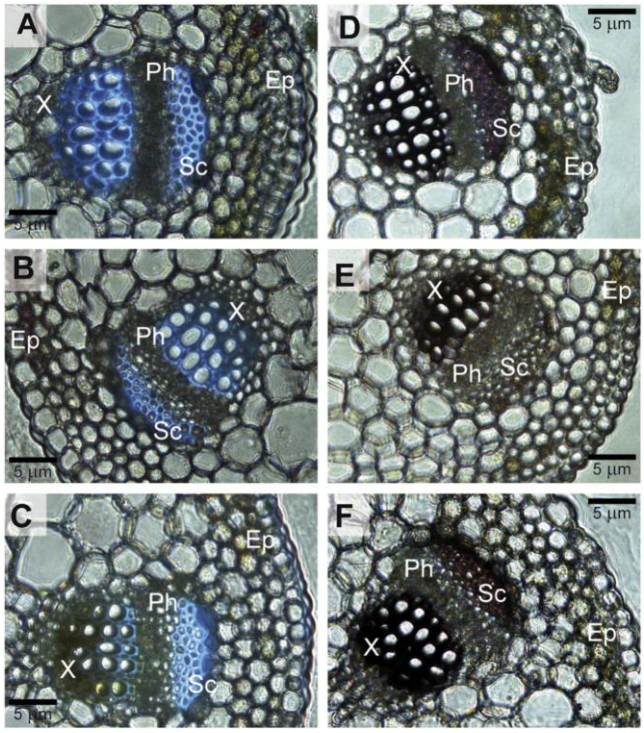

Figure A.I.4. *Microscopy analyses of Fe-deficient petioles. Micrographs of petiole sections (10×): autofluorescence (A–C) and phloroglucinol staining (D–F) from Fe-sufficient plants (A and D) and Fe-deficient plants grown in the absence (B and E) and presence of $CaCO_3$ (C and F). X: xylem; Ph: phloem; C: cortex; Ep: epidermis, and Sc: sclerenchyma. Transversal petiole slices, 60 µm thick, were obtained using a vibrating blade microtome.*

Stems of Fe-sufficient plants showed a clear blue autofluorescence in the xylem vessels and a more diffuse one in the cortex, and similar results were observed when phloroglucinol was used for lignin staining (Supplementary Figure S5). Stems from Fe-deficient plants showed similar autofluorescence and staining patterns to those of controls, irrespective of the presence of $CaCO_3$ in the nutrient solution (Supplementary Figure S5).

Lignin analysis

The lignin composition (relative molar abundances of G- and S-lignin derived markers and S/G ratios) of both stems and petioles samples was studied by Py-GC/MS. The percentages of protein markers relative to the lignin markers (lignin/protein ratio) were also estimated.

In petioles, the lignin per protein ratio increased 20 and 110 % in the Fe deficiency treatment in the absence and presence of $CaCO_3$, respectively, when compared to the Fe-sufficient controls (Table 2). The total relative abundance of S- and G- lignin markers and the S/G ratio in petioles from both Fe deficiency treatments were similar to those of controls but

significantly different between them (Table 2). However, the relative molar abundances for most of the specific G-lignin markers (six of the seven compounds measured) in Fe-deficient samples presented statistically significant differences (two compounds increased and four compounds decreased with Fe deficiency) with those of control samples (Table 2). The relative molar abundances of specific S-lignin markers changed in at least one of the Fe deficiency treatments in four of the seven measured compounds when compared to control petioles (Table 2).

***Table A.I.2**: Relative molar abundance of G- and S-lignin derived markers, S/G ratio, percentage of protein markers and lignin/protein ratio in stems and petioles of Fe-sufficient and Fe-deficient plants grown in the absence and presence of $CaCO_3$, as estimated by Py-GC/MS. Data are means ± SD of four biological replicates. Different letters within the same row and tissue indicate statistically significant differences using the Student's t-test and $p < 0.05$.*

Compounds	Petioles			Stems		
	+ Fe	− Fe	− Fe + $CaCO_3$	+ Fe	− Fe	− Fe + $CaCO_3$
G-lignin markers						
Guaiacol	19.5 ± 0.5 a	24.7 ± 2.1 b	23.9 ± 2.2 b	25.6 ± 1.5 a	27.5 ± 2.1 a	26.2 ± 1.8 a
4-Methylguaiacol	3.4 ± 0.2 b	3.1 ± 0.2 a	3.0 ± 0.1 a	3.3 ± 0.4 a	3.4 ± 0.1 a	3.2 ± 0.1 a
4-Ethylguaiacol	4.0 ± 0.7 a	6.4 ± 0.2 b	6.5 ± 0.9 b	6.4 ± 0.4 a	7.1 ± 0.3 b	7.0 ± 0.7 ab
4-Vinylguaiacol	44.2 ± 2.4 c	36.2 ± 2.0 a	40.7 ± 2.4 b	23.5 ± 1.4 a	24.2 ± 1.2 a	25.2 ± 1.9 a
Eugenol	1.9 ± 0.2 b	1.4 ± 0.2 a	1.1 ± 0.3 a	1.0 ± 0.1 a	1.1 ± 0.1 a	1.1 ± 0.2 a
cis-Isoeugenol	1.5 ± 0.0 b	1.2 ± 0.2 a	1.0 ± 0.2 a	1.2 ± 0.1 a	1.2 ± 0.1 a	1.3 ± 0.1 a
trans-Isoeugenol	7.1 ± 0.2 a	7.0 ± 0.3 a	6.1 ± 0.9 a	6.4 ± 0.5 a	6.7 ± 0.7 a	7.1 ± 0.6 a
Total G compounds	81.6 ± 1.3 ab	80.1 ± 1.2 a	82.3 ± 1.3 b	67.5 ± 3.6 a	71.0 ± 1.6 a	71.1 ± 1.0 a
***S*-lignin markers**						
Syringol	7.8 ± 0.6 a	9.1 ± 0.5 b	7.8 ± 0.9 a	15.2 ± 1.7 b	13.9 ± 0.5 b	12.8 ± 0.5 a
4-Methylsyringol	1.3 ± 0.1 b	1.2 ± 0.1 ab	1.0 ± 0.2 a	2.1 ± 0.1 b	1.7 ± 0.1 a	1.6 ± 0.1 a
4-Ethylsyringol	1.1 ± 0.2 a	1.6 ± 0.1 b	1.7 ± 0.3 b	3.2 ± 0.5 a	2.7 ± 0.2 a	2.9 ± 0.2 a
4-Vinylsyringol	5.7 ± 0.3 b	5.4 ± 0.4 ab	4.7 ± 0.6 a	8.0 ± 0.9 b	6.7 ± 0.5 a	6.7 ± 0.4 a
4-Allylsyringol	0.5 ± 0.1 a	0.4 ± 0.0 a	0.4 ± 0.1 a	0.5 ± 0.1 a	0.5 ± 0.1 ab	0.6 ± 0.0 b
cis-4-propenylsyringol	0.3 ± 0.1 a	0.3 ± 0.1 a	0.3 ± 0.0 a	0.6 ± 0.1 a	0.5 ± 0.1 a	0.7 ± 0.1 a
trans-4-propenylsyringol	1.7 ± 0.3 a	1.1 ± 0.1 a	1.8 ± 0.2 a	3.0 ± 0.4 a	3.0 ± 0.5 ab	3.7 ± 0.2 b
Total S compounds	18.4 ± 1.3 ab	19.9 ± 1.2 b	17.7 ± 1.3 a	32.5 ± 3.6 a	29.0 ± 1.6 a	28.9 ± 1.0 a
S/G ratio	0.2 ± 0.0 ab	0.3 ± 0.0 b	0.2 ± 0.0 a	0.5 ± 0.1 a	0.4 ± 0.0 a	0.4 ± 0.0 a
Protein markers*						
Phenylacetonitrile	42.9 ± 6.3 c	28.5 ± 5.5 b	12.9 ± 5.0 a	8.7 ± 1.8 b	9.3 ± 3.0 b	5.2 ± 1.4 a
Indole	138.0 ± 20.5 b	120.5 ± 16.0 b	76.7 ± 17.8 a	45.0 ± 5.2 a	57.2 ± 18.0 a	46.8 ± 15.8 a
3-Methylindole	35.9 ± 7.9 b	18.9 ± 4.1 a	15.1 ± 2.5 a	8.6 ± 1.3 a	10.0 ± 3.4 a	10.9 ± 2.8 a
Total protein markers*	216.8 ± 32.5 c	167.9 ± 25.1 b	104.7 ± 24.8 a	62.4 ± 8.2 a	76.5 ± 24.1 a	62.9 ± 19.9 a
Lignin/Protein ratio	0.5 ± 0.1 a	0.6 ± 0.1 b	1.0 ± 0.2 c	1.6 ± 0.2 a	1.4 ± 0.3 a	1.7 ± 0.4 a

** Protein-markers calculated as percentage of total lignin markers (G + S)*

On the other hand, very few changes in the stem lignin parameters were found with Fe deficiency. The lignin per protein ratios, relative molar abundances of G- and S-lignin derived

markers and S/G ratios were similar in the Fe-deficient samples, irrespective of the presence of $CaCO_3$, to those found in Fe-sufficient controls (Table A.I.2).

A.I.4. Discussion

In the present study we have characterized the differences in the protein profiles of whole stems (including petioles) from *M. truncatula* plants grown in hydroponics in two different Fe deficiency conditions, in the presence and absence of $CaCO_3$, with the aim of shedding light into processes that may be relevant in Fe deficiency induced modifications in this tissue. It should be noted that the individual specific effects of Fe deficiency and $CaCO_3$ in the proteome of stems from Fe-deficient plants grown in the presence of $CaCO_3$ cannot be discriminated using the current experimental approach. The presence of $CaCO_3$ along with Fe(III)-EDTA as an Fe source causes Fe precipitation and immobilization, therefore making unfeasible its use as a control.

Overall results from the protein profiling indicate that Fe deficiency in the presence of $CaCO_3$ has a more pronounced impact on the stem proteome than the lack of Fe alone, since a larger number of spots (31) displayed differences in relative accumulation in the presence of $CaCO_3$ than in its absence (10). This stronger effect is also supported on one hand by the fact that the functional category containing the most spots that increased in relative abundance (five) in Fe-deficient plants grown in the presence of $CaCO_3$ was the defense and stress category, whereas in the absence of $CaCO_3$ no proteins from this category were found to increase significantly (Figure A.I.2A and Table A.I.1). A similar situation was described in the proteomic profiling of roots of in the same plant species (Rodríguez-Celma et al., 2011b); this is not only the result of the lack of Fe and the presence of $CaCO_3$, but also of a combination of factors including the basic pH of the growing solution which impairs Fe mobilization in the root apoplast (Mengel et al., 1994; Martínez-Cuenca et al., 2013; Zuo et al., 2007). Furthermore, the presence of $CaCO_3$ may alter the pH of plant fluids such as the xylem sap and apoplastic fluid causing changes in the chemical speciation of Fe and therefore in Fe availability (Kosegarten et al., 1999; López-Millán et al., 2000; Nikolic and Römheld, 2002). On the other hand, the functional category containing most of the spots decreasing in relative abundance was photosynthesis, with six proteins decreasing in relative abundance in the presence of $CaCO_3$ (four of them above and two below the biological cut-off value) in comparison with the four decreasing in the absence of $CaCO_3$. The decreases in the relative abundance of the photosynthesis related proteins affect different isoforms of the Rubisco activase (spots 1, 3 and 7; Supplementary Figure S6A), the large (spot 4) and small chains (spots 2 and 6) of Rubisco, and the iron-sulfur subunit of the cytochrome b6f complex (spot 5), which imply a decreased carbon fixation capacity and are in agreement with the well-known Fe deficiency induced

impairment of the photosynthetic processes (Marschner et al., 2007). All proteins identified in the stress and defense category increased in abundance, and were related either to general defense [polyketide cyclase/ dehydratase (spot 9) and PR-5b (spot 12)] or to defense against oxidative stress [thioredoxin reductase (spot 10), glutathione peroxidase 1 (spot 11) and glutaredoxin C4 (spot 13)]. The polyketide cyclase/dehydratase contains a Betv1 domain and belongs to family 10 of plant pathogenesis-related proteins (PR-10; UniProt annotation) and PR-5b belongs to the thaumatin superfamily (Lytle et al., 2009), both with yet unknown functions. However, some members of PR5 subfamily have been described to play distinctive roles in the defense system that protects against high-salt stress or osmotic imbalance (Tachi et al., 2009), which is also likely to occur in the Fe deficiency treatment in the presence of $CaCO_3$. The same PR5b protein showed increases in abundance in roots of *M. truncatula* plants grown in the presence of $CaCO_3$ (Rodríguez-Celma et al., 2011b). Interestingly, a proteomic study on *Beta vulgaris* roots submitted to several levels of Zn toxicity, which also causes induced Fe deficiency, found that some Betv1 proteins, including some PR-10, increased in abundance in roots when Zn supply increased (Gutierrez-Carbonell et al., 2013). Therefore, we could speculate that the increases measured in both pathogenesis related proteins in the $CaCO_3$ treatment might be related to osmotic stress caused by both metal imbalances and the presence of $CaCO_3$. On the other hand, increases in proteins related to defense against oxidative stress including thioredoxin reductase (spot 10) and those associated with glutathione metabolism, such as the glutathione peroxidase (spot 11) and the glutaredoxin C4 (spot 13), found in this study, have been reported to increase upon Fe deficiency in different root proteome studies (López-Millán et al., 2013) and are probably associated with the redox imbalances caused by the lack of Fe. The existence of osmotic and redox unbalances in the high pH treatment is also supported by the de novo detection of a pyridoxal biosynthesis protein (spot 31). Pyridoxal, or vitamin B6, is a singlet oxygen quencher and may play a role in osmotic or salt tolerance as well as in oxidative stress resistance (Chen and Xiong, 2005; Tambasco-Studart et al., 2005).

Changes in the protein-related category also indicate a Fe deficiency driven stress situation which was more severe in the presence of $CaCO_3$. Relative increases were observed in three proteins of the heat shock 70 kDa (HSP70) family whose members have direct functions in managing stress situations by preventing misfolded or damaged proteins to aggregate or by facilitating their disposal by interacting with ubiquitin ligases (Luders et al., 2000). One of the HSP70 (spot 15) increased in both Fe deficiency treatments (although below the threshold level in the absence of $CaCO_3$), and its *Arabidopsis* counterpart (AtBIP1; At5g28540) is involved in the ER degradation of misfolded proteins (TAIR annotation). The decrease measured in the ubiquitin-conjugating enzyme (spot 14) which belongs to the E2 class performing the second step in the ubiquitination pathway (UniProt annotation) may also suggest a role of the ubiquitin-

dependent catabolic pathway in the Fe deficiency response. The other two HSP70 (spots 16 and 17) increased only in the presence of $CaCO_3$ and are most likely isoforms of the same protein given their localization in the 2-DE gel (Supplementary Figure S6B). These proteins blast to the same *Arabidopsis* orthologue (AtHsp70–10, At5g09590) that has been suggested to play an important role in the regulation of the Fe-S assembly pathway in mitochondria (Leaden et al., 2014). Their increases may be related to the decreases measured in Fe-S cluster proteins, including the NADH-ubiquinone reductase (spot 24) of the respiratory chain complex I, the Fe-S subunit of the cytochrome b6f complex (spot 5) and the ferredoxin nitrite reductase (spot 23).

On the other hand, significant changes in the protein translation machinery were only observed in the Fe deficiency treatment in the presence of $CaCO_3$, affecting two structural components of the ribosome (spots 19 and 21) and an elongation factor (spot 20). Changes in the abundance of some components of the ribosome induced by Fe deficiency have been described in *Arabidopsis* roots and authors speculated that these changes can control mRNA preference and bias translation efficiency towards specific sets of genes (Lan et al., 2011; Lan and Schmidt, 2012; Rodríguez-Celma et al., 2013b), but they also may indicate the need of de novo synthesis of Fe deficiency effector proteins. The fact that these changes are only observed in the presence of $CaCO_3$ reinforces the strong effect of this treatment in the stem proteome.

Several lines of evidence support that Fe deficiency causes alterations in the cell wall of stem tissues, especially in the presence of $CaCO_3$. First, the increases in relative abundance measured in two protein species involved in the phenylpropanoid biosynthesis pathway: the phenylcoumaran benzylic ether reductase (PCBER, spot 29) and a putative Omethyltrasferase similar to the caffeoyl-CoA O-methyltransferase 1 (spot 30). PCBER has been shown to be one of the most abundant proteins in the xylem of poplar (Gang et al., 2011) that participates in lignan synthesis (Vander Mijnsbrugge et al., 2000) and the O-methyltrasferase probably plays a role in the methylation steps necessary for the biosynthesis of monolignols, the lignin precursors (Do et al., 2007). Their increases suggest that Fe deficiency may cause changes in lignification. A second line of evidence is provided by the lignin Py-GC/MS analysis of the petioles, which showed a small but significant relative increase in the lignin per protein ratio in Fe-deficient petioles when compared to the controls, which was more intense in the presence than in the absence of $CaCO_3$ (Table 2). Finally, the microscopy study of petiole sections also indicates stronger alterations in plants grown in the presence than in the absence of $CaCO_3$. In petioles from plants grown in the presence of $CaCO_3$, phloroglucinol staining indicates an increase in lignin in the inner part of the xylem vessels (Figure A.I.4F), and the shift towards a green color in the autofluorescence signal in the same area suggests the existence of changes in lignin composition (Figure A.I.4C); similar shifts in autofluorescence have been associated elsewhere with changes in lignin composition (Djikanović et al., 2012). When Fe-deficient plants were

grown in the absence of $CaCO_3$, changes in the micrograph images relative to the controls were less marked (Figure A.I.4B, E). Conversely to what occurs in the petioles, in the case of the stems from Fe-deficient plants the lignin/protein ratio, the lignin composition and the autofluorescence and phloroglucinol micrographs did not differ from those of control plants, and this is likely due to the fact that these stems were developed before the onset of Fe deficiency.

Overall, cell wall-related changes observed in petioles of plants grown in the presence of $CaCO_3$ should led to an increase in cell wall rigidity, especially in the xylem vessels. Changes in cell wall composition resulting in increased lignification have been described to occur upon mineral imbalances, for instance in the roots of Fe-deficient pear and quince cultivars (Donnini et al., 2009), and have also been suggested as a detoxification strategy for excess Cd in roots (Lux et al., 2011; Redjala et al., 2011). Modification in cell wall related proteins have also been described in proteomic studies of Fe-deficient roots (López-Millán et al., 2013). It has been hypothesized that increased lignification may provide a protective barrier to avoid the lateral transport and distribution of minerals by decreasing the permeability of the cell wall (Higuchi et al., 1981). In leaves, Fe deficiency also elicits structural changes in morphology, including a reduction of the leaf xylem vessel size, which could disturb normal stomatal functioning (Eichert et al., 2010; Fernández et al., 2008).

Other effects of Fe deficiency in the stem protein profiles included increases in several spots identified as malate dehydrogenase (spots 25–27 in Table 1 and Supplementary Figure S6C) and in a serinehydroxymethyl-transferase (spot 28) in both treatments that were also described in the proteome of Fe-deficient *M. truncatula* roots (Rodríguez-Celma et al., 2011b). Increases in both proteins have been reported in physiological and proteomic studies on Fe deficiency in roots and leaves (López-Millán et al., 2013; Abadía et al., 2002) and results from this study indicate this may be a common response throughout plant organs.

Mineral analyses indicate the existence of alterations in micro- and macronutrient balances as a result of Fe deficiency. Although the stem Fe concentrations did not decrease significantly in Fe-deficient plants grown in the absence of $CaCO_3$, Fe content decreases occurred in both Fe deficiency treatments (Figure A.I.3, Supplementary Figure S3). The decrease in stem Fe concentration in the presence of $CaCO_3$ was accompanied at the proteomic level by decreases in relative abundance of three Fe containing proteins related to energy production: a subunit of a NADH-ubiquinone oxido-reductase (spot 24), the ferredoxin-nitrite reductase (spot 23), and the cytochrome b6f complex (spot 5). Decreases in abundance in Fe-containing, energy related proteins have been widely described in different proteomic studies as a result of Fe shortage (López-Millán et al., 2013), and this could ultimately account for the reduction in stem mass.

A.I.5. Conclusions

A summary of the proteomic results is shown in Figure A.I.5. Overall results indicate that Fe deficiency by itself has a mild effect on the stem proteome of *M. truncatula* plants, mainly affecting photosynthesis-related proteins. However, Fe deficiency in the presence of $CaCO_3$ has a stronger impact on the proteome, including a general increase in stress and protein metabolism related proteins not observed in Fe-deficient plants grown without $CaCO_3$, as well as a larger number of photosynthesisrelated proteins decreasing. These results probably indicate the existence of mineral and osmotic unbalances. Iron deficiency also elicited significant increases in cell wall related proteins and in the lignin per protein ratio, which were more intense in the presence of $CaCO_3$. Changes in the lignin S and G monomer composition induced by Fe deficiency and the microscopy study of petiole sections further confirm the existence of alterations in cell walls of petiole tissues. These results suggest that Fe-deficient plants, especially those grown in the presence of $CaCO_3$ as occurs in many arable soils, present an increased lignification and a probable lower capacity of cell walls to interact with ions in the xylem fluid, which ultimately may affect solute transport and distribution to the leaves.

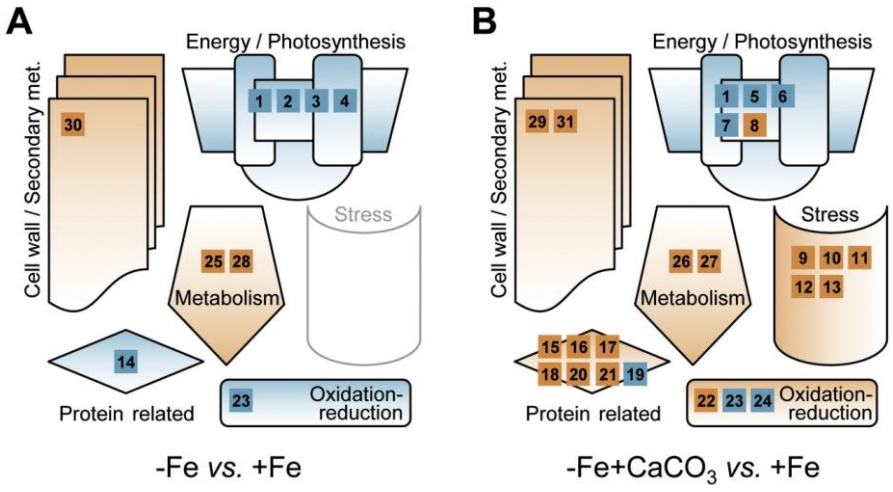

Figure A.I.5. *Changes in metabolic pathways as affected by Fe deficiency without (A) and with $CaCO_3$ (B) when compared to Fe-sufficient plants. Pathways related to the identified proteins were integrated according to the GO annotation. A statistical Student t-test was performed to show relevant changes between samples. Orange symbols mark newly detected and proteins with increased relative abundance compared to controls (using a two-fold threshold change). The same threshold (decreases larger than 50%) was selected for proteins with decreased relative abundance (blue symbols). Numbers correspond to those in Table A.1.1.*

Supplementary material

Supplementary data to this article can be found online at http://dx. doi.org/10.1016/j.jprot.2016.03.017. **Table S1.** Univariate statistical analysis of 2-DE gels; **Table S2.** List of peptides identified; **Table S3.** Summary of the 2-DE protein profiling results;

Figure S1. Stem sampling; **Figure S2.** The PCA analysis using all consistent spots and spots showing significant differences in relative abundance; **Figure S3.** The total micro- and macronutirients content in stems; **Figure S4.** The mineral composition of leaves and roots; **Figure S5.** Autofluorescence and staining patterns of lignin of Fe deficient and control plants; **Figure S6.** Localization of more relevant spots in the 2-DE gel.

References

Abadía J., López-Millán A.F., Rombolà A., Abadía A. Organic acids and Fe deficiency: a review, Plant Soil 241 (2002) 75–86.

Abadía J., Vázquez S., Rellán-Álvarez R., El-Jendoubi H., Abadía A., Álvarez-Fernández A., López-Millán A.F. Towards a knowledge-based correction of iron chlorosis, Plant Physiol. Biochem. 49 (2011) 471–482.

Álvarez-Fernández A., Paniagua P., Abadía J., Abadía A. Effects of Fe deficiency chlorosis on yield and fruit quality in peach (*Prunus persica* L. Batsch), J. Agric. Food Chem. 51 (2003) 5738–5744.

Álvarez-Fernández A., Melgar J.C., Abadía J., Abadía A. Effects of moderate and severe iron deficiency chlorosis on fruit yield, appearance and composition pear (*Pyrus communis* L.) and peach (*Prunus persica* L. Batsch), Environ. Exp. Bot. 71 (2011) 280–286.

Benedito V.A., Torres-Jerez I., Murray J.D., Andriankaja A., Allen S., Kakar K., Wandrey M., Verdier J., Zuber H., Ott T., Moreau S., Niebel A., Frickey T., Weiller G., He J., Dai X., Zhao P.X., Tang Y., Udvardi M.K. A gene expression atlas of the model legume *Medicago truncatula*, Plant J. 55 (2008) 504–513.

Cesco S., Neumann G., Tomasi N., Pinton R., Weisskopf L. Release of plant-borne flavonoids into the rhizosphere and their role in plant nutrition, Plant Soil 329 (2010) 1–25.

Chen H., Xiong L. Pyridoxine is required for post-embryonic root development and tolerance to osmotic and oxidative stresses, Plant J. 44 (2005) 396–408.

Colditz F., H.P. Braun, *Medicago truncatula* proteomics, J. Proteomics 73 (2010) 1974–1985.

Coulombe B., Chaney R., Wiebold W. Bicarbonate directly induces iron chlorosis in susceptible soybean cultivars, Soil Sci. Soc. Am.J. 48 (1984) 1297–1301.

Djikanović D., Simonović J., Savić A., Ristić I., Bajuk-Bogdanović D., Kalauzi A., Cakić S., Budinski-Simendić J., Jeremić M., Radotić K. Structural differences between lignin model polymers synthesized from various monomers, J. Polym. Environ. 20 (2012) 607–617.

Do C.T., Pollet B., Thevenin J., Sibout R., Denoue D., Barriere Y., Lapierre C., Jouanin L. Both caffeoyl Coenzyme A 3-O-methyltransferase 1 and caffeic acid Omethyltransferase 1 are involved in redundant functions for lignin, flavonoids and sinapoyl malate biosynthesis in *Arabidopsis*, Planta 226 (2007) 1117–1129.

Donnini S., Castagna A., Ranieri A., Zocchi G. Differential responses in pear and quince genotypes induced by Fe deficiency and bicarbonate, J. Plant Physiol. 166 (2009) 1181–1193.

Durrett T.P., Gassmann W., Rogers E.E. The FRD3-mediated efflux of citrate into the root vasculature is necessary for efficient iron translocation, Plant Physiol. 144 (2007) 197–205.

Eichert T., Peguero-Pina J.J., Gil-Pelegrin E., Heredia A., Fernández V. Effects of iron chlorosis and iron resupply on leaf xylem architecture, water relations, gas exchange and stomatal performance of field-grown peach (*Prunus persica*), Physiol. Plant. 138 (2010) 48–59.

Eide D., Broderius M., Fett J., Guerinot M.L. A novel iron-regulated metal transporter from plants identified by functional expression in yeast. Proc. Natl. Acad. Sci. U. S. A. 93 (1996) 5624–5628.

Fernández V., Eichert T., Del Río V., López-Casado G., Heredia-Guerrero J.A., Abadía A., Abadía J. Leaf structural changes associated with iron deficiency chlorosis in field-grown pear and peach: physiological implications, Plant Soil 311 (2008) 161–172.

Fourcroy P., Sisó-Terraza P., Sudre D., Saviron M., Reyt G., Gaymard F., Abadía A., Abadía J., Álvarez-Fernández A., Briat J.F. Involvement of the ABCG37 transporter in secretion of scopoletin and derivatives by *Arabidopsis* roots in response to iron deficiency, New Phytol. 201 (2014) 155–167.

Froelich D., Fehr W. Agronomic performance of soybeans with differing levels of iron deficiency chlorosis on calcareous soil, Crop Sci. 21 (1981) 438–441.

Gang D.R., Kasahara H., Xia Z.Q., Vander Mijnsbrugge K., Bauw G., Boerjan W., Van Montagu M., Davin L.B., Lewis N.G. Evolution of plant defense mechanisms, relationships of phenylcoumaran benzylic ether reductases to pinoresinollariciresinol and isoflavone reductases. J. Biol. Chem. 274 (1999) 7516–7527.

Garcia C.B., Grusak M.A. Mineral accumulation in vegetative and reproductive tissues during seed development in *Medicago truncatula*, Front. Plant Sci. 6 (2015) 622.

Gutierrez-Carbonell E., Lattanzio G., Sagardoy R., Rodríguez-Celma J., Rios Ruiz J.J., Matros A., Abadía A., Abadía J., López-Millán A.F. Changes induced by zinc toxicity in the 2-DE protein profile of sugar beet roots, J. Proteome 94 (2013) 149–161.

Higuchi T. Biosynthesis of lignin, In Plant Carbohydrates II, Springer, Berlin Heidelberg (1981)

Hindt M.N., Guerinot M.L. Getting a sense for signals: regulation of the plant iron deficiency response, Biochim. Biophys. Acta 1823 (2012) 1521–1530.

Hossain Z., Komatsu S. Contribution of proteomic studies towards understanding plant heavy metal stress response, Front. Plant Sci. 3 (2013).

Jorrín-Novo J.V., Maldonado A.M., Echevarria-Zomeno S., Valledor L., Castillejo M.A., Curto M., Valero J., Sghaier B., Donoso G., Redondo I. Plant proteomics update (2007–2008): second-generation proteomic techniques, an appropriate experimental design, and data analysis to fulfill MIAPE standards, increase plant proteome coverage and expand biological knowledge, J. Proteomics 72 (2009) 285–314.

Kosegarten H.U., Hoffmann B., Mengel K. Apoplastic pH and Fe^{3+} reduction in intact sunflower leaves, Plant Physiol. 121 (1999) 1069–1079.

Lan P., Li W., Wen T.N., Shiau J.Y., Wu Y.C., Lin W., Schmidt W. iTRAQ protein profile analysis of *Arabidopsis* roots reveals new aspects critical for iron homeostasis, Plant Physiol. 155 (2011) 821–834.

Lan P., Li W., Schmidt W. Complementary proteome and transcriptome profiling in phosphate-deficient *Arabidopsis* roots reveals multiple levels of gene regulation, Mol. Cell. Proteomics 11 (2012) 1156–1166.

Leaden L., Busi M.V., Gomez-Casati D.F. The mitochondrial proteins AtHscB and AtIsu1 involved in Fe-S cluster assembly interact with the Hsp70-type chaperon AtHscA2 and modulate its catalytic activity, Mitochondrion 19 (Pt B) (2014) 375–381.

Liang C., Tian J., Liao H. Proteomics dissection of plant responses to mineral nutrient deficiency, Proteomics 13 (2013) 624–636.

Lin S., Cianzio S., Shoemaker R. Mapping genetic loci for iron deficiency chlorosis in soybean, Mol. Breed. 3 (1997) 219–229.

López-Millán A.F., Morales F., Gogorcena Y., Abadía A., Abadía J. Metabolic responses in iron deficient tomato plants, J. Plant Physiol. 166 (2009) 375–384.

López-Millán A.F., Morales F., Abadía A., Abadía J. Effects of iron nutrition on the composition of the leaf apoplastic fluid and xylem sap in sugar beet: implication for iron and carbon transport, Plant Physiol. 124 (2000) 873–884.

López-Millán A.F., Grusak M.A., Abadía A., Abadía J. Iron deficiency in plants: an insight from proteomic approaches, Front. Plant Sci. 4 (2013) 254.

Lucas W.J., Groover A., Lichtenberger R., Furuta K., Yadav S.R., Helariutta Y., He X.Q., Fukuda H., Kang J., Brady S.M., Patrick J.W., Sperry J., Yoshida A., López-Millán A.F., Grusak M.A., Kachroo P. The plant vascular system: evolution, development and functions, J. Integr. Plant Biol. 55 (2013) 294–388.

Luders J., Demand J., Hohfeld J. The ubiquitin-related BAG-1 provides a link between the molecular chaperones Hsc70/Hsp70 and the proteasome, J. Biol. Chem. 275 (2000) 4613–4617.

Lux A., Vaculik M., Martinka M., Liskova D., Kulkarni M.G., Stirk W.A., Van Staden J. Cadmium induces hypodermal periderm formation in the roots of the monocotyledonous medicinal plant *Merwilla plumbea*, Ann. Bot. 107 (2011) 285–292.

Lytle B.L., Song J., De la Cruz N.B., Peterson F.C., Johnson K.A., Bingman C.A., Phillips G.N., Volkman B.F. Structures of two *Arabidopsis thaliana* major latex proteins represent novel helix-grip folds, Proteins 76 (2009) 237–243.

Marschner H. Mineral Nutrition of Higher Plants, Academic Press, London (1995)

Mártinez-Cuenca M.R., Legaz F., Forner-Giner M.A., Primo-Millo E., Iglesias D.J. Bicarbonate blocks iron translocation from cotyledons inducing iron stress responses in *Citrus* roots, J. Plant Physiol. 170 (2013) 899–905.

Mengel K. Iron availability in plant tissues–iron chlorosis on calcareous soils, Plant Soil 165 (1994) 275–283.

Nikolic M., Römheld V. Does high bicarbonate supply to roots change availability of iron in the leaf apoplast? Plant Soil 241 (2002) 67–74.

Ralph J., Hatfield R.D. Pyrolysis-GC–MS characterization of forage materials, J. Agric. Food Chem. 39 (1991) 1426–1437.

Redjala T., Zelko I., Sterckeman T., Legué V., Lux A. Relationship between root structure and root cadmium uptake in maize, Environ. Exp. Bot. 71 (2011) 241–248.

Rellán-Álvarez R., Andaluz S., Rodríguez-Celma J., Wohlgemuth G., Zocchi G., Álvarez-Fernández A., Fiehn O., López-Millán A.F., Abadía J. Changes in the proteomic and metabolic profiles of *Beta vulgaris* root tips in response to iron deficiency and resupply, BMC Plant Biol. 10 (2010a) 120.

Rellán-Álvarez R., Giner-Martinez-Sierra J., Orduna J., Orera I., Rodríguez-Castrillón J.A., García-Alonso J.I., Abadía J., Álvarez-Fernández A. Identification of a tri-iron(III), tri-citrate complex in the xylem sap of iron-deficient tomato resupplied with iron: new insights into plant iron long-distance transport, Plant Cell Physiol. 51 (2010b) 91–102.

Rellán-Álvarez R., El-Jendoubi H., Wohlgemuth G., Abadía A., Fiehn O., Abadía J., Álvarez-Fernández A. Metabolite profile changes in xylem sap and leaf extracts of strategy I plants in response to iron deficiency and resupply, Front. Plant Sci. 2 (2011) 66.

Robinson N.J., Procter C.M., Connolly E.L., Guerinot M.L. A ferric-chelate reductase for iron uptake from soils, Nature 397 (1999) 694–697.

Rodríguez-Celma J., Vázquez-Reina S., Orduna J., Abadía A., Abadía J., Álvarez-Fernández A., López-Millán A.F. Characterization of flavins in roots of Fe-deficient strategy I plants, with a focus on *Medicago truncatula*, Plant Cell Physiol. 52 (2011a) 2173–2189.

Rodríguez-Celma J., Lattanzio G., Grusak M.A., Abadía A., Abadía J., López-Millán A.F. Root responses of *Medicago truncatula* plants grown in two different iron deficiency conditions: changes in root protein profile and riboflavin biosynthesis, J. Proteome Res. 10 (2011b) 2590–2601.

Rodríguez-Celma J., Lin W.D., Fu G.M., Abadía J., López-Millán A.F., Schmidt W. Mutually exclusive alterations in secondary metabolism are critical for the uptake of insoluble iron compounds by *Arabidopsis* and *Medicago truncatula*, Plant Physiol. 162 (2013a) 1473–1485.

Rodríguez-Celma J., Pan I.C., Li W., Lan P., Buckhout T.J., Schmidt W. The transcriptional response of *Arabidopsis* leaves to Fe deficiency, Front. Plant Sci. 4 (2013b) 276.

Rombolà A., Tagliavini M. Iron nutrition of fruit tree crops, in: L.L. Barton, J. Abadía (Eds.), Iron Nutrition in Plants and Rhizospheric Microorganisms, Springer, New York 2006, pp. 61–83.

Romheld V. Different strategies for iron acquisition in higher plants, Physiol. Plant. 70 (1987) 231–234.

Roschzttardtz H., Seguela-Arnaud M., Briat J.F., Vert G., Curie C. The FRD3 citrate effluxer promotes iron nutrition between symplastically disconnected tissues throughout *Arabidopsis* development, Plant Cell 23 (2011) 2725–2737.

Santi S., Schmidt W. Dissecting iron deficiency-induced proton extrusion in *Arabidopsis* roots, New Phytol. 183 (2009) 1072–1084.

Schmidt W., Buckhout T.J. A hitchhiker's guide to the *Arabidopsis* ferrome, Plant Physiol. Biochem. 49 (2011) 462–470.

Schmid N.B., Giehl R.F., Doll S., Mock H.P., Strehmel N., Scheel D., Kong X., Hider R.C., von Wiren N. Feruloyl-CoA 6′-Hydroxylase1-dependent coumarins mediate iron acquisition from alkaline substrates in *Arabidopsis*, Plant Physiol. 164 (2014) 160–172.

Tachi H., Fukuda-Yamada K., Kojima T., Shiraiwa M., Takahara H. Molecular characterization of a novel soybean gene encoding a neutral PR-5 protein induced by highsalt stress, Plant Physiol. Biochem. 47 (2009) 73–79.

Tambasco-Studart M., Titiz O., Raschle T., Forster G., Amrhein N., Fitzpatrick T.B. Vitamin B6 biosynthesis in higher plants, Proc. Natl. Acad. Sci. U. S. A. 102 (2005) 13687–13692.

Terry N. Limiting factors in photosynthesis: I, Use of iron stress to control photochemical capacity in vivo. Plant Physiol. 65 (1980) 114–120.

Vander Mijnsbrugge K., Beeckman H., De Rycke R., Van Montagu M., Engler G., Boerjan W. Phenylcoumaran benzylic ether reductase, a prominent poplar xylem protein, is strongly associated with phenylpropanoid biosynthesis in lignifying cells, Planta 211 (2000) 502–509.

Vasconcelos M.W., Grusak M.A. Morpho-physiological parameters affecting iron deficiency chlorosis in soybean (*Glycine max* L.), Plant Soil 374 (2014) 161–172.

Watson B.S., Asirvatham V.S., Wang L., Sumner L.W. Mapping the proteome of barrel medic (*Medicago truncatula*), Plant Physiol. 131 (2003) 1104–1123.

Zocchi G. Metabolic changes in iron-stressed dicotyledoneus plants, in: L.L. Barton, J. Abadía (Eds.), Iron Nutrition in Plants and Rhizospheric Microorganisms, Springer, Dordrecht 2006, pp. 359–370.

Zuo Y., Ren L., Zhang F., Jiang R.F. Bicarbonate concentration as affected by soil water content controls iron nutrition of peanut plants in a calcareous soil, Plant Physiol. Biochem. 45 (2007) 357–364.

Last name: **Ceballos Laita** Name: **Laura**

NIF: 76923883S Date of birth: 30-04-1988 Sex: F

Current job

Institution: University of Zaragoza
Center: Institute for Biocomputation and Physics of Complex Systems (BIFI)
Advisor's name: Ramón Hurtado Guerrero
Dept.: Biochemistry Department
Postal address: Campus Río Ebro, 50018, Zaragoza
Telephone: (+34)876555422
e-mail: ceballos.laita@gmail.com

Research interests

Gel and non-gel-based proteomics techniques, including 2-DE IEF SDS-PAGE, BN SDS-PAGE and shotgun proteomics
Mass spectrometry
Iron and manganese homeostasis in plants

Academic education

Graduate (**Lic.**) in Biochemistry	University of Zaragoza, Zaragoza, Spain	September, 2011
Master ("Molecular and Cellular Biology")	University of Zaragoza, Zaragoza, Spain	June, 2012
PhD	University of Zaragoza, Zaragoza, Spain	July 2018

Scientific career

Student in practice	University Hospital Lozano Blesa (Zaragoza, Spain)	Sep 2010
Research Assistant	Biochemistry Department of University of Zaragoza (Zaragoza, Spain)	Sep 2012 - Jan 2014
Fellow FPI (CSIC)	Aula Dei Experimental Station, Zaragoza, Council for Scientific Research (EEAD-CSIC)	Jan 2014 - Jan 2018
Researcher	Biochemistry Department of University of Zaragoza (Zaragoza, Spain)	Feb 2018 - present

Languages (F = fair, C = correctly) **Spoken** **Reading** **Writing**

Spanish	C	C	C
English	F	C	C

Participation in Research Groups and Projects

Risk assessment of the impact of climate change on water: proliferation of opportunistic pathogens and potentially toxic cyanobacteria and impaired fixation of atmospheric CO_2
Financing agency: Government of Aragon, "La Caixa" Foundation and Ministry of Science and Innovation.
From: May 2012 To: Sep 2013
PI: María Francisca Fillat Castejón (University of Zaragoza, Spain)

Validation of a test to detect microcystin in water
Financing agency: Zeu-Inmunotec, S.L.

From: Jan 2012 To: Dec 2012
PI: María Luisa Peleato Sánchez (University of Zaragoza, Spain)

Consolidated Research Group recognized by the Government of Aragón: "Biología Estructural"
Financing agency: Government of Aragón
From: Jan 2013 To: Dec 2013
PI: Carlos Gómez Moreno (University of Zaragoza, Spain)

Innovative strategies to improve iron nutrition in fruit crops (ref. AGL 2012-31998)
Financing agency: Ministry of Economy, Industry and Competitiveness, Spain
From: Jan 2014 To: Dec 2015
PI: Anunciación Abadía Bayona (EEAD-CSIC, Spain)

Towards an understanding of the roles of metabolites and proteins in plant metal homeostasis (ref. AGL2013-42175-R)
Financing agency: Ministry of Economy, Industry and Competitiveness, Spain
From: Jan 2016 To: Dec 2016
PI: Javier Abadía Bayona (EEAD-CSIC, Spain)

Metals in plants: homeostasis and fertilization (AGL2016-75226-R)
Financing agency: Ministry of Economy, Industry and Competitiveness, Spain
From: Jan 2017 To: Jan 2018
PI: Javier Abadía Bayona (EEAD-CSIC, Spain)

Consolidated Research Group Recognized by the Government of Aragón: "Fisiología de estrés abiótico en plantas"
Financing agency: Government of Aragón
From: Jan 2014 To: Jan 2018
PI: Javier Abadía Bayona (EEAD-CSIC, Spain)

Papers in SCI Journals

1 **Ceballos-Laita L.**, Gutierrez-Carbonell E., Lattanzio G., Vázquez S., Contreras-Moreira B., Abadía A., Abadía J., López-Millán A.F. (2015) Protein profile of *Beta vulgaris* leaf apoplastic fluid and changes induced by Fe deficiency and Fe resupply. Front Plant Sci, 6: 145; doi: 10.3389/fpls.2015.00145.

2 **Ceballos-Laita L.**, Calvo-Beguería L., Bes M. T., Fillat M. F., Peleato M.L. (2015) Effect of several emerging contaminants on growth and microcystin production in *Microcystis aeruginosa* PCC 7806. Limnética, 34(1): 237-246.

3 **Ceballos-Laita L.**, Calvo-Beguería L., Lahoz J., Bes M.T., Fillat M.F., Peleato M.L. (2015) γ-Lindane increases microcystin synthesis in *Microcystis aeruginosa* PCC7806. Mar. Drugs, 13(9): 5666-5680; doi: 10.3390/md13095666.

4 Rodríguez-Celma J., Lattanzio G., Villarroya D., Gutierrez-Carbonell E., **Ceballos-Laita L.**, Rencoret J., Gutiérrez A., Del Río J.C., Grusak M.A., Abadía A., Abadía J., López-Millán A.F. (2016) Effects of Fe deficiency on the protein profiles and lignin composition of stem tissues from *Medicago truncatula* in absence or presence of calcium carbonate. J Proteomics, 140, 1-12; doi: 10.1016/j.jprot.2016.03.017.

5 Rodríguez-Celma J., **Ceballos-Laita L.**, Grusak M.A., Abadía J., López-Millán A.F. (2016) Plant fluid proteomics: delving into the xylem sap, phloem sap and apoplastic fluid proteomes. BBA Proteins Proteom, 1864, 991–1002; doi: 10.1016/j.bbapap.2016.03.014.

6 **Ceballos-Laita L.**, Marcuello C., Lostao A., Calvo-Beguería L., Velazquez-Campoy A., Bes M.T., Fillat M.F., Peleato M.L. (2017). Microcystin-LR binds iron, and iron promotes self-assembly. Environmental Science and Technology, 51(9): 4841-4850; doi: 10.1021/acs.est.6b05939.

7 **Ceballos-Laita L.**, Gutierrez-Carbonell E., Takahashi D., Abadía A., Uemura M., Abadía J., López-Millán A.F. (2018). Effects of Fe and Mn deficiencies on the protein profiles of tomato (*Solanum lycopersicum*) xylem sap as revealed by shotgun analyses. J Proteomics, 6(170):117-129; doi: 10.1016/j.jprot.2017.08.018.

8 **Ceballos-Laita L.**, Gutierrez-Carbonell E., Takahashi D., Abadía A., Uemura M., Abadía J., López-Millán A.F. (2018). Data on xylem sap proteins from Mn- and Fe-deficient tomato plants using shotgun proteomics. J Proteomics, 17:512-516; doi.org/10.1016/j.jprot.2017.08.018.

Submitted:

9 **Ceballos-Laita L.**, Gutierrez-Carbonell E., Imai H., Abadía A., Uemura M., Abadía J., López Millán A.F. (2018). Effects of manganese toxicity on the protein profile of tomato (*Solanum lycopersicum*) roots as revealed by two complementary proteomic approaches, two-dimensional electrophoresis and shotgun analysis. J Proteomics (Accepted).

10 **Ceballos-Laita L.**, Gutierrez-Carbonell E., Takahashi D., Abadía A., Uemura M., Abadía J., López Millán A.F. Effects of manganese toxicity on the protein profile of tomato (*Solanum lycopersicum*) xylem sap as revealed by shotgun analysis. (In preparation).

11 **Ceballos-Laita L.**, Gutierrez-Carbonell E., Imai H., Abadía A., Uemura M., Abadía J., López Millán A.F. (2018). Effects of Fe and Mn deficiencies on the protein profile of tomato (*Solanum lycopersicum*) roots as revealed by two complementary proteomic approaches, two-dimensional electrophoresis and shotgun analysis. (In preparation).

12 **Ceballos-Laita L.**, Garcia C.B., Gutierrez-Carbonell E., Uemura M., Abadía J., Grusak M.A., López Millán A.F. Effects of Fe deficiency in the seed proteome of two *Medicago truncatula* ecotypes differing in mineral accumulation patterns. (In preparation).

Short stages

Institute for Biocomputation and Physics of Complex Systems (BIFI), Zaragoza, Spain
2012-2013, One week
Subject: “Fluorimetry”

Institute for Biocomputation and Physics of Complex Systems (BIFI), Zaragoza, Spain
2012-2013, Two weeks
Subject: “Isothermal titration calorimetry”

Institute for Biocomputation and Physics of Complex Systems (BIFI), Zaragoza, Spain
2012-2013, Three months
Subject: “Surface Plasmon Resonance”

Cryobiofrontier Research Center, Faculty of Agriculture, United Graduate School of Agricultural Sciences, Morioka, Iwate, Japan
2014, One month
Subject: “Shotgun proteomics (nano-LC MS/MS)”

Cryobiofrontier Research Center, Faculty of Agriculture, United Graduate School of Agricultural Sciences, Morioka, Iwate, Japan
2015, Two months
Subject: "Shotgun proteomics (nano-LC MS/MS)"

Cryobiofrontier Research Center, Faculty of Agriculture, United Graduate School of Agricultural Sciences, Morioka, Iwate, Japan
2016, Two months
Subject: "Shotgun proteomics (nano-LC MS/MS)"

Symposia

2012 **V International Conference BIFI 2012. Protein Targets: Discovery of Bioactive Compounds (Zaragoza, Spain)**

Participant

2013 **VI National Conference BIFI 2013 (Zaragoza, Spain)**

Ceballos L., Alias M., Fillat M.F., González A., Peleato M.L., Calvo-Beguería L**.** Effect of lindane on microcystin gene cluster expression in *Microcystis aeruginosa* PCC 7806 (Poster presentation and Oral Communication)

VI National Conference BIFI 2013 (Zaragoza, Spain)

Ceballos L., Calvo-Beguería L, Bes M.T., Fillat M.F., Peleato M.L. Analysis of the interaction between NtcA and *mcyAD* promoter using Surface Plasmon Resonance (Poster presentation)

ESF-EMBO Symposium 2013. Molecular Bioenergetics of Cianobacteria: Shaping the Environment (Pultusk, Poland)

Ceballos L., Calvo-Beguería L, Alias M., Gonzalez A., Pascual M. M., Fillat M.F., Peleato M.L. Binding interactions between NtcA from *Microcystis aeruginosa* PCC 7806 and two fragments of bidirectional promoter of the microcystin gene cluster characterized by Surface Plasmon Resonance. (Poster presentation)

III Congreso Ibérico Cianotoxinas y V Reunión de la Red de Estudios en Cianotoxinas (Blanes, Spain)

Ceballos L., Calvo-Beguería L, Rodríguez-Navarro L., Martín-Brieva A., Bes M.T., M., Fillat M.F., Peleato M.L. La microcistina está relacionada con la incorporación de hierro. (Oral Communication)

III Congreso Ibérico Cianotoxinas y V Reunión de la Red de Estudios en Cianotoxinas (Blanes, Spain)

Ceballos L., Calvo-Beguería L, Lostao A., Marcuello C., Velázquez A., Gregorio I., Vela L., Bes M.T., M., Fillat M.F., Peleato M.L. Efecto de algunos contaminantes emergentes sobre los niveles de microcistina en *Microcystis aeruginosa* PCC 7806. (Poster presentation)

2014 **VI International Conference BIFI 2014. Exploring the role of computation in Science: from Biology to Physics (Zaragoza, Spain)**

Ceballos L., Alías M., Calvo-Beguería L, Peleato M.L. Study of the interaction between NtcA and *mcyAD* promoter from *Microcystis aeruginosa* PCC 7806 in the

presence of amino acids: a Surface Plasmon Resonance approach. (Poster presentation)

VI International Conference BIFI 2014. Exploring the role of computation in Science: from Biology to Physics (Zaragoza, Spain)

Ceballos L., Bes M. T., Fillat M.F., Peleato M.L. A hypothetical concanavalin A-like protein binds to *mcy* bidirectional promoter in *Microcystis aeruginosa* PCC 7806 assay. (Poster presentation)

VI International Conference BIFI 2014. Exploring the role of computation in Science: from Biology to Physics (Zaragoza, Spain)

Ceballos L., Calvo-Beguería L., Barja F., Bes M. T., Fillat M.F., Peleato M.L. γ-Lindane induces *nirA* in *Microcystis aeruginosa* PCC 7806, involved in the degradation of the pesticide. (Poster presentation)

1st INPPO World Congress on Plant Proteomics: Methodology to Biology (Hamburg, Germany)

Ceballos-Laita L., Gutierrez-Carbonell E., Lattanzio G., Abadía A., Abadía J., López-Millán A.F. Changes in the protein profiles of *Beta vulgaris* leaf apoplastic fluid with iron deficiency and iron resupply. (Poster presentation)

2015 **XXI Congreso de la Sociedad Española de Fisiología Vegetal (XIV Congreso Hispano-Luso) (Toledo, Spain)**

Gutierrez-Carbonell E., **Ceballos-Laita L.**, Takahashi D., Uemura M., Abadía A., López-Millán A.F., Abadía J. Shotgun proteomics: a tool to investigate changes in subproteomes of plants grown under stress. (Oral Communication)

WI Medicago Group Plant Proteomics Workshop 2015 (Madison, WI, USA)

Ceballos-Laita L., Garcia C., Takahashi D., Abadía A., Grusak M.A., Uemura M., Abadía J., López-Millán A.F. Changes in the protein profile of seeds from two genotypes of *Medicago truncatula* as affected by iron deficiency. (Poster presentation)

9th European Summer School Advanced Proteomics (Brixen, Italy)

Ceballos-Laita L., Garcia C., Takahashi D., Abadía A., Grusak M.A., Uemura M., Abadía J., López-Millán A.F. Changes in the protein profile of seeds from two genotypes of *Medicago truncatula* as affected by iron deficiency. (Poster presentation)

2016 **VII International Conference BIFI 2016. International Conference on Molecular Recognition (Zaragoza, Spain)**

Andreu P., Arbeloa A., **Ceballos L.**, Peleato M.L., Marin J. Proteomic analysis of *Prunus* roots growth *in vitro* under saline stress. (Poster presentation)

18th ISINIP International Symposium on Iron Nutrition and Interactions in Plants (Madrid, Spain)

Ceballos-Laita L., Takahashi D., Uemura M., Abadía A., Abadía J., López-Millán A.F. Effects of Fe and Mn deficiencies in the protein profiles of tomato (*Solanum lycopersicum*) xylem sap (Oral communication)

18th ISINIP International Symposium on Iron Nutrition and Interactions in Plants (Madrid, Spain)

Ceballos-Laita L., Garcia C.C., Takahashi D., Uemura M., Abadía A., Grusak M. A., Abadía J., López-Millán A.F. Effect of iron deficiency in the seed proteome of two *Medicago truncatula* ecotypes differing in mineral accumulation patterns. (Poster presentation)

2017 **XXII Reunión de la Sociedad Española de Fisiología Vegetal / XV Congreso Hispano-Luso de Fisiología Vegetal (Barcelona, Spain)**

Ceballos-Laita L., Imai H., Uemura M., Abadía A., Abadía J., López-Millán A.F. Effects of Mn toxicity on the protein profiles of tomato (*Solanum lycopersicum*) roots using two proteomic approaches. (Oral communication)

XVIII International Plant Nutrition Colloquium (Copenhaguen, Denmark)

Ceballos-Laita L., Gutierrez-Carbonell E., Takahashi D., Uemura M., Abadía A., Abadía J., López-Millán A.F. Effects of Mn toxicity on the protein profiles of tomato *(Solanum lycopersicum)* xylem sap and roots. (Poster presentation)

Courses

Open Day Zaragoza, Alianza Europea para la Innovación en agua
ZINNAE, Clúster urbano para el uso eficiente del agua
Zaragoza, 2013

Captación de fondos de investigación básica
Instituto de Ciencias de la Educación
Zaragoza, 2013

Horizonte 2020: Programa Marco de Investigación de la Unión Europea
Instituto de Ciencias de la Educación
Zaragoza, 2013

II Jornada sobre Bebidas Fermentadas
Cátedra Extraordinaria de Bebidas Fermentadas de la Universidad Complutense de Madrid
Zaragoza, 2013

Seminario de Alta Tecnología
Agilent Technologies
Zaragoza, 2014

Western Blot Cuantitativo: Sistema Odyssey CLx
Instituto de Investigación Sanitaria de Aragón
Zaragoza, 2015

Análisis multivariante aplicado a espectrometría de masas de tiempo de vuelo
Bruker
Zaragoza, 2016

Análisis Estadístico y Diseño de Experimentos
Consejo Superior de Investigaciones Científicas (CSIC)
Zaragoza, 2017

Writing
Consejo Superior de Investigaciones Científicas (CSIC) (On line)
Zaragoza, 2017

Cómo planificar, estructurar, diseñar y exponer presentaciones y conferencias científicas
Consejo Superior de Investigaciones Científicas (CSIC)
Zaragoza, 2017

Teaching activity

Co-tutor of internship in Biotechnology degree
Author: Elena Gárate
University: UNIVERSA, University of Zaragoza
From: Jun 2016 To: Aug 2016

Co-director of Ungraduate Research Project
Title: Effect of foliar fertilisation on the modulation of the root responses to Fe deficiency
Author: Elena Gárate
University: University of Zaragoza
Date: Jun 2017
Qualification: 8.9

Professional memberships

Member of the Institute for Biocomputation and Physics of Complex Systems. University research center, Zaragoza, Spain
From: Sep 2011 To: Dec: 2015

Member of the Spanish Proteomics Society, Madrid, Spain
From: May 2014 To: present

Member of the Spanish Society of Plant Physiology, Madrid, Spain
From: Mar 2017 To: present